Middle Atmosphere Program

ICSU

International Council of Scientific Unions

SCOSTEP

Scientific Committee on Solar-Terrestrial Physics
J. G. Roederer, President
W. I. Axford, Vice President
C. H. Liu, Scientific Secretary

MAP ORGANIZATION

MIDDLE ATMOSPHERE PROGRAM STEERING COMMITTEE

S. A. Bowhill, SCOSTEP, Chairman
K. Labitzke, COSPAR, Vice Chairman
C. H. Liu, SCOSTEP, Secretary

H. S. Ahluwalia, IUPAP
R. D. Bojkov, WMO
A. D. Danilov, COSPAR
J. C. Gille, COSPAR
I. Hirota, IUGG/IAMAP
A. H. Manson, SCOSTEP
T. Nagata, SCAR
R. G. Roper, IUGG/IAMAP
P. C. Simon, IAU
J. Taubenheim, IUGG/IAGA
T. E. VanZandt, URSI
R. A. Vincent, URSI

MAP STANDING COMMITTEES

Data Management -- G. Hartmann and I. Hirota, Co-Chairmen
Publications -- Belva Edwards, Chairman

MAP STUDY GROUPS

MSG-5 Ions and Aerosols, F. Arnold and M. P. McCormick, Co-Chairmen
MSG-8 Atmospheric Chemistry, G. Witt, Chairman
MSG-9 Measurement of Middle Atmosphere Parameters by Long Duration Balloon Flights, J. E. Blamont, Chairman

MAP PROJECTS

	Coordinator
AMA:	T. Hirasawa
ATMAP:	J. M. Forbes
DYNAMICS:	K. Labitzke
GLOBMET:	R. G. Roper
GLOBUS:	J. P. Pommereau
GOSSA:	M. P. McCormick
GRATMAP:	D. C. Fritts
MAC-EPSILON:	E. V. Thrane

	Coordinator
MAC-SINE:	E. V. Thrane
MAE:	R. A. Goldberg
MASH:	A. O'Neill
NIEO:	S. Kato
OZMAP:	D. F. Heath
SSIM:	P. C. Simon
SUPER CAMP:	E. Kopp
WINE	U. von Zahn

MAP REGIONAL CONSULTATIVE GROUP

Europe: M. L. Chanin, Chairman

MIDDLE

ATMOSPHERE

PROGRAM

HANDBOOK FOR MAP

Volume 31

Reference Models of Trace Species
for the
COSPAR International Reference Atmosphere
(Draft)

Edited by

G. M. Keating

December 1989

Published for the ICSU Scientific Committee on Solar-Terrestrial Physics (SCOSTEP) with financial assistance from the National Aeronautics and Space Administration under the 1988 Middle Atmosphere Program Management Contract and Unesco Subvention 1988-1989.

Copies available from SCOSTEP Secretariat, University of Illinois, 1406 W. Green Street, Urbana, Illinois 61801.

PREFACE

Included in the new COSPAR International Reference Atmosphere, Volume 2 (CIRA) (to be published by Pergamon Press) are reference models of ozone up to altitudes of 90 km. These ozone models, of spatial and temporal variations, are based on five recent satellite experiments. Previously, the CIRA atmospheres below 100 km had been limited to representations of the atmospheric structure and its variations without regard to trace species.

Interest in developing additional reference models of trace species has stemmed partially from two COSPAR workshops in recent years: one held in July 1986 at Toulouse, France, entitled "Proposed Reference Models of Trace Constituents of the Middle Atmosphere *(Adv. Space Res., 7,* #9, Pergamon Press, Oxford, 1987) and the other held in July 1988 at Espoo, Finland, entitled "Reference Models of the Middle Atmosphere and Lower Thermosphere and Recent Data" (*Adv. Space Res., 10,* #6, Pergamon Press, Oxford, 1990). The first workshop was cosponsored by IAGA, IAMAP, and SCOSTEP and the second by IAGA, IAMAP, SCOSTEP, and URSI. The primary purpose of these workshops was to produce a set of preliminary reference atmospheres of significant trace species which play important roles in controlling the chemistry, radiation budget, and circulation patterns of the atmosphere. These models of trace species distributions are considered to be reference models rather than standard models and thus it was not crucial that they be correct in an absolute sense. These reference models can serve as a means of comparison between individual observations, as a first guess in inversion algorithms, and as an approximate representation of observations for comparison to theoretical calculations.

On 18 July 1988 the Middle Atmosphere Program (MAP) Steering Committee met in Espoo, Finland, and invited COSPAR to compile a preliminary draft of these reference atmospheres of trace species for publication in a MAP Handbook for early distribution to the scientific community. After publication in the MAP Handbook, an improved draft will be submitted to COSPAR as a proposed addition to the COSPAR International Reference Atmosphere (CIRA).

Proposed reference models are provided here for ozone (Chapters 1 and 2) H_2O (Chapter 3), CH_4 and N_2O (Chapters 4 and 5), HNO_3 (Chapter 6), CO_2 and halogenated hydrocarbons (Chapter 7), background aerosols (Chapter 8), thermospheric NO (Chapter 10) and atomic oxygen (Chapter 11). Two chapters are devoted to comparisons between observed and calculated distributions of trace species in the middle atmosphere (Chapter 9) and in the lower thermosphere (Chapter 12). Chapter 1 gives the ozone reference model which is included in the new CIRA (to be published by Pergamon Press). Chapters 2, 3, 5, 10 and 12 are reproduced from *Adv. Space Res., 10,* and Chapters 4, 7, 8 and 9 are reproduced from *Adv. Space Res. 7,* with permission from the publishers, Pergamon Press, and the copyright holder, COSPAR. Chapters 6 and 11 are new contributions.

As may be noted, these models, which give spatial and temporal variations of trace species, are based principally on satellite data from the late 1970s and early 1980s. As more satellite, ground based and rocket and balloon data of good accuracy become available and are archived, the present models may be improved and models of additional species may be generated.

G. M. Keating, Editor
NASA Langley Research Center
Hampton, VA 23665 USA

CONTENTS

OZONE REFERENCE MODELS FOR THE MIDDLE ATMOSPHERE (NEW CIRA)

G. M. Keating[1], M. C. Pitts[2], and D. F. Young[3]

[1]Atmospheric Sciences Division, NASA Langley Research Center, Hampton, VA 23665
[2]ST Systems Corporation (STX), Hampton, VA 23666
[3]Kentron Corporation, Hampton, VA 23666

1 INTRODUCTION

Over the last 50 years, a number of measurements of ozone in the middle atmosphere have been obtained from the ground and from balloons, rockets, and satellites. Numerous models have been developed to summarize various portions of these measurements since detailed knowledge of the global distribution of ozone is important for studies of atmospheric circulation, dynamic processes, and the radiation balance and the photochemistry of the atmosphere. From the ground-based ozone network, the latitudinal-seasonal variations of total column ozone were summarized by Dutsch [1] and the longitudinal variations were included in a series of monthly atlases for the period 1957 to 1967 by London *et al.* [2]. Measurements of vertical structure obtained from balloonsondes and rocket data at midlatitudes in the Northern Hemisphere were summarized in a 45° annual model generated by A. Krueger and R. Minzner contained in the United States Standard Atmosphere Supplements, 1976 [3]. Bojkov [4] generated models of ozone vertical structure related to total column ozone amount based on Dobson data and early Umkehr measurements. Models relating the vertical structure of ozone to total ozone based on approximately 7000 balloonsondes and a number of rocketsondes were generated by Hilsenrath *et al.* [5] as a "first guess" for the Nimbus 4 Backscattered Ultraviolet (BUV) ozone experiment retrievals of total ozone and vertical structure and for the early Nimbus 7 SBUV/TOMS total ozone retrievals. Similar models based on essentially the same data base were generated by Mateer *et al.* [6] as a "first guess" for inversion of "short" Umkehr obser-vations to determine vertical structure of ozone from the ground. The 22 vertical profiles in [6] were given as a function of latitude (low, mid and high) and total column ozone, but not season. Inconsistencies between rocket and balloon data were handled differently by Mateer *et al.* [6] than by Hilsenrath *et al.* [5]. Bhartia *et al.* [7] have developed similar models using both ozonesonde and satellite data. Klenk *et al.* [8] developed a model of ozone vertical structure based on Nimbus 4 BUV data at pressures less than 15.6 mb and on balloon data at lower altitudes. This model was used as a "first guess" for vertical structure retrievals from the Nimbus 7 Solar Backscattered Ultraviolet (SBUV) ozone experiment. The model consisted of a simple parametric representation of the annual and latitudinal variations of ozone as a function of pressure and assumed symmetry between the Northern and Southern Hemispheres. Also included in this model is the ozone covariance matrix which describes the variance of ozone in individual atmospheric layers and the covariances between adjacent layers. An ozone covariance matrix is also included in the models of Mateer *et al.* [6]. Dutsch [9] compiled data on the vertical ozone distribution using chemical-type balloon soundings and early BUV results. A tabulation of monthly Nimbus 7 SBUV ozone profiles for the period November 1978 through October 1979 is provided by McPeters *et al.* [10] in 10° latitude increments from 0.17 mb to the surface. Results are given in terms of column density and its standard deviation, volume mixing ratio and number density. Heath *et al.* [11] have generated a set of atlases of total ozone for the period April 1970 - December 1976 based on Nimbus 4 BUV data. Bowman and Krueger [12] have provided a climatology of total ozone from Nimbus 7 TOMS measurements. Tolson [13] has generated a ninth-order, ninth-degree spherical harmonic model to represent the monthly mean total colum-nar ozone field over the 7-year period of the Nimbus 4 BUV data set. Annual and semiannual components are determined for both latitudinal and longitudinal variations, and

the biennial and longer term variations are determined as a function of latitude. Hasebe [14] has modeled the latitudinal and longitudinal variations in the total columnar ozone field over the 7-year period of the Nimbus 4 BUV data set using filtering techniques. Global mean total column ozone and its annual, semiannual, quasibiennial and longer term components have been determined through spherical harmonic analysis [13,15].

Data on total ozone and its vertical structure have been obtained from a number of satellite experiments. Shown in Table 1 (Krueger *et al.* [16]) is a tabulation of most satellite ozone experiments through 1978. Included are solar and stellar occultation, solar backscatter ultraviolet, and infrared types. Since then, other satellites have been launched with ozone measurement capability including Applications Explorer 2 [17], Dynamics Explorer 1 [18,19], Solar Mesosphere Explorer [20], EXOS-C [21] and instruments aboard the NOAA series of satellites (TOVS and SBUV 2) [22,23] and ERBS (SAGE II) [24].

With the wealth of recent satellite data allowing high precision determination of ozone variations with pressure, latitude, and time, it was decided to generate models of ozone vertical structure based not just on one satellite experiment, but on multiple data sets from satellites. This is the first time such models have been generated [25- 28]. The very good absolute accuracy of the individual data sets allowed the data to be directly combined to generate these models. The data used for generation of these models are from some of the most recent satellite measurements over the period 1978-1983. A discussion is provided of validation and error analyses of these data sets. Also, inconsistencies in data sets brought about by temporal variations or other factors are indicated. The models cover the pressure range from 20 to 0.003 mb (25 to 90 km). The models for pressures less than 0.5 mb represent only the day side and are only provisional since there was limited longitudinal coverage at these levels. The models start near 25 km in accord with previous CIRA models. Models are also provided of ozone mixing ratio as a function of height using the conversion from pressure to height given by Barnett and Corney [29]. The monthly standard deviation and interannual variations relative to zonal means are also provided.

In addition to the models of monthly latitudinal variations in vertical structure based on satellite measurements, monthly models of total column ozone and its characteristic variability as a function of latitude based on 4 years of Nimbus 7 measurements, models of the relation between vertical structure and total column ozone [6], and a midlatitude annual mean model similar to [3] are incorporated in this set of ozone reference atmospheres. Various systematic variations are discussed including the annual, semiannual, quasibiennial oscillations, diurnal variations, longitudinal variations, and response to solar activity variations.

Considering the good agreement among satellite data sets from 1978-1982 (generally within 10% of the interim reference models below 0.5 mb) it is expected that the present tables will be useful for many applications.

2. SATELLITE DATA FOR REFERENCE MODELS

The reference models provided here of monthly latitudinal variations of vertical structure are based on ozone data from five satellite experiments (see Table 2): Nimbus 7 Solar Backscatter Ultraviolet (SBUV), Nimbus 7 Limb Infrared Monitor of the Stratosphere (LIMS), Applications Explorer Mission-2 Stratospheric Aerosol and Gas Experiment (SAGE), Solar Mesosphere Explorer UV Spectrometer (SME-UVS), and Solar Mesosphere Explorer 1.27 μm Airglow (SME-IR). Other ozone data sets are included to define the nature of systematic variations other than the latitudinal-seasonal variation.

The nadir-viewing SBUV experiment determines the vertical structure of ozone from absorption of solar ultraviolet backscattered radiation between 250 and 340 nm. The resolution of the ozone measurements is about 8 km in the vertical. For these studies, the first 4 years of SBUV data were employed (November 1978 - September 1982) using daily zonal averages every 10° in latitude over the illuminated portion of the earth from 20 mb to 0.5 mb. Data contaminated by volcanic emissions after October 1980 (including El Chichon) have been removed [30].

Validation studies have been performed on the SBUV data employing balloon, rocket, and ground-based Umkehr measurements [31]. The precision of the SBUV measurements was found to be better than 8% for pressures between 1 and 64 mb. Constant biases of generally less than 10% between the SBUV results and the balloon and Umkehr results may be largely due to errors in ozone absorption cross-sections assumed earlier. Ozone absorption cross sections

TABLE 1 Satellite experiments to measure ozone [16]

Type	Satellite	Wavelengths	Latitude Coverage	Comments	References
		nm			
Occulta-	Echo 1	590,529.5	17°N	Dec. 1960	Venkateswaran *et al.*[106]
tion	USAF 1962	260	33°S-13°S	July 1962	Rawcliffe *et al.* [107]
Solar	Ariel 2	200-400	50°S-50°N	Apr., May, Aug. 1964	Miller and Stewart [108]
	AE-5	255.5	5°N	Dec. 1976	Guenther *et al.* [109]
Stellar	OAO-2	250	16°S-43°N	Jan. 1970 Aug. 1971	Hays and Roble [110]
	OAO-3	258-343	12°S-3°N	July 1975	Riegler *et al.* [111]
Back-	USAF 1965	284	60°S-60°N	Feb., Mar. 1965	Rawcliffe and Elliott [112]
scatter uv	USSR	225-307	60°S-60°N	Apr. 1965	Iozenas *et al.* [113]
Profile		250-330	60°S-60°N	June 1966	Iozenas *et al.* [113]
	1966-111B	175-310	80°S-80°N	1966	Elliott *et al.* [114]
	OGO-4	110-340	80°S-80°N	Sep. 1967-Jan. 1969	Anderson *et al.* [115]
	Nimbus 4 b.u.v.	255.5-305.8	80°S-80°N	Apr. 1970-Jul. 1977	Heath *et al.* [54]
	AE-5 b.u.v.	255.5-305.8	20°S-20°N	Nov. 1975-Apr. 1977	Frederick *et al.* [116]
	Nimbus 7 s.b.u.v.	255.5-305.8	80°S-80°N	Nov. 1978	Heath *et al.* [117]
Total	Nimbus 4 b.u.v.	312.5-339.8	80°S-80°N	Apr. 1970-	Mateer *et al.* [118]
	AE-5 b.u.v.	312.5-339.8	20°S-20°N	Nov. 1974-Jul. 1977	
	Nimbus 7 t.o.m.s.	312.5-339.8	global	Nov. 1978	Heath *et al.* [117]
		μm			
Infrared	Nimbus 6	9.6	65°S-90°N	Jun. 1975-	Gille *et al.* [55]
Emission	l.r.i.r.			Jan. 1976	
Profile	Nimbus 7 l.i.m.s	9.6	65°S-90°N	Oct. 1978-May 1979	Nimbus Project [119,120]
Total	Nimbus 3 i.r.i.s.	9-10 spectral scan	80°S-80°N		Hanel *et al.* [121]
	Nimbus 4 i.r.i.s.	9-10 spectral scan	80°S-80°N	Apr. 1970 Jan. 1971	Prabhakara *et al.* [58]
	Block 5 m.f.r. (4 flights)		global	Mar. 1977	Lovill *et al.* [122]
	Tiros N h.i.r.s	9.71	global	Nov. 1978	

TABLE 2 Satellite data used for interim reference ozone models

Instrument	Incorporated Pressure Range	Incorporated Time Interval
Nimbus 7 LIMS	0.4 - 20 mb	11/78 - 05/79
Nimbus 7 SBUV	0.4 - 20 mb	11/78 - 09/82
AE-2 SAGE	4 - 20 mb	02/79 - 12/79
SME UVS	0.07 - 0.5 mb	01/82 - 12/83
SME IR	0.003 - 0.5 mb	01/82 - 12/83
Nimbus 7 TOMS	Total	11/78 - 09/82

incorporated recently by the International Ozone Commission of IAMAP are employed in the inversion of the data employed in the present models (Version 5) [32-34].

The LIMS instrument, a six-channel cryogenically cooled radiometer measured O_3 and temperature in the stratosphere and mesosphere and H_2O, HNO_3, and NO_2 distributions in the stratosphere from 84°N to 64°S latitude from October 25, 1978 to May 28, 1979 [35,36]. The LIMS ozone channel measures emission near 9.6 μm with a field of view at the limb of less than 3 km in the vertical and 18 km in the horizontal (perpendicular to the line of sight).

Monthly zonal means of Kalman-filtered LIMS ozone values are incorporated in the model for the period November 1978 through May 1979 from 60°S to 80°N and from 20 mb to 0.5 mb. Non LTE effects become important above these altitudes [37]. Validation studies have been performed using balloon and rocket underflights, Umkehr soundings, and Dobson measurements [38]. Comparison with the correlative measurements shows mean differences of less than 10% at mid latitudes for balloon-borne sensors and less than 16% up to 0.3 mb for rocket data. The comparison with balloon measurements near 20 mb indicate LIMS data may be high by about 8% at low latitudes. At greater pressures there is evidence of a significant bias relative to balloon data in this region.

The SAGE instrument is a four-channel sun photometer which measured solar intensity at sunrise and sunset to derive ozone, aerosol, and NO_2 concentrations. Absorption of 0.6 μm solar radiation by ozone allowed determination of the vertical structure of ozone to be obtained up to 30 times per day from February 1979 until September 1981. After data processing, the vertical resolution of the data was estimated to be 1 km up to approximately 40 km altitude and 5 km above 40 km. The horizontal resolution was estimated to be 200 to 300 km in the viewing direction and 200 km perpendicular to the field of view [39]. Monthly latitudinal coverage depends on the time of year and solar geometry, but can extend from 78°S to 78°N. However, on any particular day, the vertical structure is obtained at a discrete latitude for sunrises or sunsets. Comparisons were made between balloon measurements and SAGE profiles from 18 to 28 km, and average differences were found to be less than 10% [17,40]. Comparisons by McCormick *et al.* [17] with rocketsondes up to 60 km yielded average differences of less than 14% . An initial comparison between SAGE and SBUV in March-April 1979 indicated agreement to generally better than 15% between 5 and 30 mb [39]. A comparative study between the three data sets SBUV, SAGE, and LIMS for March 1979 has been performed by Fleig *et al.* [41,42]. The LIMS/SBUV comparisons are shown to be very good in the upper stratosphere, while the SBUV/SAGE comparisons are shown to be very good in the lower stratosphere.

Mesospheric ozone mixing ratios are available from two limb- scanning experiments aboard the Solar Mesosphere Explorer (SME) spacecraft (which was launched 6 October 1981). The first of these, the SME-UVS, is a two-channel Ebert-Fastie spectrometer. The instrument measures the Rayleigh scattering of solar photons at the earth's limb at wavelengths of 265 nm and 296.4 nm from which the ozone profile is determined between 1.0 mb and 0.07 mb [43]. The field of view of the instrument is 3.5 km in the vertical by 35 km in the horizontal at the limb. Generally zonal means are not obtained. The primary orbits were over the longitude range from 40°W to 100°W, and the local solar time of measurement at the equator is 15 hours. An error analysis indicates total errors should range from 6% at 48 km to 15% at 68 km (1.0 to 0.1 mb) [43,44]. The data chosen for the model are over the range 0.5 mb to 0.1 mb over the period January 1982 through December 1983.

The second SME experiment, SME-IR, is a near-infrared experiment that measures 1.27 μm airglow from which ozone densities from 50 to 90 km are deduced. The dayglow is principally associated with photodissociation of ozone [45]. Monthly means from this experiment agree fairly well with the SME-UVS experiment and with Krueger and Minzner [3]. Thomas *et al.* [46] describe the error analysis of this experiment in some detail. Random errors are estimated to be less than 10% from 50 to 82 km, and increase to 20% at 90 km. Systematic errors are estimated to be 15% but could be as high as 50%. The data used for the model are monthly means over the range 0.5 mb to 0.003 mb and over the period January 1982 through December 1983. The local solar time of the measurements is again about 15 hours. Latitudinal coverage is consistent with the illuminated earth, and longitudinal coverage is principally from 40°W to 100°W.

Reviews on mesospheric ozone are found in [47-51]. Ozone measurements made in the Aladdin program [52] by several techniques on June 29-30, 1974, are in good agreement with SME

measurements below 70 km. Above 75 km, Aladdin ozone is a factor of 2-3 lower than SME-IR. It is very possible that this is a real ozone variation [53].

Other satellite instruments which have obtained measurements of the vertical structure of ozone include the Nimbus 4 BUV experiment [54] and the Nimbus 6 Limb Radiance Inversion Radiometer (LRIR) [55]. Since the Nimbus 4 BUV experiment had problems with a serious drift in bias, the Nimbus 7 SBUV data from 1978-82 was considered to be a better choice for the model. The Nimbus 7 LIMS is generally considered an improvement over the Nimbus 6 LRIR experiment and was therefore chosen for the model. More recent experiments such as SBUV 2, SAGE II, and EXOS-C are still in the validation phase.

The models of total column ozone given here are based on 4 years of Nimbus 7 TOMS measurements. The TOMS instrument is used to determine total column ozone by measuring backscattered solar ultraviolet radiation attenuated by ozone employing a simple monochrometer whose instantaneous field of view scans through the subsatellite point and perpendicular to the orbital plane. Backscattered and direct solar radiation are sampled at six wavelengths from 312.5 nm to 380 nm. The resolution of ozone measurements is about 50 km in the horizontal. For these studies the first 4 years of TOMS data were employed (November 1978 - September 1982) using daily zonal averages every 5° in latitude over the illuminated portion of the earth. Comparisons of TOMS data with ground-based Dobson and M-83 data have shown a retrieved precision of better than 2% and biases of 6% where the TOMS measurements have lower values than the Dobson measurements [56].

Global measurements of total ozone from backscattered ultraviolet measurements have also been obtained from the Nimbus 4 Backscattered Ultraviolet (BUV) and the Nimbus 7 SBUV experiments. The TOMS experiment, however, obtains more measurements per day than the other two and does not appear to have the serious drift problems which occurred on the Nimbus 4 BUV experiment. Infrared experiments which measure total column ozone from absorption of 9.6 μm radiation have included the Nimbus 4 Infrared Interferometer Spectrometer (IRIS), the DMSP Multifilter Radiometers (MFR), and the ongoing Tiros Operational Vertical Sounders (TOVS). A study of the relative biases between a limited amount of the TOMS, MFR, TOVS and SBUV total column ozone results was performed [57] showing excellent global average agreement between the TOMS and MFR (3%) but not as good agreement between SBUV and MFR (5%) or between TOVS and MFR (7%), where in each case MFR gave a lower value for total ozone. Significant latitudinal biases relative to BUV data have been noted in the Nimbus 4 IRIS data [58,59].

3. MODELS OF TOTAL COLUMN OZONE

The monthly latitudinal models of total column ozone are based on the archived first 4 years of data from the Nimbus 7 TOMS experiment. The total column ozone values tabulated here are 5.5% higher than the TOMS archived data to be more in accord with the improved ozone cross sections of Bass and Paur [33] and with Dobson measurements [56]. A more detailed correction for the future TOMS algorithm improvements is given by Fleig *et al.* [60]. Shown in Figure 1 is total column ozone in Dobson units (the Dobson unit is defined as 10^{-5} meters of ozone at 0°C and at standard sea level pressure) as a function of latitude and month. Note the high values in mid and high latitudes in spring in the Northern Hemisphere and at mid latitudes in local spring in the Southern Hemisphere. Also note the low values in September-October near 80°S. These low values reflect the recently discovered "ozone hole" in the Antarctic [61]. Much higher values of ozone were detected in the springtime Antarctic before the 1980s [61,62]. Shown in Figure 2 is the standard deviation in percent of individual ozone measurements relative to the zonal mean obtained each month for a 1-year period (November 1978 - October 1979). Minimum standard deviations occur at low latitudes while the maximum values occur near the "ozone hole." A comparison of monthly ozone values from year to year over the 4-year period (November 1978 - September 1982) gives an approximate idea of patterns of interannual variability in total ozone. Shown in Figure 3 is the interannual variability expressed as standard deviation (in percent) relative to 4-year means as a function of latitude and month. The variations are generally less than 4% (except near October, 80°S) and are strongly related to quasibiennial variations discussed briefly in the section "Other Ozone Variations." The large variations in October, 80°S again reflect the recently discovered antarctic ozone hole.

Shown in Table 3 is a tabulation of the latitudinal variation of total column ozone in Dobson units for each month based on the dayside observations of ozone over the 4-year period. The spaces indicate times when no TOMS measurements were available.

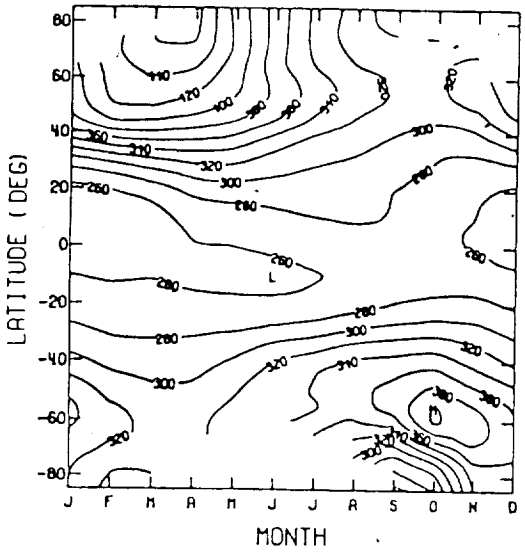

Figure 1. Zonal mean of total column ozone (Dobson units) as a function of latitude and month.

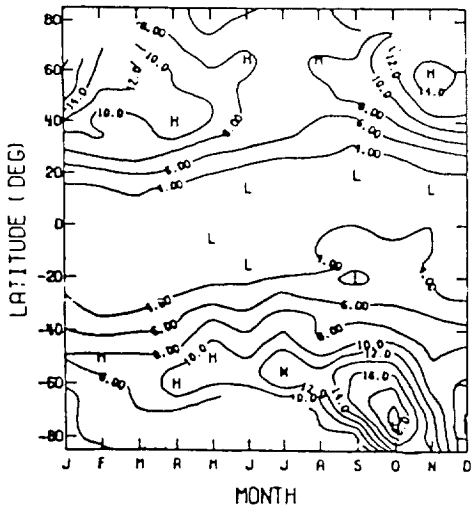

Figure. 2. Standard deviation (percent) from zonal mean of total column ozone for period January 1979 through December 1979 (Nimbus 7 TOMS data).

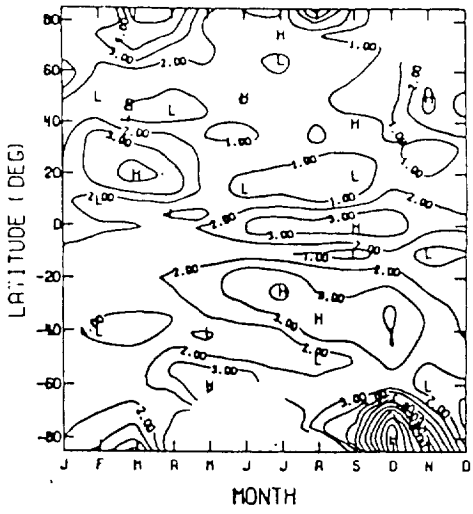

Figure 3. Interannual variability of total column ozone expressed as yearly standard deviation (percent) from 4-year zonal means (Nimbus 7 TOMS data).

TABLE 3. Zonal Mean Total Column Ozone (Dobson units)

φ	Jan	Feb	Mar	Apr	May	Jun	Jul	Aug	Sep	Oct	Nov	Dec
85°	-	-	467	467	411	371	333	311	283	-	-	-
80°	-	-	470	465	414	371	332	308	291	-	-	-
75°	-	433	460	462	416	370	332	308	302	299	-	-
70°	-	436	459	455	415	368	334	313	308	309	314	-
65°	395	432	451	444	410	367	338	320	312	315	332	-
60°	392	428	441	431	406	372	346	327	317	317	332	358
55°	390	426	433	421	402	375	350	330	318	317	327	353
50°	387	418	420	410	394	372	346	326	313	312	322	349
45°	376	402	401	395	382	360	335	319	307	302	311	338
40°	354	374	377	373	363	341	321	310	300	291	297	320
35°	322	338	347	348	342	323	310	303	295	283	284	299
30°	292	303	316	325	324	311	302	298	290	280	276	281
25°	269	278	291	304	307	301	296	291	284	275	270	267
20°	254	261	271	287	291	290	289	286	279	270	263	256
15°	248	251	260	275	279	282	284	283	279	268	261	252
10°	246	246	254	267	271	275	280	281	279	267	260	251
5°	247	248	254	261	264	268	274	277	278	263	258	251
0°	251	250	255	259	260	263	268	273	276	263	259	253
-5°	255	254	257	258	258	259	262	268	272	265	264	257
-10°	260	258	259	259	257	256	259	264	270	269	270	264
-15°	266	262	261	260	258	258	261	266	273	277	278	272
-20°	271	265	264	263	264	264	268	274	282	287	286	279
-25°	277	270	269	271	271	273	279	288	295	301	298	287
-30°	286	278	277	278	281	289	295	306	313	317	311	297
-35°	295	286	284	284	291	306	315	327	333	336	323	307
-40°	306	294	289	289	303	319	331	343	348	354	335	318
-45°	319	303	296	297	312	327	340	353	360	371	350	332
-50°	334	313	305	306	318	328	342	355	367	387	366	347
-55°	344	322	312	314	322	328	338	351	368	402	381	358
-60°	344	325	315	318	323	337	344	339	353	402	390	365
-65°	338	324	317	319	322	-	340	325	324	374	388	366
-70°	331	317	312	313	-	-	-	307	291	333	376	364
-75°	324	306	305	302	-	-	-	294	267	297	357	358
-80°	320	299	299	-	-	-	-	-	253	274	346	356
-85°	316	294	295	-	-	-	-	-	230	259	341	353

4. MODELS OF VERTICAL STRUCTURE OF OZONE

As described in section 2 the vertical structure models of monthly latitudinal variations are based on the SBUV, LIMS, SAGE, SME-UVS, and SME-IR data tabulated in Table 2. The 4-year mean of the SBUV data was given a weight of 2 due to the combination of extensive temporal and spatial coverage, while the other shorter data sets were each given a weight of 1.

Although there is interannual variability, comparison of the SBUV data over the 4-year period of measurements shows a remarkable similarity of structure from year to year. For example, shown in Figure 4 is the vertical structure at 0°, 20°N, 40°N and 60°N for November of 1978, 1979, 1980 and 1981. Note how the 0° and 20°N profiles come together near 4 mb. The 60°N profile changes in each case from the lowest profile at 4 mb to the highest at 1.5 mb.

Shown in Figure 5 is the interannual variability of zonal mean ozone expressed as standard deviation (in percent) relative to the mean of 4 years of SBUV data as a function of pressure and latitude for the months of November and July. As indicated in the previous figure, the interannual variability of zonal means in November is very low, generally less than 4%. In contrast, the month of July gave the largest variability over this 4-year period with the maximum variability occurring at high winter latitudes. The interannual variability appears to be strongly related to quasibiennial oscillations.

Figure 6 shows the average standard deviation (in percent) of the individual data points making up the monthly zonal means based on the 4 years of SBUV data. The standard deviations are shown as a function of latitude and pressure and appear considerably different from the interannual variability displayed in Figure 5. Minimum standard deviations occur near the equator and in the summer hemisphere. Standard deviations can exceed 15% at high latitudes and result from substantial longitudinal variations in ozone as well as changes in the zonal means during the month. The patterns for individual years look very similar to these 4-year mean patterns.

In Figure 7 is shown an example of the agreement between the five data sets used to generate models of the ozone vertical structure from 20 mb to 0.003 mb (25 to 90 km). Note that the mixing ratio is displayed on a log scale to allow accurate representation of the two orders of magnitude variation over this altitude range. It should be recognized that each data set represents entirely different techniques of measuring the vertical structure of ozone. The agreement shown here is fairly representative. Generally the SBUV ozone values redetermined with the improved ozone cross section (Version 5) give better agreement with the LIMS and SAGE data sets than the earlier versions.

Table 4 gives the monthly zonal mean ozone volume mixing ratios (ppmv) as a function of pressure and latitude. The standard type face indicates only one data type was used to determine the average. Italicsindicate that the percent standard deviation from the model of weighted data types exceeded 10 percent. An underlined entry indicates standard deviations from the model of less than 10 percent. The dashed entry indicates zonal means were not available at that latitude and pressure. As may be noted, in most cases at altitudes below 0.5 mb the standard deviation from the model of weighted data types was less than 10 percent. Considering the difference in techniques, this is noteworthy. Owing to the lack of longitudinal coverage for the data types used above 0.5 mb and the somewhat larger differences between data types, the (dayside) model above 0.5 mb should be considered only provisional. Nightside mesospheric ozone concentrations are generally much higher than dayside values [51]. Shown in Figure 8 are the ozone distributions given in Table 4 for the equinox and solstice months.

Comparison of entries in Table 4 shows the nature of the annual and semiannual variations of ozone in the middle atmosphere. The amplitudes of annual variations are generally highest at high latitudes, and amplitudes are especially high near 15-5 mb, 2.0-0.5 mb, and above 0.03 mb. Amplitudes are high at low and mid latitudes near 0.1 mb. There is a sharp change of phase near 4 mb with maximum ozone values in summer below this altitude and maximum values in winter in the upper stratosphere. Figure 9 shows the ozone annual variation in percent of annual mean at 50°S and 50°N over the entire range of altitudes. Notice the asymmetry between the two hemispheres. A substantial semiannual variation occurs near the equator from 15 - 3 mb, but the largest semiannual variation occurs at mid and high latitudes above 0.03 mb [63]. and at high latitudes near 1 mb. Figure 10 shows the ozone semiannual variation in percent of the annual mean at 30°S and 30°N for the entire range of altitudes. The annual and semiannual components were solved for simultaneously . Note the symmetry in the low

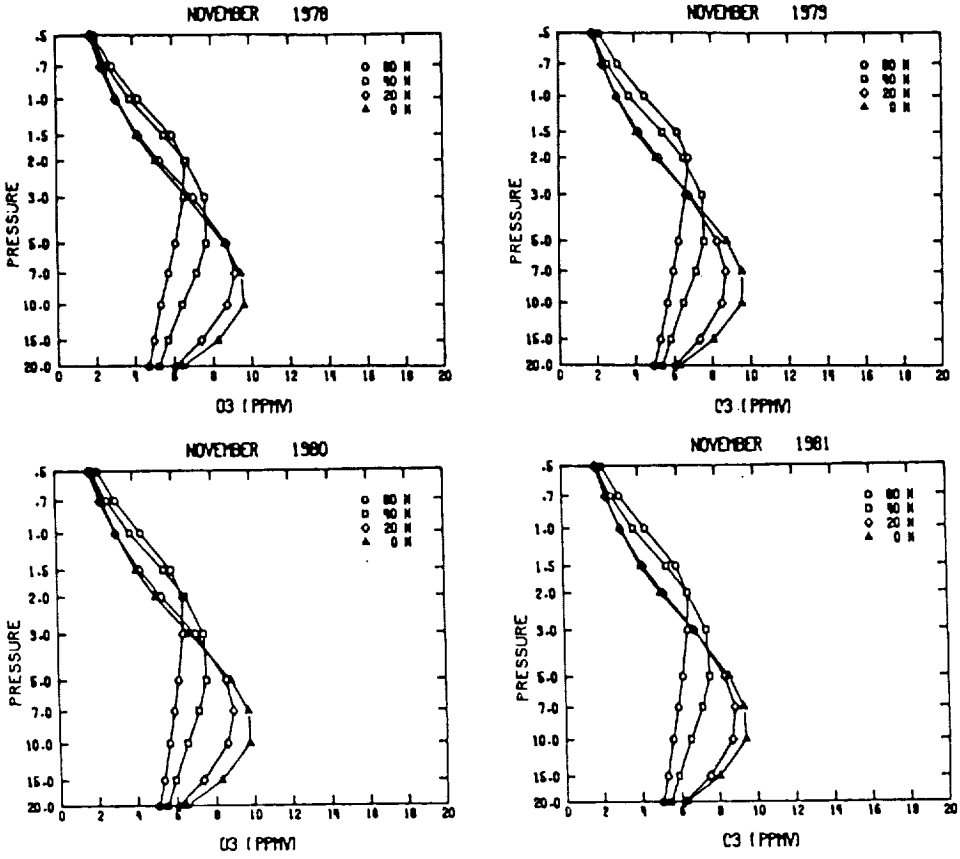

Figure 4. Similarity of ozone vertical structure in November from year to year (Nimbus 7 SBUV data).

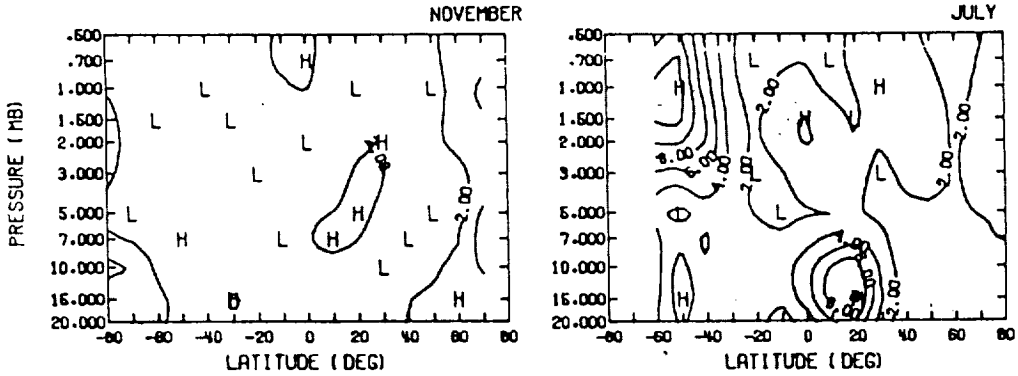

Figure 5. Interannual variability of ozone vertical structure expressed as yearly standard deviation (percent) from 4-year zonal means for the months of November and July (Nimbus 7 SBUV data).

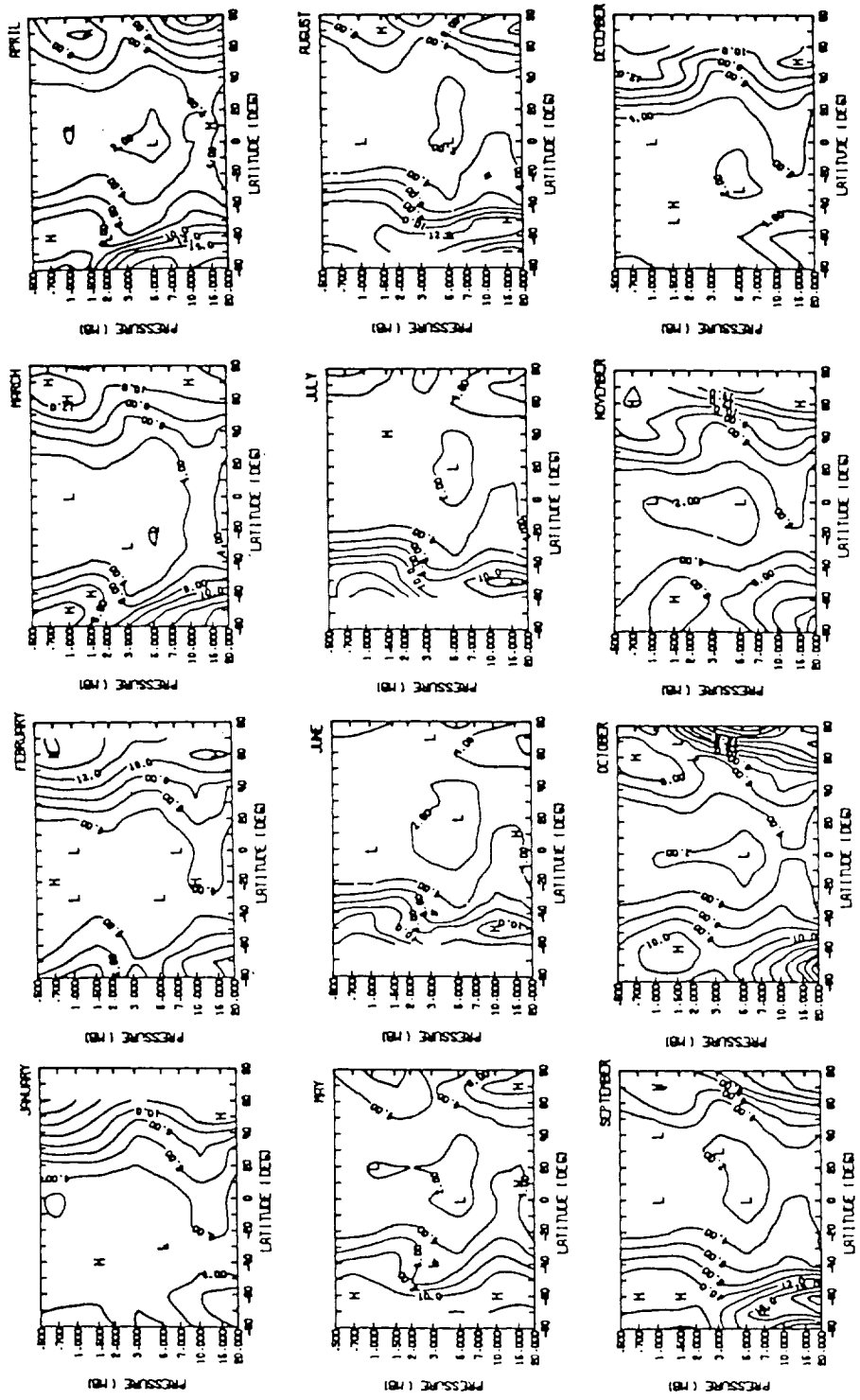

Figure 6. Average monthly standard deviation (percent) from zonal mean ozone (Nimbus 7 SBUV data)

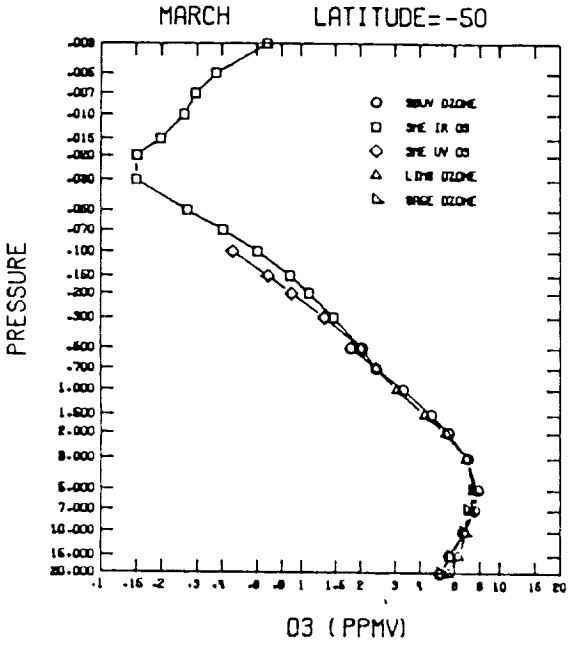

Figure 7. Comparison of measurements from five satellite experiments of zonal mean ozone volume mixing ratios for March, 50°S.

TABLE 4. Zonal Mean Ozone Mixing Ratios (ppmv) as Function of Pressure
(standard typeface: only 1 data set used in average,
italics: standard deviation of data types > 10% ,
underlined: standard deviation ≤ 10%)

average ozone (ppmv) for January

p (mb)	latitude -80°	-70°	-60°	-50°	-40°	-30°	-20°	-10°	0°	10°	20°	30°	40°	50°	60°	70°	80°
.003	.55	.72	.80	.78	.70	.63	.57	.53	.53	.52	.52	.66	.81	.84	.83	-	-
.005	.26	.35	.45	.51	.49	.46	.43	.42	.41	.38	.35	.42	.50	.52	.50	-	-
.007	.18	.21	.28	.35	.36	.36	.37	.38	.39	.37	.32	.30	.31	.30	.27	-	-
.010	.15	.15	.18	.22	.24	.26	.29	.31	.33	.34	.32	.28	.23	.19	.14	-	-
.015	.16	.15	.15	.16	.15	.16	.19	.20	.21	.23	.27	.28	.26	.23	.17	-	-
.020	.17	.16	.15	.14	.14	.13	.14	.16	.16	.17	.21	.25	.27	.28	.24	-	-
.030	.21	.19	.18	.17	.15	.14	.15	.15	.15	.16	.17	.19	.24	.32	.37	-	-
.050	.31	.28	.26	.25	.24	.22	.22	.22	.23	.23	.24	.27	.30	.37	.47	-	-
.070	.41	.38	.37	.36	.34	.32	.31	.32	.32	.32	.34	.41	.46	.49	.53	-	-
.100	.54	.53	.52	.49	.48	.48	.49	.49	.47	.46	.49	.53	.69	.69	.67	-	-
.150	.76	.74	.73	.73	.74	.76	.74	.71	.68	.68	.69	.75	.79	1.01	.93	-	-
.200	.89	.90	.92	.92	.96	.98	.96	.92	.89	.89	.92	.99	1.04	1.28	1.19	-	-
.300	1.13	1.17	1.21	1.25	1.32	1.37	1.35	1.30	1.27	1.27	1.33	1.42	1.48	1.77	-	-	-
.500	1.41	1.50	1.62	1.75	1.86	1.93	1.91	1.85	1.83	1.84	1.88	1.99	2.16	2.26	2.07	1.91	1.79
.700	1.66	1.80	1.97	2.14	2.28	2.36	2.35	2.30	2.29	2.29	2.31	2.45	2.71	2.80	2.70	2.36	2.22
1.000	2.15	2.28	2.46	2.63	2.82	2.97	3.03	3.03	3.04	3.05	3.10	3.33	3.67	3.75	3.55	3.04	2.89
1.500	2.99	3.07	3.26	3.43	3.67	3.92	4.10	4.19	4.23	4.28	4.42	4.74	5.05	5.04	4.65	3.98	3.75
2.000	3.92	3.97	4.17	4.38	4.66	4.95	5.20	5.35	5.40	5.46	5.60	5.87	6.03	5.88	5.33	4.65	4.34
3.000	5.45	5.48	5.77	6.13	6.48	6.82	7.13	7.34	7.35	7.31	7.27	7.21	7.04	6.65	5.96	5.34	5.06
5.000	5.99	6.26	6.96	7.63	8.20	8.66	9.07	9.36	9.14	8.79	8.33	7.79	7.29	6.67	6.14	5.55	5.39
7.000	5.49	5.94	6.94	7.82	8.54	9.08	9.56	9.96	9.68	9.16	8.35	7.60	6.99	6.34	6.02	5.37	5.27
10.000	4.62	5.14	6.32	7.30	8.10	8.66	9.15	9.71	9.62	9.03	7.96	7.11	6.52	5.98	5.83	5.01	4.91
15.000	3.86	4.36	5.52	6.41	7.08	7.45	7.78	8.15	8.09	7.66	6.92	6.41	6.10	5.78	5.52	4.62	4.45
20.000	3.52	3.96	4.99	5.68	6.10	6.25	6.36	6.42	6.27	6.12	5.91	5.84	5.82	5.67	5.19	4.34	4.14

average ozone (ppmv) for February

p (mb)	latitude -80°	-70°	-60°	-50°	-40°	-30°	-20°	-10°	0°	10°	20°	30°	40°	50°	60°	70°	80°
.003	.43	.56	.64	.64	.60	.57	.60	.69	.73	.70	.65	.63	.66	.73	.75	.77	-
.005	.21	.29	.37	.39	.38	.39	.44	.47	.47	.47	.44	.42	.42	.43	.41	.37	-
.007	.14	.18	.24	.28	.30	.35	.41	.42	.42	.42	.39	.33	.30	.27	.23	.18	-
.010	.13	.14	.16	.20	.23	.29	.35	.35	.36	.38	.38	.33	.27	.22	.17	.12	-
.015	.14	.13	.14	.14	.16	.18	.21	.22	.24	26	30	.32	.21	.28	.24	.20	-
.020	.15	.15	.14	.14	.13	.14	.15	.16	.17	.18	.21	.26	.30	.31	.30	.27	-
.030	.20	.19	.18	.17	.15	.15	.15	.16	.16	.16	.17	.19	.23	.29	.35	.38	-
.050	.30	.29	.28	.26	.24	.24	.23	.23	.23	.24	.25	.27	.29	.32	.39	.46	-
.070	.40	.40	.40	.38	.36	.34	.33	.32	.32	.32	.36	.40	.43	.45	.48	.52	-
.100	.56	.54	.53	.52	.50	.50	.50	.50	.50	.48	.46	.48	.52	.53	.64	.63	.64	-
.150	.76	.75	.75	.77	.78	.77	.75	.73	.71	.70	.70	.71	.72	.75	.74	.85	-
.200	.92	.92	.94	.97	1.01	1.01	.98	.94	.92	.91	.93	.94	.95	.95	.93	1.04	-
.300	1.20	1.22	1.26	1.31	1.39	1.41	1.36	1.30	1.29	1.30	1.34	1.37	1.37	1.35	1.32	1.50	-
.500	1.59	1.63	1.73	1.83	1.93	1.96	1.91	1.83	1.82	1.85	1.88	1.94	2.02	2.14	2.22	2.25	2.16
.700	2.00	2.01	2.12	2.25	2.37	2.42	2.34	2.24	2.22	2.25	2.29	2.40	2.60	2.86	2.98	2.95	2.60
1.000	2.73	2.68	2.73	2.86	3.00	3.09	3.03	2.90	2.86	2.91	3.02	3.24	3.58	3.93	4.00	3.80	3.22
1.500	3.81	3.71	3.71	3.81	3.98	4.11	4.10	3.95	3.87	3.98	4.20	4.58	5.10	5.38	5.22	4.79	4.11
2.000	4.65	4.61	4.68	4.80	4.98	5.15	5.17	5.06	4.99	5.09	5.30	5.73	6.24	6.29	5.92	5.41	4.82
3.000	5.60	5.84	6.16	6.42	6.68	6.91	7.03	7.08	7.05	7.04	7.09	7.37	7.45	7.04	6.47	6.07	5.69
5.000	5.52	6.28	7.10	7.58	8.05	8.60	9.02	9.37	9.23	8.99	8.76	8.39	7.73	7.00	6.49	6.42	6.30
7.000	4.84	5.78	6.90	7.56	8.21	9.00	9.60	10.20	10.10	9.68	9.09	8.20	7.32	6.72	6.31	6.46	6.31
10.000	3.98	4.84	6.12	7.02	7.85	8.63	9.33	10.03	10.10	9.59	8.73	7.52	6.68	6.37	6.15	6.42	6.07
15.000	3.39	4.08	5.27	6.07	6.82	7.46	7.95	8.37	8.38	7.97	7.37	6.63	6.15	6.03	6.01	6.06	5.72
20.000	3.22	3.78	4.76	5.34	5.89	6.21	6.40	6.50	6.39	6.22	6.12	5.94	5.82	5.82	5.80	5.54	5.30

TABLE 4 - continued

average ozone (ppmv) for March

p (mb)	latitude -80°	-70°	-60°	-50°	-40°	-30°	-20°	-10°	0°	10°	20°	30°	40°	50°	60°	70°	80°
.003	.37	.58	.66	.68	.74	.82	.81	.74	.69	.71	.76	.77	.68	.58	.57	.60	.61
.005	.21	.28	.31	.38	.48	.53	.52	.47	.44	.46	.49	.48	.42	.35	.33	.31	.27
.007	.15	.21	.24	.30	.38	.43	.43	.41	.40	.41	.42	.41	.36	.30	.26	.22	.16
.010	.12	.19	.22	.26	.33	.38	.37	.34	.33	.34	.37	.39	.38	.34	.28	.22	.15
.015	.12	.15	.16	.20	.24	.25	.23	.21	.20	.22	.26	.32	.38	.39	.36	.31	.23
.020	.15	.15	.14	.15	.17	.18	.16	.15	.16	.16	.19	.24	.33	.38	.39	.37	.31
.030	.20	.18	.17	.15	.14	.15	.17	.17	.17	.17	.17	.18	.23	.29	.37	.43	.41
.050	.30	.30	.29	.27	.25	.25	.25	.24	.23	.24	.25	.27	.28	.30	.37	.46	.48
.070	.40	.40	.41	.40	.38	.35	.34	.33	.31	.32	.36	.39	.41	.43	.46	.50	.52
.100	.55	.54	*.53*	*.53*	*.51*	*.50*	.51	.50	.48	.47	*.48*	*.49*	*.52*	*.54*	*.55*	*.58*	.61
.150	.79	.77	*.77*	*.78*	*.77*	*.75*	.75	.74	.73	.72	*.71*	*.72*	*.74*	*.74*	*.73*	*.74*	*.75*
.200	.99	.97	*.98*	*1.00*	*.99*	*.97*	.96	.96	.95	.94	*.93*	*.92*	*.95*	*.94*	*.91*	*.91*	*.93*
.300	1.33	1.35	1.36	1.38	1.39	1.37	1.34	1.33	1.34	1.33	1.32	*1.32*	*1.33*	*1.32*	*1.28*	*1.29*	1.35
.500	1.97	1.96	1.92	1.93	1.95	1.93	1.89	1.88	1.89	1.90	1.92	1.94	1.94	1.96	2.02	2.12	2.27
.700	2.82	2.58	2.42	2.40	2.40	2.37	2.32	2.30	2.30	2.31	2.35	2.41	2.42	2.50	2.69	2.89	3.00
1.000	3.86	3.62	3.30	3.20	3.17	3.11	2.99	2.90	2.88	2.92	3.03	3.17	3.27	3.45	3.75	3.96	3.93
1.500	5.01	5.04	4.66	4.46	4.36	4.28	4.06	3.83	3.77	3.86	4.10	4.39	4.67	5.02	5.33	5.33	5.00
2.000	5.41	5.80	5.69	5.53	5.45	5.37	5.12	4.80	4.71	4.85	5.15	5.51	5.92	6.29	6.42	6.18	5.74
3.000	5.39	6.26	6.76	6.93	7.00	7.06	6.93	6.60	6.48	6.63	6.91	7.21	7.61	7.73	7.41	6.88	6.49
5.000	5.08	6.05	7.00	7.58	8.03	8.43	8.77	8.95	8.91	8.90	8.84	8.65	8.48	7.99	7.31	6.65	6.50
7.000	4.65	5.40	6.51	7.32	8.00	8.68	9.34	9.94	10.05	9.80	9.31	8.71	8.13	7.45	6.78	6.28	6.30
10.000	4.09	4.52	5.64	6.67	7.55	8.45	9.36	10.28	10.59	10.12	9.27	8.26	7.38	6.72	6.24	6.03	6.18
15.000	3.73	3.98	4.87	5.81	6.55	7.26	7.93	8.54	8.70	8.37	7.83	7.14	6.48	6.08	5.86	5.86	5.95
20.000	3.61	3.85	4.49	5.19	5.70	6.10	6.42	6.66	6.67	6.57	6.47	6.23	5.91	5.73	5.65	5.68	5.58

average ozone (ppmv) for April

p (mb)	latitude -80°	-70°	-60°	-50°	-40°	-30°	-20°	-10°	0°	10°	20°	30°	40°	50°	60°	70°	80°
.003	-	-	.77	.83	.92	.93	.84	.77	.76	.79	.93	1.01	.83	.59	.52	.56	.63
.005	-	-	.35	.43	.54	.57	.50	.44	.43	.48	.62	.72	.61	.43	.36	.38	.42
.007	-	-	.24	.32	.41	.44	.41	.39	.39	.41	.49	.56	.51	.41	.34	.32	.30
.010	-	-	.25	.30	.35	.35	.34	.36	.36	.36	.39	.46	.48	.45	.41	.35	.26
.015	-	-	.28	.27	.26	.22	.20	.22	.23	.22	.24	.33	.41	.44	.43	.39	.29
.020	-	-	.28	.22	.19	.16	.15	.15	.16	.16	.17	.23	.31	.35	.37	.37	.31
.030	-	-	.26	.18	.16	.16	.17	.16	.17	.17	.17	.19	.21	.23	.26	.30	.33
.050	-	-	.32	.28	.27	.26	.26	.25	.25	.26	.27	.27	.28	.29	.31	.35	.39
.070	-	-	.42	.41	.40	.38	.37	.35	.34	.34	.37	.38	.39	.41	.43	.46	.49
.100	-	-	.56	*.57*	*.55*	.54	.54	.53	.50	.49	*.50*	*.49*	*.49*	*.50*	*.53*	*.55*	*.56*
.150	-	-	.80	*.81*	*.79*	*.79*	.80	.78	.76	.75	*.75*	*.74*	*.73*	*.73*	*.73*	*.73*	*.73*
.200	-	-	1.06	*1.05*	*1.02*	1.01	1.01	1.00	.98	.97	*.96*	*.95*	*.95*	*.93*	*.91*	*.90*	*.89*
.300	-	-	1.54	1.50	1.43	1.40	1.39	1.38	1.36	1.35	1.35	1.33	1.32	1.29	1.26	*1.24*	1.24
.500	2.50	2.38	2.27	2.17	2.04	1.96	1.93	1.94	1.94	1.94	1.94	1.94	1.89	1.84	1.83	1.86	1.90
.700	3.50	3.34	2.96	2.77	2.56	2.42	2.36	2.37	2.37	2.37	2.40	2.41	2.33	2.26	2.28	2.37	2.48
1.000	4.64	4.64	4.19	3.87	3.52	3.25	3.07	2.99	2.98	3.00	3.06	3.11	3.03	2.96	3.03	3.18	3.35
1.500	5.59	6.06	5.84	5.48	5.01	4.57	4.16	3.94	3.89	3.94	4.08	4.21	4.18	4.16	4.31	4.48	4.57
2.000	5.65	6.39	6.65	6.51	6.14	5.71	5.23	4.90	4.83	4.93	5.13	5.31	5.35	5.39	5.55	5.63	5.49
3.000	5.18	5.98	6.93	7.34	7.40	7.30	6.99	6.58	6.49	6.66	6.95	7.12	7.25	7.31	7.30	7.02	6.42
5.000	4.94	5.54	6.48	7.22	7.84	8.44	8.82	8.63	8.42	8.65	8.77	8.66	8.69	8.50	7.82	6.99	6.14
7.000	4.66	5.09	5.90	6.73	7.53	8.46	9.27	9.63	9.62	9.55	9.27	8.91	8.61	8.10	7.29	6.37	5.68
10.000	4.18	4.50	5.23	6.08	6.95	8.07	9.21	10.16	10.45	10.00	9.25	8.64	7.95	7.22	6.47	5.78	5.40
15.000	3.73	4.15	4.82	5.45	6.12	7.02	7.89	8.62	8.80	8.48	7.95	7.49	6.86	6.29	5.77	5.40	5.30
20.000	3.46	4.03	4.63	5.02	5.45	6.01	6.46	*6.79*	6.85	6.79	6.66	6.49	6.11	5.74	5.41	5.24	5.26

TABLE 4 - continued

average ozone (ppmv) for May

p (mb)	latitude -80°	-70°	-60°	-50°	-40°	-30°	-20°	-10°	0°	10°	20°	30°	40°	50°	60°	70°	80°
.003	-	-	-	.99	1.02	.92	.75	.65	.63	.67	.75	.85	.84	.74	.64	.56	.48
.005	-	-	-	.51	.57	.53	.46	.42	.41	.43	.52	.62	.63	.56	.49	.41	.33
.007	-	-	-	.33	.39	.39	.40	.42	.43	.43	.45	.50	.51	.46	.41	.33	.25
.010	-	-	-	.27	.30	.32	.37	.41	.42	.40	.39	.39	.38	.36	.33	.28	.21
.015	-	-	-	.24	.22	.23	.24	.27	.26	.25	.24	.25	.25	.25	.24	.21	.19
.020	-	-	-	.22	.18	.17	.17	.18	.17	.17	.17	.19	.19	.20	.19	.19	.18
.030	-	-	-	.22	.17	.16	.16	.16	.16	.17	.18	.19	.20	.20	.19	.19	.21
.050	-	-	-	.30	.28	.28	.27	.26	.27	.27	.27	.27	.28	.29	.28	.29	.31
.070	-	-	-	.41	.41	.40	.39	.38	.38	.38	.38	.37	.38	.39	.39	.40	.43
.100	-	-	-	.59	.57	.56	.57	.55	.53	.53	.53	.51	.49	.51	.53	.54	.54
.150	-	-	-	.85	.81	.81	.83	.81	.79	.79	.80	.78	.76	.76	.76	.75	.73
.200	-	-	-	1.12	1.05	1.03	1.05	1.03	1.01	1.02	1.02	1.00	.97	.95	.94	.91	.88
.300	-	-	-	1.67	1.52	1.43	1.43	1.41	1.39	1.40	1.39	1.36	1.33	1.29	1.25	1.20	1.16
.500	-	2.64	2.47	2.46	2.24	2.02	1.96	1.97	1.97	1.97	1.96	1.95	1.89	1.82	1.74	1.66	1.59
.700	-	3.66	3.50	3.35	2.89	2.54	2.43	2.42	2.42	2.42	2.42	2.40	2.33	2.23	2.12	2.04	1.97
1.000	-	4.97	4.91	4.79	4.09	3.49	3.18	3.09	3.07	3.06	3.07	3.03	2.92	2.79	2.67	2.59	2.59
1.500	-	6.30	6.39	6.61	5.85	4.98	4.33	4.10	4.05	4.04	4.06	4.02	3.88	3.74	3.62	3.54	3.64
2.000	-	6.52	6.77	7.38	6.94	6.15	5.41	5.10	5.03	5.05	5.11	5.08	4.94	4.81	4.72	4.62	4.75
3.000	-	6.07	6.39	7.46	7.76	7.54	7.06	6.74	6.68	6.77	6.93	6.92	6.82	6.73	6.60	6.31	6.30
5.000	-	5.79	5.73	6.78	7.57	8.15	8.39	8.31	8.27	8.57	8.71	8.64	8.50	8.20	7.59	6.75	6.19
7.000	-	5.46	5.31	6.21	7.12	8.03	8.77	9.12	9.18	9.27	9.20	8.98	8.70	8.16	7.35	6.26	5.47
10.000	-	4.93	4.93	5.69	6.57	7.61	8.74	9.64	9.95	9.44	8.94	8.57	8.09	7.57	6.75	5.63	4.84
15.000	-	4.43	4.74	5.33	5.95	6.72	7.60	8.28	8.55	8.39	7.91	7.59	7.10	6.57	5.92	5.06	4.43
20.000	-	4.13	4.61	5.09	5.47	5.92	6.36	6.63	6.77	6.86	6.71	6.59	6.30	5.88	5.38	4.76	4.32

average ozone (ppmv) for June

p (mb)	latitude -80°	-70°	-60°	-50°	-40°	-30°	-20°	-10°	0°	10°	20°	30°	40°	50°	60°	70°	80°
.003	-	-	-	-	.80	.78	.59	.47	.47	.54	.62	.73	.87	.94	.88	.72	.57
.005	-	-	-	-	.50	.50	.38	.34	.38	.41	.43	.51	.63	.63	.50	.39	.32
.007	-	-	-	-	.35	.37	.34	.35	.38	.39	.36	.39	.46	.42	.30	.25	.22
.010	-	-	-	-	.27	.30	.30	.31	.31	.30	.28	.27	.29	.26	.19	.18	.17
.015	-	-	-	-	.21	.22	.21	.20	.19	.19	.18	.17	.18	.18	.17	.16	.16
.020	-	-	-	-	.18	.17	.16	.15	.14	.15	.15	.15	.16	.17	.17	.17	.17
.030	-	-	-	-	.18	.17	.17	.16	.16	.17	.17	.17	.19	.20	.20	.20	.21
.050	-	-	-	-	.31	.30	.28	.26	.26	.26	.26	.27	.27	.28	.27	.28	.30
.070	-	-	-	-	.45	.45	.41	.38	.37	.37	.38	.39	.38	.38	.38	.39	.40
.100	-	-	-	-	.58	.57	.56	.57	.57	.58	.58	.55	.52	.53	.57	.55	.56
.150	-	-	-	-	.82	.82	.83	.83	.83	.85	.88	.84	.80	.80	.80	.80	.78
.200	-	-	-	-	1.06	1.04	1.05	1.06	1.06	1.08	1.11	1.08	1.03	1.01	.99	.96	.93
.300	-	-	-	-	1.53	1.44	1.44	1.47	1.47	1.48	1.49	1.45	1.39	1.35	1.30	1.24	1.18
.500	-	-	2.46	2.42	2.26	2.02	1.98	2.00	2.00	1.99	1.98	1.95	1.87	1.78	1.67	1.56	1.46
.700	-	-	3.56	3.54	2.96	2.56	2.46	2.46	2.46	2.45	2.44	2.41	2.30	2.16	1.99	1.83	1.71
1.000	-	-	5.01	5.16	4.29	3.56	3.30	3.22	3.19	3.16	3.13	3.05	2.88	2.68	2.47	2.28	2.16
1.500	-	-	6.50	7.11	6.19	5.06	4.51	4.30	4.24	4.19	4.15	3.98	3.73	3.49	3.24	3.05	2.97
2.000	-	-	6.77	7.74	7.27	6.16	5.55	5.30	5.23	5.21	5.20	5.01	4.73	4.49	4.24	4.05	4.03
3.000	-	-	6.20	7.36	7.96	7.43	7.05	6.91	6.88	6.94	7.02	6.84	6.59	6.38	6.07	5.83	5.87
5.000	-	-	5.64	6.37	7.53	7.93	8.27	8.43	8.55	8.72	8.78	8.63	8.36	7.84	7.14	6.38	6.08
7.000	-	-	5.32	5.74	7.04	7.82	8.47	8.94	9.19	9.28	9.17	8.99	8.63	7.91	7.01	5.91	5.37
10.000	-	-	5.02	5.29	6.53	7.45	8.11	8.88	9.23	9.11	8.67	8.45	7.95	7.42	6.52	5.29	4.71
15.000	-	-	4.82	5.19	5.93	6.48	7.04	7.67	7.97	7.84	7.38	7.22	6.83	6.36	5.66	4.68	4.18
20.000	-	-	4.68	5.25	5.57	5.76	5.97	6.20	6.36	6.40	6.20	6.15	6.00	5.64	5.09	4.33	3.94

TABLE 4 - continued

average ozone (ppmv) for July

p (mb)	latitude -80°	-70°	-60°	-50°	-40°	-30°	-20°	-10°	0°	10°	20°	30°	40°	50°	60°	70°	80°
.003	-	-	-	.58	.66	.63	.53	.48	.47	.51	.60	.66	.71	.85	.93	.80	.58
.005	-	-	-	.34	.41	.41	.37	.34	.37	.40	.42	.44	.49	.55	.52	.40	.31
.007	-	-	-	.24	.29	.32	.32	.33	.35	.36	.35	.34	.36	.37	.30	.23	.21
.010	-	-	-	.20	.24	.27	.29	.28	.28	.27	.25	.24	.24	.23	.19	.16	.17
.015	-	-	-	.21	.20	.20	.19	.17	.16	.16	.16	.16	.16	.16	.16	.16	.16
.020	-	-	-	.21	.17	.16	.15	.14	.14	.14	.14	.14	.15	.16	.17	.17	.17
.030	-	-	-	.22	.17	.16	.16	.16	.17	.17	.16	.16	.18	.20	.20	.20	.21
.050	-	-	-	.31	.31	.29	.26	.25	.25	.25	.24	.24	.27	.28	.28	.28	.31
.070	-	-	-	.43	.46	.45	.39	.36	.36	.36	.35	.36	.39	.39	.38	.39	.42
.100	-	-	-	.61	.60	.60	.57	.55	.55	.56	.58	.57	.55	.55	.57	.55	.56
.150	-	-	-	.89	.85	.86	.83	.82	.81	.84	.87	.88	.85	.82	.81	.81	.79
.200	-	-	-	-	1.09	1.08	1.06	1.04	1.04	1.06	1.11	1.12	1.09	1.04	1.00	.98	.95
.300	-	-	-	-	1.53	1.49	1.45	1.44	1.44	1.46	1.50	1.51	1.46	1.39	1.32	1.26	1.19
.500	-	-	2.05	2.14	2.22	2.07	2.00	1.99	1.99	1.99	2.00	2.00	1.93	1.81	1.68	1.55	1.44
.700	-	-	2.85	3.03	2.86	2.60	2.48	2.44	2.44	2.44	2.48	2.49	2.39	2.20	2.00	1.82	1.66
1.000	-	-	4.06	4.40	4.05	3.58	3.34	3.23	3.19	3.18	3.22	3.19	3.01	2.76	2.52	2.30	2.14
1.500	-	-	5.62	6.28	5.76	5.04	4.61	4.39	4.31	4.29	4.31	4.18	3.91	3.61	3.32	3.08	2.97
2.000	-	-	6.24	7.17	6.86	6.13	5.69	5.47	5.38	5.37	5.38	5.21	4.90	4.59	4.28	4.03	3.97
3.000	-	-	6.22	7.39	7.79	7.43	7.23	7.16	7.12	7.15	7.18	6.98	6.68	6.37	6.00	5.66	5.64
5.000	-	-	5.79	6.63	7.47	8.04	8.35	8.62	8.76	8.87	8.85	8.67	8.34	7.88	7.11	6.21	5.84
7.000	-	-	5.39	5.91	6.98	7.81	8.42	8.98	9.26	9.34	9.17	8.99	8.59	7.97	6.98	5.79	5.18
10.000	-	-	4.98	5.29	6.41	7.19	7.95	8.77	9.11	9.08	8.65	8.45	7.95	7.23	6.28	5.14	4.50
15.000	-	-	4.74	5.08	5.83	6.35	6.90	7.53	7.81	7.79	7.35	7.19	6.80	6.22	5.45	4.51	3.95
20.000	-	-	4.65	5.14	5.52	5.73	5.92	6.14	6.31	6.41	6.17	6.08	5.91	5.55	4.94	4.14	3.68

average ozone (ppmv) for August

p (mb)	latitude -80°	-70°	-60°	-50°	-40°	-30°	-20°	-10°	0°	10°	20°	30°	40°	50°	60°	70°	80°
.003	-	-	.62	.66	.69	.67	.61	.60	.61	.62	.65	.68	.67	.65	.67	.60	.44
.005	-	-	.37	.40	.43	.43	.41	.40	.40	.41	.44	.46	.43	.41	.41	.35	.24
.007	-	-	.26	.29	.32	.34	.35	.36	.36	.36	.38	.36	.32	.29	.28	.22	.18
.010	-	-	.23	.25	.28	.30	.32	.31	.30	.30	.31	.27	.23	.20	.18	.15	.15
.015	-	-	.25	.23	.24	.24	.22	.19	.18	.18	.19	.17	.16	.15	.14	.14	.13
.020	-	-	.24	.20	.19	.18	.16	.14	.14	.14	.15	.14	.14	.14	.14	.15	.15
.030	-	-	.24	.19	.17	.17	.17	.16	.16	16	.17	16	.16	.17	.18	.18	.19
.050	-	-	.33	.32	.31	.30	.26	.25	.25	.25	.25	.24	.25	.26	.27	.27	.29
.070	-	-	.44	.47	.48	.44	.38	.36	.36	.35	.34	.35	.36	.38	.38	.38	.39
.100	-	-	.60	.61	.62	.59	.54	.52	.53	.53	.52	.52	.53	.53	.52	.53	.54
.150	-	-	.84	.85	.88	.87	.82	.79	.79	.79	.79	.80	.81	.80	.77	.75	.73
.200	-	-	1.01	1.09	1.12	1.11	1.05	1.02	1.01	1.01	1.03	1.04	1.05	1.02	.96	.92	.90
.300	-	-	1.18	1.56	1.58	1.54	1.47	1.43	1.40	1.39	1.43	1.46	1.45	1.38	1.30	1.23	1.18
.500	-	1.90	1.90	2.19	2.22	2.11	2.00	1.97	1.95	1.94	1.97	2.02	1.98	1.85	1.74	1.64	1.56
.700	-	2.50	2.55	2.76	2.79	2.60	2.45	2.41	2.39	2.40	2.45	2.50	2.44	2.26	2.11	2.01	1.92
1.000	-	3.35	3.54	3.87	3.87	3.55	3.29	3.17	3.13	3.14	3.22	3.28	3.18	2.95	2.77	2.65	2.55
1.500	-	4.41	4.97	5.51	5.43	4.97	4.55	4.31	4.24	4.27	4.39	4.42	4.25	3.98	3.78	3.61	3.48
2.000	-	4.92	5.79	6.60	6.55	6.09	5.68	5.42	5.33	5.37	5.51	5.49	5.27	4.99	4.77	4.53	4.32
3.000	-	5.21	6.35	7.57	7.78	7.54	7.37	7.23	7.16	7.20	7.32	7.23	6.94	6.64	6.34	5.86	5.43
5.000	-	5.34	6.14	7.42	8.06	8.32	8.65	9.04	9.07	9.15	9.07	8.69	8.31	7.81	7.06	6.18	5.30
7.000	-	5.29	5.59	6.73	7.56	8.10	8.72	9.46	9.54	9.60	9.39	8.93	8.45	7.73	6.78	5.69	4.68
10.000	-	5.11	4.94	5.88	6.74	7.36	8.14	9.43	9.51	9.53	9.16	8.60	8.01	7.13	6.11	4.94	4.06
15.000	-	4.63	4.59	5.33	5.99	6.43	6.98	7.74	7.84	7.89	7.58	7.19	6.78	6.06	5.21	4.28	3.62
20.000	-	4.14	4.53	5.16	5.59	5.78	5.96	6.22	6.31	6.43	6.26	6.05	5.84	5.35	4.66	3.95	3.45

TABLE 4 - continued

average ozone (ppmv) for September

p (mb)	latitude -80°	-70°	-60°	-50°	-40°	-30°	-20°	-10°	0°	10°	20°	30°	40°	50°	60°	70°	80°
.003	.42	.58	.59	.64	.74	.79	.77	.77	.77	.75	.76	.76	.69	.61	.60	.56	.46
.005	.27	.33	.36	.39	.46	.52	.51	.48	.48	.48	.49	.53	.47	.37	.31	.28	.21
.007	.24	.26	.29	.33	.38	.43	.43	.40	.38	.38	.40	.42	.38	.29	.24	.21	.16
.010	.24	.28	.31	.35	.37	.37	.35	.32	.30	.29	.32	.34	.31	.25	.21	.19	.16
.015	.27	.32	.31	.32	.30	.27	.23	.21	.20	.19	.21	.22	.22	.19	.17	.16	.17
.020	.28	.30	.27	.25	.23	.19	.17	.16	.16	.15	.16	.17	.17	.16	.15	.15	.18
.030	.28	.28	.22	.19	.17	.16	.17	.17	.16	.16	.16	.15	.15	.16	.16	.17	.21
.050	.33	.33	.31	.31	.29	.28	.26	.24	.23	.24	.24	.23	.23	.26	.26	.27	.29
.070	.41	.43	.45	.45	.45	.42	.37	.34	.33	.34	.34	.34	.35	.38	.39	.38	.38
.100	.52	.57	*.58*	*.59*	*.58*	*.54*	*.50*	.49	.50	.49	.47	*.46*	*.48*	*.49*	*.48*	*.49*	.50
.150	.70	.80	*.80*	*.83*	*.84*	*.80*	*.77*	*.76*	.76	.74	*.72*	*.70*	*.72*	*.73*	*.70*	*.67*	*.67*
.200	-	.99	*1.01*	*1.05*	*1.06*	*1.03*	*1.00*	*.99*	.98	.97	.96	*.96*	*.97*	*.97*	*.94*	*.89*	*.86*
.300	-	1.35	1.40	*1.47*	*1.48*	*1.43*	1.41	1.41	1.38	1.36	1.38	1.40	1.40	1.40	1.36	1.28	1.25
.500	1.78	1.88	1.98	2.10	2.10	2.02	1.96	1.95	1.93	1.92	1.94	1.96	1.95	*1.92*	1.89	1.87	1.93
.700	2.38	2.34	2.48	2.67	2.64	2.47	2.38	2.36	2.35	2.36	2.38	2.40	2.38	2.36	2.37	2.41	2.48
1.000	3.19	3.18	3.38	3.66	3.62	3.36	3.16	3.06	3.04	3.07	3.15	3.23	3.23	3.23	3.30	3.37	3.34
1.500	4.26	4.38	4.72	5.10	5.07	4.71	4.35	4.13	4.08	4.15	4.34	4.48	4.51	4.54	4.66	4.69	4.33
2.000	4.86	5.16	5.72	6.23	6.26	5.90	5.50	5.21	5.13	5.21	5.45	5.60	5.59	5.60	5.67	5.52	4.87
3.000	5.34	5.89	6.86	7.58	7.80	7.63	7.36	7.08	6.97	7.04	7.25	7.31	7.17	7.03	6.82	6.23	5.22
5.000	5.36	5.94	6.86	7.76	8.45	8.81	9.04	8.99	8.96	8.98	8.98	8.80	8.41	7.89	7.17	6.07	4.97
7.000	5.28	5.62	6.45	7.31	8.06	8.64	9.20	9.54	9.61	9.57	9.34	8.98	8.43	7.63	6.67	5.47	4.58
10.000	5.15	5.18	5.81	6.61	7.34	8.02	8.80	9.25	9.39	9.31	8.84	8.35	7.71	6.74	5.75	4.71	4.14
15.000	4.38	4.51	5.12	5.85	6.38	6.83	7.31	7.81	7.94	7.91	7.45	7.04	6.58	5.76	4.94	4.13	3.75
20.000	3.50	3.97	4.75	5.42	5.79	6.00	6.14	6.30	6.38	6.42	6.15	5.92	5.71	5.18	4.54	3.89	3.53

average ozone (ppmv) for October

p (mb)	latitude -80°	-70°	-60°	-50°	-40°	-30°	-20°	-10°	0°	10°	20°	30°	40°	50°	60°	70°	80°
.003	.57	.56	.54	.61	.80	.93	.87	.80	.84	.81	.76	.84	.87	.75	.66	.65	.63
.005	.38	.41	.41	.45	.58	.66	.60	.53	.55	.54	.51	.55	.55	.44	.34	.30	.23
.007	.31	.38	.41	.44	.50	.52	.47	.42	.43	.42	.39	.42	.41	.33	.25	.19	.12
.010	.29	.38	.43	.45	.44	.39	.34	.33	.33	.32	.30	.30	.31	.28	.23	.19	.12
.015	.26	.32	.35	.35	.31	.26	.24	.24	.24	.23	.22	.22	.22	.23	.25	.25	.20
.020	.23	.24	.25	.25	.23	.19	.19	.19	.20	.18	.18	.18	.18	.20	.25	.29	.25
.030	.24	.21	.20	.19	.18	.17	.17	.18	.18	.17	.16	.16	.16	.18	.24	.33	.31
.050	.35	.33	.32	.31	.29	.26	.26	.26	.25	.24	.24	.25	.26	.26	.28	.36	.37
.070	.45	.45	.44	.43	.41	.39	.38	.37	.36	.35	.35	.36	.37	.38	.38	.40	.41
.100	.56	*.55*	*.54*	*.53*	*.50*	*.48*	*.48*	*.46*	*.46*	*.45*	.52	.53	.55	.56	.54	.51	-
.150	.78	.75	*.75*	*.76*	*.74*	*.74*	*.73*	*.71*	*.69*	*.69*	.79	*.66*	*.68*	*.70*	*.69*	.72	-
.200	.97	.93	*.94*	*.96*	*.96*	*.97*	*.96*	*.94*	*.92*	*.92*	*.93*	*.92*	*.93*	*.93*	*.91*	.94	-
.300	*1.31*	1.28	1.30	*1.33*	*1.37*	1.39	1.40	1.39	1.37	1.38	1.41	1.40	1.37	*1.36*	1.36	1.37	-
.500	1.76	1.79	1.86	1.92	1.93	*1.94*	1.96	1.97	1.97	1.97	*1.96*	*1.94*	*1.97*	2.07	2.16	2.16	2.09
.700	2.16	2.18	2.33	2.40	2.36	2.31	2.33	2.35	2.37	2.37	2.34	2.32	2.44	2.68	2.84	2.88	2.94
1.000	2.83	2.87	3.10	3.22	3.17	3.07	3.04	3.03	3.04	3.06	3.10	3.18	3.44	3.80	4.05	4.06	3.97
1.500	3.86	3.93	4.26	4.47	4.43	4.27	4.14	4.05	4.03	4.09	4.27	4.53	4.96	5.41	5.66	5.49	4.96
2.000	4.75	4.91	5.34	5.64	5.66	5.47	5.27	5.11	5.03	5.11	5.35	5.67	6.09	6.42	6.49	6.07	5.26
3.000	5.92	6.33	6.93	7.39	7.58	7.47	7.24	6.98	6.82	6.86	7.10	7.32	7.41	7.30	6.92	6.18	5.18
5.000	6.19	6.87	7.70	8.30	8.74	9.04	9.17	9.06	8.90	8.87	8.89	8.66	8.01	7.33	6.75	5.92	5.03
7.000	6.00	6.61	7.39	7.99	8.47	9.06	9.53	9.76	9.75	9.68	9.45	8.83	7.79	6.91	6.24	5.52	4.81
10.000	5.76	6.08	6.66	7.14	7.50	8.18	8.90	9.52	9.77	9.89	9.48	8.53	7.26	6.27	5.54	4.99	4.45
15.000	4.86	5.27	5.96	6.30	6.44	6.92	7.47	7.99	8.05	8.16	7.79	7.09	6.21	5.52	4.97	4.49	3.98
20.000	3.92	4.64	5.60	5.84	5.82	6.03	6.24	6.36	6.33	6.44	6.26	5.90	5.45	5.05	4.70	4.19	3.62

TABLE 4 - continued

average ozone (ppmv) for November

p (mb)	latitude -80°	-70°	-60°	-50°	-40°	-30°	-20°	-10°	0°	10°	20°	30°	40°	50°	60°	70°	80°
.003	.50	.60	.67	.74	.82	.84	.77	.76	.79	.80	.78	.84	.98	.97	.88	-	-
.005	.33	.41	.48	.54	.59	.59	.55	.53	.55	.57	.54	.54	.59	.52	.45	-	-
.007	.24	.30	.37	.42	.45	.45	.43	.43	.45	.47	.43	.41	.41	.32	.24	-	-
.010	.18	.22	.27	.31	.32	.33	.32	.33	.35	.37	.35	.33	.30	.24	.18	-	-
.015	.15	.17	.19	.21	.22	.23	.23	.24	.25	.25	.26	.25	.24	.25	.22	-	-
.020	.17	.17	.18	.18	.18	.18	.18	.20	.20	.20	.20	.20	.20	.24	.26	-	-
.030	.21	.20	.21	.20	.19	.18	.17	.18	.17	.16	.18	.18	.19	.24	.31	-	-
.050	.31	.30	.30	.30	.28	.27	.26	.25	.25	.24	.26	.27	.28	.31	.38	-	-
.070	.43	.42	.41	.41	.40	.39	.38	.37	.36	.37	.38	.39	.41	.43	.44	-	-
.100	.54	*.52*	*.52*	*.49*	*.46*	*.46*	*.46*	*.46*	*.47*	*.48*	.57	.58	.58	.59	.58	-	-
.150	.74	*.73*	*.74*	*.73*	*.72*	*.72*	*.72*	*.70*	*.70*	*.71*	*.73*	*.70*	*.70*	*.71*	.79	-	-
.200	.91	.91	*.91*	*.93*	*.93*	*.94*	*.94*	*.94*	*.93*	*.94*	*.95*	*.96*	*.95*	*.92*	-	-	-
.300	1.20	1.21	*1.24*	*1.28*	1.32	1.35	1.38	1.40	1.38	1.38	1.41	1.45	*1.43*	*1.37*	-	-	-
.500	1.59	1.64	1.72	1.80	1.85	1.90	1.94	1.98	1.98	1.98	*1.96*	*1.99*	*2.08*	*2.19*	2.09	2.09	1.84
.700	1.86	1.93	2.07	2.15	2.21	2.26	2.30	2.36	2.40	2.37	2.31	2.37	2.60	2.87	2.98	2.89	2.42
1.000	2.42	2.47	2.63	2.72	2.78	2.86	2.94	3.02	3.07	3.06	3.04	3.22	3.68	4.14	4.24	*3.98*	3.24
1.500	3.37	3.38	3.55	3.64	3.71	3.82	3.94	4.02	4.06	4.09	4.19	4.60	5.34	5.87	5.76	*5.26*	4.14
2.000	4.38	4.39	4.59	4.71	4.79	4.90	5.01	5.04	5.05	5.09	5.26	5.76	6.46	6.77	6.38	5.78	4.55
3.000	5.96	6.06	6.32	6.61	6.76	6.85	6.90	6.81	6.70	6.72	6.92	7.25	7.43	7.18	6.45	5.88	4.74
5.000	6.39	6.76	7.29	7.93	8.40	8.67	8.82	8.69	8.36	8.35	8.27	8.03	7.46	6.78	6.04	*5.67*	4.29
7.000	6.03	6.45	7.09	7.84	8.49	8.97	9.34	9.41	9.11	9.01	8.70	8.08	7.01	6.26	5.67	*5.39*	3.82
10.000	5.58	5.87	6.46	7.11	7.76	8.41	9.00	9.45	9.43	9.32	8.73	7.83	6.39	5.72	5.31	*5.00*	3.42
15.000	5.05	5.26	5.81	6.22	6.67	7.23	7.74	8.17	8.23	7.93	7.46	6.78	5.78	5.33	4.98	*4.52*	3.18
20.000	4.67	4.90	5.40	5.64	5.89	6.22	6.46	6.61	6.53	6.37	6.18	5.82	5.30	5.05	4.68	*4.11*	3.01

average ozone (ppmv) for December

p (mb)	latitude -80°	-70°	-60°	-50°	-40°	-30°	-20°	-10°	0°	10°	20°	30°	40°	50°	60°	70°	80°
.003	.54	.70	.79	.80	.75	.66	.58	.57	.55	.52	.60	.79	.94	.96	-	-	-
.005	.28	.35	.44	.52	.53	.47	.44	.45	.45	.42	.41	.49	.58	.57	-	-	-
.007	.20	.22	.27	.35	.38	.36	.37	.40	.41	.39	.36	.36	.37	.33	-	-	-
.010	.17	.17	.19	.23	.26	.26	.28	.33	.33	.33	.34	.31	.27	.21	-	-	-
.015	.17	.17	.17	.17	.17	.18	.20	.22	.22	.23	.26	.27	.26	.24	-	-	-
.020	.18	.18	.17	.16	.16	.15	.16	.17	.17	.18	.20	.23	.25	.27	-	-	-
.030	.22	.21	.20	.19	.18	.16	.16	.17	.17	.17	.17	.19	.23	.31	-	-	-
.050	.33	.30	.29	.28	.27	.25	.24	.25	.25	.24	.26	.30	.34	.39	-	-	-
.070	.43	.41	.40	.39	.39	.38	.36	.35	.35	.35	.38	.45	.49	.51	-	-	-
.100	.58	.57	*.52*	*.50*	*.48*	*.49*	*.51*	.50	.49	*.48*	*.49*	.65	.71	.70	-	-	-
.150	.78	.77	.76	*.75*	*.75*	*.77*	*.77*	.74	*.71*	*.72*	*.72*	*.76*	*.80*	.99	-	-	-
.200	.94	.93	.95	*.95*	*.96*	*1.00*	*1.01*	.97	.94	*.94*	*.97*	*1.02*	*1.04*	1.25	-	-	-
.300	1.20	1.22	1.26	1.29	*1.33*	*1.40*	1.42	1.39	1.36	1.37	1.42	*1.48*	*1.50*	1.78	-	-	-
.500	*1.47*	1.55	1.65	1.77	1.86	1.93	1.97	1.98	1.98	1.98	*1.97*	*1.99*	*2.09*	1.94	1.94	1.71	1.66
.700	1.65	1.77	1.94	2.10	2.21	2.29	2.34	2.40	2.44	2.41	2.35	2.38	2.57	2.72	2.68	2.21	2.15
1.000	2.11	2.23	2.42	2.57	2.72	2.86	2.99	3.11	3.18	3.15	3.13	3.25	3.63	3.92	3.74	3.00	2.93
1.500	2.92	3.00	3.19	3.34	3.53	3.77	4.01	4.18	4.27	4.29	4.35	4.66	5.27	5.59	5.10	4.14	4.03
2.000	3.90	3.95	4.13	4.31	4.54	4.81	5.08	5.25	5.32	5.35	5.45	5.80	6.37	6.49	5.79	4.86	4.72
3.000	5.61	5.64	5.83	6.16	6.45	6.71	6.96	7.04	6.99	6.97	7.02	7.18	7.31	6.92	6.10	5.39	5.21
5.000	6.27	6.46	7.03	7.71	8.18	8.57	8.90	8.89	8.55	8.26	7.97	7.74	7.28	6.54	5.94	5.19	4.98
7.000	5.79	6.13	6.99	7.82	8.47	8.97	9.38	9.49	9.08	8.66	8.10	7.62	6.89	6.07	5.69	4.81	4.62
10.000	4.99	5.40	6.40	7.41	8.16	8.75	9.24	9.60	9.36	8.79	7.90	7.25	6.38	5.65	*5.42*	4.37	4.25
15.000	4.35	4.72	5.62	6.41	7.01	7.44	7.77	8.04	7.93	7.53	6.87	6.44	5.85	5.42	*5.10*	4.08	4.00
20.000	4.10	4.38	5.13	5.66	6.05	6.29	6.40	6.44	6.27	6.11	5.85	5.73	5.48	5.30	4.77	3.86	3.77

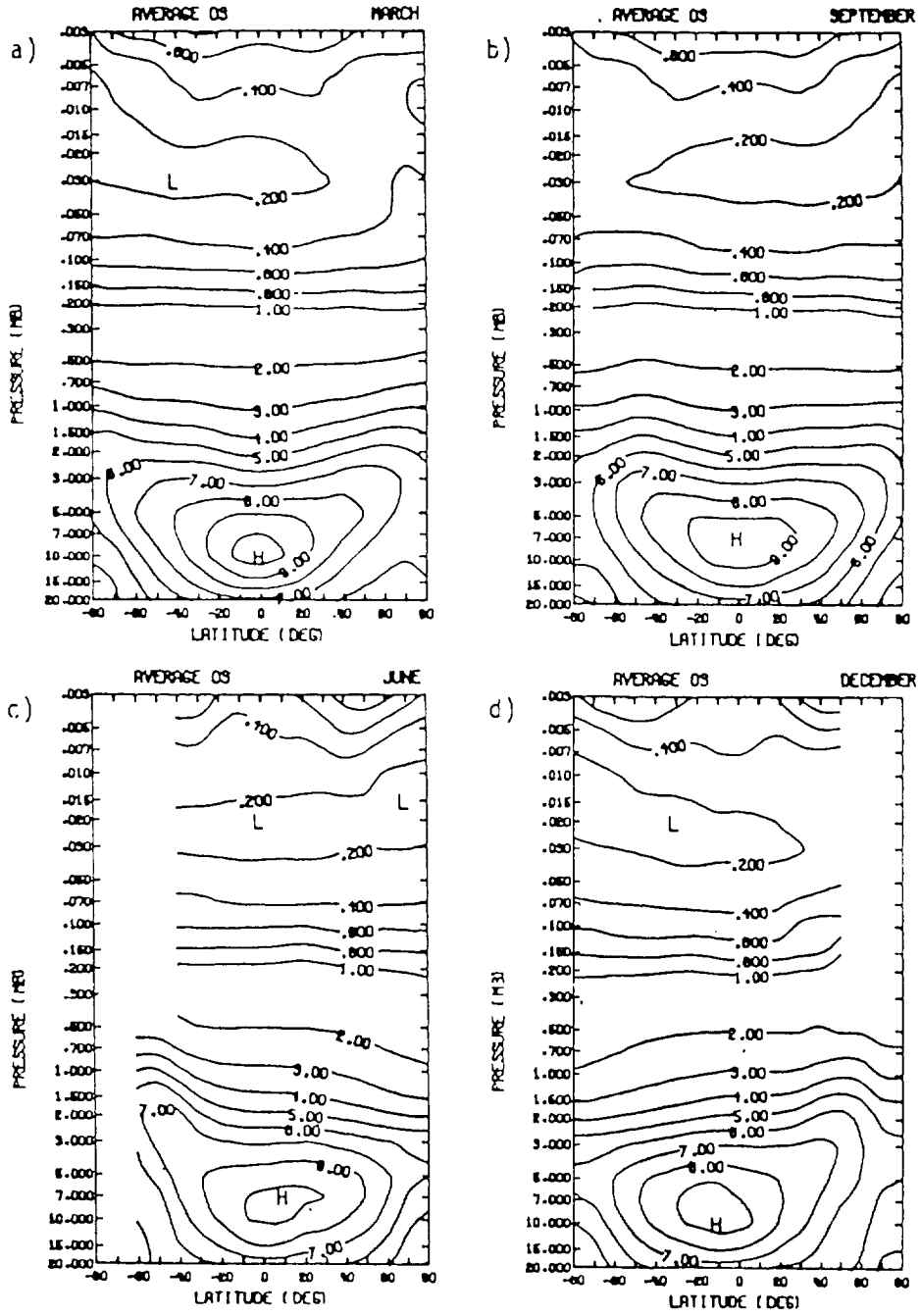

Figure 8. Monthly zonal mean ozone volume mixing ratios (ppmv) as function of latitude (deg) and pressure (mb) for (a) March, (b) September, (c) June, and (d) December.

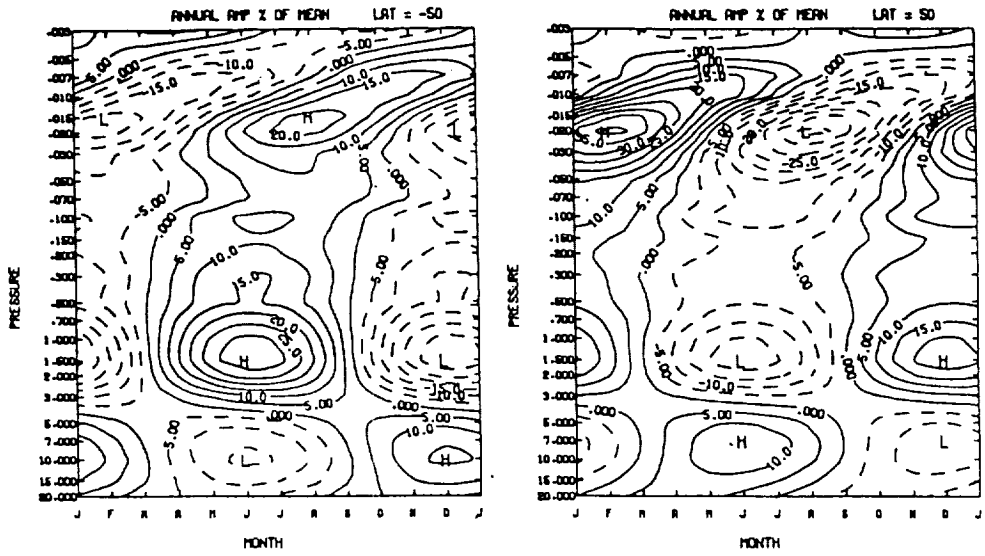

Figure 9. Annual variation of ozone volume mixing ratio in percent of annual mean at 50°S and 50°N latitude.

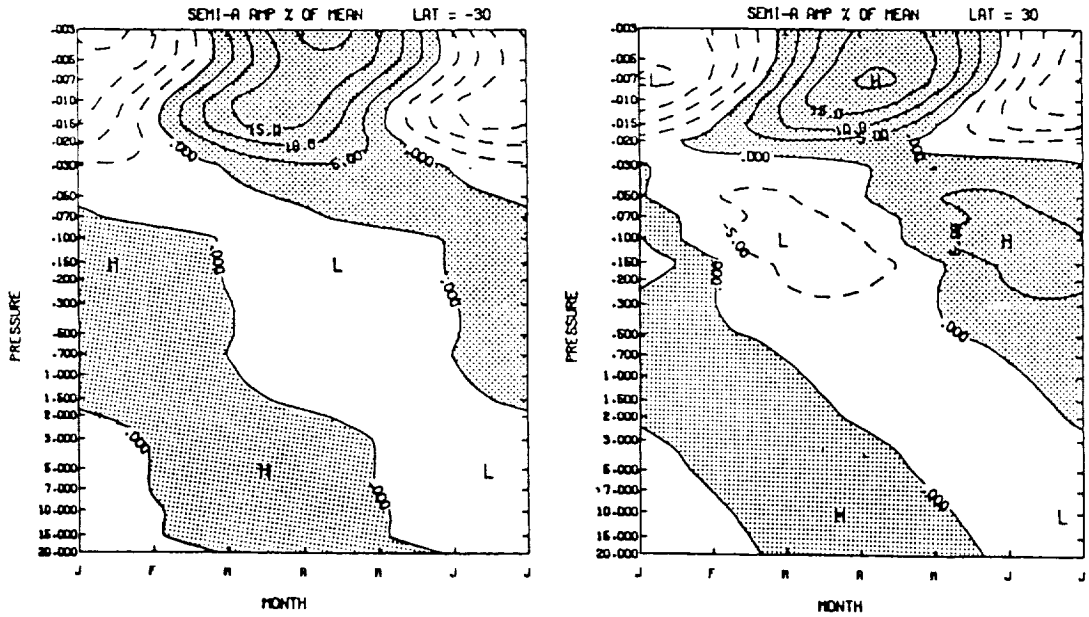

Figure 10. Semiannual variation of ozone volume mixing ratio in percent of the annual mean at 30°S and 30°N latitude.

latitude semiannual variations in the two hemispheres and evidence of propagation from the mesosphere into the stratosphere.

Shown in Figure 11 is the vertical structure of global mean ozone (weighted by cosine of latitude) and the maximum and minimum extremes of the tabulated values.

For convenience, Table 5 lists conversion factors for deriving common units for ozone measurements from volume mixing ratio.

Tabulated in Table 6 are the zonal mean ozone volume mixing ratios (ppmv) as a function of height and latitude using the conversion from pressure to height given by Barnett and Corney [29].

5. ANNUAL MEAN MIDLATITUDE MODEL

The Krueger and Minzner annual mean ozone reference model [3]of 45°N based on balloon and rocket data is compared here with this set of reference models. The Krueger and Minzner model has proven to be very useful and was included in the U. S. Standard Atmosphere, 1976. Data from rocket soundings in the latitude range of 45°N ± 15°, results of balloon soundings at latitudes from 41°N to 47°N, and latitude gradients from Nimbus 4 BUV observations were combined to give this earlier estimate of the annual mean ozone concentration and its variability at heights up to 74 km for an effective latitude of 45°N.

Shown in Figure 12a is a comparison of the vertical structure of the annual mean volume mixing ratio given by Krueger and Minzner [3] with that of the annual mean determined by averaging the monthly values at 40° and 50°N based on satellite data given in Table 4. As may be detected, there is good agreement between the balloon and rocket measurement model and the satellite measurement model. This agreement is even more noteworthy considering the lack of longitudinal coverage in the balloon and rocket measurement model. Shown in Figure 12b are the percent differences of the Krueger and Minzner model [3] from the annual mean model based on Table 4 values. Below altitudes of 0.2 mb, the agreement is generally within 10%. Above 0.2 mb, differences as large as 45% occur, but differences at all levels are within the error bars indicated by the Krueger and Minzner model. Both models give maximum mixing ratios near 5 mb.

Shown in Figure 13 is a comparison of the annual mean vertical ozone distribution from ozonesonde data from Hohenpeissenberg (FRG) (48°N, 11°E) over the period 1967-1985 and from Thalwil-Payerne (Switzerland) (47°N,7°E) over the period 1967-1982 with the 47.3°N zonal average annual mean based on the satellite data. Also the annual mean vertical structure of Umkehr data from Arosa (Switzerland) 1955-1983 is compared. These threedata sets were generously provided by R. Bojkov [64]. Considering that the ozonesonde and Umkehr data do not represent a zonal average but do represent conditions over a period of many years, the agreement is very good. Comparisons month by month of the ozonesonde data show better than 10% agreement with the zonal mean mixing ratios but show evidence of local phase shifts relative to the zonal mean variations. A number of other comparisons have been made with these satellite ozone reference models [65-68]

6. MODELS OF TOTAL OZONE-VERTICAL STRUCTURE RELATION

Mateer *et al.* [6] developed models of the vertical structure of ozone as a function of total column ozone and latitude. The models were based on balloon and rocket data. These models of the relation of total ozone to vertical structure are incorporated here. Shown in Figure 14a are low-latitude (about ±25°) profiles for ozone mixing ratios for total column ozone of 200, 230, 250 and 300 Dobson units (left to right). Shown in Figure 14b are similar mid-latitude (≈25 to 58°) profiles for total column ozone in increments of 50 Dobson units from 200 to 550 Dobson units (left to right). Finally, shown in Figure 14c are similar high-latitude (≈58 to 80°) profiles for total column ozone in increments of 50 Dobson units from 200 to 650 Dobson units (left to right). Note that the substantial variability in mixing ratio extends to lower pressures (higher altitudes) at the higher latitudes. Tabulations of the models are found in [6].

7. OTHER SYSTEMATIC VARIATIONS

A number of systematic variations of ozone in addition to latitudinal-seasonal variations have been analyzed. For brevity only a few references are included here. Empirical analyses have been performed on the quasibiennial oscillation [69], solar cycle variations [70,71] ,

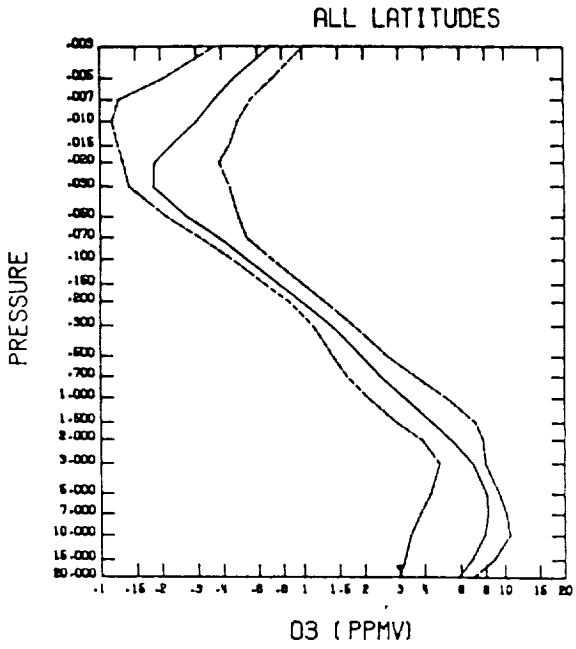

Figure 11. Global mean vertical structure of ozone volume mixing ratio (ppmv) (weighted by cosine of latitude) and the maxima and minima of Table 4 monthly latitudinal profiles.

TABLE 5. Unit Conversion

To convert from volume mixing ratio (ppmv) to the units below, multiply by:	
MASS MIXING RATIO (ppmm)	1.657
MASS DENSITY ($kg \cdot m^{-2}$)	$1.657 \cdot 10^{-8} \cdot \rho_t$
NUMBER DENSITY (m^{-3})	$2.079 \cdot 10^{19} \cdot \rho_t$
PARTIAL PRESSURE (nb)	p_t

where p_t is the total atmospheric pressure in mb (1 mb = 100 pascal) and ρ_t is the total atmospheric density in $kg \cdot m^{-3}$ at a given altitude.

Total column burden (Ω) in atm·cm (1 atm·cm = 1000 Dobson units) above a given pressure (p_0) can be calculated by integrating partial pressure $p(O_3)$ with respect to $ln(p_t)$:

$$\Omega = 7.896 \cdot 10^{-4} \cdot \int_0^{p_0} p(O_3) \cdot d\,ln(p_t)$$

TABLE 6. Zonal Mean Ozone Mixing Ratios (ppmv) as function of altitude

average ozone (ppmv) for January

alt. z(km)	latitude -80°	-70°	-60°	-50°	-40°	-30°	-20°	-10°	0°	10°	20°	30°	40°	50°	60°	70°	80°
80	.16	.15	.15	.18	.20	.23	.26	.28	.29	.31	.31	.28	.24	.23	.19	-	-
75	.26	.22	.19	.17	.15	.14	.15	.15	.15	.15	.16	.19	.23	.27	.27	.22	-
70	.48	.44	.40	.35	.30	.25	.24	.25	.26	.25	.25	.26	.27	.34	.42	-	-
65	.82	.79	.76	.69	.64	.60	.57	.56	.54	.53	.53	.54	.64	.58	.57	-	-
60	1.16	1.19	1.22	1.20	1.19	1.17	1.11	1.04	1.01	1.01	1.03	1.04	1.00	1.14	1.00	-	-
55	1.56	1.65	1.76	1.83	1.87	1.86	1.78	1.68	1.65	1.67	1.70	1.74	1.78	1.85	-	-	-
50	2.36	2.43	2.55	2.63	2.73	2.77	2.71	2.62	2.60	2.62	2.65	2.77	2.92	2.78	2.53	2.11	1.86
45	3.90	3.90	4.03	4.10	4.19	4.28	4.31	4.29	4.30	4.36	4.50	4.75	4.92	4.69	4.14	3.32	2.96
40	5.82	5.89	6.22	6.56	6.80	6.98	7.14	7.23	7.21	7.19	7.15	7.07	6.86	6.40	5.64	4.83	4.38
35	5.53	5.97	6.94	7.78	8.43	8.91	9.31	9.62	9.36	8.95	8.34	7.72	7.20	6.61	6.14	5.51	5.26
30	4.09	4.61	5.79	6.74	7.51	8.04	8.52	9.06	9.01	8.47	7.54	6.83	6.37	5.93	5.81	5.07	5.06
25	3.13	3.47	4.35	4.83	5.04	5.07	5.10	5.05	4.88	4.88	5.03	5.27	5.48	5.46	5.01	4.30	4.18

average ozone (ppmv) for February

alt. z(km)	latitude -80°	-70°	-60°	-50°	-40°	-30°	-20°	-10°	0°	10°	20°	30°	40°	50°	60°	70°	80°
80	.13	.13	.15	.17	.21	.26	.31	.31	.32	.34	.36	.33	.27	.23	.19	.14	-
75	.21	.19	.18	.16	.14	.15	.15	.16	.17	.17	.19	.23	.29	.31	.29	.25	-
70	.40	.38	.37	.33	.29	.26	.26	.26	.26	.26	.27	.27	.26	.28	.36	.42	-
65	.74	.71	.69	.67	.63	.60	.59	.58	.57	.55	.54	.54	.51	.55	.53	.56	-
60	1.15	1.15	1.17	1.19	1.21	1.18	1.12	1.08	1.06	1.07	1.07	1.02	.93	.85	.79	.87	-
55	1.65	1.67	1.76	1.83	1.89	1.87	1.78	1.71	1.70	1.73	1.75	1.73	1.67	1.57	1.45	1.51	-
50	2.67	2.61	2.65	2.75	2.85	2.86	2.74	2.59	2.55	2.61	2.67	2.75	2.83	2.82	2.75	2.58	2.26
45	4.30	4.22	4.26	4.34	4.43	4.46	4.35	4.13	4.04	4.17	4.38	4.66	4.95	4.93	4.63	4.13	3.34
40	5.65	5.99	6.39	6.64	6.87	7.06	7.08	7.03	6.97	6.98	7.03	7.23	7.21	6.77	6.19	5.64	4.95
35	5.05	5.93	6.95	7.56	8.16	8.84	9.31	9.73	9.59	9.29	8.90	8.31	7.61	6.96	6.49	6.39	6.15
30	3.65	4.41	5.62	6.46	7.26	8.02	8.69	9.34	9.42	8.93	8.18	7.17	6.50	6.29	6.13	6.42	6.12
25	3.02	3.43	4.19	4.54	4.90	4.98	5.06	5.08	4.95	4.90	5.10	5.30	5.46	5.59	5.59	5.39	5.28

average ozone (ppmv) for March

alt. z(km)	latitude -80°	-70°	-60°	-50°	-40°	-30°	-20°	-10°	0°	10°	20°	30°	40°	50°	60°	70°	80°
80	.12	.19	.21	.25	.31	.34	.33	.29	.28	.30	.33	.37	.38	.34	.28	.22	.16
75	.16	.15	.15	.15	.16	.16	.16	.16	.16	.17	.18	.21	.29	.36	.39	.36	.28
70	.28	.28	.28	.27	.27	.27	.27	.27	.26	.26	.27	.28	.27	.29	.35	.45	.45
65	.53	.53	.55	.57	.58	.58	.59	.60	.58	.57	.55	.53	.53	.52	.52	.54	.56
60	.95	.96	1.02	1.09	1.12	1.11	1.10	1.12	1.12	1.11	1.06	1.02	.98	.92	.84	.82	.82
55	1.55	1.59	1.67	1.76	1.82	1.79	1.78	1.79	1.80	1.80	1.79	1.75	1.68	1.59	1.52	1.48	1.51
50	2.87	2.76	2.73	2.80	2.84	2.79	2.71	2.66	2.65	2.67	2.73	2.76	2.71	2.64	2.67	2.74	2.77
45	4.71	4.83	4.65	4.63	4.63	4.54	4.32	4.06	3.99	4.09	4.31	4.51	4.64	4.75	4.83	4.72	4.43
40	5.40	6.16	6.66	6.93	7.05	7.11	6.99	6.63	6.50	6.65	6.90	7.11	7.37	7.34	7.02	6.54	6.08
35	5.01	5.86	6.79	7.45	8.02	8.56	9.07	9.43	9.43	9.31	9.05	8.68	8.37	7.88	7.25	6.64	6.50
30	4.00	4.34	5.32	6.25	7.03	7.85	8.68	9.51	9.79	9.38	8.67	7.81	7.06	6.54	6.16	6.01	6.16
25	3.44	3.66	4.12	4.57	4.82	4.97	5.08	5.15	5.10	5.14	5.32	5.44	5.40	5.42	5.45	5.50	5.40

TABLE 6 - continued

average ozone (ppmv) for April

alt. z(km)	latitude -80°	-70°	-60°	-50°	-40°	-30°	-20°	-10°	0°	10°	20°	30°	40°	50°	60°	70°	80°
80	-	-	.25	.30	.34	.33	.31	.32	.32	.32	.34	.41	.45	.44	.41	.36	.26
75	-	-	.28	.23	.18	.16	.16	.16	.16	.16	.17	.20	.25	.28	.31	.34	.32
70	-	-	.27	.23	.25	.27	.28	.28	.27	.28	.29	.30	.31	.32	.32	.35	.39
65	-	-	.46	.51	.55	.59	.62	.62	.60	.58	.57	.56	.56	.56	.57	.57	.57
60	-	-	.86	.97	1.04	1.10	1.15	1.16	1.15	1.13	1.10	1.08	1.07	1.03	.98	.95	.94
55	-	-	1.60	1.70	1.73	1.76	1.80	1.85	1.85	1.84	1.83	1.80	1.75	1.68	1.63	1.61	1.60
50	2.59	2.67	2.70	2.78	2.85	2.79	2.76	2.76	2.75	2.75	2.79	2.80	2.70	2.58	2.57	2.63	2.73
45	4.61	4.87	4.92	5.06	4.95	4.69	4.40	4.21	4.15	4.21	4.34	4.44	4.36	4.26	4.30	4.41	4.49
40	5.65	6.32	6.77	7.08	7.25	7.26	7.04	6.67	6.57	6.73	7.00	7.13	7.18	7.14	7.07	6.81	6.28
35	5.00	5.63	6.49	7.11	7.71	8.45	9.05	9.15	9.02	9.10	9.02	8.78	8.66	8.35	7.63	6.77	5.96
30	4.29	4.52	5.15	5.86	6.58	7.57	8.57	9.44	9.71	9.32	8.66	8.14	7.51	6.87	6.20	5.62	5.36
25	3.40	3.91	4.42	4.62	4.78	5.04	5.17	5.26	5.25	5.35	5.51	5.58	5.45	5.27	5.07	5.02	5.08

average ozone (ppmv) for May

alt. z(km)	latitude -80°	-70°	-60°	-50°	-40°	-30°	-20°	-10°	0°	10°	20°	30°	40°	50°	60°	70°	80°
80	-	-	-	.30	.31	.32	.36	.40	.40	.38	.35	.35	.34	.32	.28	.24	.19
75	-	-	-	.23	.18	.17	.17	.17	.17	.17	.17	.19	.19	.20	.19	.19	.21
70	-	-	-	.24	.23	.27	.28	.28	.29	.29	.30	.30	.32	.34	.35	.38	.42
65	-	-	-	.45	.52	.57	.63	.64	.62	.62	.62	.61	.61	.64	.67	.69	.70
60	-	-	-	.87	.97	1.06	1.16	1.18	1.16	1.16	1.16	1.15	1.14	1.14	1.13	1.11	1.10
55	-	-	-	1.68	1.73	1.73	1.81	1.86	1.86	1.85	1.86	1.86	1.83	1.78	1.72	1.67	1.63
50	-	2.45	2.54	2.90	2.91	2.85	2.82	2.81	2.80	2.80	2.82	2.81	2.73	2.63	2.54	2.49	2.50
45	-	4.55	4.90	5.45	5.41	4.96	4.54	4.36	4.31	4.31	4.36	4.35	4.24	4.12	4.07	4.05	4.21
40	-	6.44	6.76	7.41	7.52	7.41	7.07	6.81	6.75	6.86	7.04	7.04	6.94	6.84	6.70	6.42	6.34
35	-	5.92	5.90	6.79	7.45	8.10	8.58	8.74	8.75	8.94	8.98	8.83	8.61	8.18	7.45	6.44	5.70
30	-	5.18	4.97	5.62	6.34	7.21	8.20	9.00	9.29	8.95	8.43	8.08	7.60	7.07	6.32	5.31	4.60
25	-	4.13	4.49	4.83	4.98	5.15	5.22	5.17	5.22	5.45	5.53	5.58	5.47	5.17	4.82	4.41	4.15

average ozone (ppmv) for June

alt. z(km)	latitude -80°	-70°	-60°	-50°	-40°	-30°	-20°	-10°	0°	10°	20°	30°	40°	50°	60°	70°	80°
80	-	-	-	-	.30	.31	.30	.31	.31	.30	.27	.26	.26	.23	.18	.16	.16
75	-	-	-	-	.18	.17	.16	.15	.15	.15	.15	.16	.18	.20	.20	.21	.24
70	-	-	-	-	.24	.28	.28	.27	.27	.27	.27	.30	.32	.35	.38	.43	.47
65	-	-	-	-	.52	.56	.61	.64	.64	.65	.67	.66	.67	.73	.79	.83	.84
60	-	-	-	-	.93	1.05	1.15	1.19	1.19	1.21	1.24	1.24	1.23	1.26	1.27	1.24	1.20
55	-	-	-	-	1.66	1.68	1.78	1.84	1.84	1.84	1.86	1.86	1.85	1.82	1.75	1.67	1.59
50	-	-	2.35	2.71	2.84	2.81	2.86	2.86	2.84	2.82	2.84	2.84	2.75	2.62	2.48	2.38	2.33
45	-	-	4.69	5.46	5.43	4.95	4.67	4.51	4.44	4.40	4.42	4.34	4.19	4.07	3.96	3.90	3.96
40	-	-	6.70	7.67	7.67	7.25	7.04	6.96	6.93	7.00	7.12	7.03	6.88	6.68	6.38	6.19	6.19
35	-	-	5.86	6.53	7.44	7.89	8.37	8.70	8.89	9.02	9.00	8.85	8.54	7.89	7.03	5.97	5.42
30	-	-	5.12	5.28	6.32	7.02	7.59	8.29	8.63	8.49	8.00	7.78	7.30	6.77	5.95	4.85	4.31
25	-	-	4.63	5.07	5.15	5.03	4.89	4.85	4.94	5.07	5.02	5.01	5.00	4.78	4.38	3.80	3.52

TABLE 6 - continued

average ozone (ppmv) for July

alt. z(km)	latitude -80°	-70°	-60°	-50°	-40°	-30°	-20°	-10°	0°	10°	20°	30°	40°	50°	60°	70°	80°
80	-	-	-	.22	.25	.28	.29	.28	.27	.27	.24	.24	.23	.21	.17	.16	.16
75	-	-	-	.21	.18	.16	.15	.14	.15	.15	.15	.15	.16	.19	.20	.21	.25
70	-	-	-	.25	.24	.27	.26	.26	.26	.25	.24	.26	.31	.35	.38	.43	.48
65	-	-	-	.48	.55	.59	.61	.61	.61	.62	.64	.66	.69	.73	.79	.84	.85
60	-	-	-	-	1.00	1.10	1.15	1.15	1.15	1.17	1.22	1.26	1.27	1.28	1.29	1.27	1.21
55	-	-	-	-	1.72	1.75	1.79	1.80	1.79	1.79	1.83	1.88	1.88	1.84	1.77	1.67	1.56
50	-	-	2.09	2.59	2.86	2.90	2.87	2.82	2.78	2.77	2.85	2.91	2.85	2.70	2.54	2.42	2.33
45	-	-	3.94	5.00	5.29	5.00	4.74	4.55	4.45	4.42	4.50	4.48	4.35	4.20	4.05	3.92	3.94
40	-	-	6.11	7.23	7.49	7.29	7.21	7.17	7.11	7.14	7.23	7.14	6.96	6.78	6.44	6.03	5.95
35	-	-	6.04	6.77	7.36	7.94	8.38	8.81	9.01	9.11	9.03	8.87	8.52	7.95	6.99	5.82	5.18
30	-	-	5.18	5.28	6.20	6.80	7.43	8.16	8.49	8.45	7.98	7.73	7.24	6.55	5.69	4.66	4.06
25	-	-	4.66	5.03	5.15	5.02	4.89	4.83	4.95	5.10	4.97	4.87	4.80	4.63	4.18	3.57	3.24

average ozone (ppmv) for August

alt. z(km)	latitude -80°	-70°	-60°	-50°	-40°	-30°	-20°	-10°	0°	10°	20°	30°	40°	50°	60°	70°	80°
80	-	-	.24	.26	.29	.30	.31	.29	.28	.28	.29	.26	.22	.19	.16	.14	.14
75	-	-	.24	.21	.19	.18	.16	.15	.15	.15	.16	.15	.14	.16	.17	.18	.20
70	-	-	.27	.24	.26	.28	.27	.26	.26	.26	.26	.25	.27	.31	.34	.36	.39
65	-	-	.49	.53	.58	.59	.60	.60	.60	.60	.58	.59	.62	.65	.67	.70	.71
60	-	-	.88	.96	1.07	1.15	1.17	1.16	1.13	1.12	1.13	1.16	1.20	1.20	1.17	1.15	1.12
55	-	-	1.25	1.69	1.80	1.82	1.82	1.81	1.78	1.76	1.78	1.84	1.86	1.80	1.73	1.67	1.61
50	-	1.96	2.26	2.69	2.98	2.95	2.87	2.80	2.75	2.75	2.83	2.92	2.91	2.77	2.66	2.58	2.50
45	-	3.26	4.01	4.92	5.25	5.01	4.73	4.51	4.40	4.42	4.58	4.67	4.60	4.44	4.31	4.16	4.01
40	-	4.76	5.92	7.15	7.57	7.46	7.37	7.24	7.13	7.17	7.34	7.30	7.09	6.84	6.49	6.02	5.49
35	-	5.27	6.28	7.39	7.87	8.21	8.69	9.26	9.30	9.38	9.24	8.83	8.40	7.75	6.85	5.79	4.81
30	-	5.26	5.13	5.78	6.42	6.91	7.56	8.61	8.74	8.75	8.36	7.81	7.28	6.45	5.52	4.49	3.76
25	-	4.43	4.53	4.96	5.11	5.04	4.92	4.84	4.96	5.10	4.99	4.87	4.77	4.49	3.98	3.49	3.18

average ozone (ppmv) for September

alt. z(km)	latitude -80°	-70°	-60°	-50°	-40°	-30°	-20°	-10°	0°	10°	20°	30°	40°	50°	60°	70°	80°
80	.24	.27	.31	.34	.36	.36	.33	.30	.28	.27	.30	.31	.30	.25	.21	.19	.16
75	.28	.30	.27	.24	.21	.18	.17	.16	.16	.16	.16	.16	.16	.16	.15	.16	.19
70	.30	.30	.26	.26	.27	.28	.28	.26	.25	.26	.25	.24	.24	.25	.26	.26	.28
65	.47	.51	.52	.55	.57	.57	.57	.58	.59	.57	.54	.52	.52	.52	.50	.49	.50
60	-	.89	.92	.99	1.06	1.11	1.14	1.16	1.13	1.10	1.09	1.08	1.07	1.06	1.00	.90	.85
55	-	1.44	1.54	1.67	1.74	1.79	1.82	1.83	1.80	1.78	1.78	1.78	1.75	1.71	1.63	1.53	1.51
50	2.06	2.19	2.43	2.76	2.92	2.87	2.82	2.78	2.74	2.75	2.79	2.82	2.81	2.76	2.72	2.64	2.60
45	3.38	3.65	4.20	4.82	5.03	4.85	4.62	4.41	4.31	4.37	4.56	4.69	4.70	4.69	4.71	4.59	4.18
40	4.84	5.32	6.28	7.21	7.64	7.61	7.43	7.16	7.00	7.06	7.28	7.34	7.20	7.03	6.77	6.14	5.15
35	5.39	6.02	6.85	7.66	8.28	8.73	9.12	9.28	9.28	9.27	9.17	8.90	8.42	7.75	6.92	5.82	4.83
30	5.26	5.41	5.86	6.39	6.89	7.42	8.06	8.55	8.72	8.65	8.16	7.68	7.11	6.24	5.35	4.45	3.98
25	4.21	4.18	4.68	5.06	5.17	5.16	5.00	4.95	5.04	5.11	4.92	4.79	4.74	4.49	4.07	3.60	3.28

TABLE 6 - continued

average ozone (ppmv) for October

alt. z(km)	latitude -80°	-70°	-60°	-50°	-40°	-30°	-20°	-10°	0°	10°	20°	30°	40°	50°	60°	70°	80°
80	.28	.36	.40	.42	.40	.35	.31	.31	.31	.29	.28	.29	.31	.29	.24	.19	.12
75	.24	.23	.22	.22	.20	.18	.18	.19	.19	.17	.17	.17	.17	.20	.25	.27	.22
70	.37	.35	.34	.32	.31	.29	.29	.28	.27	.26	.26	.25	.24	.22	.25	.34	.33
65	.61	.59	.58	.56	.56	.56	.56	.55	.54	.53	.60	.55	.55	.51	.46	.43	-
60	1.04	1.01	1.01	1.02	1.06	1.10	1.13	1.13	1.11	1.11	1.09	1.03	.96	.87	.78	.74	-
55	1.56	1.58	1.64	1.67	1.73	1.79	1.84	1.86	1.86	1.85	1.81	1.73	1.65	1.60	1.51	1.38	-
50	2.34	2.42	2.63	2.73	2.75	2.73	2.76	2.78	2.78	2.78	2.75	2.70	2.74	2.78	2.71	2.51	2.26
45	3.69	3.86	4.26	4.51	4.59	4.52	4.45	4.36	4.31	4.36	4.50	4.64	4.90	5.09	5.00	4.53	4.07
40	5.44	5.94	6.70	7.23	7.53	7.51	7.35	7.09	6.91	6.94	7.14	7.26	7.25	7.07	6.74	6.11	5.25
35	6.20	6.86	7.61	8.17	8.61	9.05	9.37	9.43	9.33	9.29	9.18	8.74	7.92	7.21	6.68	5.93	5.06
30	5.82	6.09	6.47	6.79	6.98	7.55	8.20	8.80	8.99	9.09	8.67	7.85	6.80	6.00	5.39	4.91	4.43
25	4.07	4.53	5.27	5.29	5.10	5.09	5.07	4.97	4.93	5.02	4.94	4.82	4.71	4.59	4.38	3.93	3.42

average ozone (ppmv) for November

alt. z(km)	latitude -80°	-70°	-60°	-50°	-40°	-30°	-20°	-10°	0°	10°	20°	30°	40°	50°	60°	70°	80°
80	.16	.18	.22	.25	.28	.29	.29	.31	.33	.34	.34	.32	.32	.27	.21	-	-
75	.23	.21	.21	.19	.19	.18	.18	.19	.19	.18	.19	.20	.20	.24	.24	-	-
70	.43	.41	.39	.37	.34	.32	.30	.28	.27	.26	.27	.26	.25	.26	.34	-	-
65	.73	.71	.68	.64	.60	.58	.56	.54	.54	.55	.61	.58	.54	.49	.46	-	-
60	1.17	1.17	1.16	1.15	1.15	1.14	1.13	1.12	1.10	1.10	1.09	1.02	.89	.78	.79	-	-
55	1.65	1.70	1.76	1.79	1.82	1.84	1.85	1.85	1.85	1.84	1.80	1.72	1.63	1.48	-	-	-
50	2.40	2.45	2.57	2.61	2.63	2.66	2.71	2.75	2.78	2.76	2.68	2.65	2.67	2.66	2.43	2.17	1.77
45	3.98	4.00	4.13	4.14	4.13	4.17	4.26	4.27	4.29	4.32	4.37	4.58	4.96	5.00	4.60	3.97	3.03
40	6.10	6.27	6.53	6.80	6.91	6.97	7.00	6.87	6.74	6.75	6.89	7.07	7.14	6.96	6.40	5.78	4.42
35	6.18	6.57	7.16	7.87	8.45	8.83	9.10	9.04	8.72	8.67	8.47	8.05	7.36	6.77	6.10	5.74	4.50
30	5.37	5.58	6.13	6.65	7.21	7.84	8.40	8.88	8.91	8.71	8.18	7.41	6.19	5.64	5.29	5.04	3.53
25	4.35	4.52	4.94	5.01	5.08	5.22	5.26	5.26	5.12	5.05	5.05	4.97	4.81	4.75	4.45	3.96	2.98

average ozone (ppmv) for December

alt. z(km)	latitude -80°	-70°	-60°	-50°	-40°	-30°	-20°	-10°	0°	10°	20°	30°	40°	50°	60°	70°	80°
80	.17	.17	.17	.19	.22	.23	.26	.30	.30	.31	.32	.30	.29	.27	-	-	-
75	.26	.23	.22	.19	.17	.15	.16	.17	.17	.17	.19	.22	.25	.26	-	-	-
70	.51	.47	.42	.38	.35	.31	.28	.28	.27	.26	.27	.29	.29	.33	-	-	-
65	.85	.82	.77	.71	.66	.64	.62	.58	.56	.56	.55	.60	.64	.55	-	-	-
60	1.23	1.25	1.26	1.23	1.22	1.22	1.19	1.12	1.08	1.08	1.10	1.08	.97	1.03	-	-	-
55	1.58	1.66	1.76	1.83	1.88	1.89	1.86	1.82	1.80	1.80	1.79	1.74	1.68	1.78	-	-	-
50	2.31	2.38	2.49	2.55	2.64	2.71	2.74	2.76	2.79	2.76	2.73	2.70	2.66	2.42	2.11	1.67	1.54
45	3.87	3.88	3.95	3.98	4.07	4.18	4.29	4.36	4.42	4.44	4.51	4.67	4.93	4.66	3.93	2.84	2.58
40	6.04	6.08	6.26	6.53	6.74	6.90	7.04	7.04	6.95	6.94	6.97	7.03	7.04	6.68	5.84	4.69	4.33
35	5.84	6.18	7.00	7.79	8.37	8.80	9.14	9.17	8.78	8.43	8.03	7.69	7.19	6.54	5.98	5.28	5.13
30	4.57	4.95	5.91	6.83	7.54	8.09	8.55	8.92	8.76	8.27	7.48	6.93	6.21	5.60	5.42	4.52	4.48
25	3.75	3.94	4.56	4.86	5.07	5.18	5.16	5.08	4.90	4.92	4.96	5.10	5.11	5.08	4.59	3.83	3.81

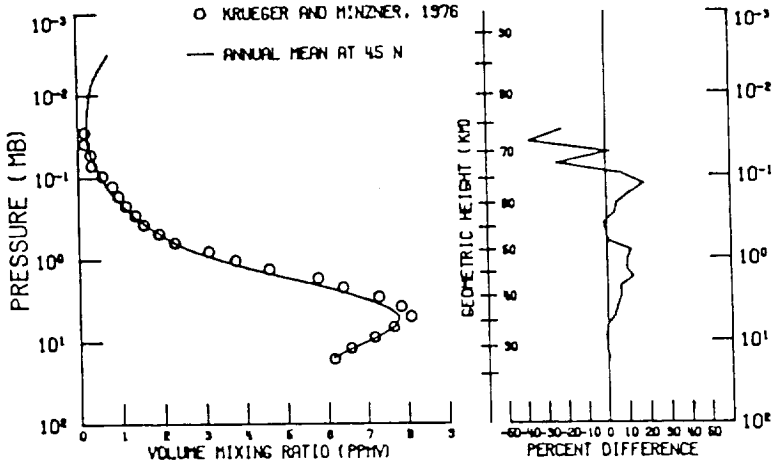

Figure 12. Comparison of annual mean ozone volume mixing ratio (ppmv) at 45°N based on the satellite data model of Table 4 and based on the balloon and rocket data model of Krueger and Minzner [3]. On the left (a) is shown the vertical structure in the two models and on the right (b) the percent difference from the satellite data model of the Krueger and Minzner model.

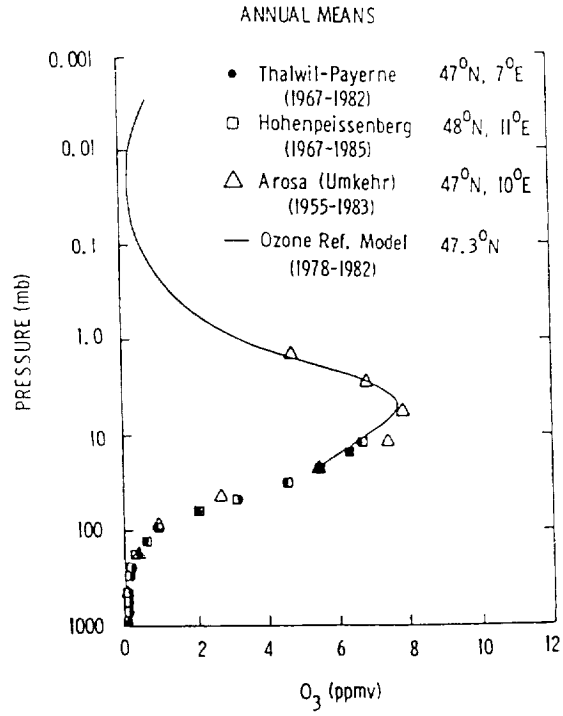

Figure 13. Comparison of annual mean ozone reference model with annual means of long-term balloon and Umkehr measurements.

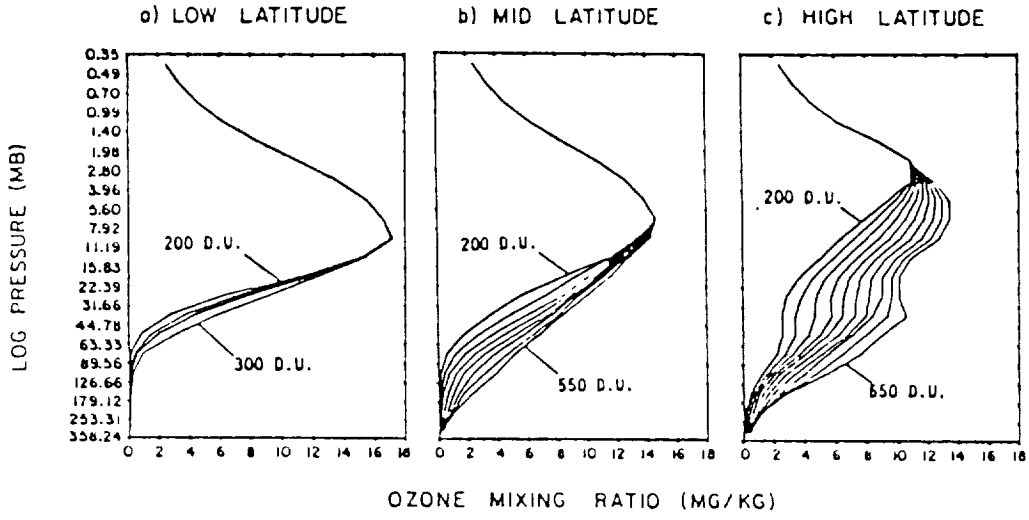

Figure 14. Variation of ozone mass mixing ratio with total ozone (from Mateer et al. [6]).
(a) low-latitude ozone profiles for total ozone of 200, 230, 250, and 300 Dobson units
(b) midlatitude ozone profiles for total ozone of 200, 250, ... 550 Dobson units
(c) high-latitude ozone profiles for total ozone of 200, 250, ..., 650 Dobson units.

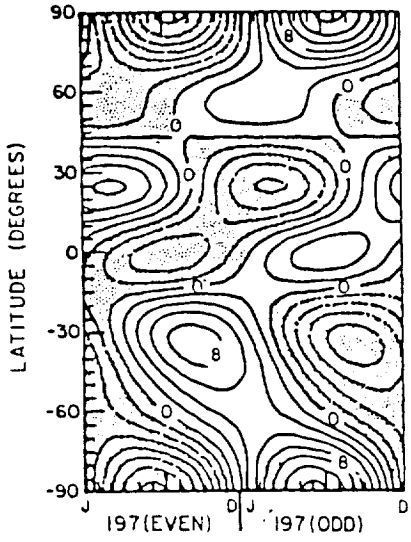

Figure 15. Biennial component of zonal mean ozone variation based on 7 years of Nimbus 4 BUV measurements. Contour interval is 2 Dobson units; solid lines are positive and the shaded area with dashed lines negative (Tolson, [13]).

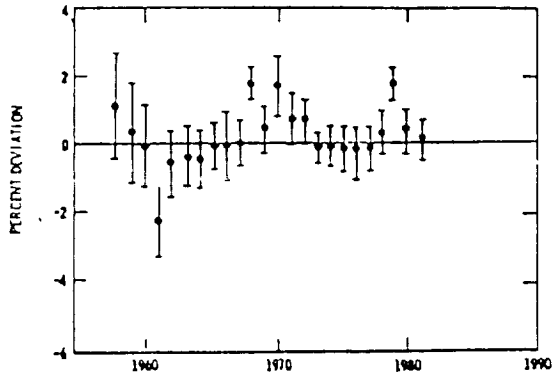

Figure 16. Variation of global yearly average total column ozone expressed as percent deviation from the mean based on ground-based Dobson spectrophotometers as well as M-83 ozonometers (Angell and Korshover, [83]).

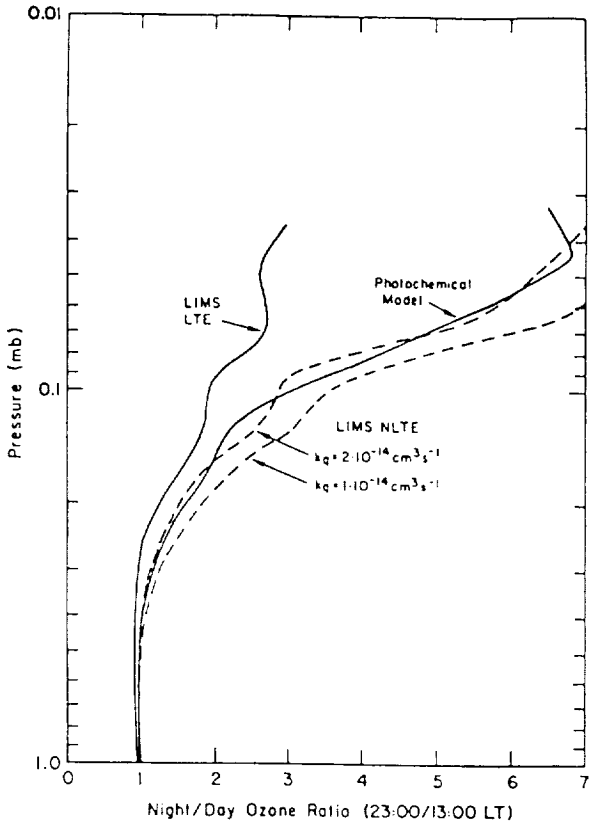

Figure 17. Vertical profile of the ozone diurnal variation calculated in a one-dimensional model and the corresponding values obtained from LIMS data after correction for non-LTE effects, assuming quenching rates of 1 and 2 x 10^{-14} cm^3 s^{-1} (from Solomon et al.[37]).

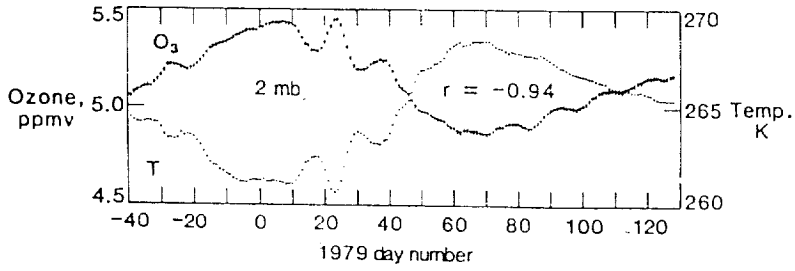

Figure 18. Comparison of Nimbus 7 LIMS measurements of zonal mean ozone and temperature obtained within 20° of the equator (Keating et al.[73]).

solar rotation variations [72-75,123] , diurnal variations [37,38,76,77] , longitudinal variations [2,11,78,79],volcanic eruptions [69,80], possible response to nuclear explosions [81], long-term trends [71,82,83], 4-year oscillations [14], response to stratospheric temperature [84-86], response to sudden winter warmings [87], and response to solar proton events [88,89].

The quasibiennial variation in ozone is thought to be related to the quasibiennial variation in equatorial zonal winds [90]. Shown in Figure 15 [13] is the biennial component of the zonal mean total ozone variation based on 7 years of Nimbus 4 BUV data. The contour interval is 2 Dobson units with the solid lines positive and the shaded area with dashed lines negative. Referring back to Figure 3, it may be seen that in the low and midlatitude regions the large interannual variations correspond to regions of large quasibiennial variation. However, since the variation is quasibiennial as opposed to biennial, the phase indicated in Figure 15 will change with time. There is also evidence that the period of the quasibiennial variation may vary somewhat with latitude [91] and that the latitude of maximum quasibiennial variation may vary somewhat with time [14].

Evidence has accumulated that variations in ozone with a period of the order of 11 years occur at various locations. On the other hand, there has been a lack of consensus as to whether these variations are related to the 11-year solar activity cycle. The early studies which were performed were reviewed by Keating [70]. Recent empirical studies on the possible response of ozone to 11-year solar variations include the works of Reinsel *et al.* [92] , Oehlert [93], Chandra [94], and Keating *et al.* [15]. From a study of Umkehr data, Reinsel *et al.* [92] estimate a 3% variation in ozone over the solar cycle near 36 km superimposed on a 3% per decade linear decline which may be associated with anthropogenic effects. Long term variations in total column ozone have been detected using the global Dobson network. Shown in Figure 16 are estimates of percent variation in global mean ozone based on those measurements as determined by Angell and Korshover [83]. Maximum values appear to occur near the times of solar maxima. It has now been established that there are solar UV variations of the order of 5% at wavelengths between 180 and 208 nm associated with the 27-day rotation period of the sun [95,96]. Analyses of satellite data are indicating a clearly detectable ozone response in both the stratosphere and mesosphere to these short-term solar variations [72-75,97,98,123]. Peak positive responses are detected near 40 km and peak negative responses (associated with solar Lyman-α radiation) are detected near 70 km [123].

The SME mesospheric measurements from which the mesospheric ozone models are based are dayside measurements. Observations and theoretical models show that mesospheric ozone is higher on the night side [37,38,51,76,77,99-103]. Shown in figure 17 is the night/day ozone ratio at the equator (January 13, 1979) based on Nimbus 7 LIMS data after correcting for non-LTE effects, assuming quenching rates of 1 and $2 \cdot 10^{-14}$ $cm^3 s^{-1}$ [37]. The photochemical model results shown in the figure employ the photochemistry in the two-dimensional model of Garcia and Solomon [104]. The night/day ratios given in Figure 17 are also in good agreement with the model of Allen *et al.* [51]. This model [51] appears to be fairly consistent with most of the measurements obtained at different latitudes, seasons, and altitudes of mesospheric diurnal variations.

Due to the temperature dependence of rate constants in the middle atmosphere, temperature decreases can result in increases of upper atmospheric ozone in regions approaching photochemical equilibrium [84]. Other processes can also lead to negative correlations between ozone and temperature [105]. The sensitivity of ozone to temperature variations reaches a maximum value near the stratopause of about 2% increase in ozone per Kelvin decrease in temperature. Shown in Figure 18 is an example of the negative response of upper stratospheric ozone to temperature variations [73]. Shown is the negative correlation between zonal mean temperature and ozone from 2 mb Nimbus 7 LIMS measurements within 20° of the equator. In addition to the stratospheric ozone response, the mesospheric ozone is found to be strongly affected by temperature variations [20].

8. RECENT RESULTS

The inversion algorithm for the SAGE ozone data has been refined and the resulting SAGE data was combined with the other satellite data sets and used to generate improved reference models [124]. However, the improved models are within 5% of the tabulations provided here. Also included in [124] are latitudinal seasonal models of nightside mesospheric ozone based on the Nimbus 7 LIMS data. Results concerning recent trends in column ozone and ozone profiles are summarized in the most recent Ozone Trends Panel report [125]. This report also identifies biases between measuring instruments.

ACKNOWLEDGMENTS

The authors wish to acknowledge the valuable contributions of the "Ad Hoc Group on Ozone Reference Models for CIRA" in reviewing an earlier manuscript. The Group includes C. A. Barth, P. K. Bhartia, D. F. Heath, K. Labitzke, C. A. Mateer, M. P. McCormick, A. J. Miller, and J. M. Russell III. Others offering valuable comments included J. S. Chang, R. Bojkov, R. J. Thomas, M. Allen, D. W. Rusch, and W. P. Chu. The authors also wish to thank B. T. Marshall and J. Y. Nicholson, III for their assistance in organizing and compiling the vast amount of ozone data.

REFERENCES

1. H.U. DUTSCH, Can. J. Chem. 52, 1491 (1974)

2. J. LONDON, R.D. BOJKOV, S.OLTMANS, and J.I. KELLEY, Atlas of the global distribution of total ozone, July 1957-June 1967, NCAR TN/113+STR, Boulder, CO (1976)

3. A.J. KRUEGER and R.A. MINZNER, J. Geophys. Res. 81, 4477 (1976)

4. R.D. BOJKOV, J.of Appl. Met. 8, 284 (1969)

5. E. HILSENRATH, P J. DUNN, and C.L. MATEER, in : Collection of Extended Summaries of Contributions Presented at the Joint Assembly CMUA Sessions IAGA/IAMAP, Seattle, WA, August 1977, National Center for Atmospheric Research, Boulder, CO, 41-1-41-6 (1977)

6. C.L. MATEER, J.J. DELUISI, and C.C. PORCO, NOAA TM ERL ARL-86 , 1980

7. P.K. BHARTIA, D. SILBERSTEIN, B. MONOSMITH, and A.J. FLEIG, in: Atmospheric Ozone ,eds C.S. Zerefos and A.Ghazi, D. Reidel Publ., Dordrecht, Holland, 1984, p. 243

8. K.F. KLENK, P.K. BHARTIA, E. HILSENRATH, and A.J. FLEIG, J. Clim. Appl. Met. 22, 2012 (1983)

9. H.U. DUTSCH, Pure Appl. Geophys. 116, 511 (1978)

10. R.D. MCPETERS, D.F. HEATH, and P.K. BHARTIA, J. Geophys. Res. 89, 5199 (1984)

11. D.F. HEATH, A.J. FLEIG, A.J. MILLER, T.G. ROGERS, R.M. NAGATANI, H.D. BOWMAN, V.G. KAVEESHWAR, K.F. KLENK, P.K. BHARTIA, and K.D. LEE, NASA Reference Publication 1098, p. A2 (1982)

12. K.P. BOWMAN and A.J. KRUEGER, J. Geophys. Res. 90, 7967 (1985)

13. R.M. TOLSON, J. Geophys. Res. 86, 7312 (1981)

14. F. HASEBE, J. Geophys. Res. 88, 6819 (1983)

15. G.M. KEATING, L.R. LAKE, J.Y. NICHOLSON III, and M. NATARAJAN, J. Geophys. Res. 86, 9873 (1981)

16. A.J. KRUEGER, B. GUENTHER, A.J. FLEIG, D.F. HEATH, E. HILSENRATH, R. MCPETERS, and C. PRABHAKARA, Phil. Trans. R. Soc. Lond. A 296, 191 (1980)

17. M.P. MCCORMICK, T.J. SWISSLER, E.HILSENRATH, A.J. KRUEGER, and M.T. OSBORN, J. Geophys. Res. 89, 5315 (1984)

18. G.M. KEATING, L. FRANK, J. CRAVEN, M. SHAPIRO, D. YOUNG, and P. BHARTIA, Adv. Space Res. 2, 183 (1983)

19. G.M. KEATING, J.D. CRAVEN, L.A. FRANK, D.F. YOUNG, and P.K. BHARTIA, Geophys. Res. Lett. 12, 593 (1985)

20. C.A. BARTH, D.W. RUSCH, R.J. THOMAS, G.H. MOUNT, G.J. ROTTMAN, G.E. THOMAS, R.W. SANDERS, and G.M. LAWRENCE, Geophys. Res. Lett. 10, 237 (1983)

21. K. SUZUKI, T. OGAWA, and S. KADOKURA, J. Geomag. Geoelectr. 37, 225 (1985)

22. J.E. FREDERICK, R.P. CEBULA, and D.F. HEATH, J. Atmos. and Oceanic Tech. 3, 472 (1986)

23. W.G. PLANET, J.H. LIENESEH AND M.L. HILL, In: Atmospheric Ozone, eds C.S. Zerefos and A. Ghazi, D. Reidel Publ., Dordrecht, Holland, 1984, p. 234

24. M.P. MCCORMICK and J.C. LARSEN, Geophys. Res. Lett. 13, 1280 (1986)

25. G.M. KEATING and D.F. YOUNG, Adv. Space Res. 5, # 7, 155 (1985)

26. G.M. KEATING and D.F. YOUNG, Handbook of MAP 16, 205 (1985)

27. G.M. KEATING, D.F. YOUNG, and M.C. PITTS, Adv. Space Res. 7, #10, 105 (1987)

28. G.M. KEATING and M.C. PITTS, Adv. Space Res. 7, #9, 37 (1987)

29. J.J. BARNETT and M.CORNEY, Handbook of MAP 16, 47 (1985)

30. Systems and Applied Sciences Corp., NASA CR NAS5-28060 (1984)

31. P.K. BHARTIA, K.F. KLENK, A.J. FLEIG, C.G. WELLEMEYER, and D. GORDON, J. Geophys. Res. 89, 5227 (1984)

32. K.F. KLENK, B. MONOSMITH and P.K. BHARTIA, In: Atmospheric Ozone, eds C.S. Zerefos and A. Ghazi, D. Reidel Publ., Dordrecht, Holland, 1984, p. 625

33. A.M. BASS and R.J. PAUR, In: Atmospheric Ozone , eds C.S. Zerefos and A. Ghazi, D. Reidel Publ., Dordrecht, Holland, 1984, p. 606

34. R.J. PAUR and A. M. BASS, In Atmospheric Ozone , eds C.S. Zerefos and A. Ghazi, D. Reidel Publ., Dordrecht, Holland, 1984, p. 611

35. J.M. RUSSELL III, Adv. Space Res. 4, #4, 107 (1984)

36. J.C. GILLE and J.M. RUSSELL III, J. Geophys. Res. 89, 5125 (1984)

37. S. SOLOMON, J.T. KIEHL, B.J. KERRIDGE, E.E. REMSBERG, and J.M. RUSSELL III, J. Geophys. Res. 91, 9865 (1986)

38. E.E. REMSBERG, J.M. RUSSELL III, J.C. GILLE, L.L. GORDLEY, P.L. BAILEY, W.G. PLANET, and J.E. HARRIES, J. Geophys. Res. 89, 5161 (1984)

39. D.M. CUNNOLD, M.C. PITTS, and C.R. TREPTE, J. Geophys. Res. 89, 5249 (1984)

40. R. REITER and M.P. MCCORMICK, Nature 300, 337 (1982)

41. A.J. FLEIG, P.K. BHARTIA, C.K. WONG, and K.F. KLENK, Proceedings of the 5th Conference on Atmospheric Radiation (AMS), Oct.31 - Nov.4, 1983 Baltimore, MD (1984)

42. A.J. FLEIG, J.C. GILLE, M.P. MCCORMICK, D.W. RUSCH, J.M. RUSSELL III, and J.M. LINDSAY, In: Atmospheric Ozone , eds C.S. Zerefos and A. Ghazi, D. Reidel Publ., Dordrecht, Holland, 1984, p. 258

43. D.W. RUSCH, G.H. MOUNT, C.A. BARTH, G.J. ROTTMAN, R.J. THOMAS, G.E. THOMAS, R.W. SANDERS, G.M. LAWRENCE, and R.S. ECKMAN, Geophys. Res. Lett. 10, 241 (1983)

44. D.W. RUSCH, G.H. MOUNT, C.A. BARTH, R.J. THOMAS, and M.T. CALLAN, J. Geophys. Res. 89, 11677 (1984)

45. R.J. THOMAS, C.A. BARTH, G.J. ROTTMAN, D.W. RUSCH, G.H. MOUNT, G.M. LAWRENCE, R.W. SANDERS, G.E. THOMAS, and L.E. CLEMENS, Geophys. Res. Lett. 10, 245 (1983)

46. R.J. THOMAS, C.A. BARTH, D.W. RUSCH, and B.W. SANDERS, J. Geophys. Res. 89, 9569 (1984)

47. A. VALLANCE JONES, Space Sci. Rev. 15, 355 (1973)

48. L. THOMAS, Phil. Trans. R. Soc. Lond. A 296, 243 (1980)

49. J.F. NOXON, Planet. Space Sci. 30, 545 (1982)

50. G. VAUGHAN, Quart. J. R. Met. Soc. 110, 239 (1984)

51. M. ALLEN, J.I. LUNINE, and Y.L. YUNG, J. Geophys. Res. 89, 4841 (1984)

52. L.H. WEEKS, R.E. GOOD, J.S. RANDHAWA, and H. TRINKS, J. Geophys. Res. 83, 978 (1978)

53. R.THOMAS, private communication (1984).

54. D.F. HEATH, C.L. MATEER, and A.J. KRUEGER, Pure Appl. Geophys. 106-108, 1238 (1973)

55. J.C. GILLE, P.L. BAILEY, and J.M. RUSSELL III, Phil. Trans. R. Soc. Lond. A 296, 205 (1980)

56. P.K. BHARTIA, A.J. FLEIG, K.F. KLENK, C.K. WONG, and D. GORDON, J. Geophys. Res. 89, 5239 (1984)

57. J.E. LOVILL and J.S. ELLIS, Geophys. Res. Lett. 10, 447 (1983)

58. C. PRABHAKARA, E.B. RODGERS, B.J. CONRATH, R.A. HANSEL, and V.G. KUNDE, J. Geophys. Res. 81, 6391 (1976)

59. E.J. PRIOR and B.J. OZA, Geophys. Res. Lett. 5, 547 (1978)

60. A.J. FLEIG, P.K. BHARTIA, C.G. WELLEMEYER, and D.S. SILBERSTEIN, Geophys. Res. Lett. 13, 1355 (1986)

61. J.C. FARMAN, B.G GARDINER, and J.D. SHANKLIN, Nature 315, 207 (1985)

62. R.D. BOJKOV, Geophys. Res. Lett. 13, 1236 (1986)

63. R.J. THOMAS, C.A BARTH, and S. SOLOMON, Geophys. Res. Lett. 11, 673 (1984)

64. R.D. BOJKOV ,private communication (1987)

65. T. WATANABE and T. OGAWA, Adv. Space Res. 7, # 9, 123 (1987)

66. B.H. SUBBARAYA and A. JAYARAMAN, Adv. Space Res. 7, # 9, 119 (1987)

67. E. LOBSIGER, J. Atmos. Terr. Phys. 49, 493 (1987)

68. R.A. BARNES, A.C. HOLLAND, and V.W.J.H. KIRCHOFF, J. Geophys. Res. 92, 5573 (1987)

69. J.K. ANGELL and J. KORSHOVER, Mon. Weather Rev. 106, 725 (1978)

70. G.M. KEATING, Solar Physics 74, 321 (1981)

71. G.C. REINSEL, G.C. TIAO, J.J. DELUISI, C.L. MATEER, A.J. MILLER, and J.E. FREDERICK, J. Geophys. Res. 89, 4833 (1984)

72. J.C. GILLE, C.M SMYTHE, and D.F. HEATH, Science 225, 315 (1984)

73. G.M. KEATING, G.P. BRASSEUR, J.Y. NICHOLSON III, and A. DERUDDER, Geophys. Res. Lett. 12, 449 (1985)

74. L.L. HOOD, J. Geophys. Res. 91, 5264 (1986)

75. S. CHANDRA, J. Geophys. Res. 91, 2719 (1986)

76. J.L. LEAN, J. Geophys. Res. 87, 4973 (1982)

77. E. LOBSIGER and K.F. KUNZI, J. Atmos. Terr. Phys. 48, 1153 (1986)

78. R.W. WILCOX, G D. NASTROM, and A.D. BELMONT, J. Appl. Meteorol. 16, 290 (1977)

79. V.I. BEKORYUKOV, V.N. GLAZKOV, and V.V. FEDOROV, Adv. Space Res. 7, # 9, 115 (1987)

80. H.U. DUTSCH, in: Atmospheric Ozone, eds C.S. Zerefos and A. Ghazi, D.Reidel Publ., Dordrecht, Holland, 1984 , p. 263

81. H. JOHNSON, G. WHITTEN, and J. BIRKS, J. Geophys. Res. 78, 6107 (1973)

82. J. LONDON and J. KELLEY, Science 184, 987 (1974)

83. J.K. ANGELL and J. KORSHOVER, J. Clim. Appl. Met. 22, 1611 (1983)

84. J.J. BARNETT, J.T. HOUGHTON, and J.A. PYLE, Quart. J. R. Met. Soc. 101, 245 (1975)

85. M.C. PITTS, Masters Thesis, Georgia Institute of Technology, Atlanta, Georgia (1981)

86. A.J. MILLER, R.M. NAGATANI, and J.E. FREDERICK, in: Atmospheric Ozone, eds C.S. Zerefos and A. Ghazi, D. Reidel Publ., Dordrecht, Holland, 1984, p. 321

87. A. GHAZI, J. Atmos. Sci. 31, 2197 (1974)

88. D.F. HEATH, A.J. KRUEGER, and P.J. CRUTZEN, Science 197, 886 (1977)

89. R.J. THOMAS, C.A. BARTH, G.J. ROTTMAN, D.W. RUSCH, G.H. MOUNT, G.M. LAWRENCE, R.W. SANDERS, G.E. THOMAS, and L.E. CLEMENS, Geophys. Res. Lett. 10, 253 (1983)

90. S.J. OLTMANS and J. LONDON, J. Geophys. Res. 87, 8981 (1982)

91. E. HILSENRATH and B.M. SCHLESINGER, J. Geophys. Res. 86, 12087 (1981)

92. G.C. REINSEL, G.C. TIAO, A.J. MILLER, D.J. WUEBBLES, P.S. CONNELL, C.L. MATEER, and J.L. DELUISI, J. Geophys. Res. 92, 2201 (1987)

93. G.W. OEHLERT, J. Geophys. Res. 91, 2675 (1986)

94. S. CHANDRA, J. Geophys. Res. 89, 1373 (1984)

95. D.F. HEATH, R.F. DONNELLY, and R.G. MERRILL, NOAA Tech. Rep. ERL 424-ARL, Boulder, CO (1983)

96. J. LONDON, G.G. BJARNASON, and G.J. ROTTMAN, Geophys. Res. Lett. 11, 54 (1984)

97. G. BRASSEUR, A. DERUDDER, G.M. KEATING, and M. C. PITTS, J. Geophys. Res. 92, 903 (1987)

98. D.F. HEATH and B.M. SCHLESINGER, in: Atmospheric Ozone, eds. C.S. Zerefos and A.Ghazi, D.Reidel Publ., Dordrecht, Holland, 1984, p. 666

99. E. HILSENRATH, J. Atmos. Sci. 28, 295 (1970)

100. G.P. ANDERSON, J.C. GILLE, P.L. BAILEY, and S. SOLOMON, paper presented at Quadrennial International Ozone Symposium, Int. Ozone Comm. and IAMAP, Boulder (1980)

101. W.J. WILSON and P.R. SCHWARTZ, J. Geophys. Res. 86, 7385 (1981)

102. G. VAUGHAN, Nature 296, 133 (1982)

103. B.D. GREEN, W.T. RAWLINS, and R.M. NADILE, J. Geophys. Res. 91, 311 (1986)

104. R.R. GARCIA, and S. SOLOMON, J. Geophys. Res. 88, 1379 (1983)

105. R.R. ROOD and A.R. DOUGLAS, J. Geophys. Res. 90, 5733 (1985)

106. S.V. VENKATESWARAN, J.G. MOORE, and A.J. KRUEGER, J. Geophys. Res. 66, 1751 (1961)

107 R.D. RAWCLIFFE, G.E. MELOY, R.M. FRIEDMAN, and E.H. ROGERS, J. Geophys. Res. 68, 6425 (1963)

108. D.E. MILLER and K.H. STEWART, Proc. R. Soc. Lond. A 288, 540 (1965)

109. B. GUENTHER, R. DASGUPTA, and D.F. HEATH, Geophys. Res. Lett. 4, 434 (1977)

110. P.B. HAYS and R.G. ROBLE, Planet. Space Sci. 21, 273 (1973)

111. G.R. RIEGLER, J.F. DRAKE, S.C. LIU, and R.J. CICERONE, J. Geophys. Res. 81, 4997 (1976)

112. R.D. RAWCLIFFE and D.D. ELLIOTT, J. Geophys. Res. 71, 5077 (1966)

113. V.A. IOZENAS, V.A. KRASNOPOL'SKI, A P. KUZNETSOV, and A.I. LEBEDINSKY, Atms. Oceanic Phys. 5, 149 (1969)

114. D.D. ELLIOTT, M.A. CLARK, and R.D. HUDSON, Aerospace Techn. Report TR-0158 (3260-10) (1967)

115. G.P. ANDERSON, C.A. BARTH, F. CAYLA, and J. LONDON, Ann. Geophys. 25, 239 (1969)

116. J.E. FREDERICK, P.B. HAYS, B.W. GUENTHER, and D.F. HEATH, J. Atmos. Sci. 34, 1987 (1977)

117. D.F. HEATH, A.J. KRUEGER, H.A. ROEDER, and B.D. HENDERSON, Opt. Engng. 14, 323 (1975)

118. C.L. MATEER, D.F HEATH , and A.J.KRUEGER, J. Atmos. Sci. 28, 1307 (1971)

119. Nimbus Project, The Nimbus 7 Users' Guide, Goddard Space Flight Center, Greenbelt, MD (1978)

120. Nimbus Project, Nimbus-7 Data Product Summary, NASA Reference Publ. 1215 (1989)

121. R.A. HANEL, B. SCHLACHMAN, F.D. CLARK, C.H. PROKESH, J.B. TAYLOR, W.M. WILSON, and L. CHANEY, Appl. Opt. 9, 1767 (1970)

122. J.E. LOVILL, T.J. SULLIVAN, R.L. WEICHEL, J.S. ELLIS, J.G. HUEBEL, J.A. KORVER, P.P. WERDHAAS, and F.A. PHELPS, Lawrence Livermore Laboratory UCRL-52473 (1978)

123. G.M. KEATING, M.C. PITTS, G. BRASSEUR, and A. DERUDDER, J. Geophys. Res. 89, 889 (1987)

124. G.M. KEATING and M.C. PITTS, Improved reference models for middle atmosphere ozone, Adv. Space Res., to be published (1989)

125. R.T. WATSON and Ozone Trends Panel, M.J. PRATHER and ad-hoc Theory Panel, and M.J. KURYLO and NASA Panel for Data Evaluation, NASA Reference Publ. 1208 (1988)

2

IMPROVED REFERENCE MODELS FOR MIDDLE ATMOSPHERE OZONE

G. M. Keating[1], M. C. Pitts[2], and C. Chen[2]

[1]Atmospheric Sciences Division, NASA Langley Research Center, Hampton, VA 23665
[2]ST Systems Corporation (STX), Hampton, VA 23666

ABSTRACT

Improvements are provided here for the ozone reference model which is to be incorporated in the COSPAR International Reference Atmosphere (CIRA). The ozone reference model will provide considerable information on the global ozone distribution, including ozone vertical structure as a function of month and latitude from approximately 25 to 90 km, combining data from five recent satellite experiments (Nimbus 7 LIMS, Nimbus 7 SBUV, AE-2 SAGE, Solar Mesosphere Explorer (SME) UVS, and SME IR). The improved models described here use reprocessed AE-2 SAGE data (sunset) and extend the use of SAGE data from 1981 to the period 1981-1983. It is found that these SAGE data agree at all latitudes and months with the ozone reference model within 15 percent and result in modifications in the reference model of less than 4 percent. In the mesosphere, a model of nighttime conditions (≈ 10 p.m.) has been added using Nimbus 7 LIMS data between pressures of 0.5 mb to 0.05 mb (≈ 54 to 70 km). Minimum nightside ozone mixing ratios occur at about 0.2 mb (≈ 61 km). The ratio of nightside LIMS data to dayside (≈ 3 p.m.) SME data gives diurnal variations as large as a factor of 6 at the highest levels. At 0.1 mb (≈ 66 km), the night-day diurnal variation can exceed 3 and maximizes during solstice periods near 45 degrees in the summer hemisphere and near the Equator during equinoctial periods. This may largely result from the dayside ozone being more strongly photodissociated by the more directly incident summer Sun at mid latitudes and the equinoctial Sun at the Equator. Comparisons are shown between the ozone reference model and various non-satellite measurements at different levels in the middle atmosphere.

INTRODUCTION

An ozone reference model is being developed for incorporation in the next COSPAR International Reference Atmosphere (CIRA). Previous versions of the Keating et al. model are described in the ozone chapter in the "Draft Reference Middle Atmosphere" published in Map Handbook Number 16 /1/ and in editions of Advances in Space Research /2, 3, 4/. The ozone vertical structure from ≈ 25 to 90 km is determined by combining results from five contemporary satellite experiments: Nimbus 7 Solar Backscatter Ultraviolet (SBUV), Applications Explorer Mission-2 Stratospheric Aerosol Gas Experiment (SAGE), Solar Mesosphere Explorer (SME) UV Spectrometer (SME-UVS), and SME 1.27 Micron Airglow (SME-IR). Total column ozone is determined using Nimbus 7 TOMS data. Monthly standard deviations in the zonal mean ozone are provided for both the vertical structure and total column ozone, indicators of the interannual variability are given, and models developed by /5/ relating vertical structure of ozone to total column ozone for low, medium, and high latitudes are also included in the Keating and Young representation. A brief discussion is also provided by Keating and Young /1/ of the various systematic variations in ozone which have been studied, including the annual and semiannual variations and quasi-biennial oscillation, estimates of solar rotation and solar-cycle variations, diurnal variations, longitudinal variations, possible variations with volcanic eruptions and nuclear explosions, response to solar proton events, response to stratospheric temperature variations, possible 4-year oscillations, and long-term trends.

In this paper, the models of vertical structure are improved using reprocessed AE-2 SAGE data as one of the data sets for the period 1981-1983. Previously, only SAGE data from 1981 had been used. Also, models of the nightside mesospheric ozone are provided using Nimbus 7 LIMS data from 0.5 mb to 0.05 mb (≈ 54 to 70 km). The reference model is compared with various non-satellite measurements of ozone.

The pressure range and time intervals of the data used in these improved models are shown in Table 1.

TABLE 1 Satellite Data Used for Improved Ozone Reference Models

Instrument	Incorporated Pressure Range	Incorporated Time Interval
Nimbus 7 LIMS	0.5 - 20 mb 0.05 - 0.5 mb (night)	11/78 - 5/79 11/78 - 5/79
Nimbus 7 SBUV	0.5 - 20 mb	11/78 - 9/82
AE-2 SAGE	5 - 20 mb	2/79 - 11/81
SME UVS	0.07 - 0.5 mb	1/82 - 12/83
SME IR	0.003 - 0.5 mb	1/82 - 12/83
Nimbus 7 TOMS	TOTAL	11/78 - 9/82

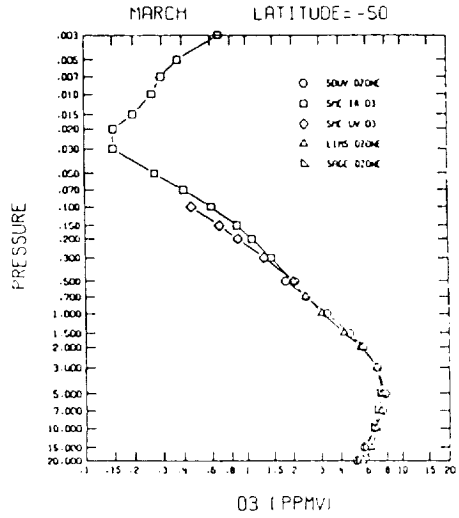

Figure 1. Comparison of ozone mixing ratios from five satellite experiments.

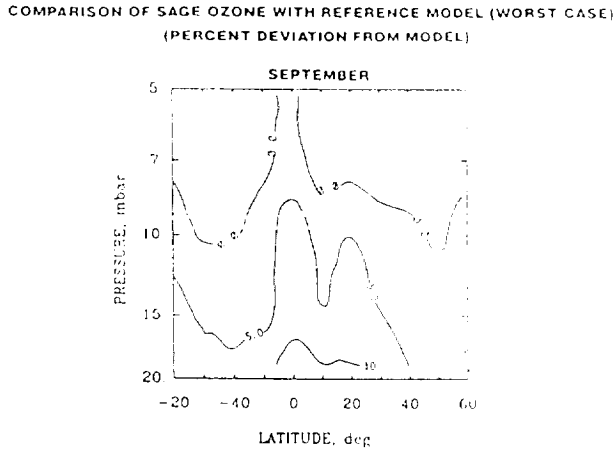

Figure 2. Comparison of reprocessed SAGE ozone data with improved reference model. The percent deviation from the model shown here represents the maximum deviations detected.

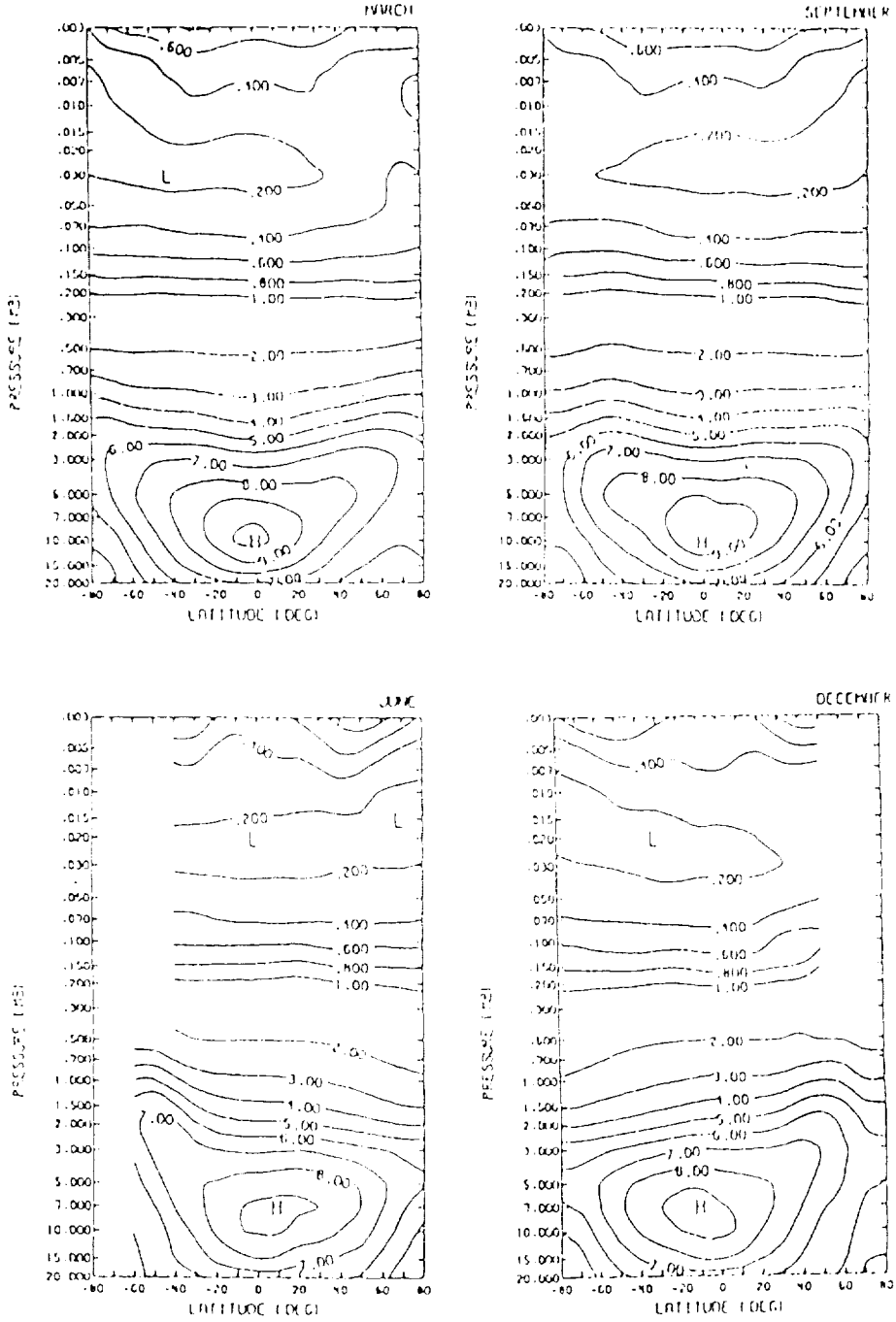

Figure 3. Improved reference model of ozone volume mixing ratios (ppmv).

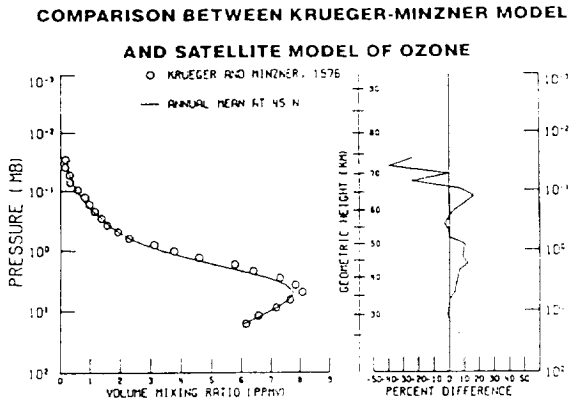

Figure 4. Comparison between Krueger-Minzner annual mean ozone model (45°N) and model of ozone based on satellite data.

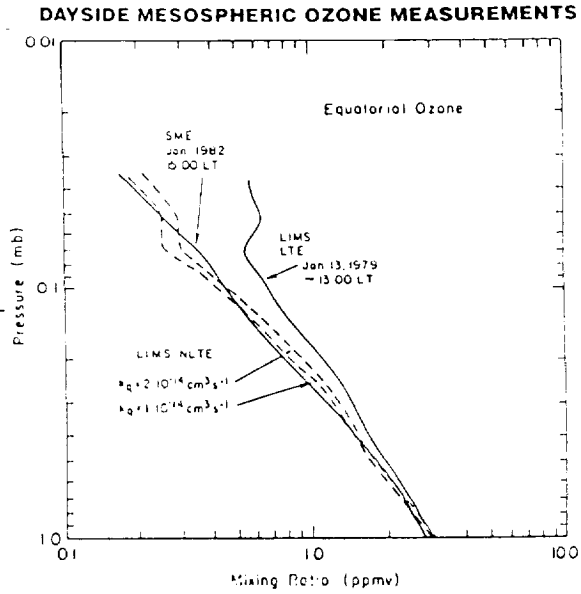

Figure 5. Nimbus 7 LIMS measurements of dayside equatorial ozone (Jan. 13, 1979) before (LIMS LTE) and after (LIMS NLTE) correction for non-LTE effects. The two LIMS NLTE curves are for different quenching rates. Also shown is a comparison between SME dayside ozone measurements in January 1982 and the LIMS measurements corrected for non-LTE effects from (/16/).

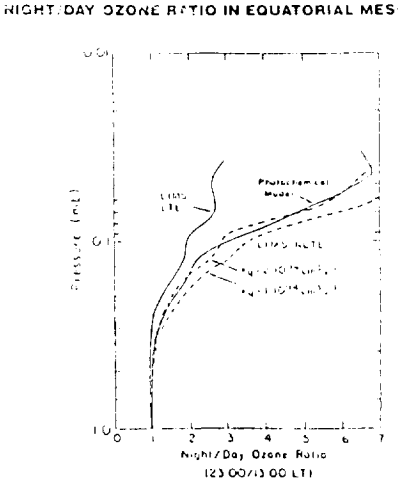

Figure 6. Night-to-day ozone ratio based on LIMS nightside measurements and the uncorrected (LIMS LTE) and corrected (LIMS NLTE for the two quenching rates) LIMS dayside measurements. The observations are compared with the photochemical model of Garcia and Solomon /21/ (from /16/).

COMPARISONS WITH SAGE

The Applications Explorer Mission-2 Stratospheric Aerosol and Gas Experiment (SAGE) used a four-channel Sun photometer which measured solar intensity at sunrise and sunset to derive ozone, aerosols, and NO_2 concentrations. Absorption of 0.6 micron solar radiation by ozone allowed determination of the vertical structure of ozone to be obtained up to 30 times per day from February 1979 until November 1981. The early validation of the SAGE measurements is described in some detail by /6/ and /7/. Recently, the algorithm for determining ozone mixing ratios has been refined. We incorporate here a provisional version of the refined (sunset) data which has been provided by the experimenter. The data have been interpolated to the model latitudes, times, and pressures.

The reprocessed SAGE data is found to have very good agreement with the ozone reference model. Shown in Figure 1 is an example of the agreement between the five data sets used to generate the models of the ozone vertical structure from 20 mb to 0.003 mb (≈ 25-90 km). Note that the mixing ratio is displayed on a log scale to allow accurate representation of the two orders of magnitude variation over this altitude range. It should be recognized that each data set represent entirely different techniques of measuring the vertical structure of ozone. The agreement shown is fairly representative. The reprocessed monthly SAGE data is shown by right triangles and closely matches the other data sets.

The vertical structure models are generated giving the 4-year mean of the SBUV data a weight of 2 due to the combination of extensive temporal and spatial coverage, while the other shorter data sets are given a weight of 1. The resulting updated model is compared with the reprocessed SAGE data in Figure 2. Over the latitudinal range of SAGE data provided for September, the SAGE data gives values near the Equator which are less than 15 percent higher than the reference model. This is the worst case of all months and results in less than a 4 percent modification in the reference model at 20 mb near the Equator for September. Thus, there are very small differences between this reference model, which is available upon request, and the Keating and Pitts tabulation /4/.

The resulting ozone distributions for the equinox and solstice months are shown in Figure 3. Shown in Figure 4 is a comparison of the Krueger and Minzner /8/ annual mean ozone reference model of 45N latitude, which is given in the U.S. Standard Atmosphere, 1976, and the updated ozone reference model provided here. The Krueger and Minzner model is based on rocket and balloon soundings and takes into account the latitudinal gradients in ozone near 45N from Nimbus 4 BUV observations. As may be seen, there is good agreement between the balloon and rocket model and the satellite measurement model, especially over the pressure range of the SAGE measurements incorporated here.

NIGHTSIDE MESOSPHERIC MODEL

The SME mesospheric measurements from which the mesospheric ozone models are based are dayside measurements (≈ 3 p.m.). Observations and theoretical models show that mesospheric ozone is higher on the nightside (Hilsenrath /9/; Anderson et al. /10/; Wilson and Schwartz /11/; Lean /12/; Vaughan /13/; Remsberg et al. /14/; Allen et al. /15/; Solomon et al. /16/; Green et al. /17/; Lobsiger and Kunzi /18/; Bjarnason et al. /19/). The Nimbus 7 Limb Infrared Monitor of the Stratosphere (LIMS) (Russell /20/) obtained mesospheric measurements on both the nightside and dayside. The LIMS instrument, a six-channel cryogenically cooled radiometer, had a number of channels to measure temperature and various species and included an ozone channel near 9.6 microns. Detailed validation studies have been described by Remsberg et al. /14/. Solomon et al. /16/ have shown that the LIMS dayside measurements of the mesosphere should be corrected for nonlocal thermodynamic equilibrium (non-LTE) effects. Shown in Figure 5 is an example of a LIMS dayside profile before (LIMS LTE) and after (LIMS NLTE) correction for non-LTE effects. After this correction, Solomon et al. /16/ point out there was good agreement between dayside LIMS and SME measurements. Shown in Figure 6 is the night-day ozone ratio based on LIMS nightside measurements and the uncorrected (LIMS LTE) and corrected (LIMS NLTE for two quenching rates) LIMS dayside measurements. As may be seen after the non-LTE correction, the ozone ratio is in good agreement with the photochemical model. The photochemical model results shown in the figure employ the photochemistry in the 2-dimensional model of Garcia and Solomon /21/. Since the correction for non-LTE effects in the dayside mesosphere have not been applied to the LIMS data as a whole, we have chosen to use only the SME data to represent the dayside mesosphere and nightside LIMS data to represent the nightside mesosphere.

Shown in Table 2 are the monthly nightside (ascending) zonal means of Kalman-filtered LIMS ozone volume mixing ratios (ppmv) (Remsberg et al. /22/) from the LIMS Map Archival Tape

TABLE 2 Nightside Mesospheric Ozone Volume Mixing Ratios (ppmv)

O3 ZONAL MEAN OCT

	-60.	-50.	-40.	-30.	-20.	-10.	0.	10.	20.	30.	40.	50.	60.	70.	80.
0.05	———	———	———	———	———	———	———	———	———	1.47	1.39	1.36	1.59	2.08	2.17
0.07	———	———	———	———	———	———	———	———	———	1.36	1.32	1.35	1.42	1.61	1.66
0.10	1.48	1.59	1.55	1.52	1.47	1.61	1.63	1.57	1.42	1.30	1.29	1.33	1.31	1.30	1.31
0.15	1.46	1.48	1.45	1.44	1.41	1.46	1.46	1.43	1.38	1.31	1.28	1.29	1.26	1.22	1.21
0.20	1.49	1.48	1.45	1.45	1.43	1.45	1.43	1.41	1.42	1.37	1.34	1.34	1.31	1.27	1.24
0.30	1.58	1.55	1.53	1.54	1.54	1.56	1.53	1.53	1.55	1.51	1.49	1.47	1.45	1.45	1.43
0.50	1.92	1.87	1.86	1.87	1.88	1.90	1.88	1.87	1.89	1.91	1.94	1.99	2.03	2.08	1.96

O3 ZONAL MEAN NOV

	-60.	-50.	-40.	-30.	-20.	-10.	0.	10.	20.	30.	40.	50.	60.	70.	80.
0.05	———	———	———	———	———	———	———	———	———	1.51	1.40	1.39	1.80	2.20	2.14
0.07	———	———	———	———	———	———	———	———	———	1.42	1.33	1.31	1.49	1.68	1.73
0.10	———	1.63	1.60	1.56	1.48	1.50	1.46	1.49	1.44	1.37	1.30	1.27	1.29	1.33	1.43
0.15	———	1.49	1.48	1.46	1.39	1.39	1.36	1.38	1.40	1.35	1.30	1.25	1.24	1.22	1.24
0.20	———	1.47	1.46	1.46	1.41	1.39	1.36	1.39	1.43	1.40	1.36	1.31	1.29	1.24	1.22
0.30	———	1.53	1.54	1.56	1.52	1.51	1.47	1.52	1.56	1.54	1.50	1.44	1.42	1.38	1.33
0.50	———	1.83	1.84	1.87	1.87	1.89	1.86	1.89	1.92	1.94	1.99	2.01	2.03	1.95	1.85

O3 ZONAL MEAN DEC

	-60	-50	-40	-30	-20	-10	0	10	20	30	40	50	60	70	80
0.05	———	———	———	———	1.46	1.42	1.40*	———	1.56*	1.40*	1.54*	1.63	2.17	2.31	2.06
0.07	———	———	———	———	1.43	1.36	1.33	———	1.38	1.40	1.42	1.47	1.70	1.78	1.72
0.10	———	1.72	1.75	1.60	1.41	1.33	1.30	1.32	1.33	1.41	1.36	1.36	1.38	1.41	1.45
0.15	———	1.55	1.55	1.46	1.37	1.31	1.27	1.30	1.35	1.41	1.38	1.31	1.27	1.28	1.27
0.20	———	1.51	1.50	1.45	1.40	1.35	1.32	1.35	1.41	1.46	1.41	1.35	1.29	1.24	1.23
0.30	———	1.56	1.56	1.54	1.51	1.48	1.45	1.49	1.54	1.57	1.52	1.46	1.41	1.38	1.26
0.50	———	1.84	1.85	1.86	1.87	1.90	1.90	1.92	1.92	1.94	1.96	1.96	1.88	1.70	1.63

O3 ZONAL MEAN JAN

	-60	-50	-40	-30	-20	-10	0.	10.	20	30.	40	50.	60	70.	80.
0.05	———	———	———	———	1.41	1.43	1.47*	1.51*	1.49	1.48*	1.41*	1.72*	2.06*	2.32	2.28
0.07	———	———	———	———	1.32	1.35	1.39	1.43	1.40	1.43	1.43	1.56	1.71	1.84	1.80
0.10	———	1.73	1.73	1.46	1.29	1.31	1.34	1.37	1.35	1.40	1.45	1.46	1.47	1.49	1.47
0.15	———	1.55	1.55	1.41	1.31	1.32	1.33	1.34	1.34	1.41	1.45	1.42	1.39	1.35	1.32
0.20	———	1.52	1.51	1.45	1.38	1.37	1.37	1.37	1.39	1.47	1.52	1.47	1.42	1.34	1.31
0.30	———	1.59	1.60	1.56	1.51	1.46	1.43	1.47	1.52	1.61	1.64	1.61	1.55	1.45	1.40
0.50	———	1.89	1.92	1.92	1.89	1.83	1.78	1.84	1.91	2.01	2.11	2.11	2.05	1.88	1.78

O3 ZONAL MEAN FEB

	-60.	-50.	-40.	-30	-20.	-10.	0.	10.	20.	30.	40.	50	60.	70.	80.
0.05	———	———	———	———	1.35*	1.50*	1.63	1.68*	1.50	1.44	1.50	1.60	2.01	2.52	2.65
0.07	———	———	———	———	1.31	1.43	1.51	1.52	1.42	1.37	1.45	1.50	1.71	1.93	2.01
0.10	1.12	1.69	1.58	1.34	1.30	1.40	1.44	1.46	1.38	1.35	1.42	1.44	1.51	1.53	1.58
0.15	1.23	1.54	1.46	1.35	1.32	1.39	1.40	1.40	1.36	1.37	1.41	1.40	1.43	1.43	1.48
0.20	1.34	1.52	1.49	1.41	1.39	1.43	1.42	1.42	1.40	1.43	1.46	1.46	1.47	1.47	1.51
0.30	1.52	1.61	1.60	1.55	1.56	1.52	1.50	1.52	1.54	1.58	1.61	1.61	1.64	1.67	1.71
0.50	1.90	1.94	1.98	1.97	1.83	1.86	1.82	1.86	1.91	2.01	2.09	2.16	2.25	2.27	2.21

O3 ZONAL MEAN MAR

	-60.	-50	-40.	-30	-20	-10	0.	10.	20.	30	40.	50.	60.	70.	80
0.05	1.83	———	———	———	———	———	———	———	1.77*	1.57*	1.70	1.74	1.77	2.07	1.88
0.07	1.59	———	———	———	———	———	———	———	1.62	1.49	1.57	1.64	1.78	1.88	1.62
0.10	1.44	1.48	1.38	1.36	1.45	1.61	1.65	1.60	1.52	1.44	1.48	1.56	1.63	1.62	1.46
0.15	1.42	1.45	1.38	1.37	1.43	1.52	1.53	1.48	1.45	1.41	1.44	1.47	1.51	1.51	1.44
0.20	1.47	1.48	1.44	1.42	1.47	1.52	1.52	1.48	1.48	1.45	1.47	1.49	1.52	1.54	1.53
0.30	1.59	1.59	1.56	1.54	1.57	1.61	1.59	1.58	1.59	1.59	1.59	1.61	1.63	1.67	1.76
0.50	1.98	1.97	1.96	1.93	1.93	1.94	1.91	1.94	1.99	2.01	2.02	2.04	2.12	2.27	2.45

O3 ZONAL MEAN APR

	-60	-50.	-40	-30	-20	-10.	0.	10	20.	30	40	50.	60.	70.	80.
0.05	1.39	1.34	1.37*	1.58	———	———	———	———	———	1.79*	2.17	2.38	2.26	1.68	———
0.07	1.34	1.29	1.27	1.37	———	———	———	———	———	1.68	1.88	2.02	1.99	1.58	———
0.10	1.31	1.27	1.23	1.31	1.53	1.75	1.79	1.76	1.65	1.60	1.63	1.76	1.77	1.51	———
0.15	1.27	1.28	1.28	1.35	1.48	1.60	1.62	1.59	1.55	1.52	1.53	1.59	1.59	1.44	———
0.20	1.32	1.35	1.36	1.41	1.50	1.58	1.59	1.57	1.56	1.53	1.54	1.57	1.56	1.47	———
0.30	1.48	1.51	1.50	1.53	1.60	1.65	1.66	1.66	1.66	1.65	1.65	1.65	1.64	1.61	———
0.50	2.02	2.00	1.94	1.92	1.98	1.99	1.98	2.01	2.04	2.04	2.03	2.00	2.00	2.01	———

O3 ZONAL MEAN MAY

	-60.	-50	-40.	-30.	-20.	-10.	0.	10.	20.	30.	40.	50.	60.	70.	80.
0.05	1.84*	1.16*	1.18*	1.37*	———	———	———	———	———	———	———	———	———	———	———
0.07	1.52	1.20	1.20	1.30	———	———	———	———	———	———	———	———	———	———	———
0.10	1.31	1.25	1.23	1.27	1.46	1.68	1.74	1.72	1.65	1.72	1.85	1.94	1.86	———	———
0.15	1.23	1.24	1.25	1.38	1.42	1.55	1.59	1.58	1.55	1.59	1.66	1.72	1.65	———	———
0.20	1.28	1.32	1.33	1.37	1.45	1.54	1.57	1.56	1.56	1.59	1.63	1.67	1.60	———	———
0.30	1.43	1.51	1.51	1.52	1.56	1.63	1.65	1.66	1.69	1.70	1.71	1.72	1.66	———	———
0.50	2.11	2.13	2.04	1.95	1.94	1.95	1.96	1.99	2.05	2.06	2.05	2.03	1.96	———	———

* ESTIMATED ERROR EXCEEDS 20 PERCENT

(LAMAT) interpolated to the standard levels in the models. An "*" is placed after values where the error in zonal mean is estimated to exceed 20 percent. Values are shown between 0.5 mb and 0.05 mb (when available) from 60S to 80N. Values between 50S and 60N are near 10 p.m. At the highest latitudes, earlier local solar times occur.

Shown in Figure 7 is the reference model for January, Equator. The LIMS nighttime values from 1 mb to 0.05 mb are seen to depart from the dayside model above 0.5 mb (≈ 54 km). Below 0.5 mb, little diurnal variability occurs due to the lower dayside O/O, ratio at lower altitudes resulting in less production of ozone on the nightside. In Figure 8, a similar pattern is shown for January, 60N (winter). Again, substantial day-night variations do not appear to occur below 0.5 mb. Referring to the table, it may be seen that a minimum mixing ratio generally occurs on the nightside near 0.2 mb (≈ 61 km). As may be seen in Figures 7 and 8, a dayside minimum occurs at much higher altitudes, 75 or 80 km.

Shown in Figure 9 is the night-day ozone ratio for January, based on 1980 LIMS (≈ 10 p.m.) and 1982-1983 SME (≈ 3 p.m.) data, as a function of latitude and pressure. It should be taken into consideration that as opposed to all of the difference being diurnal, part may be due to interannual variations and biases of SME data relative to LIMS data, even though the agreement between dayside SME and LIMS in Figure 9 appears to be in accord with the observed and predicted values given in Figure 6.

Figure 10 gives a detailed view of latitudinal-seasonal variations in the night-day ozone ratio at 0.1 mb (≈ 66 km). Ratios at this level can exceed a factor of 3 and maximize during solstice periods near 45 degree latitude in summer and near the Equator during equinox periods. This may largely result from the dayside ozone being more strongly photodissociated by the more directly incident summer Sun at mid latitudes and the equinoctial Sun at the Equator.

COMPARISON OF MODEL WITH OTHER MEASUREMENTS

It is of interest to compare the ozone vertical structure model, which is based on satellite measurements, with ozone measurements obtained by other techniques. In Figure 4, a comparison has already been shown with the Krueger and Minzer (1976) model based on balloon and rocket data. Shown in Figure 11 is a comparison with the satellite data model (47°N, annual mean) of the annual mean vertical distribution from ozonesonde data from Hohenpeissenberg (FRG) (48°N, 11°E) over the period 1967-1985 and from Thalwil-Payerne (Switzerland) (47°N, 7°E) over the period 1967-1982, and the annual mean vertical structure from Umkehr data from Arosa, Switzerland (47°N, 10°E), over the period 1955-1983. The three data sets were generously provided by R. D. Bojkov /23/. Considering that the ozonesonde and Umkehr data do not represent a zonal average, but do represent conditions over a period of many years, the agreement is very good.

Over the period April 1984 to April 1985, a microwave radiometer was operated at Bern, Switzerland (47°N, 7°E), measuring the thermal emission of the rotational ozone transition at 142.2 GHZ to determine stratospheric and mesospheric ozone abundances in the range of 25 to 75 km. Monthly mean ozone partial pressures for Umkehr layers 6-10 were calculated from over 300 daytime profiles. Shown in Figure 12 (Lobsinger /24/) are the resulting ozone profiles obtained by the microwave measurements (solid line) compared with Umkehr measurements from Arosa (dashed line), 20-year monthly mean Arosa Umkehr (crosses), and the Keating and Young /1/ ozone reference model (open circles). The differences with the reference model may be partially due to local year-to-year phase shifts relative to the zonal mean variations. Note the excellent agreement in the annual variation at Umkehr levels 7 and 8 between the reference model and Arosa Umkehr (20 years) measurements.

A comparison with other information is also made between the annual mean of the microwave measurements in Figure 13. Residuals are shown relative to the microwave measurements (Lobsinger /24/). The solid line is the 20-year annual average of Arosa Umkehr measurements, the dash-dotted line the Krueger and Minzner /8/ model, and the dashed line the Keating and Young MAP model /1/. With the exception of Umkehr levels 5 (≈ 22 mb) and 14 (≈ 0.04 mb), the annual microwave measurements agree very closely with other information.

An ozone measurement campaign was conducted at Natal, Brazil (6°S, 35°W) in March-April 1985, resulting in seven profiles from ROCOZ-A ozonesondes (Barnes et al. /25/). Shown in Figure 14 is comparison of a mean of the ROCOZ-A ozone measurements with the MAP Interim Ozone Model /1/. The agreement is excellent, with the Natal measurements averaging 2 percent higher than the MAP model with a 3 percent standard deviation. The agreement between ozone data in the mid-1980's with a model based on satellite data in the late 1970's and early 1980's has interesting implications concerning the amplitude of long-term trends.

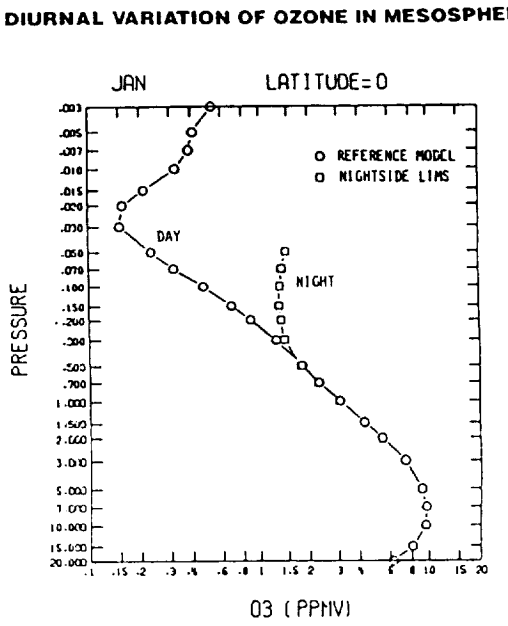

Figure 7. Diurnal variation of mesospheric ozone from satellite data. Comparison of ozone reference model (dayside above 0.5 mb) with the LIMS nightside measurements (0.05 mb to 1 mb) for Equator in January.

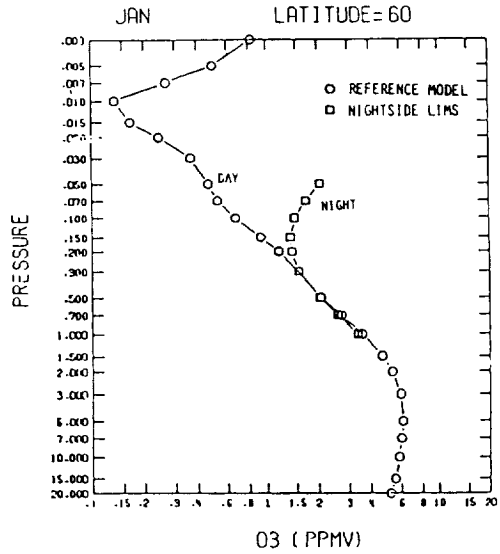

Figure 8. Same as Figure 7 but for 60°N in January.

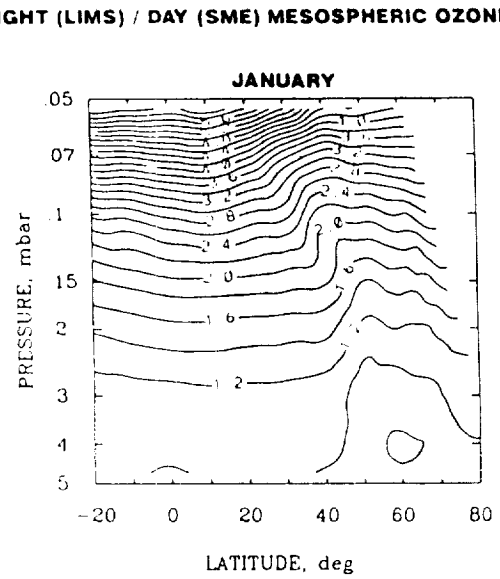

Figure 9. Night to day ozone ratio for January based on 1980 LIMS nightside data and 1982-1983 SME dayside data as a function of latitude and pressure.

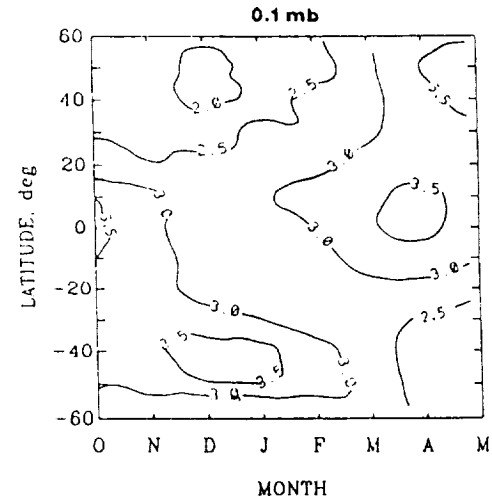

Figure 10. Night (LIMS) to day (SME) mesospheric ozone ratio at 0.1 mb (≈ 66 km) as a function of latitude and season.

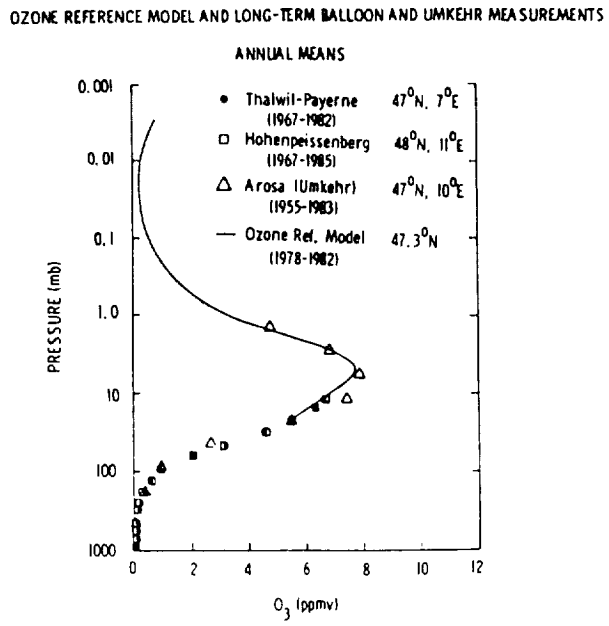

Figure 11. Comparison of ozone reference model based on satellite data with annual means of long-term balloon and Umkehr measurements.

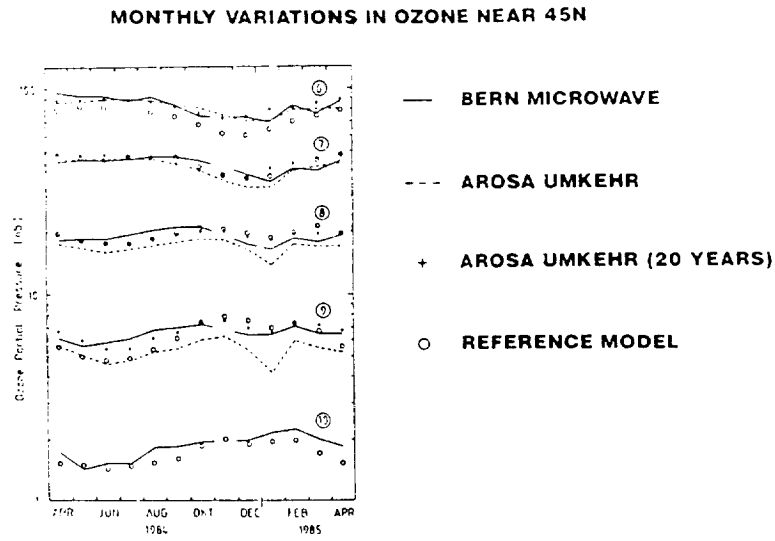

Figure 12. Comparison of monthly variations in ozone partial pressure from (a) microwave measurements from Bern, Switzerland, (b) simultaneous Umkehr measurements from Arosa, Switzerland, (c) 20 years of Umkehr measurements from Arosa, Switzerland, and (d) the ozone reference model based on satellite data (from /24/).

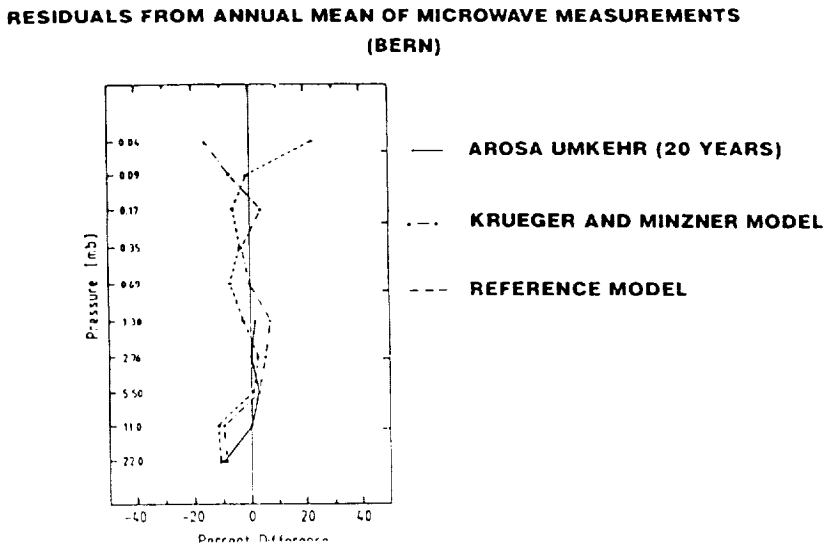

Figure 13. Residuals from annual mean of microwave ozone measurements from Bern, Switzerland of (a) 20 years of measurements from Arosa, Switzerland, (b) The Krueger and Minzner model /8/, and (c) the ozone reference model based on satellite data (from /24/).

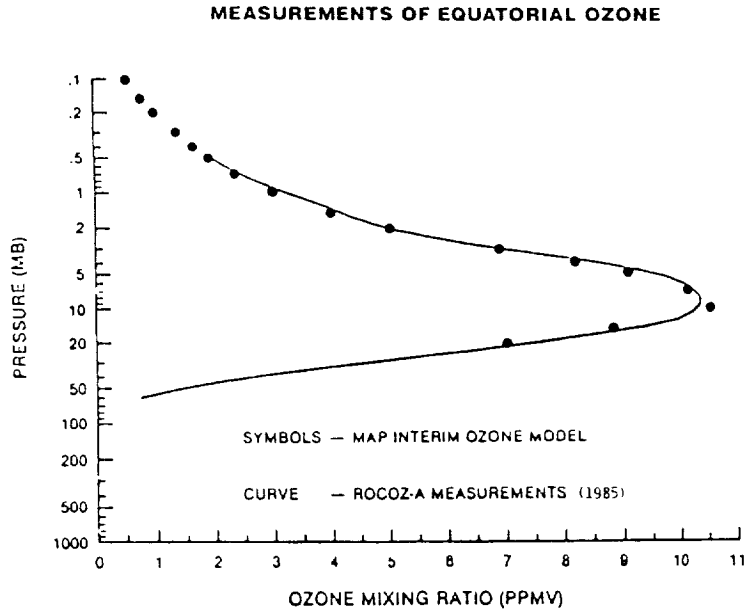

Figure 14. Comparison of equatorial ozone measurements obtained from 7 ROCOZ-A ozonesondes in 1985 with the ozone reference model based on satellite data (from /25/).

REFERENCES

1. G.M. Keating and D.F. Young, Handbook of MAP, 16, 205 (1985)

2. G.M. Keating and D.F. Young, Adv. Space Res., 5, #7, 155 (1985)

3. G.M. Keating, D.F. Young, and M.C. Pitts, Adv. Space Res., 7, #10, 105 (1987)

4. G.M. Keating and M.C. Pitts, Adv. Space Res., 7, #9, 37 (1987)

5. C.L. Mateer, J.J. Deluisi, and C.C. Porco, NOAA TM ERL ARL-86, (1980)

6. M.P. McCormick, T.J. Swissler, E. Hilsenrath, A.J. Krueger, and M.T. Osborn, J. Geophys. Res., 89, 5315 (1984)

7. D.M. Cunnold, M.C. Pitts, and C.R. Trepte, J. Geophys. Res., 89, 5249 (1984)

8. A.J. Krueger and R.A. Minzner, J. Geophys. Res., 81, 4477 (1976)

9. E. Hilsenrath, J. Atmos. Sci., 28, 295 (1970)

10. G.P. Anderson, J.C. Gille, P.L. Bailey, and S. Solomon, paper presented at Quadriennial International Ozone Symposium, Int. Ozone Comm. and IAMAP, Boulder (1980)

11. W.J. Wilson and P.R. Schwartz, J. Geophys. Res., 86, 7385 (1981)

12. J.L. Lean, J. Geophys. Res., 87, 4973 (1982)

13. G. Vaughan, Nature, 296, 133 (1982)

14. E.E. Remsberg, J.M. Russell III, J.C. Gille, L.L. Gordley, P.L. Bailey, W.G. Planet, and J.E. Harries, J. Geophys. Res., 89, 5161 (1984)

15. M. Allen, J.I. Lunine, and Y.L. Yung, J. Geophys. Res., 89, 4841 (1984)

16. S. Solomon, J.T. Kiehl, B.J. Kerridge, E.E. Remsberg, and J.M. Russell III, J. Geophys. Res., 91, 9865 (1986)

17. B.D. Green, W.T. Rawlins, and R.M. Nadile, J. Geophys. Res., 91, 311 (1986)

18. E. Lobsinger and K.F. Kunzi, J. Atmos. Terr. Phys., 48, 1153 (1986)

19. G.G. Bjarnason, S. Solomon, and R.R. Garcia, J. Geophys. Res., 92, 5609 (1987)

20. J.M. Russell III, Adv. Space Res., 4, #4, 107 (1984)

21. R.R. Garcia and S. Solomon, J. Geophys. Res., 88, 1379 (1983)

22. E.E. Remsberg, R.J. Kurzeja, K.V. Haggard, J.M. Russell III, and L.L. Gordley, NASA Technical Report 2625 (1986)

23. R.D. Bojkov, private communication (1987)

24. E. Lobsinger, J. Atmos. Terr. Phys., 49, 493 (1987)

25. R.A. Barnes, A.C. Holland, and V.W.J.H. Kirchoff, J. Geophys. Res., 92, 5573 (1987)

AN INTERIM REFERENCE MODEL FOR THE VARIABILITY OF THE MIDDLE ATMOSPHERE H_2O VAPOR DISTRIBUTION

E. E. Remsberg[1], J. M. Russell III[1], and C. Y. Wu[2]

[1]Atmospheric Science Division, NASA Langley Research Center, Hampton, VA 23665
[2]ST Systems Corporation (STX), Hampton, VA 23666

ABSTRACT

Water vapor is an important minor constituent in the studies of the middle atmosphere for a variety of reasons, including its role as a source for active HO_y chemicals and its use in analysis of transport processes. A number of in situ and remote techniques have been employed in the determination of water vapor distributions. Two of the more complete data sets have been used to develop an interim reference profile. First, there are the 7 months of Nimbus 7 LIMS data obtained during November 1978 to May 1979 over the range 64S to 84N latitude and from about 100-mb to 1-mb. By averaging radiances before retrieval, LIMS random errors have been reduced, and the results have been improved and extended recently from 1.5-mb to 0.5-mb. Secondly, the ground-based microwave emission technique has provided many profiles from 0.2-mb to 0.01-mb in the mid mesosphere at several fixed Northern Hemisphere mid latitude sites. These two data sets have been combined to give a mid latitude, interim reference water vapor profile for the entire vertical range of the middle atmosphere and with accuracies of better than 25 percent. The daily variability of stratospheric water vapor profiles about the monthly mean has also been established from these data sets for selected months. Information is also provided on the longitudinal variability of LIMS water vapor profiles about the daily, weekly, and monthly zonal means. Generally, the interim reference water vapor profile and its variability are consistent with prevailing ideas about chemistry and transport.

INTRODUCTION

Water vapor (H_2O) is an important minor constituent in the middle atmosphere for several reasons. It is a major source of the active chemical radicals, OH and HO_2, which affect the ozone distribution in the mesosphere /1/ and upper stratosphere /2/. Water vapor plays a significant role in the ion cluster chemistry of the mesosphere /3, 4/. Condensed phase water in the form of nacreous or polar stratospheric clouds at high latitudes of the winter hemisphere is regulated by the water vapor mixing ratio and atmospheric temperatures needed to reach saturation /5/. Similar constraints apply for the noctilucent or polar mesospheric clouds that occur near the summer polar mesopause /6/. The infrared emission from water vapor in the upper troposphere helps determine the temperature distribution at the lower boundary of the middle atmosphere. Water vapor also contributes in a minor way to the radiative balance throughout the middle atmosphere /7/. For most of the middle atmosphere, water vapor can be used as a tracer molecule to describe a net global transport or circulation there /8, 9/. Knowledge of the peak mesospheric H_2O mixing ratio, the altitude of the peak value, and the rate of mixing ratio decrease above the altitude peak is needed to validate chemical/transport models and to gain an improved understanding of seasonal changes in the mesosphere /10/. Finally, the long-term trend in middle atmosphere water vapor can be an indicator of trends in minimum tropical tropopause temperatures, coupled with the effect in the upper stratosphere of the increase in methane, which is a source gas of water vapor there /11/.

Russell /12/ presented a comprehensive review with references for those satellite and in situ data sets that are generally available for defining the distribution of middle atmosphere water vapor. The primary data source for those distributions was derived from the 7 months of observations from the Nimbus 7 Limb Infrared Monitor of the Stratosphere (LIMS) experiment which began operations in late October 1978. Data were obtained from 64S to 84N latitude and from about 1-mb to 100-mb. Those data were supplemented with results from the Grille Spectrometer on Spacelab 1 /13/ and the host of microwave radiometer measurements of water vapor (e.g. /14/) to produce a Northern Hemisphere mid latitude reference profile for the winter/spring seasons from about 100- to 0.005-mb. Profiles of water vapor by several different techniques from rocket soundings at high latitudes of the Northern Hemisphere are also available (e.g. /15/), and they may be used

to supplement LIMS results above 1-mb. The rocket data and techniques were reviewed in /7/. Because those soundings have occurred sporadically over a 10-year period, no attempt has been made to develop a reference profile of water vapor variability for the high latitude mesosphere. Information is lacking on mesospheric water vapor measurements at low latitudes or in the Southern Hemisphere. Finally, measurements of water vapor using balloon-borne and airborne techniques have provided considerable information about the water vapor profile in the mid to low stratosphere /2/. In particular, Mastenbrook and Oltmans /16/ report a 16-year time series of measurements using frost-point hygrometer soundings near Washington, D.C. A similar series is now available for 1981-1986 from measurements at Boulder, Colorado /17/.

Although a climatology of middle atmosphere water vapor has yet to be achieved, there is now sufficient information for establishing a reference model for some latitudes and seasons. This model is heavily weighted by the extensive LIMS data set (see /12/ for details). Tabulated reference profiles are given in this paper, along with their estimated uncertainties. In addition, new information is presented on the longitudinal variations about the zonal mean profiles, on the monthly variations of the zonal mean distributions, and time series of the zonal mean and wave amplitudes on a pressure surface. Variability of mesospheric water vapor on daily to seasonal timescales is also presented using data from ground-based microwave radiometers at Northern Hemisphere mid latitudes. All of these results should provide adequate information about middle atmospheric water vapor for initial scientific studies and for use in comparisons with modeled distributions of water vapor and the association of the HO_x and O_x chemical families.

MONTHLY ZONAL MEAN LIMS WATER VAPOR DISTRIBUTIONS

The quality of the individual LIMS water vapor profiles (LAIPAT tapes) archived at the National Space Sciences Data Center (NSSDC) in Greenbelt, Maryland, has been discussed in /12, 18, 19/. An extensive study was conducted to validate the LIMS data and to establish any limitations of the results. Table 1 from /12/ summarizes those results and is reproduced here. Note that the measured precision in orbit (geophysical plus instrument effects) is about 0.2 to 0.3 ppmv from 50- to 2-mb, decreasing to 0.7 ppmv at 1-mb. Single profile accuracy at mid and high latitudes varies from 30 percent near the stratopause to 20 percent in the mid stratosphere and 37 percent at 50-mb. Accuracy estimates are better for zonal mean LAIPAT profiles, becoming 27 percent, 17 percent, and 20 percent, respectively /20/.

Russell et al. /18/ noted that there is an apparent diurnal variation in water vapor (day values higher than night values) of as much as 1 to 2 ppmv near 1-mb, decreasing to 0.2 ppmv near 10-mb. Kerridge and Remsberg /21/ have found that the probable explanation for the difference is the presence during daytime of small radiance contributions from vibrationally excited water vapor and, especially, NO_2 at the long wavelength side of the LIMS water vapor channel. Correction for these effects in the retrieval eliminates the bias between day and night water vapor. Because corrections for these mechanisms have not been applied to the archived data and because these mechanisms are inoperative at night, we have chosen to present LIMS reference profiles and variability using only nighttime water vapor data.

Over most of the stratosphere, the other principal systematic error in water vapor is due to bias errors in temperature through the retrieval. Such biases can affect either night or day data. An extreme example of this occasional problem was pointed out in /22/, Figs. 6c and 7, for a situation when large vertical and horizontal gradients in temperature existed at high northern latitudes in early February 1979. The effect on water vapor there is of the order of several ppmv. On the other hand, a much more prevalent, positive temperature bias occurs near the tropical tropopause. That bias is estimated to yield water vapor values that are too low between ±15 degrees latitude by about 0.3 ppmv at 50-mb and 0.6 ppmv at 70-mb, with only half that bias at ±25 degrees latitude /19/. However, no such corrections have been applied to the archived data.

The monthly mean profiles derived from the archived vertical profile tapes (LAIPAT) were presented for the latitude zones 32S-56S, 28S-28N, 32N-56N, and 56N-84N in /12/--his Tables 4 and 5. The average profile for 28S-28N was adjusted for the temperature bias effect at 50-mb and 70-mb. Results for each latitude zone have been interpolated linearly in log pressure to yield the reference profiles in Tables 2 and 3. The zonal mean distributions are shown in Fig. 1 (a through g). Similar figures have been produced from the LIMS Map Archive Tapes (LAMAT) at NSSDC /23/, and a detailed description of that product is given in /22/.

Tables 2 and 3 also contain information about the standard deviation of the daily nighttime zonal means about the monthly nighttime zonal mean and, in general, the changes

TABLE 1 LIMS H_2O Estimated Accuracy and Correlative Measurement Comparison Statistics

Pressure (mb)	Measured On-Orbit Precision (ppmv)	Estimated Accuracy (%)†	Comparison with Correlative Measurements*	
			Mean Difference (%)	RMS Difference (%)
5	0.2	24	-20.9	41.1
7			-18.0	47.2
10		20	- 6.5	24.8
15			7.1	28.7
20			16.3	23.5
30	0.3	23	21.4	27.6
50		37	10.1	28.4
70			- 7.7	28.8
100		39	18.6	28.9

†Based on measured instrument parameters and computer simulations based on 13 comparisons with balloon remote and in situ H_2O measurements.

*Based on 13 comparisons with balloon remote and in situ H_2O measurements.

TABLE 2 LIMS Monthly Zonal Mean H_2O Mixing Ratio Profiles in the 32°S - 56°S and 28°S - 28°N Latitude Ranges For November 1978 through May 1979

Pressure (mb)	MEAN WATER VAPOR MIXING RATIO (ppmv) ± STANDARD DEVIATION (ppmv) OF THE DAILY ZONAL MEAN ABOUT THE MONTHLY MEAN													
	32°S - 56°S							28°S - 28°N*						
	Nov.	Dec.	Jan.	Feb.	March	April	May	Nov.	Dec.	Jan.	Feb.	March	April	May
1.5	4.9±.28	4.9±.27	4.9±.25	4.7±.26	4.5±.31	4.4±.38	4.4±.45	5.4±.36	5.1±.41	5.0±.33	5.0±.34	5.2±.32	5.1±.32	5.1±.33
2.0	4.9±.22	4.9±.22	4.9±.19	4.7±.20	4.4±.25	4.2±.30	4.2±.35	5.1±.27	4.9±.30	4.8±.25	4.7±.25	4.9±.24	4.9±.24	4.9±.26
3.0	4.8±.16	4.9±.16	4.9±.14	4.7±.16	4.4±.17	4.2±.23	4.1±.30	4.8±.20	4.6±.23	4.5±.20	4.4±.19	4.6±.19	4.6±.18	4.7±.21
5.0	4.7±.13	4.8±.14	4.7±.12	4.6±.12	4.4±.13	4.3±.19	4.1±.21	4.3±.16	4.2±.18	4.1±.16	4.1±.16	4.2±.15	4.3±.14	4.3±.15
7.0	4.6±.12	4.7±.12	4.6±.10	4.5±.10	4.5±.12	4.4±.16	4.3±.19	4.1±.14	4.0±.15	4.0±.15	4.0±.13	4.1±.13	4.1±.11	4.1±.12
10.0	4.7±.12	4.7±.10	4.7±.09	4.6±.09	4.7±.11	4.6±.14	4.6±.18	4.1±.12	4.1±.12	4.1±.11	4.0±.11	4.0±.11	4.0±.09	4.0±.10
16.0	4.8±.12	4.7±.11	4.7±.09	4.7±.09	4.8±.11	4.8±.13	4.8±.18	4.2±.09	4.2±.12	4.1±.11	4.0±.11	4.0±.09	3.9±.07	4.0±.10
30.0	4.7±.12	4.7±.13	4.6±.10	4.6±.11	4.8±.12	4.9±.12	5.0±.19	3.9±.09	3.9±.11	3.7±.12	3.7±.11	3.7±.11	3.8±.10	3.9±.10
50.0	4.1±.15	3.9±.15	3.8±.11	3.8±.12	4.1±.17	4.5±.17	4.8±.23	2.8±.12	2.7±.13	2.6±.14	2.5±.12	2.6±.13	2.7±.13	2.8±.11
70.0	3.9±.18	3.7±.16	3.5±.14	3.5±.14	3.8±.20	4.4±.23	4.9±.30	2.8±.23	2.6±.26	2.6±.27	2.4±.25	2.4±.30	2.5±.26	2.7±.22
100.0	4.5±.25	4.2±.30	4.1±.24	4.2±.25	4.6±.23	5.3±.30	5.8±.47	3.9±.41	3.6±.64	3.7±.51	3.5±.61	3.4±.60	3.6±.55	3.9±.46

*Mixing ratios at the 50-mb and 70-mb levels have been increased by + 0.15 and 0.3 ppmv, respectively, to account for water vapor bias effects described in /18, 19/.

TABLE 3 LIMS Monthly Zonal Mean H_2O Mixing Ratio Profiles in the 32°N - 56°N and 56°N - 84°N Latitude Ranges For November 1978 through May 1979

Pressure (mb)	MEAN WATER VAPOR MIXING RATIO (ppmv) ± STANDARD DEVIATION (ppmv) OF THE DAILY ZONAL MEAN ABOUT THE MONTHLY MEAN													
	32°N - 56°N							56°N - 84°N						
	Nov.	Dec.	Jan.	Feb.	March	April	May	Nov.	Dec.	Jan.	Feb.	March	April	May
1.5	5.2±.49	4.9±.45	4.9±.37	4.9±.34	5.2±.37	5.4±.26	5.5±.24	5.0±.64	4.4±.62	4.5±.94	4.6±.46	5.2±.41	5.2±.24	5.1±.20
2.0	4.8±.37	4.7±.41	4.7±.30	4.7±.27	5.0±.32	5.2±.22	5.3±.19	4.7±.51	4.3±.55	4.4±.95	4.5±.36	4.8±.35	5.0±.21	5.1±.16
3.0	4.5±.29	4.5±.40	4.7±.26	4.7±.23	4.9±.26	5.2±.10	5.3±.15	4.6±.46	4.5±.51	4.6±.62	4.6±.32	4.7±.28	5.0±.23	5.1±.12
5.0	4.4±.24	4.4±.31	4.6±.22	4.6±.19	4.8±.18	4.9±.15	5.0±.13	4.7±.39	4.7±.47	4.7±.40	4.7±.27	4.8±.23	5.0±.20	5.1±.11
7.0	4.5±.21	4.4±.26	4.5±.22	4.5±.17	4.7±.14	4.8±.13	4.9±.12	4.7±.33	4.8±.44	4.8±.36	4.8±.25	4.8±.20	4.9±.16	5.0±.10
10.0	4.7±.18	4.5±.25	4.6±.20	4.6±.16	4.7±.12	4.7±.12	4.7±.12	4.9±.31	4.9±.42	5.0±.32	5.0±.27	4.9±.16	5.0±.13	5.1±.09
16.0	4.8±.17	4.7±.23	4.7±.20	4.6±.15	4.6±.12	4.7±.11	4.7±.12	5.0±.29	4.8±.34	5.0±.30	5.3±.30	5.0±.15	5.0±.13	5.1±.09
30.0	4.5±.17	4.6±.23	4.7±.22	4.8±.17	4.6±.13	4.7±.11	4.7±.11	5.0±.24	4.8±.33	4.9±.35	5.5±.23	5.3±.19	5.1±.11	5.2±.13
50.0	4.1±.21	4.1±.28	4.3±.24	4.4±.22	4.3±.19	4.4±.12	4.0±.13	4.9±.23	4.8±.34	4.7±.37	5.1±.39	5.3±.19	5.0±.13	4.9±.13
70.0	4.1±.27	4.2±.34	4.4±.29	4.4±.27	4.1±.29	4.4±.16	3.8±.15	5.2±.28	5.1±.43	4.8±.39	5.2±.46	5.4±.22	5.1±.18	4.8±.15
100.0	5.2±.41	5.0±.55	[illegible]	5.0±.46	4.7±.52	6.0±.28	4.3±.28	6.6±.43	6.4±.64	5.7±.58	6.0±.59	6.0±.32	5.7±.26	5.2±.21

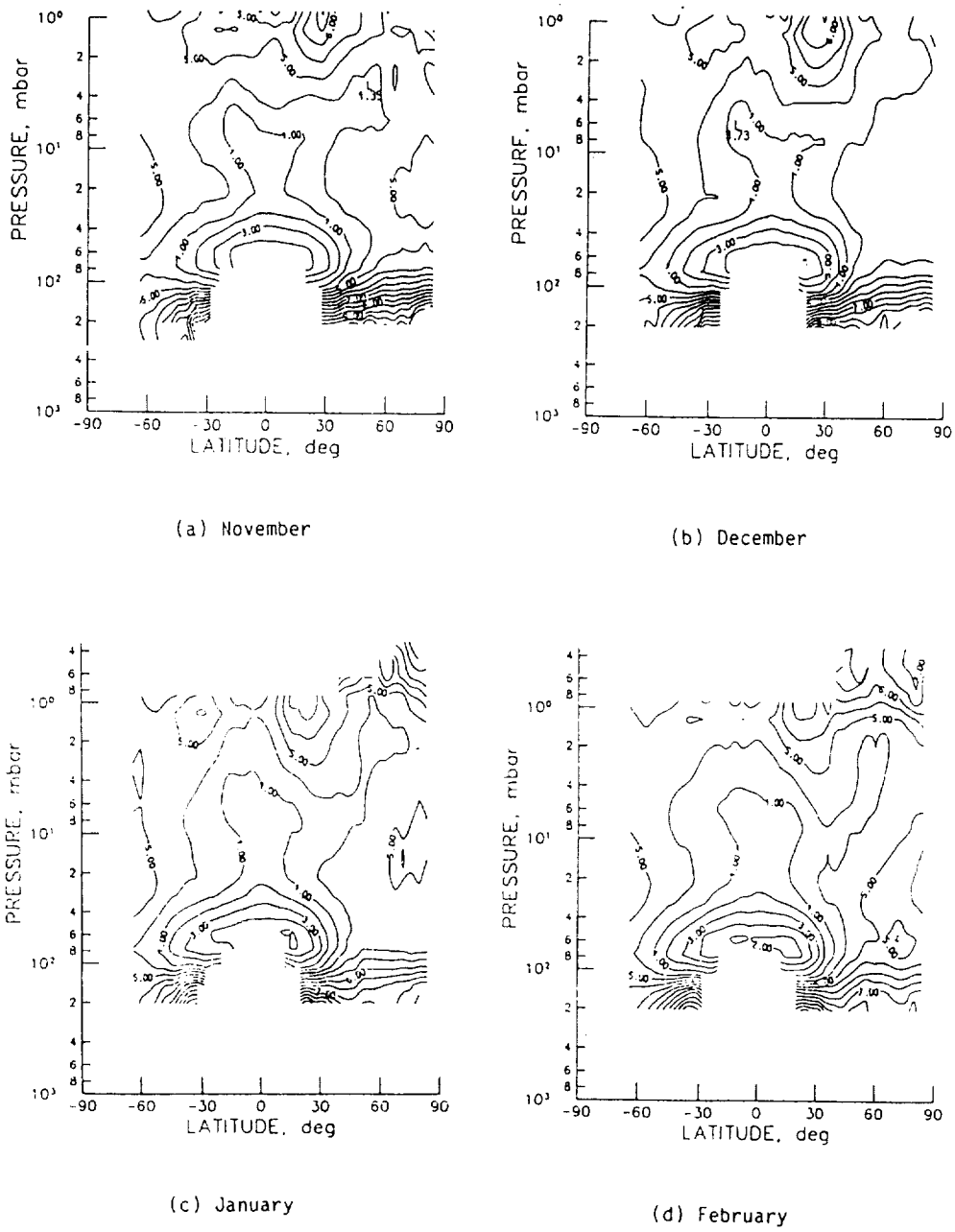

Figure 1. LIMS H_2O zonal mean pressure versus latitude cross section for descending orbital data. Countour interval 0.5 ppmv. (a) November, (b) December, (c) January, (d) February, (3) March, (f) April and (g) May.

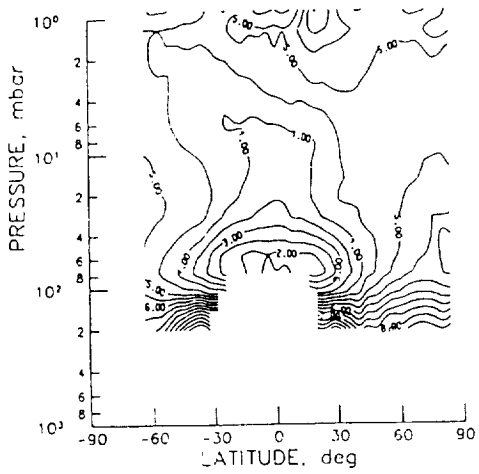

(e) March

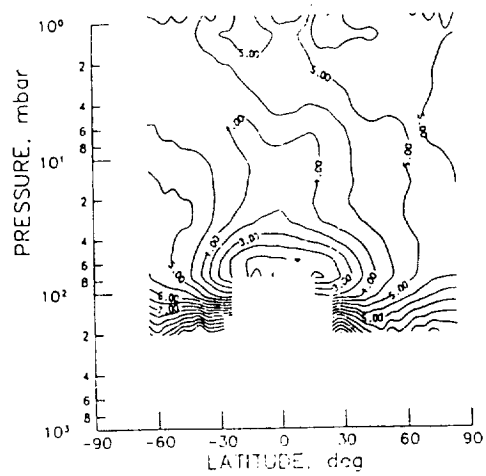

(f) April

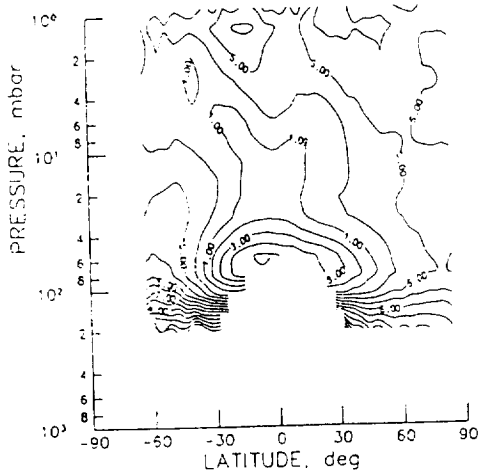

(g) May

Figure 1 continued.

are very small. Figure 2 (a,b) shows those results for the months of November and May. Zonal mean deviations are minimal in the mid stratosphere, and they are a bit smaller for late autumn versus late spring, possibly due to a stronger net transport during late autumn.

Day-to-day zonal mean variability in Fig. 2 near 1-mb is about 15 percent, which is larger than expected for the real atmosphere. However, a significant fraction of that variability is due to random error in the measured radiances and from uncertainties in the retrieval at the tops-of-profiles. According to /18/, radiance signal-to-noise (S/N) for individual profiles is only about 2 to 3 at 1-mb. In fact, variations near 1-mb may be more indicative of data quality there than independent simulations of known LIMS error mechanisms. In that regard, it is also noted that variability at 1-mb decreases at 60S in November (Fig. 2a) and at 60N in May (Fig. 2b).

Seasonal mean mixing ratios are given in Table 4 from the LIMS data, along with the daily variations about the seasonal means. If one compares the northern and southern mid latitude zones (32-56 degrees latitude), it is clear that more change is occurring in winter versus summer, i.e., standard deviations are larger by a factor of 2 in winter. This difference is most likely related to the relative absence of net transport due to stratospheric wave activity in mid latitude summer /24/.

Changes in the monthly zonal mean water vapor cross sections (Fig. 1) occur smoothly with time over the 7 months. In fact, the November and May distributions are nearly mirror images. Between 10-mb and 1-mb, the largest change in the distribution occurs from January to March at a time when the diabatic circulation is undergoing a similar shift /25/. These changes in the net circulation are also being influenced by strong gradients in radiative cooling in the Northern Hemisphere in response to the poleward heat transport by enhanced planetary wave activity.

Seasonal changes are also apparent at mid latitudes of the lower stratosphere, but water vapor variations at the tropical hygropause are less apparent from the zonal mean data. Tropical forcing due to the semiannual oscillation (SAO) is most pronounced in late winter to early spring, which must contribute to the appearance of a double minimum in water vapor near 7-mb on either side of the Equator during April and May /26/.

The relative water vapor maxima near 1-mb and above and between 60N and 84N in January and February 1979 (Fig. 1 c,d) are not believed to be real for the following reasons. The production of nitric oxide (NO) by auroral particle precipitation followed by partitioning between NO and NO_2, and downward transport by the mean meridional circulation in the polar winter mesosphere has been analyzed /27/. Kerridge and Remsberg /21/ have shown that the vibrationally excited emission from this relatively large amount of mesospheric NO, in polar night must be accounted for during the H_2O retrieval in order to give accurate water vapor levels. After correcting for these effects, the water vapor values are not elevated there, and they appear to be more in line with the idea that there is a net downward transport of relatively dry air from mesosphere to stratosphere at high latitudes of the winter hemisphere /28/.

Global-average estimates of the LIMS water vapor have been prepared for December-January-February and March-April-May, along with estimates of accuracy in the zonal mean (Fig. 3). Water vapor values for each 4 degree latitude zone are multiplied by the fractional global area due to that zone, followed by a sum over all zones, to yield an area-weighted profile for comparison with one-dimensional models. Mixing ratios at 64S were extended to 90S and values at 84N were extended to 90N, but because those areas represent only 5 percent of the globe, the uncertainty due to the extrapolation is small. The average mixing ratio is nearly constant at 4.4 ppmv from 30- to 5-mb, decreasing to 3.5 ppmv at 50-mb. Mixing ratios increase from 4.4 ppmv at 5-mb to 5.0 ppmv at 1.5-mb, consistent with the idea of methane oxidation as a source of water vapor in the upper stratosphere (see also /19, 29/). The estimated accuracy at 1-mb is poorer than the difference between the mean values at 1-mb and 1.5-mb, so interpretations of the increase from 1.5- to 1-mb are not meaningful; this is not the case at 50-mb.

Prior to the existence of the LIMS data set, there was still some uncertainty about the magnitude and even the sign of the meridional gradient of water vapor. Given the precision, accuracy, and general physical consistency of the LIMS water vapor, there is no reason to doubt results such as those displayed for 2 January 1979, in Fig. 4, where meridional gradients are shown at 50-mb, 10-mb, and 3-mb. Based on current understanding of the measurements, the only caveat to these gradients would be a probable H_2O underestimate of 0.3 ppmv between ±15 degrees latitude at 50-mb.

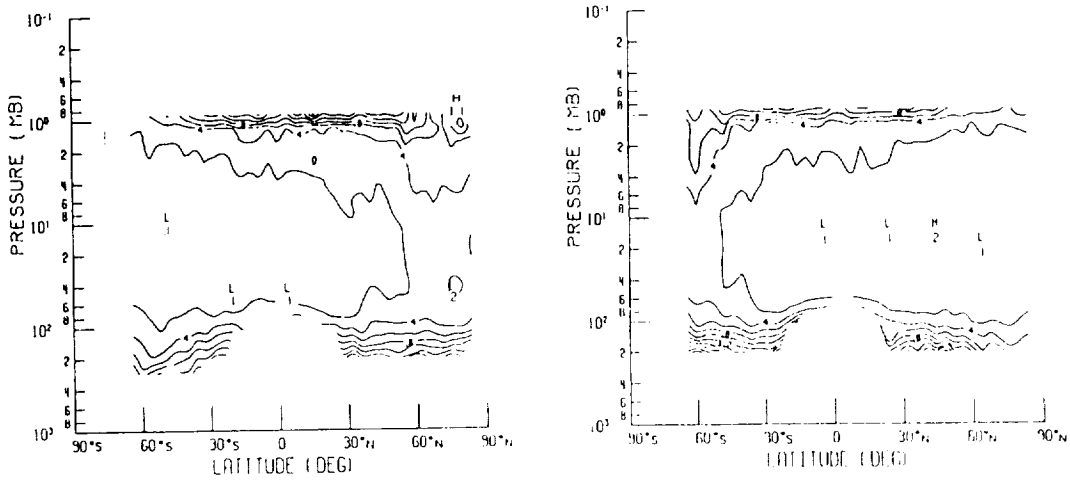

2(a) November

2(b) May

Figure 2. LIMS H_2O standard deviation (ppmv) of daily zonal mean profiles about the monthly zonal mean. (a) November and (b) May.

TABLE 4 LIMS Zonal Mean H_2O Profiles (ppmv) ± Standard Deviation of the Daily Zonal Mean about the Seasonal Mean for Various Latitude Bands for Northern Hemisphere winter (November, December, January) and Spring (March, April, May).

Pressure	32°N - 56°N**		28°S - 28°N*		32°N - 56°N		56°N - 84°N	
(mb)	Summer	Autumn	Winter	Spring	Winter	Spring	Winter	Spring
1.5	4.9±.29	4.5±.42	5.2±.41	5.1±.37	5.0±.49	5.4±.27	4.6±.61	5.2±.38
2.0	4.9±.23	4.3±.35	4.9±.32	4.9±.29	4.8±.38	5.2±.27	4.4±.51	5.0±.38
3.0	4.8±.16	4.2±.30	4.6±.26	4.6±.22	4.6±.33	5.1±.27	4.6±.46	5.0±.35
5.0	4.7±.13	4.2±.24	4.2±.20	4.3±.17	4.5±.28	4.9±.21	4.7±.42	4.9±.26
7.0	4.6±.12	4.3±.20	4.0±.17	4.1±.14	4.4±.26	4.8±.17	4.7±.39	4.9±.20
10.0	4.7±.11	4.6±.17	4.1±.14	4.0±.12	4.6±.26	4.7±.16	4.9±.39	5.0±.16
16.0	4.7±.12	4.8±.16	4.2±.12	4.0±.10	4.7±.23	4.7±.14	4.9±.36	5.0±.14
30.0	4.7±.13	4.9±.16	3.8±.14	3.8±.13	4.6±.22	4.7±.12	4.9±.36	5.2±.18
50.0	3.9±.17	4.5±.32	2.8±.16	2.7±.17	4.2±.27	4.1±.18	4.8±.35	5.1±.24
70.0	3.7±.24	4.3±.47	2.7±.29	2.5±.31	4.2±.32	3.9±.27	5.1±.41	5.1±.30
100.0	4.3±.33	5.2±.62	3.7±.54	3.7±.57	5.1±.53	4.5±.39	6.2±.64	5.7±.44

*Mixing ratios at the 50-mb and 70-mb levels have been increased by 0.15 and 0.3 ppmv, respectively, to account for water vapor bias effects described in /18, 19/.

**The November, December, and January average is summer in the Southern Hemisphere and March, April, and May is autumn.

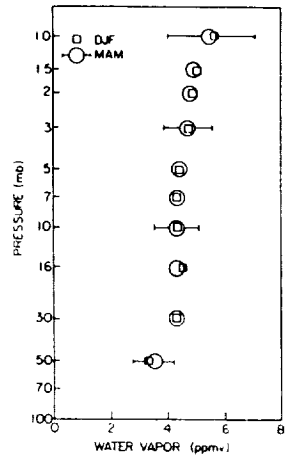

Figure 3. Global area-weighted average LIMS H_2O nighttime profiles for December, January, and February (□) and March, April, and May (O). Horizontal bars represent accuracy of zonal mean.

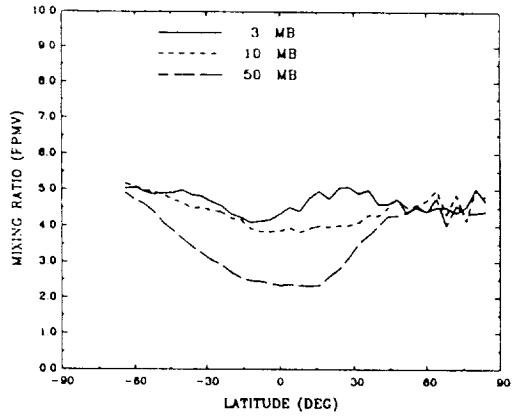

Figure 4. LIMS zonal mean H_2O mixing ratio versus latitude at 3-, 10-, and 50-mb on January 2, 1979.

ZONAL VARIATIONS IN LIMS WATER VAPOR

Estimates of variations about the zonal mean have been determined from the archived LAIPAT by calculating a 5-day zonal mean cross section and determining the standard deviation in ppmv of the individual profiles about the mean result. Figure 5a is an example for 5 days of data between 20-26 May 1979. These variations include both "noise" and real wave activity. Minimum May standard deviations of 0.4 ppmv occur near 20-mb at low latitudes and in the Northern Hemisphere when wave activity is expected to be weak. Variations in the upper stratosphere are related more to the noise associated with the low signal-to-noise at tops of profiles, while increases in the absolute variations at 100-mb and below are due, in part, to the fact that water vapor mixing ratios increase sharply at these levels such that small variations in the pressure registration of the water vapor radiance profiles have become significant. The larger standard deviations in the mid stratosphere at 40S to 64S are most likely due to enhanced wave amplitudes there during late autumn (see also /30/). Figure 5b is similar to 5a, but for 27-31 October 1978. Again, the hemispheric mirror image is apparent between the two periods.

Water vapor variability is presented for another period, 1-5 February 1979, that was dynamically active in the Northern Hemisphere. Figures 6a and 6b show results for ascending (or day) and descending (or night) data at 5-mb and 50-mb. Note that regardless of the day/night difference of about 0.5 ppmv (not shown) that exists in the zonal mean result at 5-mb and Equator, the standard deviations about the respective ascending and descending zonal means are very similar in Fig. 6a. At 5-mb, there appears to be a gradual increase in variability from 60S to North Pole. However, if the water vapor field near 5-mb possesses weak meridional and vertical gradients (Fig. 1d), the effect of atmospheric waves on the field will be unnoticed. Conversely, variations at 50-mb (Fig. 6b) are nearly constant at 0.4 ppmv from 64S to 30N, but by 60N, they have increased by a factor of 3 to 1.2 ppmv. From Fig. 1d, one can see that there are strong meridional gradients at 50-mb at mid latitudes of both hemispheres, so low standard deviations in the Southern Hemisphere are indicative of little wave activity, while such activity is more apparent in the Northern Hemisphere. For example, the north polar vortex is shifted off the Pole in early February 1979, so a strong wave 1 amplitude should be evident. A time series of the wave 1 amplitude in ppmv at 5-mb and 50-mb was determined from the zonal, Fourier coefficient form of the LIMS data set /22/. The Fourier analysis yields wave 1 amplitudes of 0.2 to 0.4 ppmv at 5-mb for day 100 (1 February) or about one-half the variability in Fig. 6a. Figure 7 for 50-mb shows that the wave 1 amplitudes for day 100 are 0.6 to 1.0 ppmv from 60N to 80N, accounting for most of the variation in Fig. 6b. Previous analyses have also shown good correspondence in the patterns of the large-scale water vapor fields and coincident maps of geopotential height or potential vorticity, in line with ideas about water vapor being an appropriate tracer of transport processes throughout the middle atmosphere /22, 31/.

VARIABILITY OF MESOSPHERIC WATER VAPOR

Information about mesospheric water vapor and its variations is available from two extensive data sets. First, because of the analyses conducted in /21/, more confidence can be placed in the lower mesospheric nighttime water vapor values reported by /32/ from LIMS results (winter/spring 1978-1979) between 0.5-mb and 1.5-mb as retrieved from specially processed, averaged radiance profiles. Secondly, sets of water vapor profiles derived from ground-based measurements of microwave emission were reported for spring 1984 at Jet Propulsion Laboratory (JPL), California (34N, 50- to 85-km) /33/, for winter/spring 1985 from JPL at 60- to 80-km by /34/, and for spring 1984 at Pennsylvania State University (PSU) (41N, 65- to 80-km) by /35/. The microwave measurement technique and earlier H_2O results are summarized briefly in /12/.

Bevilacqua et al. /33/ reported a monthly increase in water vapor of a factor of 2 at 75-km from April to June 1984, and they concluded that the change was due to a seasonal variation in mixing due to gravity wave breaking. Comparisons of the 1984 and 1985 profiles at 34N indicate general agreement in shape and magnitude from 60- to 80-km. Comparisons with data obtained in the early 1980's at Haystack Observatory (43N) reported by /36, 14/, indicate slightly lower mixing ratios for spring than at JPL. Tsou et al. /35/ find a similar difference between the 1984 results at JPL and PSU, which they attribute to latitudinal and/or longitudinal variations in the occurrence of breaking gravity waves. Gordley et al. /32/ also found a definite latitudinal variation in LIMS zonal mean water vapor in the lower mesosphere with values at 34N being greater than those at 41N and 43N by about 1 ppmv. Thus, LIMS provides supporting evidence that there are latitudinal variations in mesospheric water vapor.

An estimate of a mean water vapor profile in the mesosphere at Northern Hemisphere mid latitudes has been derived for spring (April and May) from 1.5-mb to 0.01-mb by using the radiance-averaged LIMS data from 1.5- to 0.5-mb, plus the microwave results above that.

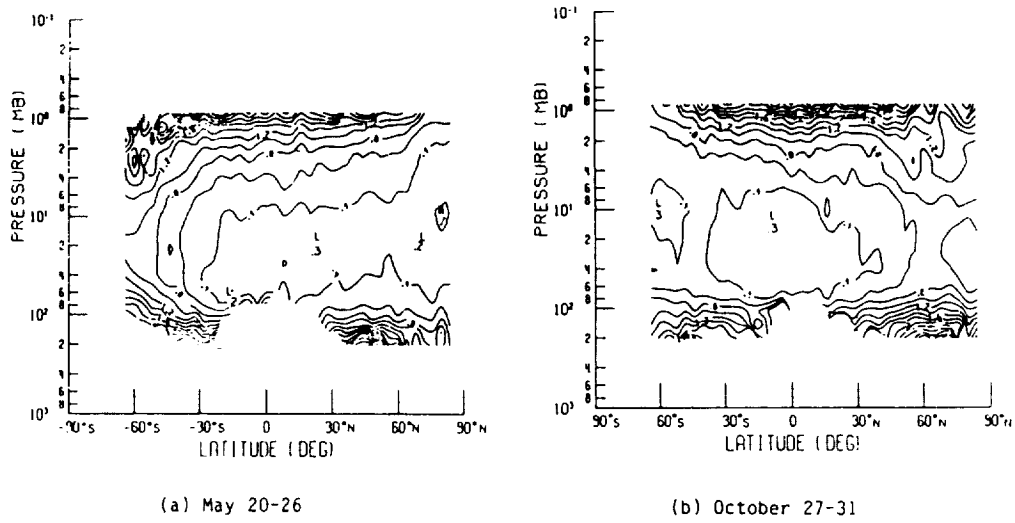

Figure 5. LIMS H_2O standard deviation (ppmv) of individual profiles about the zonal mean for (a) May 20-26 and (b) October 27-31.

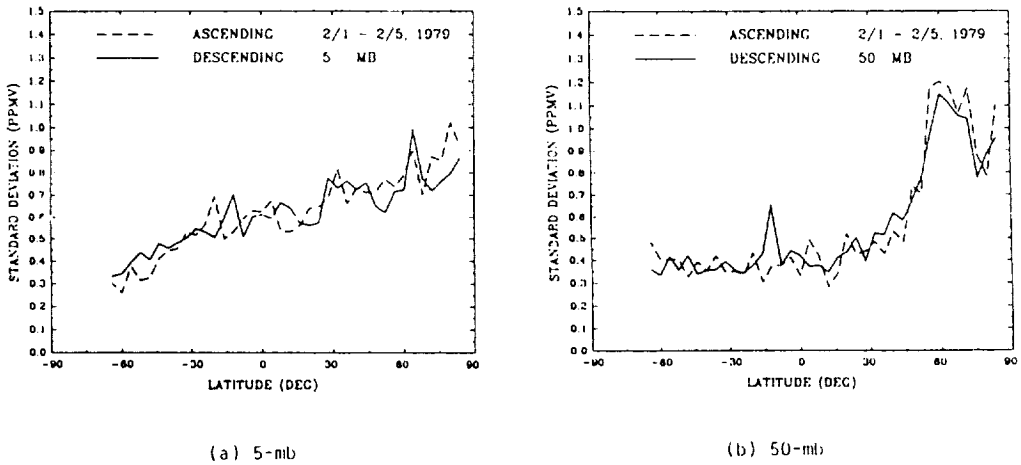

Figure 6. LIMS H_2O standard deviation (ppmv) versus latitude for individual profiles about the 5-day zonal mean for February 1-5, 1979, at (a) 5-mb and (b) 50-mb.

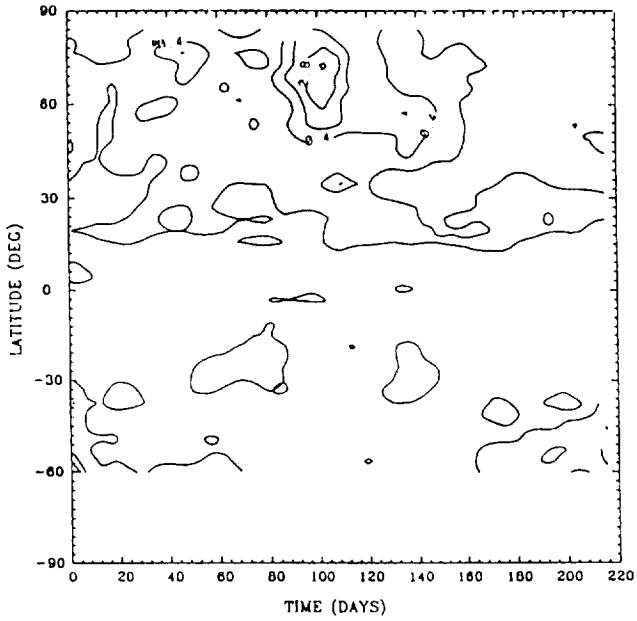

Figure 7. LIMS descending mode H_2O wave 1 amplitude (ppmv) for October 25, 1978 to May 28, 1979 at 50-mb.

Table 5 contains the 2-month average, plus the monthly difference profiles from the combined data sets. Data from Fig. 8 of /35/ were used from 0.1- to 0.01-mb, and LIMS data prepared in the manner described in /32/ were used for 1.5- to 0.5-mb. The average values at 0.2-mb (near 60-km) in Table 5 were obtained from the Haystack results (43N) of /36/, their Fig. 2, plus the JPL results (Fig. 4 of /33/).

A REFERENCE WATER VAPOR PROFILE AND ITS VARIABILITY

A springtime, Northern Hemisphere, mid latitude water vapor profile and its variability were constructed from the data in Table 5 and from the mean spring results at 32N to 56N in Table 4 from 2.0-mb to 100-mb. Variability from 2.0-mb to 100-mb for mid latitude spring was derived by combining data on variations of single LIMS profiles about the 5-day zonal mean as in Fig. 5, plus the variation of the daily zonal mean profiles about the seasonal mean in Table 4. Variations from 0.5- to 1.5-mb were set to those at 2.0-mb, since information on variability about the zonal mean is lacking for that region. Variations from 0.2- to 0.01-mb were derived by averaging the differences between the April and May profiles at 34N, 41N, and 43N from /35/ and /36/. Figure 9 in /35/ contains information about the larger water vapor variations for the daily time series for each month, but because these variations were not tabulated, they were not included in the variability for the reference profile. This means that the real atmospheric variability at those levels is being underestimated here. The final combined profile is given in Table 6 and Fig. 8. It is also noted that this profile is somewhat different from the combined profile in Table 7 of /12/ because that earlier profile contained an average of several different kinds of mid latitude mesospheric measurements, it was derived as a winter/spring average, and for the LIMS data, it only contained variations of the daily zonal means about the seasonal means.

The profile in Fig. 8 contains only LIMS data, plus monthly averages of microwave emission results, some of which were published in the past year. The profile is also only appropriate for Northern Hemisphere spring. Nevertheless, this reference model has a constant mixing ratio of 4.7 ppmv from 30- to 7-mb, gradually increasing to 6.0 ppmv at 0.2-mb, then decreasing rapidly to 1.3 ppmv at 0.01-mb. The determination of the vertical position and magnitude of the peak mixing ratio at 0.2-mb must be considered uncertain because the one sigma error for that measurement is about 1.5 ppmv /33/. Obviously, more mesospheric data are needed at other seasons and latitudes and longitudes before additional reference profiles can be prepared for the middle atmosphere. Mean mixing ratios decrease to 4.0 ppmv at 50- to 70-mb, reflecting the net poleward transport of relatively dryer air from tropical latitudes.

DISCUSSION AND CONCLUSIONS

This analysis is an update of the review by /12/ on interim reference profiles for middle atmospheric water vapor. New emphasis is given to estimates of the observed variability of stratospheric water vapor using the winter/spring data from the Nimbus 7 LIMS experiment from 64S to 84N. Some initial results obtained by averaging the LIMS radiance data before retrieval are used to decrease the uncertainty in archived LIMS results from 1- to 2-mb, as well as to extend results upward to 0.5-mb. Monthly zonal mean LIMS cross sections are shown to vary smoothly over the 7 months of the data set, and these results plus global average estimates of the seasonal mean water vapor profile are physically consistent with prevailing ideas about the sources, sinks, and mechanisms affecting the water vapor distributions. Longitudinal variations about the zonal mean distribution are generally small, except in the lower stratosphere where the meridional gradient in water vapor is also large enough to reflect the effects of transport and mixing due to waves during dynamically active periods of the winter hemisphere. An extensive set of microwave emission measurements of mesospheric water vapor is included, along with LIMS data, to determine a mesospheric reference profile from 0.2- to 0.01-mb for Northern Hemisphere mid latitudes in spring. The observed variability for spring appears to be real and probably is related to variations in mean vertical advection.

Several additional water vapor data sets are expected shortly. The most extensive will be the multiyear, near-global data set from the Stratospheric Aerosol and Gas Experiment (SAGE II) underway since late 1984 /37/. This experiment is providing water vapor profiles by solar occultation for the entire stratospheric altitude range. Data from the Spacelab 3 ATMOS experiment in May 1985 should also be available soon, and they are expected to extend from 20- to 80-km. Peter et al. /38/ will report H_2O results from 20 to 70 km and 45N to 75N for December 1986 using an airborne millimeter-wave instrument. The stratospheric results are consistent with those from LIMS. In the near future, it is also anticipated that permanent millimeter-wave emission instruments will be installed at sites to be designated as part of a proposed Network for the Detection of Stratospheric Change (NDSC). Based on the LIMS results in the lower mesosphere, it appears that the profile at low latitudes is somewhat different from that at mid latitudes, so a continuous measurement is needed there.

TABLE 5 Mesospheric Mean Water Vapor Profile for Northern Hemisphere Spring at Mid Latitudes

Pressure (mb)	H_2O Mixing Ratios (ppmv)*
0.01	1.4 ± 0.6
0.025	2.0 ± 0.6
0.05	3.3 ± 0.9
0.1	5.0 ± 0.7
0.2	6.0 ± 1.0
0.5	5.5 ± 0.6
0.7	5.5 ± 0.5
1.0	5.1 ± 0.3
1.5	5.0 ± 0.2

*Specially averaged LIMS data are from 1.5-mb to 0.5-mb. Microwave data are from 0.2-mb to 0.01-mb. Variability is defined in the text.

TABLE 6 Mid Latitude Interim Reference Profile for 32°N - 56°N Spring Obtained Using LIMS Data from 100-mb to 0.5-mb and Microwave Data from 0.2-mb to 0.01-mb. Variability is defined in the text.

Pressure (mb)	H_2O Mixing Ratios (ppmv)
0.01	1.4 ± 0.6
0.025	2.0 ± 0.6
0.05	3.3 ± 0.9
0.1	5.0 ± 0.7
0.2	6.0 ± 1.0
0.5	5.5 ± 1.2
0.7	5.5 ± 1.2
1.0	5.1 ± 1.2
1.5	5.0 ± 1.2
2.0	5.2 ± 0.9
3.0	5.1 ± 0.8
5.0	4.9 ± 0.5
7.0	4.8 ± 0.4
10.0	4.7 ± 0.4
16.0	4.7 ± 0.4
30.0	4.7 ± 0.4
50.0	4.1 ± 0.4
70.0	3.9 ± 0.5
100.0	4.5 ± 0.7

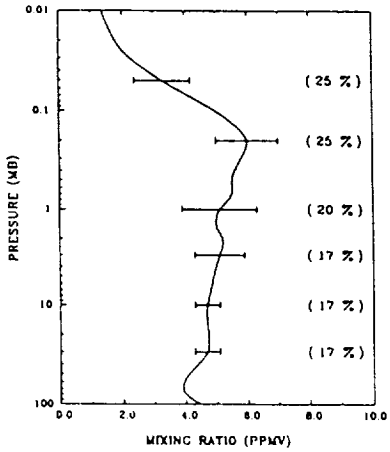

Figure 8. H_2O interim reference profile for Northern Hemisphere midlatitude springtime. Bars represent variability of the data. Numbers in parentheses represent estimated accuracies.

In the lower stratosphere, the time series of frost-point hygrometer measurements at Boulder is continuing /17/. Results will soon be available from the comprehensive tropical Stratospheric/Tropospheric Exchange Project (STEP) experiment conducted out of Darwin, Australia, in early 1987. These data should be useful in defining the water vapor fluxes, which contribute to the overall H_2O distribution in the hygropause region. Finally, preliminary results were reported from the 1987 Airborne Antarctic Ozone Expedition (AAOE), along with some balloon-borne measurements of water vapor from McMurdo Base during the National Ozone Expedition (NOZE2) and the measurements from SAGE II (see /39/). According to the measurements, it appears that a separate water vapor reference profile may be required for the special conditions associated with cold lower stratospheric temperatures over the Antarctic region, at least during winter and spring. Air for those periods is dehydrated with mixing ratios equivalent to those at the tropical hygropause (2 to 3 ppmv). With the addition of these new data sets, it should be possible to know the seasonal distribution of water vapor for the entire stratosphere and for limited, but representative, locations for the mesosphere.

REFERENCES

1. M. Nicolet, On the photodissociation of water vapour in the mesosphere, Planet. Space Sci. 32, 871 (1984).

2. WMO, Atmospheric Ozone 1985, Report 16, Geneva (1986).

3. S. Solomon, E.E. Ferguson, D.W. Fahey, and P.J. Crutzen, On the chemistry of H_2O, H_2 and meteoritic ions in the mesosphere and lower thermosphere, Planet. Space Sci. 30, 1117 (1982).

4. G. Brasseur and S. Solomon, Aeronomy of the Middle Atmosphere, Reidel, Dordrecht, 441 pp (1984).

5. J. Austin, E.E. Remsberg, R.L. Jones, and A.F. Tuck, Polar stratospheric clouds inferred from satellite data, Geophys. Res. Letts. 13, 1256 (1986).

6. J.J. Olivero and G.E. Thomas, Climatology of polar mesospheric clouds, J. Atmos. Sci. 43, 1263 (1986).

7. J. Kiehl and S. Solomon, On the radiative balance of the stratosphere, J. Atmos. Sci. 43, 1525 (1986).

8. J. Holton, Troposphere-stratosphere exchange of trace constituents: The water vapor puzzle, in: Dynamics of the Middle Atmosphere, (J.R. Holton and T. Matsuno, eds.), Terrapub, Tokyo, 369 (1984).

9. E. Remsberg, Analysis of the mean meridional circulation using satellite data. In Transport Processes in the Middle Atmosphere, eds. G. Visconti and R. Garcia, Reidel, 401 (1987).

10. D.F. Strobel, M.E. Summers, R.M. Bevilacqua, M.T. DeLand, and M. Allen, Vertical constituent transport in the mesosphere, J. Geophys. Res. 92, 6691 (1987).

11. D.R. Blake and S.F. Rowland, Continuing worldwide increase in tropospheric methane, 1978 to 1987, Science 239, 1129 (1988).

12. J.M. Russell III, An interim reference model for the middle atmosphere water vapor distribution. Adv. Space Res. 7, # 9, 5 (1987).

13. C. Lippens, C. Muller, J. Vercheval, M. Ackerman, J. Laurent, M.P. Lemaitre, J. Besson, and A. Girard, Trace constituent measurements deduced from spectrometric observations onboard Spacelab, Adv. Space Res. 4, # 6, 75 (1984).

14. R.M. Bevilacqua, J.J. Olivero, P.R. Schwartz, C.J. Gibbins, J.M. Bologna, and D.L. Thacker, An observational study of water vapor in the mid latitude mesosphere using ground-based microwave techniques, J. Geophys. Res. 88, 8523 (1983).

15. H.G. Bruckelmann, K.U. Grossmann, and D. Offermann, Rocket-borne measurements of atmospheric infrared emissions by spectrometic techniques, Adv. Space Res. 7, # 10, 43 (1987).

16. H.J. Mastenbrook and S.J. Oltmans, Stratospheric water vapor variability for Washington, D.C./Boulder, Colorado: 1964-82, J. Atmos. Sci. 40, 2157 (1983).

17. Geophysical Monitoring for Climatic Change (GMCC), Summary Report 1986 15, NOAA/ERL, Boulder, Colorado, 61 (1987).

18. J.M. Russell III, J.C. Gille, E.E. Remsberg, L.L. Gordley, P.L. Bailey, H. Fischer, A. Girard, S.R. Drayson, W.F.J. Evans, and J.E. Harries, Validation of water vapor results measured by the limb infrared monitor of the stratosphere (LIMS) experiment on Nimbus 7, J. Geophys. Res. 89, # D4, 5115 (1984).

19. E.E. Remsberg, J.M. Russell III, L.L. Gordley, J.C. Gille, and P.L. Bailey, Implications of the stratospheric water vapor distribution as determined from the Nimbus 7 LIMS experiment, J. Atmos. Sci. 41, 2934 (1984).

20. E.E. Remsberg and J.M. Russell III, The near global distributions of middle atmospheric H_2O and NO_2 measured by the Nimbus 7 LIMS experiment, in: Transport Processes in the Middle Atmosphere, eds. G. Visconti and R. Garcia, Reidel, 87 (1987).

21. B. Kerridge and E.E. Remsberg, Evidence from LIMS data for non-local thermodynamic equilibrium in the ν_3 mode of mesospheric water vapor and the ν_4 mode of stratospheric nitrogen dioxide, submitted to J. Geophys. Res. (1988).

22. K.W. Haggard, B.T. Marshall, R.J. Kurzeja, E.E. Remsberg, and J.M. Russell III, Description of data on the Nimbus 7 LIMS Map Archive Tape - Water Vapor and nitrogen dioxide, NASA Technical Paper 2761, 66 pp. (1988).

23. J.M. Russell III, S. Solomon, M.P. McCormick, A.J. Miller, J.J. Barnett, R.L. Jones, and D.W. Rusch, Middle atmosphere composition revealed by satellite observations, MAP Handbook # 22, 302 pp. (1986).

24. D.G. Andrews, J.R. Holton, and C.B. Leovy, Middle Atmosphere Dynamics, Academic Press (1987).

25. S. Solomon, J.T. Kiehl, R.R. Garcia, and W.L. Grose, Tracer transport by the diabatic circulation deduced from satellite observations, J. Atmos. Sci. 43, 1603 (1986).

26. L.J. Gray and J.A. Pyle, The semiannual oscillation and equatorial tracer distributions, Q.J.R. Meteorol. Soc. 112, 387 (1986).

27. R.R. Garcia, S. Solomon, R.G. Roble, and D.W. Rusch, A numerical response of the middle atmosphere to the 11-year solar cycle, Planet. Space Sci. 32, 411 (1984).

28. H. LeTexier, S. Solomon, and R.R. Garcia, The role of molecular hydrogen and methane oxidation in the water vapor budget of the stratosphere, Q.J.R. Meteorol. Soc. 114, 281 (1988).

29. R.L. Jones, J.A. Pyle, J.E. Harries, A.M. Zavody, J.M. Russell, and J.C. Gille, The water vapor budget of the stratosphere studied using LIMS and SAMS satellite data, Q.J.R. Meteorol. Soc. 122, 1127 (1986).

30. C.B. Leovy, C-R. Sun, M.H. Hitchman, E.E. Remsberg, J.M. Russell III, L.L. Gordley, J.C. Gille, and L.V. Lyjak, Transport of ozone in the middle stratosphere: Evidence for planetary wave breaking, J. Atmos. Sci. 42, 230 (1985).

31. N. Butchart and E.E. Remsberg, The area of the stratospheric polar vortex as a diagnostic for tracer transport on an isentropic surface, J. Atmos. Sci. 43, 1319 (1986).

32. L.L. Gordley, J.M. Russell III, and E.E. Remsberg, Global lower mesospheric water vapor revealed by LIMS observations, in: Atmospheric Ozone, eds. C.S. Zerefos and A. Ghazi, Reidel, 139 (1985).

33. R.M. Bevilacqua, W.J. Wilson, W.B. Ricketts, P.R. Schwartz, and R.J. Howard, Possible seasonal variability of mesospheric water vapor, Geophys. Res. Letts. 12, 397 (1985).

34. R.M. Bevilacqua, W.J. Wilson, and P.R. Schwartz, Measurements of mesospheric water vapor in 1984 and 1985: results and implications for middle atmospheric transport, J. Geophys. Res. 92, 6679 (1987).

35. J-J. Tsou, J.J. Olivero, and C.L. Croskey, Study of variability of mesospheric H_2O during spring 1984 by ground-based microwave radiometric observations, J. Geophys. Res. 93, 5255 (1988).

36. P.R. Schwartz, C.L. Croskey, R.M. Bevilacqua, and J.J. Olivero, Microwave spectroscopy of H_2O in the stratosphere and mesosphere, Nature 305, 294 (1983).

37. M.P. McCormick, SAGE II: An overview, Adv. Space Res. 7, # 3, 219 (1987).

38. R. Peter, K. Kunzi, and G. K. Hartmann, Latitudinal survey of water vapor in middle atmosphere using an airborne millimeter-wave sensors, Geophys. Res. Letts. 15, 1173 (1988).

39. Polar Ozone Workshop Abstracts, NASA Conference Publication #10014, Snowmass, Colorado, 9-13 May (1988).

4

PROPOSED REFERENCE MODELS FOR NITROUS OXIDE AND METHANE IN THE MIDDLE ATMOSPHERE

F. W. Taylor, A. Dudhia, and C. D. Rodgers

Department of Atmospheric Physics, Oxford University
Clarendon Laboratory, Oxford OX1 3PU, United Kingdom

ABSTRACT

Data from the Stratospheric and Mesospheric Sounder (SAMS) on the Nimbus 7 satellite, for the three years from January 1979-December 1981, are used to prepare a reference model for the long-lived trace gases methane (CH_4) and nitrous oxide (N_2O) in the stratosphere. The model is presented in tabular form on seventeen pressure surfaces from 20 to 0.1 mb, in 10^o latitude bins from 50S to 70N, and for each month of the year. The means by which the data quality and interannual variability, and some of the more interesting globally and seasonally variable features of the data are discussed briefly.

INTRODUCTION

N_2O and CH_4 are both important minor constituents of the stratosphere for several reasons. Neither gas has a known photochemical source in the middle atmosphere, both originating near the surface by a variety of processes which includes anthropogenic sources in each case /1/. As both gases have fairly long lifetimes against photochemical destruction (ranging from about a year for methane in the lower stratosphere to a few weeks for nitrous oxide near the stratopause), they are important tracers of the transfer process across the tropopause and of the stratospheric mean circulation. Methane is a source of water vapour in the middle atmosphere as a result of a series of reactions equivalent to

$$CH_4 + 2O_2 = CO_2 + 2\,H_2O$$

while nitrous oxide is the main source of stratospheric NO_x by a series equivalent to

$$2N_2O + O_2 = 4NO$$

and subsequent reactions.

The Stratospheric and Mesospheric Sounder (SAMS) made observations from the Nimbus 7 spacecraft from 1978 to 1983. The SAMS instrument has been described by Drummond et al /2/ and examples of the results from the experiment are presented and discussed in the articles by Barnett et al /3/ and Jones and Pyle /4/. The last-named paper discusses the methane and nitrous oxide observations in particular detail, including the retrieval of abundances from radiance observations and an analysis of the error budget. The data used here are essentially the same as those used by Jones and Pyle, with some reprocessing and considerable reformatting and manipulation. Our goal is to produce standard tables which represent the mean distribution of methane and nitrous oxide as a function of height, latitude and month.

DESCRIPTION OF THE MEASUREMENTS

SAMS is a nine-channel, limb-viewing infrared radiometer employing the pressure-modulation technique /5/ to observe thermal emission from carbon dioxide (for temperature retrievals) and five other atmospheric minor constituents. Methane was observed in the ν_4 band near 7.6 μm and nitrous oxide in the ν_1 band near 7.8 μm. Both channels shared the same pyroelectric detector and the instrument had a 75% duty cycle; hence the observations of

either species occupied about one-third of each month on average.

The vertical resolution of the measurements is 8 to 10 km. Profiles were actually retrieved at seven altitudes, including a fixed base value at 1.4 scale heights (250 mb). The other levels were 2.6, 3.8, 5.0, 6.2, 7.4, and 8.6 scale heights (75, 20, 7, 2, 0.6, and 0.2 mb respectively). Most of the useful information is restricted to levels between 0.2 (0.6 for N_2O) and 20 mb.

The SAMS N_2O and CH_4 observations are not entirely independent,since their spectral bands overlap and data from one species is required by the retrieval program to determine the other. Vertical correlations are introduced by the finite field of view of the instrument and temporal correlations by the 'sequential maximum likelihood operator' approach used for the retrieval /4/. There is also some latitudinal interdependence in the data introduced by the temperature retrieval algorithm /6/. All of these effects are small, however, especially in monthly averages.

For the purposes of producing the present model, an additional filter was applied to the data. The smoothing was based on a $\log_{10}$ (mixing ratio) grid of 5 (altitudes) x 12 (latitudes) x 14 (months), (i.e. replicating January and December at each end to ensure continuity in time). Each grid point was then combined with a value obtained from the interpolation of up to 13 pairs of adjacent grid points, each reduced to 10% weighting. This gives a relatively small amount of smoothing which removed a few rogue points and smoothed out the sharper features which although real were probably atypical.

The accuracy of the retrieved zonal mean as determined by Jones and Pyle /4/, who combined conservative estimates of all of the known sources of error including spectroscopic and retrieval uncertainties, and noise due to instrumental sources and spacecraft jitter, varies with height but is at best 20% for CH_4 and 25% for N_2O. The corresponding precision is $\sim$ 3% for CH_4 and $\sim$ 6% for N_2O. The 'confidence limits' established by the same authors for the vertical range of the measurements is 20 mb ($\simeq$25 km) to 0.2 mb ($\simeq$60 km) for CH_4 and 0.6 mb ($\simeq$53 km) for N_2O.

COMPARISON WITH OTHER MEASUREMENTS

The lower part of the SAMS retrieved profiles can be compared with balloon measurements /7/, which extend up to about 7 mb and therefore overlap the lowest two SAMS vertical resolution elements. Jones and Pyle /4/ made such comparisons and found that, while the in-situ and satellite data agree quite well near the top of the region of overlap, lower down discrepancies of nearly a factor of two occur with the SAMS amounts being higher. More recent measurements /8/ of both CH_4 and N_2O by a cryogenic sampling technique in 1979, 1982 and 1985 confirm the discrepancy but its origin is still a mystery. One possibility is the spectroscopic data used in the SAMS retrieval, which may not include enough weak lines of the fundamental or some overlapping band. This possibility is under investigation and the data set may be completely revised at some later date. For the meantime, even if it can be assumed that the responsibility for the discrepancy lies entirely with the satellite data, which is probably not the case as the in-situ data shows a considerable scatter, we cannot correct our model without more information on the extent to which the difference depends on (a) altitude, (b) latitude, (c) month, and (d) natural variability of the atmosphere. We do provide, however, (Table 1) a list of the estimated mean differences between the two kinds of data for the latitudes and times at which comparisons are possible. It should further be noted that, according to Schmidt /8/, not only the absolute amounts but also the trend with time in late summer at 45°N is in disagreement. Balloon data show lower abundances in October/November than in September, in contrast to SAMS findings. Again, the reason for this is under investigation but in this case a spectroscopic explanation seems unlikely. It also illustrates the risk of using the ratios in table 1 simply as a universal 'correction factor'.

Table 1

Approximate ratios between SAMS data and mean values from in-situ data/7/ at 30 to 45°N

Pressure (mb)	(N_2O) in-situ/SAMS	(CH_4) in-situ/SAMS
20	0.60	0.80
15	0.69	0.85
10	0.84	0.93
7 and lower	1.00	1.00

MODELS OF VERTICAL STRUCTURE OF METHANE AND NITROUS OXIDE

Models were produced by averaging the SAMS data for the three year period from January 1979 through December 1981 and applying some smoothing. SAMS actually made observations from shortly after launch on 24 October 1978 until June 1984, but the early data consists mainly of instrument checkout modes while those obtained after March 1982 were rendered more difficult to interpret by the volcanic dust injected into the stratosphere by the eruption of El Chichon and will require further validation.

Averages were formed first by day and by latitude, the latter in 10° bins. The daily data and their estimated errors were then used to produce an error-weighted average by month, before the corresponding months for the three years were combined. Thereafter, the 'error' was taken to be the square root of the greater of either the variance or the inverse sum of the weights of the contributing data. This approach brings in the standard deviation of the profiles contributing to the mean. For any further manipulation of the data, each point was weighted by the inverse square of this 'error'. The extension of the N_2O data to 0.2 mb was done simply by subtracting 0.5 from the log (mixing ratio) at 0.6 mb, accompanied by an increase in the variance of the log mixing ratio of 0.1, i.e. an additional error in the mixing ratio of about a factor of 2.

Table 2 gives the monthly zonal mean nitrous oxide and methane mixing ratios in ppbv and ppmv respectively, as a function of latitude and height, for each month. The height intervals are the standard ones chosen by Keating and Young /9/ for their model of middle atmosphere ozone. In the table, the value for mixing ratio is accompanied by an indication of the uncertainty of the number due to instrument noise, to daily variance and to extrapolation outside the 'confidence limits' for the original measurements.

DISCUSSION OF MAJOR FEATURES

A programme of scientific analysis of these data is going on, and in particular a detailed discussion of the features present in the time-averaged data used to produce the model tabulated here will shortly appear in a paper now in preparation /10/. A scientific interpretation of the structure which appears in the distribution profiles of stratospheric methane and nitrous oxide is clearly beyond the scope of the present paper, but the following brief phenomenological description of the main features may assist one's understanding of the model.

Firstly, the overall structure seen in abundance charts for either CH_4 and N_2O is qualitatively the same, as might be expected of long-lived species whose distribution is controlled more by dynamics than chemistry. The following remarks, therefore, apply to both gases, and always (in this paper) to zonal mean abundances.

The highest absolute amounts occur towards the end of Summer, i.e. in September/October in the Northern Hemisphere and March/April in the Southern. At any given latitude, the zonal mean abundance tends to peak earlier at higher altitudes, the opposite to the behavior to be expected if material from the troposphere was simply being advected vertically. At high altitudes (near the 0.2 mb level) there is a pronounced semi-annual oscillation in the abundances of CH_4 and N_2O which, incidentally, is not present in the thermal structure when averaged in the same way. Remarkably, this feature is present in the Southern but not the Northern Hemisphere.

TABLE 2

Monthly mean mixing ratios for nitrous oxide in parts per billion (10^9) by volume (ppbv) then methane in parts per million by volume (ppmv). An indication of the reliability of the values as a model of the actual amounts to be expected in any given year is given by the letter following each entry. These represent the standard deviation or standard error of the data making up the value, as given in the key and described in the text. Absence of a letter means less than ten percent deviation in the data. Annual averages are given at the end of the set of monthly means.

Average N_2O (ppbv) for JANUARY

Press.	Latitude (°N)												
(mb)	-50°	-40	-30	-20	-10	0	+10	+20	+30	+40	+50	+60	+70°
0.10*	0.21^D	0.50^D	0.88^D	1.18^D	1.47^D	1.17^D	0.91^D	0.94^D	0.86^D	0.73^D	0.61^D	0.59^D	0.66^D
0.15*	0.24^D	0.58^D	1.01^D	1.36^D	1.68^D	1.33^D	1.03^D	1.06^D	0.98^D	0.83^D	0.70^D	0.67^D	0.76^D
0.20*	0.28^D	0.66^D	1.16^C	1.57^D	1.91^D	1.51^D	1.18^D	1.19^D	1.11^D	0.94^D	0.79^D	0.77^D	0.86^D
0.30*	0.37^D	0.87^D	1.54^C	2.09^C	2.48^C	1.96^C	1.52^D	1.51^C	1.42^C	1.21^D	1.03^D	1.00^C	1.11^D
0.40*	0.49^D	1.15^C	2.04^C	2.77^C	3.21^C	2.53^C	1.96^C	1.92^C	1.82^C	1.56^C	1.33^C	1.29^C	1.44^C
0.50*	0.65^D	1.52^C	2.70^C	3.68^C	4.16^C	3.28^C	2.54^C	2.44^C	2.33^C	2.02^C	1.72^C	1.68^C	1.86^C
0.70	1.00^C	2.26^C	4.04^B	5.54^B	6.10^B	4.81^B	3.69^B	3.43^B	3.29^D	2.89^B	2.49^B	2.40^B	2.56^B
1.00	1.45^C	3.05^B	5.41^B	7.62^B	8.34^B	6.63^B	5.01^B	4.44^B	4.14^B	3.72^B	3.27^B	2.99^B	2.88^B
1.50	2.71^C	5.04^B	8.81^B	12.96^D	14.07^B	11.32^B	8.32^B	6.83^B	6.07^B	5.67^B	5.19^B	4.31^B	3.52^C
2.00	5.08^C	8.33^B	14.35^B	22.02^b	23.73^B	19.34^B	13.83^B	10.49^B	8.91^B	8.64^B	8.22^B	6.23^B	4.30^C
3.00	8.06^C	12.53^B	20.70^B	31.40^B	35.14^B	29.80^B	21.83^B	16.58^B	13.84^B	13.07^B	11.85^B	8.81^B	6.15^C
4.00	12.48^B	18.52^B	29.31^B	43.82^B	51.01^B	45.02^D	33.86^B	25.90^B	21.29^B	19.52^B	16.80^B	12.32^D	8.78^C
5.00	19.32^D	27.37^B	41.50^D	61.17^b	74.05^B	68.02^D	52.53^B	40.44^D	32.74^B	29.17^B	23.83^B	17.23^D	12.53^C
7.00	42.23^A	54.96^B	76.97^B	110.28^D	142.90^D	141.32^D	114.87^B	89.65^B	70.79^B	60.14^B	45.30^D	32.10^B	24.07^C
10.00	54.25^B	67.61^B	89.74^B	123.61^D	159.90^D	165.77^B	143.20^D	114.31^b	92.04^B	81.08^B	67.90^B	50.73^C	35.58^C
15.00	82.36^C	95.50^B	115.91^B	149.51^B	192.83^B	216.29^D	206.77^B	171.40^D	142.57^b	133.38^B	133.31^B	108.73^C	68.23^C
20.00	125.04^C	134.90^C	149.71^D	180.83^B	232.55^b	282.19^B	298.56^B	257.01^B	220.83^D	219.42^B	261.73^B	233.07^C	130.87^C

Average N_2O (ppbv) for FEBRUARY

Press.	Latitude (°N)												
(mb)	-50*	-40	-30	-20	-10	0	+10	+20	+30	+40	+50	+60	+70*
0.10*	0.54^D	1.08^D	1.40^D	1.30^D	1.05^D	0.75^D	0.76^D	1.06^D	1.17^D	0.89^D	0.68^D	0.57^D	0.49^D
0.15*	0.62^D	1.22^D	1.60^D	1.50^D	1.22^D	0.88^D	0.88^D	1.20^D	1.32^D	1.01^D	0.78^D	0.65^D	0.56^D
0.20*	0.70^D	1.39^D	1.83^D	1.74^D	1.42^D	1.03^D	1.02^D	1.37^D	1.49^D	1.15^D	0.89^D	0.74^D	0.64^D
0.30*	0.90^D	1.78^D	2.41^C	2.34^C	1.93^C	1.42^D	1.38^C	1.77^C	1.90^C	1.49^D	1.16^D	0.98^D	0.85^D
0.40*	1.16^D	2.28^C	3.16^C	3.14^C	2.62^C	1.96^C	1.86^C	2.29^C	2.42^C	1.93^C	1.52^C	1.28^C	1.11^C
0.50*	1.50^D	2.92^C	4.15^C	4.22^C	3.56^C	2.70^C	2.50^C	2.96^C	3.09^C	2.50^C	1.99^C	1.68^C	1.46^C
0.70	2.11^C	4.10^C	6.09^B	6.47^B	5.61^B	4.33^C	3.86^B	4.30^B	4.37^B	3.59^C	2.92^C	2.50^C	2.20^C
1.00	2.60^C	5.13^C	8.02^B	9.12^B	8.24^B	6.39^B	5.48^B	5.75^B	5.65^B	4.64^B	3.88^B	3.43^B	3.07^C
1.50	3.67^C	7.44^B	12.65^D	16.17^b	15.85^D	12.23^B	9.79^B	9.32^B	8.66^B	7.12^B	6.23^B	5.79^B	5.38^C
2.00	5.19^C	10.78^B	19.98^B	28.65^B	29.73^B	23.42^B	17.51^B	15.11^B	13.28^B	10.92^B	10.00^B	9.80^B	9.43^B
3.00	8.24^C	15.93^D	27.66^B	38.8[illegible]	41.82^B	35.07^B	27.05^B	22.64^B	18.90^B	15.54^B	14.13^B	13.51^B	12.84^C
4.00	13.01^B	23.27^B	37.63^B	50.87^B	57.16^B	51.10^B	40.87^B	33.34^B	26.49^B	21.78^B	19.62^B	18.21^B	17.07^C
5.00	20.53^B	34.01^B	51.18^B	66.91^B	78.14^B	74.46^B	61.77^B	49.10^B	37.13^B	30.52^B	27.23^B	24.56^B	22.68^C
7.00	46.69^A	66.99^B	88.50^B	109.07^b	136.15^B	145.19^B	128.51^B	97.96^B	68.21^B	56.08^B	49.49^B	42.44^B	37.77^C
10.00	64.57^B	83.09^B	102.59^B	125.26^B	156.33^B	169.30^B	152.26^B	120.21^B	87.05^B	72.02^B	67.78^B	57.89^B	45.43^C
15.00	110.86^B	118.96^B	131.24^B	157.75^B	196.82^B	218.70^B	201.99^B	169.10^B	130.73^B	109.27^B	114.50^B	97.14^B	61.78^C
20.00	190.32^C	170.32^C	167.90^B	198.68^B	247.81^B	282.52^b	267.96^B	237.85^B	196.33^B	165.80^B	193.42^B	162.99^C	84.03^C

Average N_2O (ppbv) for MARCH

Press.	Latitude (°N)												
(mb)	-50*	-40	-30	-20	-10	0	+10	+20	+30	+40	+50	+60	+70*
0.10*	1.10^D	1.55^D	1.86^D	1.30^D	0.74^D	0.56^D	0.61^D	0.80^D	1.03^D	1.08^D	0.74^D	0.52^D	0.43^D
0.15*	1.24^D	1.76^D	2.11^D	1.49^D	0.86^D	0.66^D	0.72^D	0.92^D	1.16^C	1.23^D	0.84^D	0.59^D	0.49^D
0.20*	1.39^D	1.99^D	2.39^C	1.71^D	1.01^D	0.77^D	0.84^D	1.07^D	1.35^C	1.39^D	0.96^D	0.68^D	0.57^D
0.30*	1.77^D	2.55^C	3.09^C	2.27^C	1.38^C	1.07^C	1.14^C	1.42^C	1.76^C	1.80^C	1.26^D	0.90^D	0.74^C
0.40*	2.24^D	3.28^C	3.98^C	3.00^C	1.89^C	1.47^C	1.56^C	1.89^C	2.30^C	2.32^C	1.64^C	1.19^C	0.97^C
0.50*	2.84^C	4.20^C	5.13^C	3.97^C	2.58^C	2.03^C	2.12^C	2.51^C	3.01^C	3.00^C	2.14^C	1.57^C	1.27^C
0.70	3.76^C	5.84^B	7.35^B	5.99^B	4.11^B	3.27^B	3.34^B	3.82^B	4.43^B	4.28^B	3.12^B	2.34^B	1.90^B
1.00	4.01^C	6.95^B	9.52^B	8.40^B	6.10^B	4.86^B	4.86^B	5.42^B	5.96^B	5.48^B	4.09^B	3.20^B	2.65^B
1.50	4.45^C	9.29^B	14.67^B	14.77^B	11.76^B	9.39^B	9.08^B	9.67^B	9.74^B	8.27^B	6.41^B	5.37^B	4.61^B
2.00	4.94^B	12.40^B	22.60^B	25.96^B	22.67^B	18.14^B	16.95^B	17.26^B	15.93^B	12.49^B	10.06^B	9.01^B	8.02^C
3.00	7.83^B	17.56^B	30.45^D	36.50^B	34.23^B	28.77^B	26.49^B	25.68^B	22.50^B	17.37^B	14.15^B	12.82^B	11.74^C
4.00	12.50^B	24.70^B	40.32^b	50.09^B	50.30^B	44.47^B	40.42^B	37.33^B	31.17^B	23.82^B	19.59^B	17.86^B	16.80^B
5.00	19.96^D	34.73^B	53.39^B	68.76^A	73.91^B	68.73^B	61.67^B	54.26^B	43.18^B	32.65^B	27.10^B	24.85^B	24.06^B
7.00	46.30^B	64.21^B	88.47^B	120.66^B	146.02^B	148.61^B	130.32^B	105.30^B	77.19^B	57.55^B	48.84^B	45.57^B	46.53^B
10.00	82.52^B	82.85^B	107.63^b	138.59^b	167.66^B	175.08^B	153.23^D	122.25^D	91.12^B	71.13^B	64.43^B	64.82^B	70.35^C
15.00	103.14^B	126.69^b	149.22^D	174.59^B	211.76^B	230.07^D	200.71^B	156.78^B	120.16^B	101.27^B	102.26^B	116.89^C	140.14^C
20.00	170.15^B	193.73^B	206.89^B	219.93^B	267.13^B	302.34^b	262.90^B	201.06^B	158.45^b	144.18^B	162.31^B	209.72^C	279.14^D

* Extrapolated from original data.

Variation in data <10%, >10%^{A}, >20%^{B}, >50%^{C}, >100%^{D}

Average N_2O (ppbv) for APRIL

Press.	Latitude (°N)												
(mb)	-50°	-40	-30	-20	-10	0	+10	+20	+30	+40	+50	+60	+70°
0.10°	1.87^{D}	1.63^{D}	1.21^{D}	0.59^{D}	0.37^{D}	0.41^{D}	0.53^{D}	0.79^{D}	1.03^{D}	1.13^{D}	0.78^{D}	0.43^{D}	0.29^{D}
0.15°	2.08^{D}	1.84^{D}	1.39^{C}	0.69^{D}	0.44^{D}	0.47^{D}	0.62^{D}	0.91^{C}	1.18^{C}	1.28^{D}	0.88^{D}	0.49^{D}	0.34^{D}
0.20°	2.31^{D}	2.08^{D}	1.60^{C}	0.81^{C}	0.51^{C}	0.55^{C}	0.72^{C}	1.05^{C}	1.35^{C}	1.44^{C}	1.00^{D}	0.57^{D}	0.38^{D}
0.30°	2.85^{D}	2.66^{C}	2.11^{C}	1.11^{C}	0.71^{C}	0.75^{C}	0.97^{C}	1.39^{C}	1.77^{C}	1.82^{C}	1.27^{C}	0.74^{C}	0.51^{D}
0.40°	3.52^{D}	3.40^{C}	2.78^{C}	1.53^{C}	0.98^{C}	1.02^{C}	1.30^{C}	1.83^{C}	2.31^{C}	2.32^{C}	1.61^{C}	0.97^{C}	0.67^{C}
0.50°	4.35^{C}	4.35^{C}	3.66^{C}	2.10^{C}	1.35^{C}	1.39^{C}	1.75^{C}	2.42^{C}	3.03^{C}	2.94^{C}	2.05^{C}	1.27^{C}	0.88^{C}
0.70	5.65^{C}	6.08^{B}	5.47^{B}	3.40^{B}	2.22^{B}	2.22^{B}	2.75^{B}	3.68^{B}	4.46^{B}	4.12^{B}	2.88^{B}	1.87^{B}	1.32^{B}
1.00	6.22^{C}	7.47^{B}	7.56^{D}	5.22^{B}	3.53^{B}	3.43^{B}	4.11^{B}	5.26^{B}	6.03^{B}	5.27^{B}	3.71^{B}	2.54^{B}	1.84^{B}
1.50	7.28^{B}	10.54^{B}	12.89^{B}	10.67^{B}	7.67^{B}	7.04^{B}	8.02^{B}	9.58^{B}	9.97^{B}	7.96^{B}	5.64^{B}	4.20^{B}	3.22^{C}
2.00	8.53^{B}	14.86^{B}	22.03^{B}	21.82^{B}	16.66^{D}	14.45^{B}	15.65^{B}	17.43^{B}	16.48^{B}	12.00^{B}	8.58^{B}	6.95^{B}	5.63^{C}
3.00	12.05^{B}	20.57^{B}	30.46^{B}	32.17^{B}	26.80^{B}	24.16^{B}	25.35^{B}	26.35^{B}	23.58^{B}	16.95^{B}	12.33^{B}	10.24^{B}	8.60^{B}
4.00	17.03^{D}	28.17^{B}	41.18^{B}	45.95^{B}	41.73^{B}	39.28^{B}	40.04^{B}	38.89^{B}	33.07^{B}	23.61^{B}	17.47^{D}	14.81^{B}	12.85^{B}
5.00	24.08^{B}	38.58^{B}	55.68^{B}	65.63^{B}	64.99^{B}	63.86^{B}	63.22^{B}	57.40^{B}	46.39^{B}	32.87^{B}	24.76^{B}	21.41^{B}	19.20^{B}
7.00	45.32^{B}	68.23^{B}	95.72^{B}	123.76^{B}	142.35^{B}	150.63^{B}	141.54^{B}	114.09^{D}	84.54^{B}	59.49^{B}	46.52^{B}	41.94^{B}	40.01^{B}
10.00	64.50^{B}	89.43^{B}	117.4^{C}	146.24^{B}	167.37^{B}	175.90^{B}	162.50^{B}	128.41^{B}	97.02^{B}	73.24^{B}	61.99^{B}	60.08^{B}	60.44^{C}
15.00	116.16^{D}	140.40^{B}	165.22^{D}	193.15^{B}	219.22^{B}	227.79^{B}	204.54^{B}	156.38^{B}	122.05^{B}	103.58^{B}	100.01^{B}	109.35^{C}	120.19^{C}
20.00	209.17^{C}	220.41^{B}	232.39^{B}	255.10^{B}	287.13^{B}	294.98^{B}	257.46^{B}	190.43^{B}	153.53^{D}	146.49^{B}	161.34^{B}	199.03^{C}	239.03^{D}

Average N_2O (ppbv) for MAY

Press.	Latitude (°N)												
(mb)	-50°	-40	-30	-20	-10	0	+10	+20	+30	+40	+50	+60	+70°
0.10°	1.05^{D}	0.85^{D}	0.59^{C}	0.38^{D}	0.32^{D}	0.38^{D}	0.59^{C}	0.93^{D}	1.07^{D}	0.92^{D}	0.57^{D}	0.37^{D}	0.33^{D}
0.15°	1.21^{D}	0.98^{D}	0.68^{C}	0.44^{C}	0.38^{D}	0.45^{D}	0.68^{C}	1.07^{C}	1.22^{C}	1.04^{D}	0.65^{D}	0.42^{D}	0.38^{D}
0.20°	1.38^{D}	1.12^{C}	0.79^{C}	0.52^{C}	0.44^{D}	0.52^{C}	0.79^{C}	1.22^{C}	1.40^{C}	1.18^{C}	0.73^{C}	0.49^{D}	0.44^{D}
0.30°	1.81^{D}	1.47^{C}	1.05^{C}	0.70^{C}	0.61^{C}	0.71^{C}	1.05^{C}	1.60^{C}	1.82^{C}	1.52^{C}	0.94^{C}	0.63^{D}	0.58^{D}
0.40°	2.36^{C}	1.94^{C}	1.39^{C}	0.96^{C}	0.85^{C}	0.98^{C}	1.40^{C}	2.10^{C}	2.36^{C}	1.95^{C}	1.21^{C}	0.83^{C}	0.76^{D}
0.50°	3.09^{C}	2.55^{C}	1.85^{B}	1.30^{C}	1.17^{C}	1.33^{C}	1.87^{B}	2.76^{C}	3.07^{C}	2.50^{C}	1.55^{C}	1.08^{C}	1.00^{C}
0.70	4.50^{B}	3.80^{B}	2.86^{B}	2.09^{B}	1.92^{B}	2.14^{B}	2.89^{B}	4.12^{B}	4.48^{B}	3.66^{B}	2.22^{B}	1.59^{B}	1.47^{C}
1.00	6.82^{B}	5.22^{B}	4.25^{B}	3.28^{B}	2.99^{B}	3.26^{B}	4.24^{D}	5.77^{B}	5.99^{B}	4.56^{D}	2.88^{B}	2.10^{B}	1.91^{C}
1.50	8.94^{B}	8.87^{B}	8.21^{B}	6.93^{B}	6.28^{B}	6.61^{B}	8.05^{B}	10.11^{B}	9.68^{B}	6.90^{B}	4.48^{B}	3.36^{B}	2.93^{C}
2.00	13.72^{B}	15.07^{B}	15.86^{B}	14.65^{B}	13.19^{B}	13.39^{B}	15.29^{B}	17.71^{B}	15.67^{B}	10.43^{B}	6.96^{B}	5.37^{B}	4.50^{B}
3.00	19.52^{B}	22.10^{B}	24.22^{B}	23.79^{B}	22.13^{B}	22.17^{D}	24.21^{B}	26.99^{B}	22.22^{B}	16.03^{B}	10.29^{B}	8.13^{B}	6.92^{B}
4.00	27.37^{B}	31.75^{B}	36.00^{B}	37.46^{B}	36.07^{B}	35.71^{B}	37.39^{B}	37.29^{B}	30.92^{B}	21.36^{B}	14.98^{B}	12.13^{B}	10.52^{B}
5.00	38.37^{B}	45.60^{B}	53.50^{B}	59.00^{B}	58.78^{B}	57.52^{B}	57.75^{B}	53.51^{B}	43.05^{B}	30.36^{B}	21.81^{B}	18.09^{B}	16.00^{B}
7.00	70.72^{D}	87.41^{B}	108.46^{D}	131.71^{B}	150.20^{D}	153.75^{B}	124.61^{B}	101.43^{D}	77.66^{B}	57.17^{B}	43.03^{B}	37.32^{B}	34.21^{A}
10.00	93.54^{B}	111.37^{D}	133.41^{D}	154.22^{B}	161.64^{B}	159.38^{D}	145.71^{B}	116.53^{D}	92.48^{D}	73.38^{D}	58.42^{B}	52.29^{B}	49.65^{D}
15.00	149.06^{C}	166.78^{B}	188.38^{B}	200.61^{B}	207.36^{B}	213.48^{D}	189.09^{B}	146.85^{B}	123.74^{B}	111.23^{B}	97.22^{B}	91.76^{B}	92.38^{C}
20.00	237.54^{C}	249.77^{B}	265.96^{B}	280.95^{B}	286.01^{B}	285.93^{B}	245.30^{B}	185.06^{B}	165.55^{B}	168.60^{B}	181.81^{B}	181.01^{C}	171.89^{C}

Average N_2O (ppbv) for JUNE

Press.	Latitude (°N)												
(mb)	-50°	-40	-30	-20	-10	0	+10	+20	+30	+40	+50	+60	+70°
0.10°	0.27^{D}	0.25^{D}	0.28^{C}	0.37^{C}	0.43^{C}	0.52^{D}	0.78^{C}	1.08^{D}	1.21^{D}	0.91^{D}	0.50^{D}	0.47^{D}	0.75^{D}
0.15°	0.31^{D}	0.30^{D}	0.33^{C}	0.43^{C}	0.50^{C}	0.60^{C}	0.90^{C}	1.23^{C}	1.38^{C}	1.04^{D}	0.67^{D}	0.53^{D}	0.84^{D}
0.20°	0.36^{C}	0.34^{D}	0.39^{C}	0.49^{C}	0.57^{C}	0.69^{C}	1.03^{C}	1.42^{C}	1.57^{C}	1.18^{C}	0.65^{D}	0.61^{D}	0.95^{D}
0.30°	0.48^{D}	0.48^{C}	0.52^{C}	0.65^{C}	0.76^{C}	0.92^{C}	1.37^{C}	1.87^{C}	2.05^{C}	1.52^{C}	0.84^{C}	0.79^{C}	1.21^{D}
0.40°	0.64^{D}	0.67^{C}	0.71^{C}	0.86^{C}	1.00^{C}	1.22^{C}	1.81^{C}	2.46^{C}	2.68^{C}	1.96^{C}	1.10^{C}	1.02^{C}	1.54^{C}
0.50°	0.86^{C}	0.92^{C}	0.97^{B}	1.13^{B}	1.32^{B}	1.61^{C}	2.39^{C}	3.24^{C}	3.50^{C}	2.53^{C}	1.42^{C}	1.33^{C}	1.95^{C}
0.70	1.37^{C}	1.50^{B}	1.56^{B}	1.75^{B}	2.03^{B}	2.47^{B}	3.62^{B}	4.84^{B}	5.09^{B}	3.80^{B}	2.06^{B}	1.92^{B}	2.67^{C}
1.00	2.18^{C}	2.36^{D}	2.45^{D}	2.68^{D}	3.00^{B}	3.60^{D}	5.13^{D}	6.84^{D}	6.66^{D}	4.51^{D}	2.68^{D}	2.47^{B}	3.14^{C}
1.50	4.73^{C}	5.03^{B}	5.20^{B}	5.46^{B}	5.77^{B}	6.76^{B}	9.17^{B}	11.25^{B}	10.42^{B}	6.68^{B}	4.16^{B}	3.75^{B}	4.11^{C}
2.00	10.29^{C}	10.71^{D}	11.06^{B}	11.13^{B}	11.06^{B}	12.70^{B}	16.35^{C}	19.07^{B}	16.32^{B}	9.82^{B}	6.45^{B}	5.68^{B}	5.38^{B}
3.00	16.78^{C}	17.27^{B}	18.60^{D}	18.88^{D}	18.52^{D}	20.80^{B}	25.03^{B}	27.42^{B}	22.86^{B}	14.29^{D}	9.66^{D}	8.46^{B}	7.97^{B}
4.00	23.38^{C}	27.00^{B}	30.37^{B}	31.18^{B}	30.21^{B}	32.33^{B}	37.38^{B}	38.60^{B}	31.48^{B}	20.55^{B}	14.25^{B}	12.42^{B}	11.76^{B}
5.00	34.65^{C}	42.20^{B}	49.56^{B}	51.48^{B}	49.28^{B}	50.99^{B}	55.82^{B}	54.35^{B}	43.36^{B}	29.54^{B}	21.03^{B}	18.23^{B}	17.35^{B}
7.00	70.54^{B}	93.82^{B}	118.41^{B}	125.36^{B}	117.58^{B}	114.67^{B}	113.80^{B}	99.81^{B}	76.92^{B}	56.71^{B}	42.39^{B}	36.54^{B}	35.16^{B}
10.00	96.27^{B}	121.89^{B}	147.74^{B}	154.99^{B}	146.26^{B}	141.99^{B}	135.39^{B}	116.42^{D}	93.47^{B}	72.30^{B}	56.19^{B}	50.14^{B}	50.04^{B}
15.00	161.66^{B}	188.53^{B}	213.66^{B}	220.73^{B}	210.45^{B}	202.72^{B}	180.84^{B}	150.49^{B}	129.35^{B}	108.36^{B}	89.90^{B}	84.95^{B}	90.09^{B}
20.00	271.46^{B}	291.60^{B}	308.99^{B}	314.35^{B}	302.81^{B}	289.43^{B}	241.56^{B}	194.52^{B}	178.99^{B}	162.41^{B}	143.83^{B}	143.93^{B}	162.20^{C}

* Extrapolated from original data.

Variation in data <10%, >10%^{A}, >20%^{B}, >50%^{C}, >100%^{D}

Average N_2O (ppbv) for JULY

Press.	Latitude (°N)												
(mb)	-90°	-40	-30	-20	-10	0	+10	+20	+30	+40	+50	+60	+70°
0.10*	0.31[D]	0.24[D]	0.30[D]	0.45[D]	0.49[D]	0.70[D]	1.19[C]	1.56[C]	1.52[C]	0.99[D]	0.56[D]	0.59[D]	0.98[D]
0.15*	0.35[D]	0.28[D]	0.36[D]	0.51[C]	0.56[C]	0.80[C]	1.36[C]	1.79[C]	1.73[C]	1.12[D]	0.64[D]	0.66[D]	1.10[D]
0.20*	0.40[D]	0.32[D]	0.40[D]	0.59[C]	0.65[C]	0.92[C]	1.56[C]	2.04[C]	1.97[C]	1.28[C]	0.73[D]	0.75[D]	1.23[D]
0.30*	0.51[D]	0.44[D]	0.55[C]	0.77[C]	0.86[C]	1.22[C]	2.04[C]	2.67[C]	2.56[C]	1.65[C]	0.94[C]	0.96[D]	1.54[D]
0.40*	0.66[D]	0.59[C]	0.74[C]	1.02[C]	1.14[C]	1.62[C]	2.68[C]	3.48[C]	3.32[C]	2.12[C]	1.21[C]	1.23[C]	1.93[C]
0.50*	0.85[D]	0.81[C]	1.00[C]	1.34[C]	1.52[C]	2.14[C]	3.50[C]	4.55[B]	4.30[C]	2.74[C]	1.56[C]	1.57[C]	2.41[C]
0.70	1.25[C]	1.26[C]	1.57[B]	2.00[B]	2.28[B]	3.22[B]	5.16[B]	6.64[B]	6.16[B]	3.87[B]	2.21[B]	2.17[B]	3.15[B]
1.00	1.76[C]	1.84[C]	2.24[B]	2.73[B]	3.09[B]	4.41[B]	6.94[B]	8.74[B]	7.81[B]	4.78[B]	2.73[B]	2.58[B]	3.36[B]
1.50	3.11[C]	3.43[C]	4.07[B]	4.56[B]	5.17[B]	7.45[B]	11.35[B]	13.82[B]	11.62[B]	6.80[B]	3.89[B]	3.35[B]	3.73[B]
2.00	5.50[C]	6.39[B]	7.39[B]	7.63[B]	8.62[B]	12.59[B]	18.57[B]	21.85[B]	17.27[B]	9.67[B]	5.55[B]	4.40[B]	4.14[B]
3.00	9.18[C]	10.70[B]	12.19[B]	12.73[B]	14.29[B]	19.62[B]	27.44[B]	31.11[D]	24.41[B]	14.23[B]	8.52[B]	6.74[B]	6.26[B]
4.00	15.06[C]	17.52[D]	19.70[D]	20.92[B]	23.30[D]	30.03[B]	39.82[B]	43.55[B]	34.02[B]	20.73[B]	12.97[B]	10.30[B]	9.51[B]
5.00	24.68[C]	28.67[B]	31.83[B]	34.37[B]	38.01[B]	45.96[B]	57.78[B]	60.95[B]	47.43[B]	30.21[B]	19.74[B]	15.72[B]	14.47[D]
7.00	60.34[B]	69.50[B]	75.33[B]	83.79[B]	91.30[B]	98.57[B]	112.21[B]	110.75[B]	85.93[B]	59.44[B]	42.06[B]	33.86[B]	31.16[B]
10.00	90.09[B]	96.54[B]	103.50[B]	115.37[D]	123.36[D]	129.27[B]	135.48[B]	128.09[B]	104.06[B]	76.60[B]	56.92[B]	48.74[B]	48.13[B]
15.00	175.67[B]	166.94[B]	175.77[C]	196.61[C]	203.72[D]	203.12[B]	185.46[B]	163.21[B]	143.17[B]	116.92[B]	94.21[B]	89.46[B]	9..35[B]
20.00	342.58[B]	238.67[B]	298.49[C]	335.05[C]	336.42[B]	319.17[b]	253.88[B]	207.98[b]	196.97[B]	178.46[B]	155.95[B]	164.19[D]	205.06[B]

Average N_2O (ppbv) for AUGUST

Press.	Latitude (°N)												
(mb)	-50°	-40	-30	-20	-10	0	+10	+20	+30	+40	+50	+60	+70°
0.10*	0.58[D]	0.37[D]	0.41[D]	0.68[D]	0.85[D]	1.08[D]	1.56[D]	1.91[C]	1.90[D]	1.31[D]	0.79[D]	0.52[D]	0.34[D]
0.15*	0.65[D]	0.43[D]	0.47[D]	0.77[D]	0.97[D]	1.24[D]	1.78[C]	2.18[C]	2.16[C]	1.48[D]	0.89[D]	0.60[D]	0.38[D]
0.20*	0.73[D]	0.50[D]	0.55[D]	0.87[C]	1.10[C]	1.41[C]	2.03[C]	2.49[C]	2.45[C]	1.68[D]	1.00[D]	0.67[D]	0.44[D]
0.30*	0.92[D]	0.68[D]	0.74[C]	1.12[C]	1.41[C]	1.83[C]	2.65[C]	3.25[C]	3.15[C]	2.14[C]	1.27[C]	0.85[D]	0.57[D]
0.40*	1.16[D]	0.91[C]	0.99[C]	1.45[C]	1.82[C]	2.38[C]	3.45[C]	4.24[C]	4.07[C]	2.73[C]	1.61[C]	1.08[C]	0.74[C]
0.50*	1.46[C]	1.22[C]	1.33[C]	1.87[C]	2.34[C]	3.09[C]	4.50[C]	5.53[B]	5.24[C]	3.48[C]	2.04[C]	1.37[C]	0.96[C]
0.70	1.96[C]	1.83[C]	2.04[B]	2.70[B]	3.38[B]	4.51[B]	6.58[B]	8.07[B]	7.48[B]	4.86[B]	2.77[B]	1.85[B]	1.33[B]
1.00	2.28[C]	2.40[C]	2.78[B]	3.59[B]	4.51[B]	6.08[B]	8.81[B]	10.61[B]	9.80[B]	6.00[B]	3.20[B]	2.08[B]	1.54[B]
1.50	2.91[C]	3.75[C]	4.66[B]	5.79[B]	7.31[B]	9.99[B]	14.31[B]	16.76[B]	14.54[B]	8.52[B]	4.07[B]	2.52[B]	1.94[C]
2.00	3.72[C]	5.88[B]	7.83[B]	9.33[B]	11.86[B]	16.40[B]	23.24[B]	26.47[B]	22.04[B]	12.11[B]	5.19[B]	3.06[B]	2.46[C]
3.00	6.17[C]	9.39[B]	12.16[B]	14.40[B]	18.00[B]	24.16[B]	32.81[B]	35.86[B]	29.57[B]	17.18[B]	8.03[B]	4.87[B]	3.86[C]
4.00	10.22[C]	14.81[B]	18.57[B]	21.88[B]	26.89[B]	34.93[B]	45.46[B]	47.68[B]	39.03[B]	24.13[B]	12.42[B]	7.76[B]	6.06[C]
5.00	16.93[C]	23.36[B]	28.34[B]	33.24[B]	40.17[B]	50.50[B]	62.99[B]	63.39[B]	51.52[B]	33.89[B]	19.21[B]	12.38[B]	9.53[B]
7.00	42.23[C]	53.36[B]	61.12[B]	70.94[B]	83.00[B]	98.06[B]	113.10[B]	105.90[B]	85.03[B]	62.55[B]	42.16[B]	28.82[B]	21.70[B]
10.00	63.91[C]	79.04[B]	89.96[B]	101.79[B]	114.70[B]	127.34[b]	140.02[B]	130.11[B]	105.08[B]	81.00[B]	58.71[B]	42.88[B]	33.66[B]
15.00	127.53[C]	152.15[B]	171.32[C]	185.82[C]	196.66[B]	196.80[B]	199.86[B]	183.37[B]	149.45[B]	124.64[B]	101.94[B]	83.15[B]	69.95[B]
20.00	254.48[C]	292.87[C]	326.26[C]	339.20[C]	337.19[B]	304.18[B]	288.27[B]	258.42[B]	212.61[B]	191.77[B]	177.00[B]	161.28[B]	146.38[B]

Average N_2O (ppbv) for SEPTEMBER

Press.	Latitude (°N)												
(mb)	-90°	-40	-30	-20	-10	0	+10	+20	+30	+40	+50	+60	+70°
0.10*	0.91[D]	0.82[D]	0.69[D]	0.66[D]	0.90[D]	1.23[D]	1.49[D]	1.82[D]	2.02[C]	1.86[D]	1.29[D]	0.74[D]	0.43[D]
0.15*	1.03[D]	0.93[D]	0.78[D]	0.75[D]	1.02[D]	1.40[D]	1.70[D]	2.08[C]	2.31[C]	2.09[D]	1.43[D]	0.82[D]	0.49[D]
0.20*	1.17[D]	1.06[D]	0.89[C]	0.86[C]	1.17[C]	1.60[C]	1.94[C]	2.38[C]	2.63[C]	2.36[C]	1.59[D]	0.92[D]	0.56[D]
0.30*	1.50[D]	1.36[C]	1.15[C]	1.13[C]	1.62[C]	2.07[C]	2.53[C]	3.11[C]	3.42[C]	2.98[C]	1.97[C]	1.15[C]	0.73[D]
0.40*	1.92[D]	1.75[C]	1.50[C]	1.48[C]	1.98[C]	2.69[C]	3.30[C]	4.07[C]	4.44[C]	3.76[C]	2.43[C]	1.44[C]	0.94[C]
0.50*	2.46[C]	2.24[C]	1.94[C]	1.94[C]	2.59[C]	3.49[C]	4.29[C]	5.32[C]	5.77[B]	4.79[C]	3.00[C]	1.80[C]	1.21[C]
0.70	3.44[C]	3.17[B]	2.82[B]	2.87[D]	3.79[B]	5.08[B]	6.31[B]	7.81[B]	8.31[B]	6.59[B]	3.97[B]	2.37[B]	1.59[B]
1.00	4.13[C]	3.97[B]	3.73[B]	3.94[B]	5.13[B]	6.84[B]	8.57[B]	10.43[B]	10.65[B]	8.00[B]	4.64[B]	2.58[B]	1.53[B]
1.50	5.63[C]	5.78[B]	5.94[B]	6.65[B]	8.49[B]	11.20[B]	14.28[B]	16.87[B]	16.10[B]	11.03[B]	6.00[B]	2.98[B]	1.42[B]
2.00	7.66[C]	8.41[B]	9.47[B]	11.23[B]	14.04[B]	18.36[B]	23.80[B]	27.30[B]	24.35[B]	15.22[B]	7.77[B]	3.43[B]	1.32[B]
3.00	10.94[C]	12.31[B]	14.00[B]	16.65[B]	20.90[B]	27.19[B]	34.41[B]	37.59[B]	32.59[B]	20.76[B]	11.15[B]	5.32[B]	2.23[B]
4.00	15.49[C]	17.82[B]	20.38[B]	24.20[B]	30.52[B]	39.56[B]	48.79[B]	50.77[B]	42.92[B]	28.05[B]	15.94[B]	8.28[B]	3.86[B]
5.00	21.95[B]	25.78[B]	29.65[B]	35.18[B]	44.58[B]	57.58[B]	69.17[B]	68.57[B]	56.51[B]	37.89[B]	22.77[B]	12.89[B]	6.67[B]
7.00	41.75[B]	50.65[B]	58.75[B]	69.51[B]	88.48[B]	112.77[B]	128.87[B]	117.24[B]	92.76[B]	65.40[B]	43.51[B]	28.79[B]	18.13[B]
10.00	64.68[B]	74.09[B]	84.42[B]	99.17[B]	120.68[B]	143.81[B]	153.88[B]	137.73[B]	113.10[B]	85.31[B]	59.48[B]	42.86[B]	31.54[B]
15.00	134.14[B]	139.67[B]	154.49[B]	179.30[C]	202.46[B]	215.68[B]	206.80[B]	180.14[B]	157.38[B]	132.84[B]	100.15[B]	83.21[B]	79.40[B]
20.00	278.22[C]	263.29[B]	282.72[C]	324.18[C]	339.65[C]	323.45[B]	277.94[B]	235.61[B]	218.99[B]	206.86[B]	168.63[B]	161.54[B]	199.87[B]

* Extrapolated from original data.

Variation in data <10%, >10%[A], >20%[B], >50%[C], >100%[D]

Average N_2O (ppbv) for OCTOBER

Press. (mb)	Latitude (°N)												
	-50°	-40	-30	-20	-10	0	+10	+20	+30	+40	+50	+60	+70°
0.10°	1.12^{D}	1.01^{D}	0.72^{D}	0.60^{D}	0.82^{D}	0.80^{D}	0.98^{D}	1.18^{D}	1.41^{D}	1.53^{D}	1.25^{D}	0.84^{D}	0.52^{D}
0.15°	1.26^{D}	1.22^{D}	0.82^{D}	0.70^{D}	0.94^{D}	1.02^{D}	1.12^{D}	1.35^{D}	1.60^{D}	1.73^{C}	1.41^{C}	0.94^{D}	0.59^{D}
0.20°	1.43^{D}	1.37^{D}	0.94^{D}	0.80^{D}	1.07^{D}	1.16^{C}	1.28^{C}	1.54^{C}	1.82^{C}	1.96^{C}	1.59^{C}	1.05^{D}	0.66^{D}
0.30°	1.82^{D}	1.72^{D}	1.23^{C}	1.07^{C}	1.40^{C}	1.52^{C}	1.68^{C}	2.00^{C}	2.35^{C}	2.51^{C}	2.00^{C}	1.32^{C}	0.84^{D}
0.40°	2.32^{D}	2.18^{C}	1.60^{C}	1.42^{C}	1.83^{C}	1.99^{C}	2.21^{C}	2.61^{C}	3.04^{C}	3.21^{C}	2.53^{C}	1.66^{C}	1.08^{C}
0.50°	2.95^{C}	2.75^{C}	2.08^{C}	1.89^{C}	2.39^{C}	2.61^{C}	2.89^{C}	3.39^{C}	3.92^{C}	4.12^{C}	3.20^{C}	2.10^{C}	1.37^{C}
0.70	4.01^{C}	3.77^{C}	3.05^{B}	2.87^{B}	3.51^{B}	3.86^{B}	4.29^{B}	5.00^{B}	5.69^{B}	5.80^{B}	4.41^{B}	2.83^{B}	1.83^{B}
1.00	4.56^{C}	4.59^{B}	4.07^{D}	3.96^{B}	4.74^{B}	5.24^{D}	5.86^{B}	6.86^{B}	7.61^{D}	7.28^{B}	5.37^{B}	3.30^{B}	1.94^{C}
1.50	5.64^{C}	6.35^{D}	6.58^{D}	6.80^{B}	7.79^{D}	8.75^{D}	9.85^{B}	11.61^{B}	12.37^{B}	10.64^{B}	7.46^{B}	4.25^{C}	2.15^{C}
2.00	6.97^{B}	8.80^{B}	10.64^{D}	11.66^{B}	12.83^{B}	14.59^{B}	16.57^{B}	19.87^{B}	20.09^{B}	15.54^{B}	10.38^{B}	5.48^{C}	2.38^{C}
3.00	10.89^{B}	13.20^{B}	15.56^{B}	17.57^{B}	20.18^{B}	23.44^{B}	26.80^{B}	[illegible]15^{B}	28.59^{B}	21.59^{B}	14.53^{B}	7.98^{C}	3.72^{C}
4.00	17.03^{B}	19.65^{B}	22.37^{B}	25.96^{B}	31.22^{B}	37.01^{D}	42.61^{D}	45.33^{B}	39.92^{B}	29.62^{B}	20.14^{B}	11.57^{B}	5.84^{C}
5.00	26.63^{B}	29.25^{B}	32.14^{B}	38.35^{B}	48.30^{B}	58.46^{D}	67.75^{B}	68.16^{B}	55.74^{B}	40.63^{B}	27.92^{B}	16.78^{D}	9.18^{C}
7.00	59.18^{B}	59.84^{B}	61.95^{D}	77.31^{B}	105.20^{D}	131.63^{B}	153.45^{D}	140.02^{B}	101.29^{B}	71.89^{B}	50.45^{D}	33.01^{B}	21.02^{C}
10.00	75.74^{C}	79.13^{B}	83.38^{B}	100.37^{B}	132.03^{B}	160.71^{B}	175.36^{B}	158.82^{D}	123.17^{B}	91.68^{B}	66.28^{B}	47.31^{B}	34.21^{B}
15.00	114.25^{D}	126.06^{C}	130.77^{B}	155.07^{B}	192.79^{B}	224.14^{B}	219.04^{B}	195.91^{B}	170.66^{B}	137.50^{B}	104.36^{B}	86.18^{B}	77.04^{B}
20.00	172.34^{D}	200.83^{C}	224.35^{C}	239.59^{C}	281.52^{B}	312.61^{B}	273.60^{B}	241.67^{B}	236.46^{D}	206.20^{B}	164.37^{B}	157.00^{B}	173.51^{D}

Average N_2O (ppbv) for NOVEMBER

Press. (mb)	Latitude (°N)												
	-50°	-40	-30	-20	-10	0	+10	+20	+30	+40	+50	+60	+70°
0.10°	0.29^{D}	0.51^{D}	0.67^{D}	0.63^{D}	0.73^{D}	0.71^{C}	0.55^{C}	0.55^{D}	0.70^{D}	0.99^{C}	0.85^{C}	0.60^{C}	0.61
0.15°	0.33^{D}	0.5[illegible]^{D}	0.76^{D}	0.73^{D}	0.84^{D}	0.82^{C}	0.63^{C}	0.64^{C}	0.80^{C}	1.12^{C}	0.97^{C}	0.68^{C}	0.68
0.20°	0.38^{D}	0.67^{D}	0.87^{D}	0.85^{D}	0.97^{C}	0.94^{C}	0.72^{C}	0.74^{C}	0.92^{C}	1.28^{C}	1.09^{C}	0.77^{C}	0.76
0.30°	0.51^{D}	0.88^{D}	1.14^{C}	1.13^{C}	1.29^{C}	1.23^{C}	0.96^{C}	0.98^{C}	1.22^{C}	1.65^{C}	1.41^{C}	0.98^{B}	0.94
0.40°	0.68^{D}	1.15^{C}	1.50^{C}	1.52^{C}	1.72^{C}	1.62^{C}	1.26^{C}	1.29^{C}	1.60^{C}	2.12^{C}	1.81^{C}	1.25^{B}	1.17
0.50°	0.91^{D}	1.50^{C}	1.96^{C}	2.03^{C}	2.28^{C}	2.13^{C}	1.67^{B}	1.72^{C}	2.11^{C}	2.73^{C}	[illegible]2^{B}	1.60^{B}	1.45
0.70	1.39^{C}	2.21^{C}	2.89^{B}	3.10^{B}	3.44^{B}	3.18^{B}	2.54^{B}	2.61^{B}	3.14^{B}	3.87^{B}	3.27^{B}	2.21^{B}	1.82^{A}
1.00	1.93^{C}	2.96^{C}	3.92^{B}	4.35^{B}	4.73^{B}	4.37^{B}	3.66^{B}	3.73^{B}	4.24^{B}	4.84^{B}	4.07^{B}	2.60^{B}	1.73^{B}
1.50	3.36^{C}	4.84^{B}	6.50^{B}	7.65^{B}	8.05^{B}	7.43^{B}	6.69^{B}	6.74^{B}	7.03^{B}	7.01^{B}	5.87^{B}	3.41^{B}	1.59^{B}
2.00	5.86^{C}	7.90^{B}	10.78^{B}	13.45^{B}	13.70^{B}	12.65^{B}	12.24^{B}	12.20^{B}	11.65^{B}	10.18^{B}	8.47^{B}	4.47^{B}	1.47^{B}
3.00	9.17^{C}	12.11^{B}	16.24^{B}	20.77^{B}	22.15^{B}	20.96^{B}	20.47^{B}	20.39^{B}	19.00^{B}	15.87^{B}	12.51^{B}	6.78^{B}	2.53^{B}
4.00	14.09^{B}	18.25^{B}	24.04^{B}	31.42^{B}	35.19^{B}	34.16^{B}	33.53^{B}	33.42^{B}	30.50^{B}	24.58^{B}	18.29^{B}	10.24^{B}	4.45^{B}
5.00	21.63^{B}	27.50^{B}	35.59^{B}	47.51^{B}	55.91^{B}	55.68^{B}	54.92^{B}	54.75^{B}	48.97^{B}	38.08^{B}	26.74^{B}	15.47^{B}	7.84^{C}
7.00	46.96^{C}	57.43^{B}	71.47^{B}	98.61^{B}	126.69^{B}	131.90^{B}	131.04^{B}	130.73^{B}	113.14^{B}	83.13^{B}	53.19^{B}	32.77^{B}	21.80^{C}
10.00	86.48^{C}	74.96^{C}	85.44^{B}	112.39^{B}	147.60^{B}	153.95^{B}	150.24^{B}	150.14^{B}	133.67^{B}	104.57^{B}	72.66^{B}	48.32^{B}	33.94^{C}
15.00	118.64^{D}	116.86^{C}	115.06^{B}	139.76^{B}	190.39^{B}	199.19^{B}	188.71^{B}	189.11^{B}	176.49^{B}	153.29^{B}	122.19^{B}	92.27^{C}	70.97^{B}
20.00	211.73^{D}	182.16^{D}	154.94^{B}	173.81^{B}	245.58^{B}	257.71^{B}	237.02^{B}	238.19^{B}	233.03^{B}	224.71^{B}	205.49^{C}	176.21^{C}	148.41^{B}

Average N_2O (ppbv) for DECEMBER

Press. (mb)	Latitude (°N)												
	-50°	-40	-30	-20	-10	0	+10	+20	+30	+40	+50	+60	+70°
0.10°	0.14^{D}	0.31^{D}	0.60^{D}	0.97^{D}	1.09^{D}	0.81^{C}	0.58^{C}	0.51^{D}	0.57^{D}	0.77^{D}	0.74^{C}	0.56^{D}	0.50^{D}
0.15°	0.16^{D}	0.36^{D}	0.70^{D}	1.11^{C}	1.24^{C}	0.93^{C}	0.66^{C}	0.59^{C}	0.66^{D}	0.87^{D}	0.84^{C}	0.64^{D}	0.57^{D}
0.20°	0.19^{D}	0.41^{D}	0.81^{C}	1.28^{C}	1.42^{C}	1.06^{C}	0.75^{C}	0.67^{C}	0.78^{C}	0.99^{C}	0.94^{C}	0.73^{C}	0.65^{D}
0.30°	0.26^{D}	0.56^{D}	1.07^{C}	1.67^{C}	1.86^{C}	1.38^{C}	0.98^{C}	0.88^{C}	0.95^{C}	1.26^{C}	1.20^{C}	0.94^{C}	0.84^{D}
0.40°	0.35^{D}	0.75^{C}	1.43^{C}	2.19^{C}	2.43^{C}	1.80^{C}	1.28^{C}	1.15^{C}	1.28^{C}	1.62^{C}	1.52^{C}	1.21^{C}	1.09^{C}
0.50°	0.47^{D}	1.01^{C}	1.90^{C}	2.86^{C}	3.17^{C}	2.35^{B}	1.66^{B}	1.50^{C}	1.68^{C}	2.06^{C}	1.93^{B}	1.56^{C}	1.41^{C}
0.70	0.73^{C}	1.56^{C}	2.89^{B}	4.26^{B}	4.69^{B}	3.47^{B}	2.44^{B}	2.21^{B}	2.45^{B}	2.89^{B}	2.65^{B}	2.14^{B}	1.88^{B}
1.00	1.08^{C}	2.21^{C}	4.04^{D}	5.90^{D}	6.43^{B}	4.76^{B}	3.33^{B}	2.94^{B}	3.16^{B}	3.59^{B}	3.18^{B}	2.41^{B}	1.92^{B}
1.50	2.05^{C}	3.97^{B}	7.03^{B}	10.16^{D}	10.90^{B}	8.06^{B}	5.57^{B}	4.75^{B}	4.83^{B}	5.13^{B}	4.29^{B}	2.94^{B}	1.99^{B}
2.00	3.92^{C}	7.12^{B}	12.26^{B}	17.49^{B}	18.46^{B}	13.64^{B}	9.34^{B}	7.66^{B}	7.39^{B}	7.34^{B}	5.79^{B}	3.58^{B}	2.06^{B}
3.00	6.63^{C}	11.08^{B}	18.08^{D}	26.14^{D}	28.71^{D}	21.97^{D}	15.55^{B}	13.20^{B}	12.80^{B}	12.10^{B}	9.22^{D}	5.61^{B}	3.12^{B}
4.00	10.95^{B}	16.89^{B}	26.09^{B}	38.29^{B}	43.84^{B}	34.79^{D}	25.48^{B}	22.48^{B}	21.98^{B}	19.81^{B}	14.62^{B}	8.78^{B}	4.80^{B}
5.00	18.10^{B}	25.73^{B}	37.65^{B}	56.07^{B}	66.93^{B}	55.09^{B}	41.76^{B}	38.28^{B}	37.75^{B}	32.44^{B}	23.19^{B}	13.76^{B}	7.37^{C}
7.00	44.42^{B}	54.57^{B}	72.23^{B}	109.70^{B}	140.88^{B}	124.40^{B}	100.44^{B}	98.21^{B}	98.13^{B}	78.26^{B}	53.44^{B}	31.18^{C}	16.21^{C}
10.00	59.11^{C}	68.65^{B}	84.97^{B}	120.29^{B}	155.71^{B}	149.08^{B}	124.85^{B}	119.72^{B}	117.36^{B}	102.70^{B}	78.12^{B}	47.35^{C}	26.10^{C}
15.00	95.19^{D}	100.66^{C}	111.40^{B}	140.27^{B}	183.98^{B}	201.54^{B}	179.40^{B}	166.55^{B}	158.13^{B}	161.52^{B}	147.07^{C}	95.15^{C}	57.75^{C}
20.00	153.29^{D}	147.56^{C}	146.04^{B}	163.58^{B}	217.38^{B}	272.46^{B}	257.78^{B}	231.69^{B}	213.07^{B}	254.04^{B}	276.89^{C}	191.23^{C}	127.78^{C}

* Extrapolated from original data.

Variation in data ^{A}<10%, ^{B}>10%, ^{C}>20%, ^{D}>50%, ^{E}>100%

Average CH_4 (ppmv) for JANUARY

Press.	Latitude (°N)												
(mb)	−50*	−40	−30	−20	−10	0	+10	+20	+30	+40	+50	+60	+70*
0.10*	0.14	0.12	0.10[A]	0.09[A]	0.10[A]	0.11[A]	0.12[A]	0.12[A]	0.12[A]	0.11[A]	0.09[A]	0.08[A]	0.07[B]
0.15*	0.14	0.12	0.11[A]	0.10[A]	0.11[A]	0.12[A]	0.13[A]	0.14[A]	0.13[A]	0.12[A]	0.10[A]	0.09[A]	0.08[B]
0.20	0.14	0.13	0.12[A]	0.11[A]	0.12[A]	0.13[A]	0.14[A]	0.15[A]	0.14[A]	0.13[A]	0.11[A]	0.09[A]	0.08[B]
0.30	0.15	0.15[A]	0.14[A]	0.15[A]	0.16[A]	0.17[A]	0.17[A]	0.17[A]	0.16[A]	0.15[A]	0.13[A]	0.11[A]	0.09[B]
0.40	0.15[A]	0.16[A]	0.18[A]	0.19[A]	0.21[A]	0.21[A]	0.21[A]	0.21[A]	0.19[A]	0.18[A]	0.16[A]	0.13[A]	0.10[A]
0.50	0.16[A]	0.18[A]	0.22[A]	0.25[A]	0.26[A]	0.26[A]	0.26[A]	0.25[A]	0.22[A]	0.20[A]	0.19[A]	0.16[A]	0.12[A]
0.70	0.17[A]	0.22[A]	0.28[A]	0.35[A]	0.37[A]	0.35[A]	0.33[A]	0.30[A]	0.27[A]	0.25[A]	0.23[A]	0.20[A]	0.14[A]
1.00	0.20[A]	0.25[A]	0.32[A]	0.40[A]	0.42[A]	0.40[A]	0.38[A]	0.34[A]	0.30[A]	0.27[A]	0.26[A]	0.22[A]	0.16[A]
1.50	0.24[A]	0.31[A]	0.40[A]	0.51[A]	0.54[A]	0.50[A]	0.46[A]	0.40[A]	0.35[A]	0.32[A]	0.30[A]	0.26[A]	0.19[B]
2.00	0.29[A]	0.38[A]	0.50	0.64	0.69	0.63	0.55	0.47[A]	0.40[A]	0.37[A]	0.35[A]	0.31[B]	0.23[B]
3.00	0.34[A]	0.44[A]	0.56[A]	0.69	0.76	0.70	0.63	0.54[A]	0.47[A]	0.43[A]	0.41[A]	0.35[B]	0.26[B]
4.00	0.41[A]	0.50[A]	0.61[A]	0.75	0.82	0.78	0.71	0.61[A]	0.54[A]	0.51[A]	0.48[A]	0.40[A]	0.29[B]
5.00	0.49	0.57[A]	0.67[A]	0.80	0.89	0.87	0.79	0.70	0.63[A]	0.60[A]	0.55[A]	0.45[A]	0.32[B]
7.00	0.67	0.71	0.79[A]	0.91	1.02[A]	1.05	0.99	0.89	0.82	0.79	0.72[A]	0.58[A]	0.41[B]
10.00	0.76[A]	0.78[A]	0.83[A]	0.94[A]	1.06[A]	1.14[A]	1.10[A]	0.99[A]	0.92[A]	0.90[A]	0.83[A]	0.69[A]	0.56[B]
15.00	0.93[B]	0.90[A]	0.91[A]	0.99[A]	1.14[A]	1.31[A]	1.31[A]	1.18[A]	1.12[A]	1.11[B]	1.03[B]	0.95[B]	0.94[B]
20.00	1.15[B]	1.05[B]	1.00[A]	1.04[A]	1.22[A]	1.50[A]	1.57[A]	1.42[B]	1.35[B]	1.37[B]	1.28[B]	1.29[B]	1.57[B]

Average CH_4 (ppmv) for FEBRUARY

Press.	Latitude (°N)												
(mb)	−50*	−40	−30	−20	−10	0	+10	+20	+30	+40	+50	+60	+70*
0.10*	0.18[B]	0.11[A]	0.08[A]	0.08[A]	0.09[A]	0.10[A]	0.10[A]	0.10[A]	0.09[A]	0.09[A]	0.09[A]	0.08[A]	0.07[B]
0.15*	0.17[A]	0.12[A]	0.09[A]	0.09[A]	0.11[A]	0.11[A]	0.12[A]	0.11[A]	0.10[A]	0.10[A]	0.09[A]	0.08[A]	0.07[B]
0.20	0.17[A]	0.13[A]	0.10[A]	0.11[A]	0.12[A]	0.13[A]	0.13[A]	0.12[A]	0.11[A]	0.11[A]	0.10[A]	0.09[A]	0.08[B]
0.30	0.17[A]	0.15[A]	0.14[A]	0.15[A]	0.16[A]	0.16[A]	0.16[A]	0.15[A]	0.14[A]	0.14[A]	0.13[A]	0.11[A]	0.10[B]
0.40	0.17[A]	0.17[A]	0.18[A]	0.20[A]	0.21[A]	0.20[A]	0.19[A]	0.19[A]	0.18[A]	0.17[A]	0.16[A]	0.13[A]	0.12[B]
0.50	0.17[A]	0.20[A]	0.24[A]	0.27[A]	0.28[A]	0.25[A]	0.24[A]	0.24[A]	0.23[A]	0.21[A]	0.19[A]	0.16[A]	0.14[B]
0.70	0.18[A]	0.25[A]	0.33[A]	0.40[A]	0.39[A]	0.34[A]	0.32[A]	0.33[A]	0.31[A]	0.28[A]	0.25[A]	0.21[A]	0.18[B]
1.00	0.20[A]	0.28[A]	0.38[A]	0.46[A]	0.45[A]	0.39[A]	0.37[A]	0.37[A]	0.34[A]	0.31[A]	0.27[A]	0.23[A]	0.21[B]
1.50	0.25[A]	0.34[A]	0.46[A]	0.56[A]	0.57[A]	0.51	0.47[A]	0.44[A]	0.40[A]	0.36[A]	0.32[A]	0.28[A]	0.27[B]
2.00	0.29[A]	0.42[A]	0.57[A]	0.70[A]	0.72[A]	0.65	0.59	0.54[A]	0.47[A]	0.42[A]	0.37[A]	0.35[A]	0.34[B]
3.00	0.36[A]	0.48[A]	0.62	0.75	0.79[A]	0.73	0.67	0.61[A]	0.53[A]	0.47[A]	0.42[A]	0.39[A]	0.38[B]
4.00	0.41[A]	0.53	0.67	0.80	0.85	0.81	0.74	0.68	0.59	0.52[A]	0.48[A]	0.45[A]	0.41[B]
5.00	0.49[A]	0.60	0.73	0.86	0.92	0.89	0.83	0.76	0.66	0.58	0.54[A]	0.51[A]	0.45[B]
7.00	0.65	0.73	0.84	0.96	1.04	1.06	1.00	0.92	0.81	0.71	0.68[A]	0.63[A]	0.54[B]
10.00	0.71[A]	0.78[A]	0.87	0.98	1.08[A]	1.14[A]	1.12[A]	1.02[A]	0.89[A]	0.80[A]	0.79[A]	0.75[A]	0.68[B]
15.00	0.83[B]	0.86[A]	0.93	1.02[A]	1.15[A]	1.29[A]	1.33[A]	1.20[A]	1.03[B]	0.99[B]	1.00[B]	1.00[B]	0.99[B]
20.00	0.97[B]	0.95[A]	0.99[A]	1.06[A]	1.21[A]	1.46[A]	1.[illegible][A]	1.40[B]	1.20[B]	1.23[B]	1.28[B]	1.32[B]	1.43[B]

Average CH_4 (ppmv) for MARCH

Press.	Latitude (°N)												
(mb)	−50*	−40	−30	−20	−10	0	+10	+20	+30	+40	+50	+60	+70*
0.10*	0.18	0.11[A]	0.08[B]	0.08[A]	0.10[A]	0.10[A]	0.10[A]	0.09[A]	0.08[A]	0.08	0.08	0.06[A]	0.05[B]
0.15*	0.18[A]	0.12[A]	0.09[B]	0.09[A]	0.11[A]	0.11[A]	0.11[A]	0.10[A]	0.09[A]	0.09	0.08	0.07[A]	0.06[B]
0.20	0.18[A]	0.13[A]	0.11[B]	0.11[A]	0.12[A]	0.13[A]	0.12[A]	0.12[A]	0.11[A]	0.10	0.09[A]	0.08[A]	0.06[B]
0.30	0.18[A]	0.17[A]	0.15[A]	0.15[A]	0.16[A]	0.16[A]	0.15[A]	0.15[A]	0.14[A]	0.13[A]	0.11[A]	0.09[A]	0.08[B]
0.40	0.19[A]	0.21[A]	0.22[A]	0.21[A]	0.20[A]	0.19[A]	0.18[A]	0.18[A]	0.18[A]	0.16[A]	0.14[A]	0.12[A]	0.10[A]
0.50	0.19[A]	0.26[A]	0.31[A]	0.29[A]	0.26[A]	0.24[A]	0.23[A]	0.23[A]	0.23[A]	0.20[A]	0.17[A]	0.14[A]	0.13[A]
0.70	0.19[A]	0.34[A]	0.47[A]	0.43[A]	0.35[A]	0.31[A]	0.30[A]	0.31[A]	0.31[A]	0.27[A]	0.22[A]	0.19[A]	0.18[A]
1.00	0.22[A]	0.36[A]	0.50[A]	0.48[A]	0.41[A]	0.36[A]	0.35[A]	0.36[A]	0.35[A]	0.30[A]	0.24[A]	0.21[A]	0.20[A]
1.50	0.26[A]	0.40[A]	0.55[A]	0.58[A]	0.53[A]	0.47	0.45	0.46[A]	0.43[A]	0.36[A]	0.30[A]	0.27[A]	0.2[illegible]
2.00	0.31[A]	0.45[A]	0.61	0.70[A]	0.68[A]	0.61	0.58	0.58	0.53	0.44	0.36[A]	0.33[A]	0.32[A]
3.00	0.36[A]	0.50[A]	0.66	0.76[A]	0.75[A]	0.69	0.66	0.65	0.59	0.49	0.41[A]	0.39[A]	0.37[A]
4.00	0.41[A]	0.55[A]	0.71	0.81[A]	0.82[A]	0.76	0.74	0.72	0.65	0.54	0.46[A]	0.44[A]	0.43[A]
5.00	0.48[A]	0.61[A]	0.76	0.87	0.89	0.85	0.83	0.80	0.71	0.59	0.52[A]	0.51[A]	0.50[A]
7.00	0.62	0.73	0.86	0.99	1.04	1.03	1.02	0.96	0.84	0.70[A]	0.65[A]	0.66[A]	0.66[A]
10.00	0.68[A]	0.78[A]	0.90	1.02	1.08[A]	1.11[A]	1.12[A]	1.05[A]	0.92[A]	0.82[A]	0.76[A]	0.76[A]	0.79[A]
15.00	0.82[A]	0.86[A]	0.97[A]	1.08[A]	1.18[A]	1.24[A]	1.31[A]	1.22[A]	1.08[A]	1.08[A]	1.00[A]	0.97[A]	1.05[A]
20.00	0.97[B]	0.96[A]	1.04[A]	1.18[A]	1.22[A]	1.39[A]	1.52[A]	1.41[B]	1.26[B]	1.34[B]	1.31[B]	1.24[A]	1.40[A]

* Extrapolated from original data.

Variation in data <10%, >10%[A], >20%[B], >50%[C], >100%[D]

Average CH_4 (ppmv) for APRIL

Press. (mb)	Latitude (°N)												
	−50°	−40	−30	−20	−10	0	+10	+20	+30	+40	+50	+60	+70°
0.10*	0.14[A]	0.11[B]	0.09[B]	0.09[A]	0.11[A]	0.11[A]	0.10[A]	0.10[A]	0.09[A]	0.09[A]	0.08	0.06[A]	0.05[B]
0.15*	0.15[A]	0.12[B]	0.10[B]	0.10[A]	0.12[A]	0.12[A]	0.12[A]	0.11[A]	0.10[A]	0.10[A]	0.08	0.06[A]	0.05[B]
0.20	0.16[A]	0.14[B]	0.12[B]	0.12[A]	0.13[A]	0.13[A]	0.13[A]	0.12[A]	0.11[A]	0.11[A]	0.09	0.07[A]	0.06[B]
0.30	0.17[A]	0.17[B]	0.16[B]	0.15[A]	0.16[A]	0.16[A]	0.16[A]	0.16[A]	0.15[A]	0.13[A]	0.11[A]	0.08[A]	0.07[B]
0.40	0.19[A]	0.20[A]	0.20[A]	0.19[A]	0.19[A]	0.19[A]	0.19[A]	0.20[A]	0.19[A]	0.16[A]	0.13[A]	0.10[A]	0.08[B]
0.50	0.21[A]	0.25[A]	0.26[A]	0.25[A]	0.23[A]	0.23[A]	0.24[A]	0.25[A]	0.25[A]	0.20[A]	0.15[A]	0.12[A]	0.10[B]
0.70	0.24[A]	0.32[A]	0.36[A]	0.34[A]	0.30[A]	0.29	0.31[A]	0.34[A]	0.34[A]	0.26[A]	0.19[A]	0.15[A]	0.13[A]
1.00	0.26[A]	0.34[A]	0.41[A]	0.40[A]	0.35[A]	0.33	0.35	0.39[A]	0.38[A]	0.29[A]	0.21[A]	0.18[A]	0.15[A]
1.50	0.29[A]	0.40[A]	0.49[A]	0.50[A]	0.45[A]	0.42	0.44	0.47	0.44[A]	0.35[A]	0.26[A]	0.22[A]	0.20[A]
2.00	0.34[A]	0.45[A]	0.58[A]	0.63[A]	0.59[A]	0.54	0.55	0.58	0.53	0.42	0.33	0.28	0.25
3.00	0.39[A]	0.52[A]	0.65[A]	0.71[A]	0.67[A]	0.63	0.63	0.65	0.59	0.47	0.37	0.33	0.31
4.00	0.45[A]	0.58[A]	0.72[A]	0.78[A]	0.76[A]	0.72	0.71	0.71	0.65	0.52	0.42[A]	0.38	0.37
5.00	0.52[A]	0.66[A]	0.79[A]	0.86[A]	0.85	0.82	0.80	0.79	0.73	0.58[A]	0.47[A]	0.44	0.45
7.00	0.68[A]	0.81[A]	0.94	1.02	1.05	1.04	1.00	0.95	0.88	0.71[A]	0.58[A]	0.59[A]	0.63
10.00	0.74[A]	0.87[A]	0.99	1.06	1.09[A]	1.11	1.08	1.02	0.96[A]	0.82[A]	0.72[A]	0.74[A]	0.78
15.00	0.85[A]	0.96[A]	1.08[A]	1.14[A]	1.18[A]	1.25[A]	1.25[A]	1.16[A]	1.11[A]	1.06[A]	1.04[A]	1.07[A]	1.13[A]
20.00	0.98[A]	1.07[A]	1.19[A]	1.23[A]	1.24[A]	1.40[A]	1.43[A]	1.32[A]	1.29[A]	1.36[A]	1.48[B]	1.56[A]	1.62[A]

Average CH_4 (ppmv) for MAY

Press. (mb)	Latitude (°N)												
	−50°	−40	−30	−20	−10	0	+10	+20	+30	+40	+50	+60	+70°
0.10*	0.05[A]	0.08[A]	0.11[A]	0.11[A]	0.12[A]	0.12[A]	0.11[A]	0.11[A]	0.10[A]	0.09[A]	0.07[A]	0.06[B]	0.06[B]
0.15*	0.06[A]	0.09[A]	0.12[A]	0.12[A]	0.12[A]	0.13[A]	0.12[A]	0.12[A]	0.11[A]	0.10[A]	0.08[A]	0.07[B]	0.06[B]
0.20	0.07[A]	0.10[A]	0.13[A]	0.13[A]	0.13[A]	0.14[A]	0.14[A]	0.13[A]	0.13[A]	0.11[A]	0.08[A]	0.07[B]	0.07[B]
0.30	0.09[B]	0.13[A]	0.15[A]	0.15[A]	0.15[A]	0.16[A]	0.17[A]	0.17[A]	0.16[A]	0.13[A]	0.10[A]	0.08[A]	0.07[B]
0.40	0.11[B]	0.15[A]	0.18[A]	0.17[A]	0.18[A]	0.19[A]	0.20[A]	0.21[A]	0.20[A]	0.15[A]	0.11[A]	0.09[A]	0.08[B]
0.50	0.14[B]	0.19[A]	0.21[A]	0.20[A]	0.21[A]	0.22[A]	0.25[A]	0.26[A]	0.25[A]	0.18[A]	0.13[A]	0.11[A]	0.09[B]
0.70	0.20[B]	0.24[A]	0.26[A]	0.25[A]	0.25	0.28	0.32[A]	0.35[A]	0.33[A]	0.23[A]	0.16[A]	0.13[A]	0.10[A]
1.00	0.23[B]	0.28[A]	0.30[A]	0.29[A]	0.30	0.32	0.36[A]	0.40[A]	0.37[A]	0.26[A]	0.19[A]	0.15[A]	0.12[A]
1.50	0.30[B]	0.36[A]	0.39[A]	0.38[A]	0.39	0.41	0.45[A]	0.48[A]	0.44[A]	0.32	0.23[A]	0.19[A]	0.16[A]
2.00	0.38[A]	0.46[A]	0.50[A]	0.50[A]	0.50	0.52[A]	0.57	0.59	0.52	0.39	0.29[A]	0.24[A]	0.21[A]
3.00	0.45[A]	0.53[A]	0.57[A]	0.58[A]	0.59	0.60	0.64	0.66	0.58	0.44	0.34[A]	0.29[A]	0.27[A]
4.00	0.53[A]	0.61[A]	0.66[A]	0.68	0.68	0.69	0.72	0.73	0.65	0.50	0.39[A]	0.35[A]	0.33[A]
5.00	0.63[A]	0.70[A]	0.75	0.78	0.79	0.78	0.80	0.80	0.72	0.56[A]	0.45[A]	0.42[A]	0.40[A]
7.00	0.83[A]	0.89[A]	0.96	1.02	1.03	0.99	0.98	0.96	0.86	0.70[A]	0.60[A]	0.58[A]	0.58
10.00	0.87[A]	0.97[A]	1.04	1.08	1.10	1.08	1.06	1.00	0.91[A]	0.80[A]	0.73[A]	0.73[A]	0.74[A]
15.00	0.94[A]	1.10[A]	1.20[A]	1.21[A]	1.22	1.24	1.20[A]	1.09[A]	1.00[A]	1.00[A]	1.04[A]	1.07[A]	1.10[A]
20.00	1.01[A]	1.24[A]	1.38[A]	1.35[A]	1.37	1.42[A]	1.35[A]	1.18[A]	1.09[A]	1.25[B]	1.48[B]	1.57[A]	1.63[A]

Average CH_4 (ppmv) for JUNE

Press. (mb)	Latitude (°N)												
	−50°	−40	−30	−20	−10	0	+10	+20	+30	+40	+50	+60	+70°
0.10*	0.06	0.10	0.13[A]	0.12[A]	0.12[A]	0.12[A]	0.12[A]	0.11[A]	0.10[A]	0.09[A]	0.07[A]	0.06[A]	0.06[B]
0.15*	0.06	0.10	0.13[A]	0.13[A]	0.13[A]	0.13[A]	0.13[A]	0.12[A]	0.11[A]	0.10[A]	0.08[A]	0.07[A]	0.07[B]
0.20	0.07	0.11	0.14[A]	0.14[A]	0.14[A]	0.14[A]	0.14[A]	0.14[A]	0.13[A]	0.11[A]	0.08[A]	0.07[A]	0.07[B]
0.30	0.08[A]	0.13[A]	0.16[A]	0.16[A]	0.16[A]	0.17[A]	0.18[A]	0.18[A]	0.16[A]	0.13[A]	0.10[A]	0.08[A]	0.07[B]
0.40	0.10[A]	0.14[A]	0.18[A]	0.18[A]	0.19[A]	0.20[A]	0.22[A]	0.22[A]	0.20[A]	0.15[A]	0.11[A]	0.09[A]	0.08[B]
0.50	0.12[B]	0.16[A]	0.20[A]	0.21[A]	0.22[A]	0.24[A]	0.27[A]	0.29[A]	0.24[A]	0.18[A]	0.12[A]	0.10[A]	0.08[B]
0.70	0.15[B]	0.20[B]	0.23[A]	0.25[A]	0.27	0.30[A]	0.36[A]	0.38[A]	0.32[A]	0.23[A]	0.15[A]	0.11[A]	0.09[B]
1.00	0.18[B]	0.23[B]	0.27[A]	0.29[A]	0.31[A]	0.34[A]	0.40[A]	0.43[A]	0.36[A]	0.26[A]	0.17[A]	0.13[A]	0.11[A]
1.50	0.24[B]	0.29[A]	0.34[A]	0.35[A]	0.38[A]	0.42[A]	0.49[A]	0.52[A]	0.44[A]	0.31[A]	0.21[A]	0.17[A]	0.15[A]
2.00	0.32[B]	0.38[A]	0.42[A]	0.44[A]	0.47[A]	0.52[A]	0.59	0.62	0.54	0.38	0.26[A]	0.22[A]	0.20[A]
3.00	0.38[B]	0.46[A]	0.51[A]	0.52[A]	0.55[A]	0.60[A]	0.67	0.68	0.60	0.44	0.32[A]	0.27[A]	0.25[A]
4.00	0.45[B]	0.55[A]	0.61[A]	0.61[A]	0.63[A]	0.69[A]	0.74	0.75	0.66	0.50	0.38[A]	0.33[A]	0.30[A]
5.00	0.53[B]	0.65[A]	0.72[A]	0.72[A]	0.73[A]	0.79	0.83	0.82	0.73	0.57	0.46[A]	0.41[A]	0.37[A]
7.00	0.71[A]	0.90[A]	1.00	0.96[A]	0.96[A]	1.00	1.01	0.96	0.87	0.73	0.64	0.60	0.55
10.00	0.85[A]	1.02[A]	1.09[A]	1.04[A]	1.03[A]	1.08	1.07	1.00	0.91[A]	0.81[A]	0.75[A]	0.73	0.71
15.00	1.16[B]	1.27[A]	1.28[A]	1.19[A]	1.17[A]	1.21[A]	1.18[A]	1.07[A]	0.96[A]	0.94[A]	0.97[A]	1.02[A]	1.10
20.00	1.58[B]	1.57[B]	1.49[A]	1.36[A]	1.33[A]	1.36[A]	1.30[A]	1.15[A]	1.02[A]	1.11[B]	1.27[A]	1.43[A]	1.72[A]

* Extrapolated from original data.

Variation in data <10%, >10%[A], >20%[B], >50%[C], >100%[D]

Average CH_4 (ppmv) for JULY

Press.	Latitude (°N)												
(mb)	-50*	-40	-30	-20	-10	0	+10	+20	+30	+40	+50	+60	+70*
0.10*	0.08	0.10	0.12[A]	0.13[A]	0.12[A]	0.12[A]	0.12[A]	0.10[A]	0.09[A]	0.09[A]	0.08[A]	0.08[B]	0.07[B]
0.15*	0.09	0.11	0.13[A]	0.13[A]	0.13[A]	0.14[A]	0.13[A]	0.12[A]	0.11[A]	0.10[A]	0.09[A]	0.08[B]	0.07[B]
0.20	0.09	0.11	0.14[A]	0.14[A]	0.15[A]	0.15[A]	0.15[A]	0.14[A]	0.12[A]	0.11[A]	0.09[A]	0.08[A]	0.07[B]
0.30	0.09	0.13[A]	0.16[A]	0.17[A]	0.17[A]	0.19[A]	0.19[A]	0.18[A]	0.16[A]	0.13[A]	0.10[A]	0.09[A]	0.07[B]
0.40	0.09[A]	0.14[A]	0.18[A]	0.19[A]	0.21[A]	0.23[A]	0.25[A]	0.24[A]	0.21[A]	0.16[A]	0.12[A]	0.09[A]	0.07[B]
0.50	0.10[A]	0.15[A]	0.20[A]	0.22[A]	0.25[A]	0.28[A]	0.32[A]	0.32[A]	0.27[A]	0.19[A]	0.13[A]	0.10[A]	0.07[A]
0.70	0.11[B]	0.18[A]	0.24[A]	0.27[A]	0.31[A]	0.37[A]	0.43[A]	0.45[A]	0.38[A]	0.25[A]	0.15[A]	0.11[A]	0.08[A]
1.00	0.13[B]	0.20[A]	0.26[A]	0.29[A]	0.33[A]	0.40[A]	0.48[A]	0.50[A]	0.42[A]	0.28[A]	0.17[A]	0.12[A]	0.10[A]
1.50	0.19[B]	0.25[A]	0.30[A]	0.34[A]	0.39[A]	0.47[A]	0.56[A]	0.59[A]	0.50[A]	0.33[A]	0.21[A]	0.16[A]	0.13[A]
2.00	0.26[B]	0.31[B]	0.35[A]	0.39[A]	0.45[A]	0.55[A]	0.67[A]	0.69	0.58	0.40[A]	0.26[A]	0.20[A]	0.17[A]
3.00	0.32[B]	0.38[A]	0.42[A]	0.46[A]	0.52[A]	0.62[A]	0.73	0.74	0.64	0.46[A]	0.32[A]	0.25[A]	0.23[A]
4.00	0.37[A]	0.46[A]	0.51[A]	0.54[A]	0.61[A]	0.70[A]	0.80	0.79	0.70	0.53[A]	0.38[A]	0.32[A]	0.29
5.00	0.44[A]	0.54[A]	0.60[A]	0.64[A]	0.70[A]	0.79[A]	0.86	0.85	0.76	0.60[A]	0.46[A]	0.40[A]	0.38
7.00	0.60	0.75[A]	0.84[A]	0.87[A]	0.92[A]	0.98	1.00	0.95	0.89	0.76[A]	0.65[A]	0.61	0.60
10.00	0.82	0.93[A]	0.96[A]	0.96[A]	1.00[A]	1.05[A]	1.06	1.00	0.92[A]	0.83[A]	0.74[A]	0.73	0.76
15.00	1.39	1.30[A]	1.20[A]	1.13[A]	1.16[A]	1.19[A]	1.17[A]	1.08[A]	0.98[A]	0.94[A]	0.92[A]	0.98	1.15
20.00	2.33	1.83[A]	1.60[A]	1.32[A]	1.33[A]	1.35[A]	1.29[A]	1.17[A]	1.05[A]	1.07[B]	1.14[A]	1.33[A]	1.72

Average CH_4 (ppmv) for AUGUST

Press.	Latitude (°N)												
(mb)	-50*	-40	-30	-20	-10	0	+10	+20	+30	+40	+50	+60	+70*
0.10*	0.09	0.10	0.11	0.13[A]	0.13[A]	0.13[B]	0.12[A]	0.10[A]	0.10[A]	0.10[A]	0.11[A]	0.11[A]	0.11[B]
0.15*	0.09	0.11	0.12	0.14[A]	0.15[A]	0.15[B]	0.14[A]	0.12[A]	0.11[A]	0.11[A]	0.12[A]	0.11[A]	0.10[B]
0.20	0.10	0.12	0.14	0.15[A]	0.16[A]	0.17[B]	0.16[A]	0.14[A]	0.13[A]	0.13[A]	0.12[A]	0.11[A]	0.10[B]
0.30	0.11	0.14	0.17	0.19[A]	0.19[A]	0.21[A]	0.21[A]	0.20[A]	0.18[A]	0.16[A]	0.13[A]	0.11[A]	0.09[B]
0.40	0.12[A]	0.17[A]	0.21	0.23[A]	0.25[A]	0.26[A]	0.28[A]	0.28[A]	0.25[A]	0.20[A]	0.15[A]	0.11[A]	0.08[A]
0.50	0.13[A]	0.20[A]	0.26[A]	0.28[A]	0.28[A]	0.32[A]	0.37[A]	0.39[A]	0.34[A]	0.24[A]	0.16[A]	0.11[A]	0.08[A]
0.70	0.16[B]	0.25[A]	0.34[A]	0.35[A]	0.35[A]	0.42[A]	0.52[A]	0.58[A]	0.49[A]	0.32[A]	0.19[A]	0.11[A]	0.07[A]
1.00	0.18[B]	0.26[A]	0.33[A]	0.35[A]	0.37[A]	0.45[A]	0.60[A]	0.61[A]	0.52[A]	0.34[A]	0.20[A]	0.13[A]	0.09[A]
1.50	0.24[B]	0.28[A]	0.33[A]	0.35[A]	0.41[A]	0.52[A]	0.62[A]	0.66	0.57[A]	0.39[A]	0.23[A]	0.15[A]	0.11[A]
2.00	0.31[B]	0.30[A]	0.32[A]	0.36[A]	0.45[A]	0.60[A]	0.70	0.71	0.62	0.45[A]	0.26[A]	0.17[A]	0.15[A]
3.00	0.37[B]	0.36[A]	0.38[A]	0.42[A]	0.51[A]	0.66[A]	0.78	0.77	0.67	0.50[A]	0.31[A]	0.22[A]	0.19[A]
4.00	0.43[B]	0.43[A]	0.46[A]	0.50[A]	0.59[A]	0.73[A]	0.81	0.82	0.73	0.56[A]	0.38[A]	0.28[A]	0.25[A]
5.00	0.50[A]	0.52[A]	0.54[A]	0.59[A]	0.68[A]	0.79[A]	0.88	0.88	0.79	0.62[A]	0.45[A]	0.36[A]	0.33[A]
7.00	0.67[A]	0.72[A]	0.75[A]	0.79[A]	0.87[A]	0.94	1.00	1.00	0.90	0.76[A]	0.63[A]	0.57[A]	0.53
10.00	0.87[A]	0.86[A]	0.84[A]	0.86[A]	0.95[A]	1.02[A]	1.06[A]	1.04[A]	0.96[A]	0.83[A]	0.72[A]	0.68[A]	0.68[A]
15.00	1.36[A]	1.16[A]	1.02[A]	1.00[A]	1.10[A]	1.17[A]	1.15[A]	1.12[A]	1.05[A]	0.96[A]	0.88[A]	0.91[A]	1.06[A]
20.00	2.13[A]	1.56[A]	1.24[A]	1.17[A]	1.28[A]	1.34[A]	1.26[A]	1.19[A]	1.16[A]	1.11[A]	1.08[A]	1.23[A]	1.64[A]

Average CH_4 (ppmv) for SEPTEMBER

Press.	Latitude (°N)												
(mb)	-50*	-40	-30	-20	-10	0	+10	+20	+30	+40	+50	+60	+70*
0.10*	0.10[B]	0.10[B]	0.10[A]	0.13[A]	0.14[A]	0.14[A]	0.12[A]	0.10[A]	0.10[A]	0.13[A]	0.15[A]	0.15[A]	0.15
0.15*	0.11[B]	0.11[B]	0.12[A]	0.14[A]	0.16[A]	0.16[A]	0.14[A]	0.12[A]	0.12[A]	0.14[A]	0.16[A]	0.15[A]	0.14
0.20	0.12[B]	0.12[A]	0.13[A]	0.16[A]	0.17[A]	0.18[A]	0.16[A]	0.14[A]	0.14[A]	0.16[A]	0.17[A]	0.15[A]	0.13
0.30	0.13[B]	0.15[A]	0.17[A]	0.19[A]	0.21[A]	0.22[A]	0.21[A]	0.19[A]	0.19[A]	0.20[A]	0.19[A]	0.15[A]	0.11
0.40	0.15[B]	0.19[A]	0.22[A]	0.24[A]	0.25[A]	0.28[A]	0.28[A]	0.27[A]	0.26[A]	0.25[A]	0.21[A]	0.14[A]	0.10
0.50	0.18[A]	0.24[A]	0.28[A]	0.29[A]	0.31[A]	0.34[A]	0.36[A]	0.37[A]	0.36[A]	0.32[A]	0.23[A]	0.14[A]	0.08
0.70	0.21[A]	0.31[A]	0.38[A]	0.37[A]	0.39[A]	0.45[A]	0.50[A]	0.54[A]	0.52[A]	0.42[A]	0.26[A]	0.14[A]	0.07
1.00	0.24[A]	0.32[A]	0.39[A]	0.39[A]	0.42[A]	0.49[A]	0.54[A]	0.58[A]	0.56[A]	0.44[A]	0.27[A]	0.14[A]	0.07
1.50	0.28[A]	0.34[A]	0.40[A]	0.43[A]	0.48[A]	0.56[A]	0.63[A]	0.66[A]	0.63[A]	0.48[A]	0.28[A]	0.15[A]	0.08[A]
2.00	0.32[A]	0.36[B]	0.41[B]	0.47[A]	0.54[A]	0.63	0.72	0.75	0.70	0.53[A]	0.30[A]	0.15[A]	0.09[A]
3.00	0.38[A]	0.41[A]	0.45[B]	0.52[A]	0.60[A]	0.69	0.77	0.80	0.75	0.58[A]	0.35[A]	0.20[A]	0.12[A]
4.00	0.45[A]	0.47[A]	0.51[B]	0.57[A]	0.66[A]	0.75	0.83	0.85	0.79	0.63[A]	0.41[A]	0.26[A]	0.18[A]
5.00	0.53[A]	0.54[A]	0.56[A]	0.62[A]	0.72[A]	0.82	0.88	0.90	0.84	0.69[A]	0.49[A]	0.34[A]	0.25[A]
7.00	0.71[B]	0.69[A]	0.69[A]	0.73[A]	0.85[A]	0.95	1.00	0.99	0.93	0.80[A]	0.67[A]	0.55	0.46[A]
10.00	0.84[A]	0.79[A]	0.77[A]	0.81[A]	0.93[A]	1.05	1.06	1.03[A]	0.98[A]	0.87[A]	0.75[A]	0.67	0.63[A]
15.00	1.11[A]	0.99[B]	0.93[B]	0.95[A]	1.08[A]	1.23[A]	1.18[A]	1.10[A]	1.07[A]	0.99[A]	0.91[A]	0.93[A]	1.04[A]
20.00	1.47[A]	1.24[B]	1.13[B]	1.12[A]	1.26[A]	1.46[A]	1.32[A]	1.17[A]	1.17[A]	1.12[A]	1.11[A]	1.30[A]	1.72[A]

* Extrapolated from original data. Variation in data <10%, >10%[A], >20%[B], >50%[C], >100%[D]

Average CH_4 (ppmv) for OCTOBER

Press.	Latitude (°N)												
(mb)	-50*	-40	-30	-20	-10	0	+10	+20	+30	+40	+50	+60	+70*
0.10*	0.10	0.10^A	0.11^A	0.12^A	0.15^A	0.16^A	0.14^A	0.12^A	0.12^A	0.13^A	0.14^A	0.14^A	0.15^A
0.15*	0.10	0.11^A	0.12^A	0.14^A	0.16^A	0.18^A	0.16^A	0.14^A	0.13^A	0.15^A	0.15^A	0.14^A	0.14^A
0.20	0.11	0.12^A	0.13^A	0.15^A	0.18^A	0.19^A	0.17^A	0.15^A	0.15^A	0.16^A	0.16^A	0.14^A	0.13^A
0.30	0.13	0.15^A	0.16^A	0.16^A	0.21^A	0.23^A	0.22^A	0.20^A	0.20^A	0.20^A	0.18^A	0.15^A	0.11^A
0.40	0.15	0.17^A	0.20^A	0.22^A	0.24^A	0.27^A	0.27^A	0.26^A	0.26^A	0.24^A	0.20^A	0.15^A	0.10^A
0.50	0.18	0.21^A	0.24^A	0.27^A	0.29^A	0.31^A	0.33^A	0.34^A	0.34^A	0.29^A	0.23^A	0.16^A	0.09^A
0.70	0.21^A	0.26^A	0.31^A	0.34^A	0.36	0.39	0.43^A	0.47^A	0.46^A	0.36^A	0.27^A	0.16^A	0.08^A
1.00	0.23^A	0.28^A	0.33^A	0.37^A	0.39^A	0.43^A	0.47^A	0.51^A	0.50^A	0.39^A	0.28^A	0.16^A	0.08^A
1.50	0.26^A	0.31^A	0.37^A	0.43^A	0.47^A	0.51^A	0.56^A	0.59^A	0.57^A	0.45^A	0.30^A	0.17^A	0.08^A
2.00	0.30^A	0.35^A	0.42^A	0.49^A	0.55^A	0.61^A	0.67	0.69	0.65^A	0.51^A	0.32^A	0.17^A	0.08^A
3.00	0.35^A	0.40^A	0.47^A	0.55^A	0.62^A	0.68	0.73	0.75	0.70^A	0.56^A	0.38^A	0.21^A	0.11
4.00	0.42^A	0.47^A	0.53^A	0.60^A	0.68^A	0.75	0.79	0.81	0.76^A	0.62^A	0.44^A	0.28^A	0.16
5.00	0.49^A	0.54^A	0.60^A	0.66^A	0.76^A	0.83	0.86	0.88	0.82	0.68	0.52^A	0.36^A	0.23
7.00	0.67^A	0.71^A	0.74^A	0.78^A	0.91	0.99	1.01	1.01	0.94^A	0.82	0.69	0.56^A	0.44
10.00	0.81^A	0.82^A	0.81^A	0.85^A	0.99	1.10	1.10^A	1.07^A	1.00^A	0.90^A	0.78^A	0.68^A	0.57^A
15.00	1.15^A	1.02^A	0.95^B	0.97^A	1.15	1.31	1.26^A	1.17^A	1.12^A	1.05^A	0.96^A	0.92^A	0.89^A
20.00	1.57	1.28^B	1.11^B	1.11^A	1.33	1.57^A	1.45^A	1.28^B	1.26^B	1.23^A	1.19^A	1.25^A	1.39^A

Average CH_4 (ppmv) for NOVEMBER

Press.	Latitude (°N)												
(mb)	-50*	-40	-30	-20	-10	0	+10	+20	+30	+40	+50	+60	+70*
0.10*	0.10^A	0.11^B	0.13^A	0.13^A	0.14^A	0.15^A	0.14^A	0.13^A	0.13^A	0.13^A	0.11^A	0.09^A	0.08
0.15*	0.11^A	0.12^A	0.13^A	0.14^A	0.15^A	0.16^A	0.15^A	0.14^A	0.14^A	0.14^A	0.12^A	0.10^A	0.08^A
0.20	0.11^A	0.13^A	0.14^A	0.15^A	0.16^A	0.18^A	0.17^A	0.16^A	0.16^A	0.15^A	0.13^A	0.10^A	0.09^A
0.30	0.13^A	0.14^A	0.16^A	0.17^A	0.19^A	0.20^A	0.20^A	0.19^A	0.19^A	0.18^A	0.15^A	0.11^A	0.09^A
0.40	0.14^A	0.16^A	0.18^A	0.20^A	0.22^A	0.23^A	0.24^A	0.24^A	0.23^A	0.21^A	0.17^A	0.13^A	0.09^A
0.50	0.16^A	0.18^A	0.20^A	0.23^A	0.25^A	0.27^A	0.29^A	0.29^A	0.28^A	0.24^A	0.19^A	0.14^A	0.10^A
0.70	0.19^B	0.21^A	0.24^A	0.28^A	0.31^A	0.33^A	0.36^A	0.37^A	0.36^A	0.30^A	0.23^A	0.16^A	0.10^A
1.00	0.20^A	0.24^A	0.27^A	0.32^A	0.35^A	0.37^A	0.40^A	0.41^A	0.39^A	0.33^A	0.25^A	0.17^A	0.11^B
1.50	0.23^A	0.28^A	0.33^A	0.39^A	0.44^A	0.46^A	0.48^A	0.49^A	0.47^A	0.39^A	0.29^A	0.20^A	0.12^B
2.00	0.27^A	0.33^A	0.40^A	0.47^A	0.54	0.57^A	0.57^A	0.58^A	0.56^A	0.46^A	0.34^A	0.22^A	0.15^B
3.00	0.32^A	0.39^A	0.47^A	0.54^A	0.61	0.65	0.65	0.66^A	0.63^A	0.53^A	0.40^A	0.27^A	0.17^B
4.00	0.38^A	0.46^A	0.54^A	0.61^A	0.68	0.73	0.74	0.74^A	0.70^A	0.60^A	0.47^A	0.33^A	0.22^B
5.00	0.45^A	0.54^A	0.63^A	0.70^A	0.77	0.81	0.83	0.83^A	0.78^A	0.68^A	0.55^A	0.41^A	0.29^A
7.00	0.62^A	0.72^A	0.81	0.87^A	0.94	1.00	1.03	1.03	0.96	0.86	0.74^A	0.60^A	0.48^A
10.00	0.77^A	0.83^A	0.88^A	0.93^A	1.03^A	1.12	1.13^A	1.10^A	1.05^A	0.97^A	0.84^A	0.71^A	0.61^A
15.00	1.11^A	1.08^A	1.01^A	1.04^A	1.20^A	1.34^A	1.31^A	1.24^A	1.21^A	1.17^A	1.04^A	0.93^A	0.91^A
20.00	1.61^A	1.33^A	1.16^A	1.16^A	1.39^A	1.61^A	1.53^A	1.39^B	1.40^B	1.42^A	1.28^A	1.23^A	1.35^A

Average CH_4 (ppmv) for DECEMBER

Press.	Latitude (°N)												
(mb)	-50*	-40	-30	-20	-10	0	+10	+20	+30	+40	+50	+60	+70*
0.10*	0.11^A	0.12^A	0.12^A	0.12^A	0.12	0.12^A	0.13^A	0.13^A	0.14^A	0.13^A	0.10^A	0.08	0.07^A
0.15*	0.12^A	0.13^A	0.13^A	0.13^A	0.13	0.13^A	0.14^A	0.14^A	0.15^A	0.14^A	0.11^A	0.09^A	0.07^A
0.20	0.12^A	0.13^A	0.14^A	0.14^A	0.14	0.14^A	0.15^A	0.15^A	0.16^A	0.15^A	0.11^A	0.09^A	0.08^A
0.30	0.13^A	0.15^A	0.15^A	0.17^A	0.17^A	0.17^A	0.18^A	0.18^A	0.18^A	0.16^A	0.13^A	0.10^A	0.08^A
0.40	0.14^A	0.16^A	0.18^A	0.20^A	0.21^A	0.21^A	0.21^A	0.21^A	0.21^A	0.18^A	0.15^A	0.12^A	0.09^A
0.50	0.16^B	0.18^A	0.20^A	0.24^A	0.25^A	0.25^A	0.25^A	0.24^A	0.24^A	0.21^A	0.17^A	0.13^A	0.10^A
0.70	0.17^B	0.20^A	0.24^A	0.30^A	0.32^A	0.32^A	0.31^A	0.30^A	0.28^A	0.25^A	0.20^A	0.15^A	0.12^A
1.00	0.18^B	0.22^A	0.28^A	0.34^A	0.37^A	0.37^A	0.35^A	0.34^A	0.31^A	0.27^A	0.22^A	0.17^A	0.12^A
1.50	0.21^A	0.27^A	0.35^A	0.42^A	0.46^A	0.46^A	0.43^A	0.41^A	0.38^A	0.33^A	0.27^A	0.19^A	0.13^A
2.00	0.23^A	0.32^A	0.43^A	0.52	0.57^A	0.58^A	0.54^A	0.50^A	0.46^A	0.40^A	0.32^A	0.22^A	0.14^A
3.00	0.28^A	0.38^A	0.50^A	0.59^A	0.65^A	0.66^A	0.61^A	0.58^A	0.54^A	0.47^A	0.38^A	0.27^A	0.18^A
4.00	0.35^A	0.46^A	0.56	0.66^A	0.73^A	0.74^A	0.70	0.67^A	0.62^A	0.54^A	0.45^A	0.33^A	0.23^A
5.00	0.44^A	0.54^A	0.64	0.74^A	0.82^A	0.83	0.80	0.77	0.72^A	0.64^A	0.54^A	0.40^A	0.29^A
7.00	0.65^A	0.74	0.81	0.90^A	1.01^A	1.03	1.00	1.00	0.94	0.85	0.74^A	0.58^A	0.44^A
10.00	0.79^A	0.82^A	0.87^A	0.95^A	1.08^A	1.14	1.10	1.08^A	1.06^A	1.00^A	0.87^A	0.70^A	0.58^A
15.00	1.08^A	0.99^A	0.97^A	1.05^A	1.22^A	1.34	1.29^A	1.23^A	1.27^A	1.32^A	1.14^A	0.96^A	0.90^A
20.00	1.49^B	1.19^A	1.09^A	1.15^A	1.36^A	1.59	1.52^A	1.41^A	1.54^B	1.78^A	1.51^A	1.30^A	1.41^A

* Extrapolated from original data.

Variation in data ^{A}<10%, ^{B}>10%, ^{C}>20%, ^{D}>50%, ^{E}>100%

Annual Average N_2O (ppbv)

Press. (mb)	Latitude (°N)												
	−50°	−40	−30	−20	−10	0	+10	+20	+30	+40	+50	+60	+70°
0.10°	0.53^{C}	0.63^{C}	0.69^{C}	0.69^{C}	0.70^{C}	0.72^{C}	0.82^{B}	1.01^{D}	1.14^{B}	1.05^{B}	0.75^{B}	0.55^{B}	0.50^{B}
0.15°	0.60^{C}	0.72^{C}	0.79^{C}	0.80^{C}	0.81^{C}	0.83^{B}	0.94^{B}	1.16^{B}	1.29^{B}	1.19^{B}	0.85^{B}	0.63^{B}	0.57^{B}
0.20°	0.69^{C}	0.82^{C}	0.91^{C}	0.92^{C}	0.93^{C}	0.96^{B}	1.08^{B}	1.32^{B}	1.47^{B}	1.35^{B}	0.96^{B}	0.71^{B}	0.64^{A}
0.30°	0.89^{C}	1.08^{C}	1.20^{C}	1.22^{C}	1.24^{C}	1.27^{B}	1.43^{B}	1.73^{B}	1.91^{B}	1.74^{B}	1.23^{B}	0.92^{B}	0.83^{A}
0.40°	1.15^{C}	1.42^{C}	1.59^{C}	1.62^{C}	1.65^{C}	1.69^{B}	1.89^{B}	2.27^{B}	2.49^{B}	2.23^{B}	1.58^{B}	1.19^{B}	1.07^{A}
0.50°	1.49^{C}	1.86^{C}	2.11^{C}	2.16^{C}	2.20^{C}	2.24^{B}	2.49^{B}	2.96^{B}	3.23^{B}	2.86^{B}	2.02^{B}	1.53^{B}	1.38^{A}
0.70	2.14^{C}	2.74^{C}	3.16^{C}	3.28^{C}	3.35^{B}	3.41^{B}	3.75^{B}	4.38^{B}	4.67^{B}	4.04^{B}	2.84^{B}	2.16^{B}	1.91^{B}
1.00	2.75^{C}	3.63^{C}	4.37^{C}	4.66^{C}	4.77^{B}	4.84^{D}	5.26^{B}	5.96^{B}	6.11^{B}	5.08^{B}	3.56^{B}	2.65^{B}	2.20^{B}
1.50	4.16^{C}	5.81^{C}	7.48^{C}	8.36^{C}	8.57^{B}	8.66^{D}	9.21^{B}	9.98^{B}	9.57^{B}	7.46^{B}	5.20^{B}	3.74^{B}	2.80^{C}
2.00	6.30^{B}	9.30^{B}	12.80^{B}	14.98^{C}	15.42^{D}	15.50^{B}	16.14^{B}	16.69^{D}	14.98^{B}	10.95^{B}	7.58^{B}	5.28^{B}	3.57^{C}
3.00	9.81^{B}	14.07^{B}	19.04^{B}	22.69^{B}	24.09^{B}	24.46^{B}	25.13^{B}	25.07^{B}	21.80^{B}	15.95^{B}	11.16^{B}	7.88^{B}	5.46^{C}
4.00	15.08^{B}	20.96^{B}	27.76^{B}	33.60^{B}	36.79^{D}	37.79^{D}	38.33^{D}	36.95^{B}	31.24^{D}	22.94^{B}	16.23^{B}	11.63^{B}	8.33^{C}
5.00	23.20^{B}	31.22^{B}	40.47^{B}	49.76^{B}	56.19^{D}	58.36^{B}	58.47^{B}	54.46^{B}	44.76^{B}	33.00^{D}	23.60^{A}	17.19^{B}	12.71^{B}
7.00	50.44^{A}	63.93^{B}	79.54^{B}	100.20^{B}	119.33^{B}	126.37^{A}	123.64^{A}	108.43^{A}	85.06^{A}	63.45^{A}	46.52^{A}	34.98^{A}	27.48^{B}
10.00	70.11^{B}	84.37^{B}	100.73^{B}	122.88^{B}	144.95^{B}	153.47^{A}	147.12^{A}	127.91^{A}	103.22^{A}	81.36^{A}	63.76^{A}	50.73^{B}	41.54^{B}
15.00	121.37^{B}	133.97^{B}	149.34^{B}	172.65^{B}	200.46^{B}	212.17^{A}	196.59^{A}	168.46^{A}	142.51^{A}	123.13^{A}	107.79^{B}	94.25^{B}	82.74^{B}
20.00	210.13^{B}	212.72^{B}	221.41^{B}	242.57^{B}	277.24^{D}	293.32^{A}	262.70^{A}	221.87^{A}	196.75^{A}	186.35^{B}	182.25^{B}	175.11^{B}	164.79^{A}

° Extrapolated from original data. Variation in data <10%, >10%^{A}, >20%^{B}, >50%^{C}, >100%^{D}

Annual Average CH_4 (ppmv)

Press. (mb)	Latitude (°N)												
	50°	−40	−30	−20	−10	0	+10	+20	+30	+40	+50	+60	+70°
0.10°	0.10^{B}	0.10^{A}	0.10	0.11^{A}	0.12^{A}	0.12^{A}	0.12^{A}	0.11	0.10^{A}	0.10^{B}	0.09^{B}	0.08^{B}	0.08^{B}
0.15°	0.11^{B}	0.11^{A}	0.12^{A}	0.12^{A}	0.13^{A}	0.14^{A}	0.13^{A}	0.12	0.12^{A}	0.11^{B}	0.10^{B}	0.09^{B}	0.08^{B}
0.20	0.11^{B}	0.12^{A}	0.13^{A}	0.13^{A}	0.14^{A}	0.15^{A}	0.15^{A}	0.14^{A}	0.13^{A}	0.12^{B}	0.11^{B}	0.09^{B}	0.08^{B}
0.30	0.13^{B}	0.14^{A}	0.16^{A}	0.16^{A}	0.17^{A}	0.18^{A}	0.18^{A}	0.18^{A}	0.17^{A}	0.15^{B}	0.13^{B}	0.10^{B}	0.09^{B}
0.40	0.14^{B}	0.17^{B}	0.19^{A}	0.20^{A}	0.21^{A}	0.22^{A}	0.22^{A}	0.22^{A}	0.21^{A}	0.18^{B}	0.15^{B}	0.12^{B}	0.09^{B}
0.50	0.15^{B}	0.20^{B}	0.23^{B}	0.25^{A}	0.26^{A}	0.27^{A}	0.28^{A}	0.29^{B}	0.27^{B}	0.22^{B}	0.17^{B}	0.13^{B}	0.10^{B}
0.70	0.18^{A}	0.24^{B}	0.30^{B}	0.32^{B}	0.33^{A}	0.34^{A}	0.37^{B}	0.39^{B}	0.36^{B}	0.28^{D}	0.20^{B}	0.15^{B}	0.11^{D}
1.00	0.20^{A}	0.27^{B}	0.33^{B}	0.36^{B}	0.37^{A}	0.37^{A}	0.41^{A}	0.43^{B}	0.39^{B}	0.31^{A}	0.23^{B}	0.16^{B}	0.12^{B}
1.50	0.25^{A}	0.32^{A}	0.39^{B}	0.43^{B}	0.45^{A}	0.48^{A}	0.50^{A}	0.51^{A}	0.46^{A}	0.36^{A}	0.27^{B}	0.19^{B}	0.14^{D}
2.00	0.30	0.37^{A}	0.45^{B}	0.51^{D}	0.56^{A}	0.58^{A}	0.61^{A}	0.60^{A}	0.54^{A}	0.43^{A}	0.31^{A}	0.23^{D}	0.17^{D}
3.00	0.36	0.43^{A}	0.51^{B}	0.58^{B}	0.63^{A}	0.66	0.68	0.67^{A}	0.60^{A}	0.48^{A}	0.37^{A}	0.28^{D}	0.22^{B}
4.00	0.42	0.50^{A}	0.58^{A}	0.65^{A}	0.70^{A}	0.74	0.75	0.74^{A}	0.67^{A}	0.55^{A}	0.43^{A}	0.34^{B}	0.28^{B}
5.00	0.49	0.58^{A}	0.66^{A}	0.73^{A}	0.79^{A}	0.82	0.83	0.81	0.74^{A}	0.61^{A}	0.50^{A}	0.42^{B}	0.34^{B}
7.00	0.67	0.76^{A}	0.83^{A}	0.90^{A}	0.97	1.01	1.00	0.97	0.89	0.76	0.66	0.59	0.52^{A}
10.00	0.79^{A}	0.85^{A}	0.90^{A}	0.95^{A}	1.03	1.09	1.09	1.03	0.95	0.86^{A}	0.77^{A}	0.71	0.67
15.00	1.04^{B}	1.03^{B}	1.03^{A}	1.06^{A}	1.16	1.26	1.24	1.15	1.08^{A}	1.04^{A}	0.99^{A}	0.98^{A}	1.02
20.00	1.38^{B}	1.25^{B}	1.18^{A}	1.18^{A}	1.29	1.45	1.42^{A}	1.29^{A}	1.22^{A}	1.27^{A}	1.28^{A}	1.33^{A}	1.54

° Extrapolated from original data. Variation in data <10%, >10%^{A}, >20%^{B}, >60%^{C}, >100%^{D}

The absolute abundance maxima and minima have an interesting distribution in latitude as well as time. As already noted, the absolute maxima occur in the Summer; they are centred on about 20° latitude. In the Northern Hemisphere, the low-latitude summer maximum is matched by a high-latitude(centred on about 60°) minimum, and vice-versa in the winter. Unfortunately, the asymmetrical latitudinal coverage of SAMS does not permit us to say whether the Southern Hemisphere low-latitude maxima and minima are also accompanied by high-latitude extrema of the opposite sign.

Consider now the variations with latitude and season which take place on constant height (log pressure) surfaces. Starting at the highest levels at which CH_4 was observed, i.e. around 60 km (N_2O is below the noise level at this height), a non-seasonal trend is observed whereby all latitudes in both hemispheres tend to have maxima around September, and minima around March. Lower down, the pattern described above with a low latitude Summer maximum and a high-latitude Summer minimum emerges, until at about 35 km all latitudinal and seasonal variability becomes subdued. The reason for this is clear when lower levels are examined; the pattern reverses phase to give low-latitude Summer minima and Winter maxima.

CONCLUSION AND FUTURE MODEL REFINEMENTS

Models of the zonally averaged, time averaged mixing ratios of nitrous oxide and methane have been derived from three years of the data from the Stratospheric and Mesospheric Sounder on the Nimbus 7 satellite. The distributions of both species are similar, as would be expected since both originate in the troposphere and both have long photochemical lifetimes. Considerable latitudinal and seasonally-varying structure is present in the observed distributions. This has been described in a phenomenological way but with no attempt to explain the mechanisms underlying the features. This aspect is still under study and will be reported at a later date.

It is likely that small improvements in the data set and hence in the model presented here will be possible as a result of further processing of the SAMS radiances, in particular to reduce the temperature error which contributes to the uncertainty in the constituent retrievals. The discrepancy between the satellite and balloon measurements suggests that errors of up to 50% in N_2O and 25% in CH_4 may remain at the lowest level sounded. We intend to reprocess the SAMS results with an improved treatment of the spectroscopy and examine longitudinal and other trends to see if any reason for this can be found.

An improved version of SAMS (ISAMS) is being built for the Upper Atmosphere Research Satellite, and a major revision of the model will be possible when these data become available early in the next decade.

REFERENCES

1. R.P.Wayne, Chemistry of Atmospheres, O.U.P. (1985).
2. J.R. Drummond et al. Phil.Trans.R.Soc.Lond. A296, 219-241(1979).
3. J.J. Barnett et al. Nature, 313, 439-443 (1985).
4. R.L. Jones and J.A. Pyle. J.Geophys.Res., 89, 5263-5279 (1984).
5. F.W. Taylor. Pressure Modulator Radiometry, Spectrometric Techniques, 3, 137-197 (1983).
6. C.D. Rodgers, J.J. Barnett and R.L. Jones. J.Geophys.Res. 89, 5280-5286 (1984).
7. WMO. The Stratosphere 1981: Theory and Measurements. Report No. 11, Global Ozone Research and Monitoring Project (1982).
8. U. Schmidt, personal communication.
9. G.M. Keating and D.F. Young. Adv.Space Res., 5, 155-166 (1985).
10. F.W. Taylor et al. In preparation.

5

REFERENCE MODEL FOR CH_4 AND N_2O AND TRENDS

F. W. Taylor and A. Dudhia

Department of Atmospheric, Oceanic and Planetary Physics
Oxford University, Clarendon Laboratory, Oxford OX1 3PU, United Kingdom

ABSTRACT

Data from the Stratospheric and Mesospheric Sounder on Nimbus 7 have been used as the basis for a model of the abundances of nitrous oxide and methane in the stratosphere. A version of this was produced two years ago (Taylor, Dudhia and Rodgers, /1/ - hereafter called paper 1) and in this new paper we consider some of the possible error sources in more detail, as well as long-term trends. The principal source of error in the SAMS retrievals is thought to be the use of climatological ozone profiles to invert the temperature profile data. However, we find that the effect is too small, and of the opposite sign, to explain the discrepancies between satellite and *in-situ* measurements, noted in paper 1. As expected, no systematic trends which exceed the estimated error in the data are found in either methane or nitrous oxide.

INTRODUCTION

Nitrous oxide and methane are two of the important minor constituents of the atmosphere. The former is the principal source of stratospheric NO_x which plays a significant role in the photochemistry of ozone, while methane is an important 'greenhouse' gas and the only in-situ source (through its photo-oxidation) of stratospheric water vapour. Accordingly, data on the mean abundance of these species is an important input to models and other studies of the middle atmosphere, currently a region of much research interest.

The only comprehensive data set on these two gases, covering most latitudes and all seasons over a period of several years, is that obtained by the Nimbus 7 Stratospheric and Mesospheric Sounder (SAMS- see Drummond et al. /2/ for a description of the instrument and Taylor /3/ for a discussion and overview of the results obtained). These data were used in paper 1 to construct a three-year average (1979 to 1981 inclusive) from which tables of mean monthly abundance versus log(pressure) and in ten degree latitude bins were constructed. Seventeen pressure levels from 20 mb. (about 25 km) to 0.1 mb (about 65 km) and thirteen latitude bins (from 50^{o} S to 70^{o} N) were presented.

The purpose of the present paper is primarily to re-evaluate the model in the light of work that has been done in the meantime to further validate the SAMS data and to investigate certain discrepancies with balloon data which have been uncovered. We also examine the data set for signs of trends in the abundances of both species and present tables of results for these.

EFFECTS OF OZONE ON SAMS DATA

(A) Sensitivity of temperature retrievals to ozone

In paper 1 we showed evidence for discrepancies between SAMS data and in-situ measurements from balloons, particularly below the 10 mb pressure level. In investigating this, we decided that, if the discrepancy was due to a systematic error in SAMS, the most likely cause was the use of climatological ozone profiles in the retrievals of temperature from SAMS 15μm carbon dioxide emission observations. A correction has to be applied to the transmission function in the temperature sounding channels because of

the overlapping opacity of the 16 μm ozone band. The constituent abundances which are retrieved depend strongly on the temperatures, since the emission which is measured is of course a function of both. Jones and Pyle /4/ quote variations in retrieved mixing ratio of as much as 50% for both gases with a ±2K temperature variation at 20 mb, although this sensitivity decreases rapidly with pressure and is around 10% at higher altitudes.

In the present work, we have made use of new data on the ozone distribution derived from a combination of SBUV and LIMS measurements which provides profiles for a particular month and latitude. November 1979 was chosen for these tests since balloon data for CH4 and N2O is available for that month (Schmidt, personal communication). The main differences between the original and the new ozone profiles for that month are

(1) higher values in the new profiles above 0.05 mb

(2) higher values in the peak at 10 mb., in the new low latitude profiles (but lower values at $\pm 60^{\circ}$ latitude).

Barnett and Corney /5/ suggested a 30% decrease in total ozone would produce typically a +1K increase in retrieved temperature between 150-20 mb and a 2K increase between 20 to 2.5 mb. To examine the effect of the temperature retrieval on the vertical structure of the ozone variations, a comparison was made between the zonal mean temperature retrievals for Day 305, 1979, using the original (climatological) ozone profile, and the retrievals obtained after perturbing this profile at various levels. The perturbation applied was a 20% increase at a selected level, decreasing above and below by 4% per 0.2 scale heights, so that the unperturbed value resumes at ± 1 scale height either side of the perturbation. The results are listed in Table 1 for perturbations applied at 8 different levels. The standard deviation refers to the variation in result across the twelve latitude bands ($45^{\circ}S$-$65^{\circ}N$).

Table 1
Response of Retrieved Temperature (units: 0.01K) to O_3 Perturbations of +20%

Level of Max. Perturbation	Response at level: 70mb	20mb	7mb	2mb	0.6mb	0.2mb	0.06mb	0.02mb
70mb	−42 ± 9	−11 ± 3	+1 ± 2	0 ± 3	0 ± 2	0 ± 2	−9 ± 3	−6 ± 2
20mb	+48 ± 17	−86 ± 11	−4 ± 6	+1 ± 5	+4 ± 4	−7 ± 11	+27 ± 4	23 ± 4
7mb	−33 ± 28	+35 ± 13	−6 ± 8	−22 ± 4	+25 ± 8	+103 ± 7	+21 ± 7	−17 ± 2
2mb	−26 ± 15	+9 ± 10	−13 ± 5	−15 ± 6	+14 ± 5	+33 ± 12	+28 ± 6	−2 ± 4
0.6mb	+10 ± 8	−2 ± 2	−1 ± 1	−1 ± 2	+1 ± 2	0 ± 2	0 ± 1	+1 ± 1
0.2mb	+13 ± 16	−4 ± 7	−1 ± 4	+3 ± 4	−3 ± 3	−9 ± 10	0 ± 2	+4 ± 4
0.06mb	+3 ± 16	−5 ± 7	−1 ± 4	+3 ± 4	−3 ± 3	−9 ± 10	+1 ± 2	+4 ± 3
0.02mb	+1 ± 1	0 ± 0	0 ± 0	0 ± 0	0 ± 0	0 ± 0	0 ± 0	0 ± 0

One particularly significant result is that the temperature retrievals below 10 mb are just as sensitive to the shape of the ozone profile at those levels as they are to the total column amount, so the effect of introducing the more specific ozone profiles on the temperature cannot be generalized.

(b) Sensitivity of constituent retrievals to temperature

The sensitivity of the retrieved constituent profiles to the shape of the temperature profile was tested in a similar manner. The amplitude of the perturbation was 1K and the shape the same as for ozone. For each

perturbation, temperature and constituent retrievals were performed for the whole of November, 1979. The resulting changes in the monthly profiles are shown in tables 2 and 3.

As expected, the sign of the perturbation is negative down the diagonal elements of each table (a higher local temperature implying a lower concentration for a given radiance). The conclusion here is that, in order to account for the approximately 50% reduction in mixing ratios implied by the balloon measurements at 20 mb, the actual atmospheric temperatures would have to be 5 to 10K higher than was measured by SAMS. This is a factor of 5 greater than the estimated error in SAMS temperatures from all sources.

Table 2
% Response of Retrieved N_2O to Temperature Perturbations of +1K

Level of Max. Perturbation	Response at level: 70mb	20mb	7mb	2mb	0.6mb	0.2mb
70mb	−2.8 ± 11.5	−1.2 ± 3.1	+0.4 ± 0.8	−0.3 ± 0.6	+0.2 ± 0.7	−0.7 ± 5.8
20mb	+5.1 ± 8.5	−12.5 ± 5.2	+1.3 ± 0.6	−0.8 ± 1.2	+1.4 ± 1.7	+5.6 ± 5.6
7mb	+5.6 ± 7.3	−3.0 ± 7.6	−8.2 ± 2.7	+2.1 ± 1.6	+1.3 ± 5.5	+3.5 ± 3.9
2mb	+2.7 ± 2.4	−0.2 ± 1.8	−0.5 ± 0.4	−4.0 ± 0.8	+1.0 ± 0.7	+1.1 ± 1.2
0.6mb	−2.4 ± 13.0	−1.2 ± 3.3	+0.2 ± 0.8	−0.3 ± 0.5	−1.8 ± 0.9	−1.4 ± 6.6
0.2mb	+0.5 ± 2.6	−0.2 ± 1.7	−0.1 ± 0.4	+0.0 ± 0.2	−0.2 ± 0.3	−0.1 ± 1.0

Table 3
% Response of Retrieved CH_4 to Temperature Perturbations of +1K

Level of Max. Perturbation	Response at level: 70mb	20mb	7mb	2mb	0.6mb	0.2mb
70mb	−0.3 ± 2.0	−0.2 ± 1.6	+0.2 ± 0.3	−0.1 ± 0.2	+0.1 ± 0.4	+0.0 ± 1.1
20mb	4.3 ± 6.3	−5.5 ± 5.3	−0.7 ± 0.7	+0.3 ± 0.3	−0.1 ± 0.2	+2.2 ± 3.1
7mb	5.1 ± 7.5	−5.1 ± 6.2	−6.8 ± 2.6	−0.4 ± 2.3	+1.4 ± 2.9	+1.2 ± 3.7
2mb	3.2 ± 1.8	+0.5 ± 1.3	−1.1 ± 0.3	−5.1 ± 0.3	−0.1 ± 0.4	+1.7 ± 1.1
0.6mb	3.1 ± 1.6	+0.8 ± 0.9	−0.2 ± 0.2	−1.5 ± 0.3	−4.8 ± 0.6	+1.6 ± 1.3
0.2mb	1.0 ± 0.6	+0.4 ± 0.3	−0.1 ± 0.2	−0.1 ± 0.1	−0.8 ± 0.2	−0.9 ± 0.6

(c) New retrievals of N_2O and CH_4

The final experiment of this set was to retrieve temperatures for the whole of November 1979 using the SBUV/LIMS ozone set rather than the global/annual mean used in the original retrievals, and then to re-retrieve N_2O and CH_4 for this month using the new temperature profile for each day. The resulting differences in the monthly mean are given in Table 4.

Table 4
Effect of using specific O_3 profile on November 1979 Retrievals

Constituent	% Change in vmr at level: 20mb	7mb	2mb	0.6mb	0.2mb
N_2O	+4.3 ± 11.3	+8.4 ± 11.6	−1.4 ± 3.6	+3.7 ± 4.2	+4.0 ± 7.6
CH_4	+2.6 ± 3.0	+7.4 ± 7.8	−1.6 ± 1.1	+0.2 ± 1.8	−2.2 ± 2.3

The results show that use of a specific ozone profile results in a general increase in the constituent mixing ratios. If table 4 is compared to Table 1 of paper 1, it can be seen that the effect is too small, and of the opposite sign, to that required to explain the discrepancies between SAMS and in-situ measurements for that month.

SEARCH FOR TRENDS IN CH_4 AND N_2O ABUNDANCES

Both nitrous oxide and methane are increasing in the troposphere and it is interesting to consider whether this is reflected in the stratospheric abundances at various levels. The use of satellite data to look for trends must be approached with caution, however, since the measurements techniques are novel and subject to errors, while the expected trends are quite small. The data of Rowland /6/, for example, shows methane trends of +1.25% per annum between 1979 and 1985 at the surface, which we might expect to see repeated in the stratosphere if it has been going on long enough. With 5 years of data to examine, a total change of around 6% would be expected; small compared to the estimated uncertainty in the data (20% or more, see paper 1) but perhaps just possible to detect since most of the errors in the data are systematic. In fact, the results (see tables below) are inconclusive.

In each case we have looked at three year means, using the same data set as in paper 1, and also five year means, using the entire SAMS data set. The latter are obviously better in some ways in looking for trends, except that the data from SAMS was of poorer quality towards the beginning and end of its lifetime. In the former case, the instrument was still being characterized and was used in various exploratory modes; in the latter, there were problems with the instrument, leading to intermittent data taking, and with the atmosphere, which was atypical in behaviour due to the eruption of *el Chichon*. In fact, similar results were obtained from both sets. Table 1 shows the temperatures and their standard deviations. A warming of around 0.15 degrees *may*be present near the 2mb level. Tables 2 and 3 show the percentage changes in the minor constituents; again, some levels exhibit changes which appear marginally statistically significant but the evidence is unconvincing. The main conclusion to be drawn from this study is that a longer data set of more precise data is needed to identify trends.

Table 5. Temperature trends and standard deviations

Pressure level (mb)	^{o}K change/yr (3 year set)	^{o}K change/yr (5 year set)
20	0.09±0.12	0.31±0.14
7	-0.06±0.13	-0.10±0.08
2	0.14±0.07	0.17±0.04
0.6	-0.10±0.16	-0.25±0.11
0.2	0.15±0.21	0.01±0.14

Table 6. Methane trends and standard deviations

Pressure level (mb)	% change/yr (3 year set)	% change/yr (5 year set)
20	10.97 ± 5.21	5.50 ± 5.53
7	5.53 ± 4.08	6.84 ± 2.08
2	-12.12 ± 4.27	-5.55 ± 5.99
0.6	-5.47 ± 6.67	0.51 ± 10.24
0.2	4.38 ± 5.79	4.81 ± 5.08

Table 7. Nitrous oxide trends and standard deviations

Pressure level (mb)	% change/yr (3 year set)	% change/yr (5 year set)
20	-21.52 ±15.15	-7.34 ± 8.63
7	7.37 ± 8.94	5.19 ± 4.94
2	-14.31 ± 11.6	0.38 ± 10.61
0.6	-6.38 ± 24.64	-2.25 ± 14.27
0.2	11.89 ± 25.27	-17.04 ± 12.21

CONCLUSIONS

The results of this work are summarized as follows:

1. The model presented in paper 1 with monthly values for the vertical and latitudinal distribution of methane and nitrous oxide is the best which can be produced with present data.

2. There do seem to be real discrepancies between satellite and balloon data at lower levels in the middle atmosphere, but we have been unable to explain these by limitations in the data reduction methods used for SAMS.

3. There are no systematic trends in the middle atmosphere abundances of the two species studied which can be detected reliably with the data available; this is consistent with expectations based on other data.

4. Further progress awaits new instruments like those forming the scientific payload of the Upper Atmosphere Research Satellite /7/. This will include an improved version of SAMS, called ISAMS, which will measure methane and nitrous oxide with much greater sensitivity and precision.

REFERENCES

1. Taylor, F.W., Dudhia, A., and Rodgers, C.D. Reference models for CH_4 and N_2O in the middle atmosphere. *Adv. Sp. Res.*, 7, 9, 49-62, (1987).

2. Drummond, J.R., Houghton, J.T., Peskett, G.D., Rodgers, C.D., Wale, M.J., Whitney, J.G., and Williamson, E.J. The Stratospheric and Mesospheric Sounder on Nimbus 7. *Phil. Trans. Roy. Soc. Lond.*, **A 296**, 219-241, (1980).

3. Taylor, F.W. Remote sounding of the middle atmosphere from satellites: the Stratospheric and Mesospheric Sounder experiment on Nimbus 7. Surveys in Geophysics, 9, 123-148, (1987).

4. Jones, R.L., and Pyle, J.A., J. Geophys. Res., 89, 5263-5279, (1984).

5. Barnett, J.J. and Corney.M. Temperature comparisons between the Nimbus 7 SAMS, Rocket/radiosondes, and the NOAA 6 SSU. J Geophys. Res., 89, 5294-5302, (1984).

6. Rowland, S. In 'Present State of Knowledge of the Upper Atmosphere, NASA Reference Publication 1162, (1986).

7. Taylor, F.W. The Upper Atmosphere Research Satellite. *Spaceflight*, 26, 455-457 (1984).

6

REVISED REFERENCE MODEL FOR NITRIC ACID

J. C. Gille, P. L. Bailey, and C. A. Craig

National Center for Atmospheric Research
Boulder, CO 80307

ABSTRACT

A nearly global set of data on the nitric acid distribution was obtained for seven months by the Limb Infrared Monitor of the Stratosphere (LIMS) experiment on the Nimbus 7 spacecraft. The evaluation of the accuracy, precision and resolution of these data is described, and a description of the major features of the nitric acid distributions is presented. The zonal mean for nitric acid is distributed in a stratospheric layer that peaks near 30 mb, with the largest mixing ratios occurring in polar regions, especially in winter.

INTRODUCTION

Nitric acid was first identified in the stratosphere by Murcray *et al.* /1/, who measured its infrared absorption spectrum from a balloon. It has subsequently been measured many times from balloons /2/, aircraft /3/ and more recently the shuttle /4/. In addition, it has been observed by direct collection on filters from balloons and aircraft /5/. Nitric acid is formed by the three body reaction

$$NO_2 + OH + M \rightarrow HNO_3 + M$$

although other processes may be involved during high latitude winter conditions. It is destroyed by the reactions

$$HNO_3 + h\nu \rightarrow OH + NO_2$$

and

$$HNO_3 + OH \rightarrow NO_3 + H_2O.$$

The time scales are several days /6/, indicating that the distribution will be strongly influenced by atmospheric motions.

The only near-global observations were obtained by the Limb Infrared Monitor of the Stratosphere (LIMS), which flew on the Nimbus 7 spacecraft. Because these are in good agreement with the other data, they are the basis for the nitric acid model proposed here. The LIMS was a 6 channel infrared radiometer that scanned the earth's limb, measuring emitted radiances that could be inverted to yield profiles of nitric acid and other quantities. The experiment and the data reduction have been described by Gille and Russell /7/; other discussions are contained in Russell and Gille /8/ and Gille *et al.* /9/. The features of IR limb scanning relevant to the measurement of HNO_3 include the long viewing paths, giving maximum sensitivity to small amounts of the gas, high vertical resolution if narrow field of view detectors are used, and the ability to obtain measurements on both the day and night sides of the orbit. However, to obtain high signal to noise ratios with the narrow detectors required that they be cooled. The use of a solid cryogen limited the LIMS lifetime to about 7 months.

Over this period, from 25 October 1978 to 28 May 1979, the instrument operated extremely well. On the average, over 1000 profiles were derived each day, from 64°S to 84°N. These profiles were then objectively analyzed using the Kalman filter approach suggested by Rodgers /10/ and described in more detail by Kohri /11/. This leads to daily estimates of the zonal mean mixing ratio and the coefficients describing 6 waves in longitude. Only a model for the zonal mean distribution is presented here.

ACCURACY AND PRECISION OF THE NITRIC ACID DATA

The characteristics of the LIMS HNO_3 data were discussed by Gille *et al.* /12/. The vertical range of the data is set by the region of adequate signal to noise ratio, and, at the bottom, by the frequent occurrence of clouds. For the HNO_3 signal, the upper limit occurred at about the 2 mb pressure level, or around 45 km altitude. Clouds usually impose a lower limit at or above the 100 mb pressure level in the tropics. Retrievals to lower altitude are possible at higher latitudes, but with rather small signal to noise ratios. In this discussion the lower boundary is taken to be 100 mb.

The precision of the profiles, or scan-to-scan repeatability, is about 0.05-0.1 ppbv in undisturbed regions where atmospheric variability does not contribute to the variations. This intrinsic precision is of the order of 2% up to 7 mb, rising to only 5% at 4 mb. When natural atmospheric variability is included, which may incorporate real variations on scales smaller than the approximately 100 km inter-scan spacing, a repeatability at almost all latitudes and altitudes of 0.1 ppbv is found.

The accuracy is much more difficult to establish. Gille *et al.* /12/ estimated the errors presented in Table 1. These estimates, at least away from the top levels, are thought to be rather conservative. Again, these were checked through comparison with 15 balloon-borne measurements from 100 to 10 mb. These differences are also collected in Table 1. They are approximately the errors associated with the balloon-borne measurements. However, the LIMS results become increasingly larger than the correlative measurements with altitude, leading the authors to suggest that they were in error. In addition, chemical consistency suggests that the original values are too large /13/. Subsequently Bailey and Gille /14/ have shown that an instrumental correction should be applied that slightly reduces the radiances at all altitudes. This has the effect of significantly reducing the HNO_3 mixing ratios above 10 mb, where the signals are small. The results presented here have now been corrected for this effect. These results therefore differ at the upper levels from those presented in Gille *et al.* /15/.

TABLE 1 LIMS Nitric Acid Errors[+]

Pressure Level (mb)	No. of Comparisons	Estimated Systematic Errors (%)	Differences from Correlative Measurements (%)
80		42	
70	4		-19 ± 24
50	14	41	4 ± 8
30	14	33	9 ± 7
10	12	29	27 ± 11
7	11		53 ± 11
5	6		90 ± 4
3		65	

[+] From Gille *et al.* /12/.

NITRIC ACID DISTRIBUTION

Vertical Distribution

Vertical profiles of HNO_3 at 60°S, 32°S, the equator, 32°N and 60°N are shown in Figure 1. At the equator, there is little vertical variation. A slight maximum of between 2 and 3 ppbv is located near 20 mb, but the seasonal variation is quite small. At 32°S the maximum of about 7 ppbv is shifted down to 30 mb. There is a minimum in mid-summer with a maximum observed value in May, suggesting an annual variation with largest values in winter. Temporal variations are shown in more detail below. A similar variation (shifted by 6 months) is shown at 32°N.

The variation is similar but much larger at 60°S. The peak values, again at 30 mb, are over 10 ppbv. At 60°N the largest values are in winter, with maxima of nearly 10 ppbv, again at 30 mb.

In summary, the tropics are characterized by low mixing ratios, and have a small seasonal variation. At higher latitudes the mixing ratios are larger, and have an annual variation characterized by a fall-winter maximum. There is very little variation in the pressure of the peak values, which increases from 20 mb in the tropics to 30 mb at high latitudes.

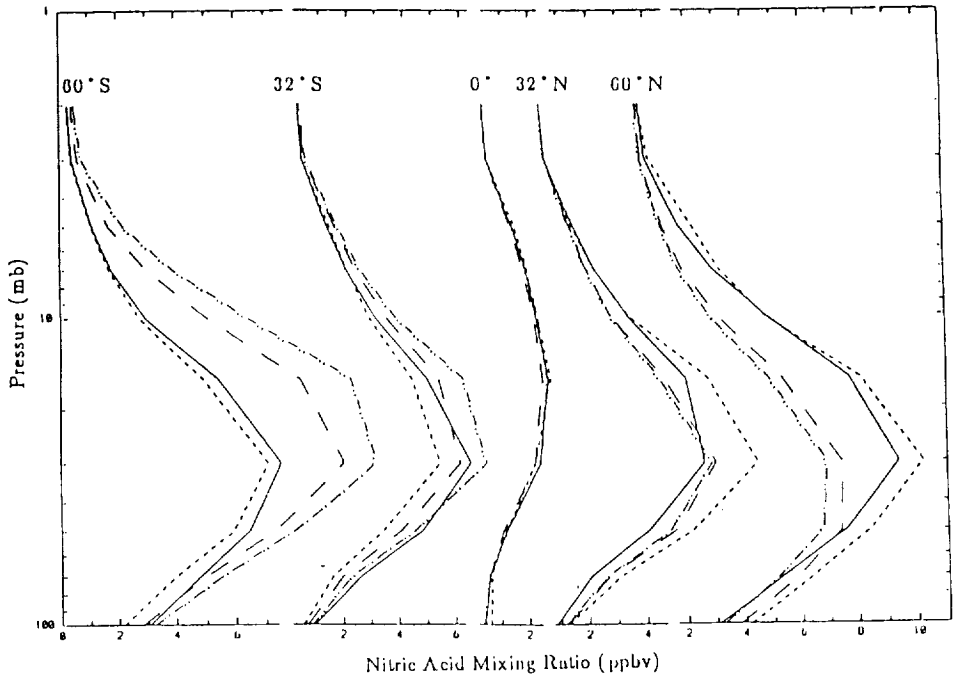

Figure 1. Vertical profiles of monthly average zonal mean HNO_3 mixing ratios at five latitudes for October (——), January (- - -), April (— —), and May (– · · –).

Monthly Average Zonal Mean Cross-Sections

At every location there are short-term variations, associated with dynamical effects, as well as seasonal changes. Even after taking the zonal mean, there are short period temporal variations. However, over a month the standard deviation of these variations are usually small. Figure 2, for January (1979) shows that the standard deviation of the daily values is less than 5% except at upper levels in the winter hemisphere, where it can be over 30%. (The increased values at the tropical tropopause are due in part to incomplete removal of cloud contaminated profiles, and in part to the difficulty of accurately following the sharp radiance decrease above clouds, in conjunction with the low mixing ratios there.) In contrast, in April (Figure 3) the standard deviation is less than 5% almost everywhere, and never greater than 15%. The standard deviation of the monthly averaged zonal means (these values divided by $\sqrt{N}$, where N is the number of days with data in the month) are therefore less than 1%, except for the high upper polar winter stratosphere, where they are still only 6%, so the random uncertainties associated with the following mean cross-sections are rather small. These standard deviations are tabulated in Table 2.

The monthly average zonal mean nitric acid distributions for October through May are presented in Figures 4-11, and in tabular form in Table 3. The general features of the nitric acid distribution are illustrated by the October data (Figure 4). There is a broad saddle in the tropics, centered near 20 mb, and characterized by values of 2-3 ppbv. Mixing ratios decrease slowly above and below this level, indicating profiles characterized by low and relatively constant values. Maximum values increase toward both poles, with the altitude of the maximum decreasing to the 30 mb level at high latitudes. In the Northern Hemisphere (NH), the maximum of 3 ppbv at 20 mb for 10° N progresses to a maximum of 12 ppbv at 30 mb for 84°N. The latitudinal variations are similar in the Southern Hemisphere (SH) as far as they can be seen. Note also that the isolines are relatively flat on the upper side of the layer, but have fairly steep slopes on the lower side. Finally, there is an indication of slightly higher values at high northern latitudes and high altitudes.

There is a regular progression in the monthly mean values. In November (Figure 5), the northern polar maximum has increased to its maximum value, while the maximum at 64°S has decreased. By December (Figure 6), the northern maximum has dropped back to less than 11 ppbv, while the southern maximum has fallen further.

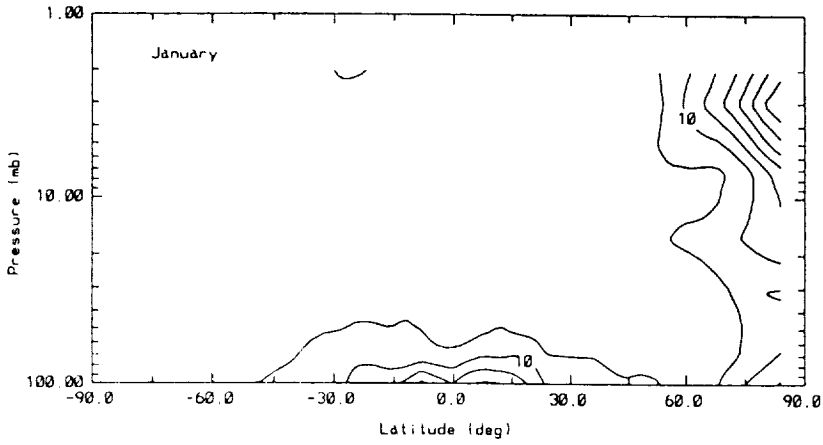

Figure 2. Cross section of the standard deviation of the daily HNO_3 mixing ratios from the monthly average, as a percent of the average value, for January. Contour interval is 5%.

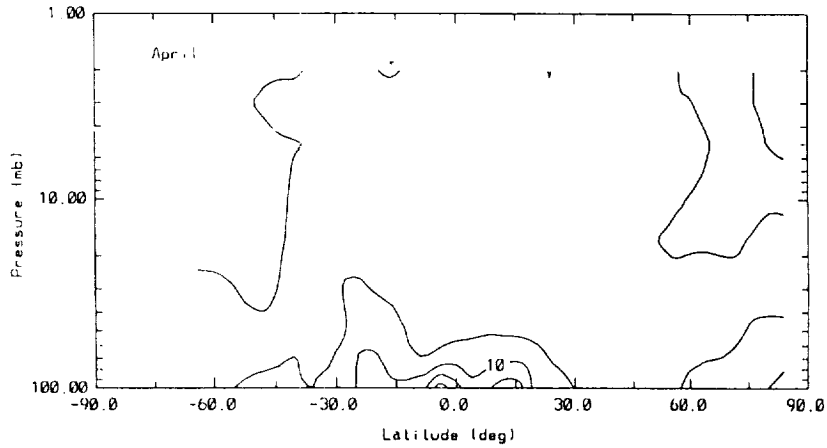

Figure 3. Same as Figure 2, but for April.

Table 2. Standard deviation of monthly average zonal mean mixing ratios (as a percent of the zonal mean)

January

Pressure (mb)	-84	-60	-50	-40	-30	-20	-10	0	10	20	30	40	50	60	70	80
2.00	0.37	0.44	0.66	0.76	0.89	0.81	0.64	0.66	0.71	0.41	0.64	0.39	0.64	1.66	3.08	5.16
3.00	0.38	0.29	0.44	0.67	0.35	0.60	0.60	0.60	0.62	0.68	0.61	0.68	0.68	1.96	3.70	6.31
5.00	0.20	0.30	0.49	0.63	0.45	0.63	0.50	0.53	0.38	0.42	0.84	0.61	0.78	1.33	1.83	4.15
7.00	0.43	0.45	0.35	0.61	0.43	0.40	0.38	0.26	0.25	0.62	0.66	0.41	0.62	0.80	0.87	2.42
10.00	0.43	0.43	0.42	0.40	0.20	0.24	0.24	0.31	0.25	0.43	0.60	0.36	0.71	0.66	1.06	2.12
16.00	0.43	0.41	0.34	0.21	0.18	0.33	0.33	0.61	0.67	0.80	0.76	0.63	0.87	1.05	1.54	2.29
30.00	0.41	0.33	0.12	0.14	0.60	0.77	0.67	0.65	0.34	0.54	0.33	0.42	0.36	0.39	0.82	0.89
50.00	0.30	0.19	0.22	0.55	0.83	0.92	0.92	0.42	0.84	0.56	0.42	0.40	0.60	0.64	0.66	1.13
70.00	0.26	0.14	0.42	0.83	1.38	1.51	1.11	1.10	1.03	1.60	0.88	0.73	0.60	0.57	0.65	1.52
100.00	0.23	0.32	0.89	1.23	1.59	2.32	3.39	2.69	3.71	2.54	1.61	1.11	1.04	0.62	1.13	2.34

April

Pressure (mb)	-84	-60	-50	-40	-30	-20	-10	0	10	20	30	40	50	60	70	80
2.00	1.32	1.33	1.12	1.04	0.60	0.90	0.84	0.74	0.72	0.80	0.76	0.75	0.74	1.08	1.61	2.19
3.00	1.22	1.57	0.90	0.68	0.75	0.45	0.70	0.48	0.53	0.74	0.48	0.68	0.69	0.87	1.48	1.97
5.00	1.66	1.56	1.16	0.95	0.59	0.66	0.62	0.38	0.54	0.61	0.62	0.44	0.60	0.62	1.23	1.85
7.00	1.80	1.60	1.43	0.85	0.46	0.42	0.36	0.35	0.29	0.31	0.40	0.23	0.33	0.70	1.32	1.40
10.00	1.65	1.61	1.62	0.80	0.58	0.35	0.27	0.24	0.25	0.22	0.14	0.25	0.42	0.97	1.24	1.04
16.00	1.22	1.23	1.38	0.75	0.70	0.69	0.32	0.30	0.44	0.41	0.30	0.38	0.80	1.03	1.01	0.66
30.00	0.72	0.74	1.07	0.49	0.63	0.86	0.25	0.52	0.29	0.17	0.31	0.42	0.59	0.62	0.71	0.58
50.00	0.49	0.48	0.72	0.75	0.63	1.51	0.78	0.59	0.81	0.46	0.36	0.59	0.37	0.66	0.73	1.11
70.00	0.57	0.53	0.72	0.93	1.01	1.93	0.95	1.50	1.51	1.59	0.64	0.64	0.38	0.76	0.98	1.54
100.00	0.87	0.83	1.11	0.93	1.21	2.55	2.38	3.13	2.95	1.52	0.00	0.83	0.49	1.15	1.43	1.83

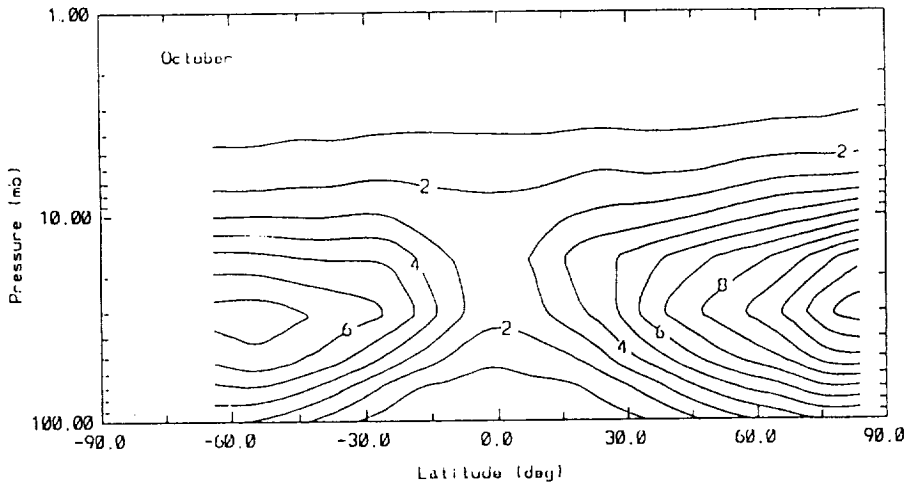

Figure 4. Monthly averaged zonal mean cross section of HNO_3 mixing ratio (ppbv) for October (last 7 days).

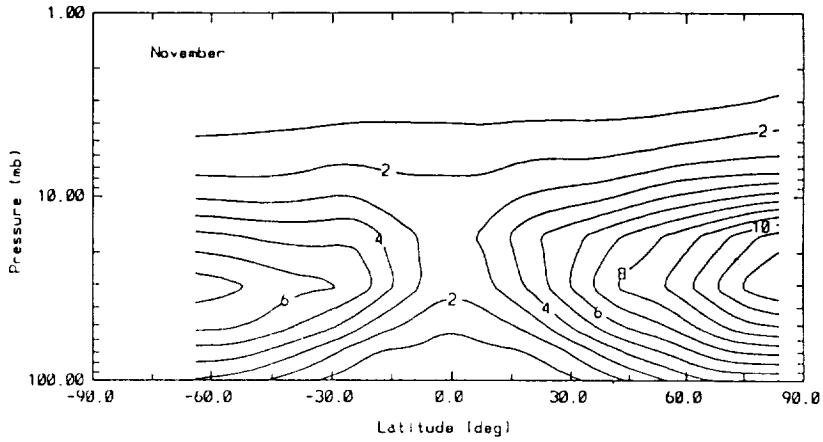

Figure 5. Same as Figure 4, but for November.

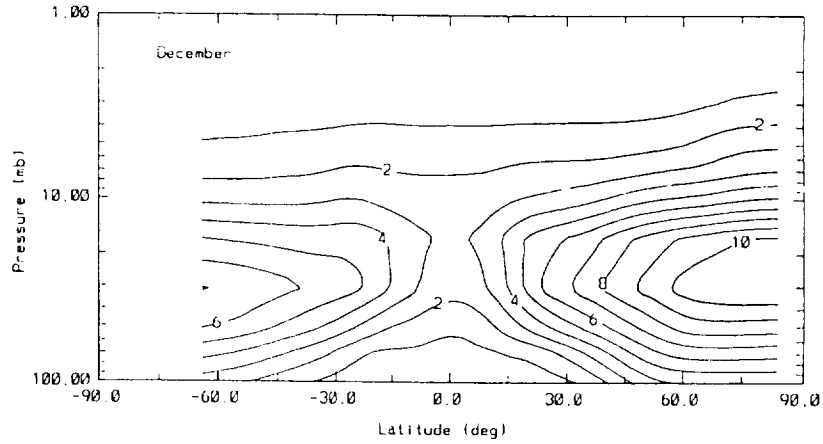

Figure 6. As Figure 4, but for December.

January's distribution (Figure 7) is much like December's, but with some increase in the winter polar upper stratosphere. This latter feature is largely gone in February (Figure 8), and the NH high latitude maximum has decreased below 10 ppbv, while that in the SH has increased. These seasonal changes continue in March (Figure 9) and April (Figure 10), until by May (Figure 11) the NH maximum is only slightly above 7 ppbv, while the SH max at 64°S is over 11 ppbv. In addition, there has been an increase in the SH (winter) polar upper stratosphere.

A comparison of November and May, the two nearly complete months that are 6 months apart, indicates little change in the tropics. However, they show a 7 ppbv contour in the SH in November that is not present at 64°N in May. Similarly, in May the mixing ratios near 60°S are larger than those near 60°N in November. It is clear that the SH maxima and minima have larger mixing ratios than those in the NH, indicating an asymmetry between the hemispheres in nitrogen compounds. This has also been seen in NO_2, and estimates of the total odd nitrogen.

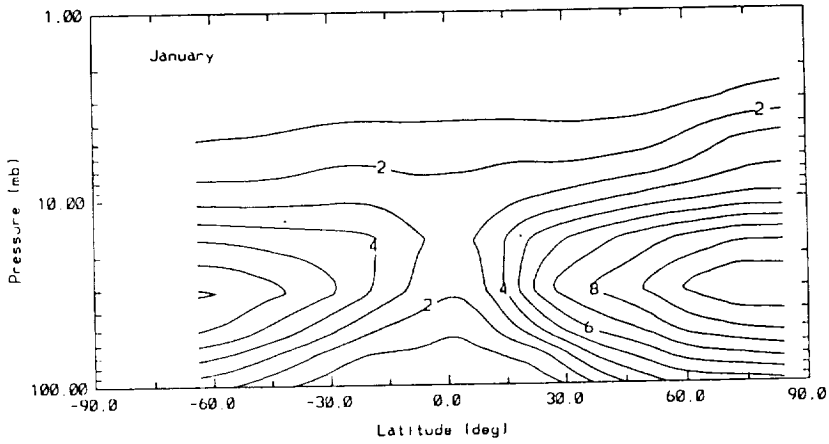

Figure 7. As Figure 4, but for January.

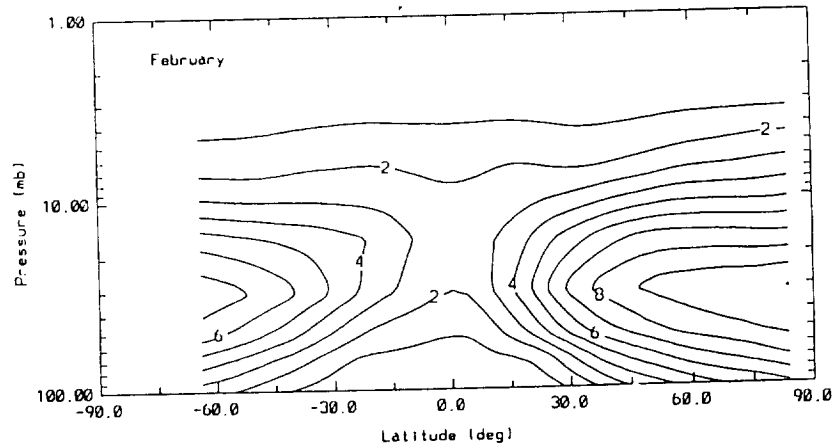

Figure 8. As Figure 4, but for February.

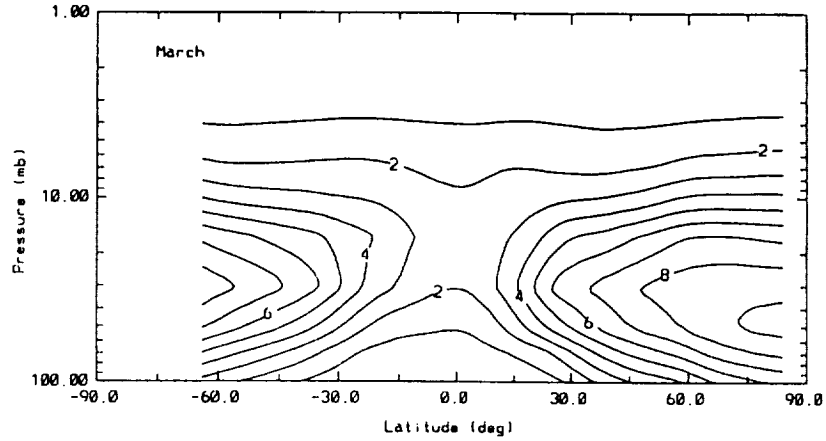

Figure 9. As Figure 4, but for March.

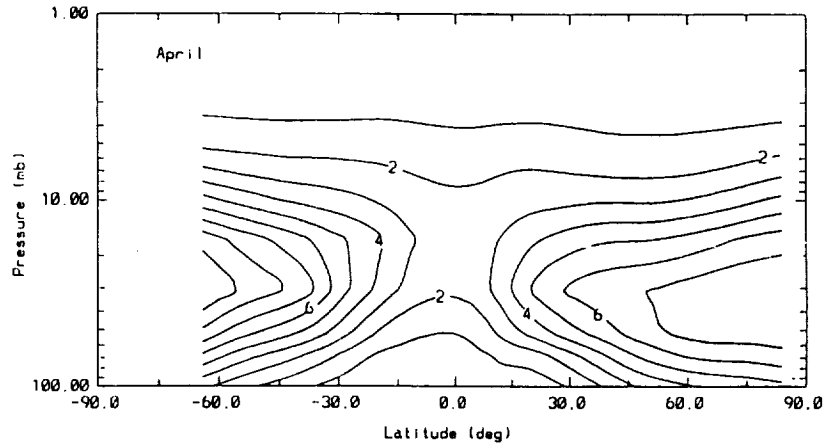

Figure 10. As Figure 4, but for April.

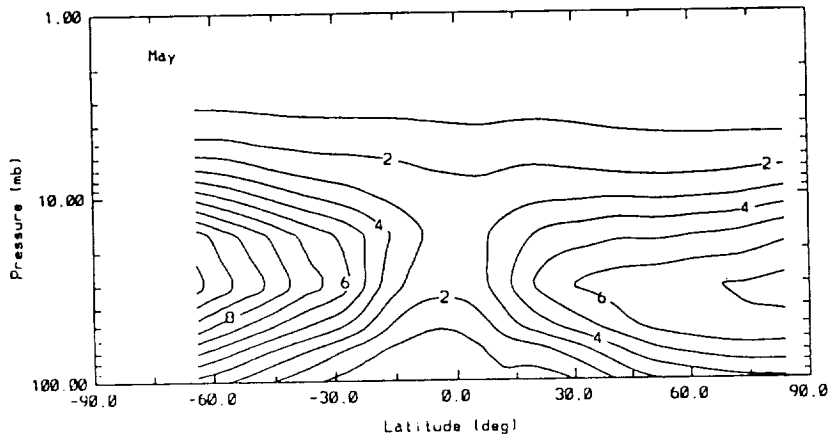

Figure 11. As Figure 4, but for May (first 28 days).

Temporal Variations

The temporal variation of the zonal mean is conveniently displayed by time-height cross sections. At the equator (Figure 12) there is a semi-annual oscillation, where the HNO_3 maxima occur at the beginning of January and (probably) July at 16 and 10 mb. The minimum at each level is close to the mid-point between the maxima. This is consistent with semi-annual vertical motions, having maximum strength in March, with minimum motions in December and June as found by Gille *et al.* /16/.

At 32°N and S (not shown), the patterns are similar to those at 60°, but the variations are weaker. The NH maxima and SH minima occur in February at 50 and 30 mb, which also shows the higher SH values in late autumn than in the NH. Again, there is a suggestion that the NH maximum occurs earlier than the SH minimum.

At 60°N and S (Figures 13 and 14) there is an annual variation, which is out of phase between the two hemispheres, with the NH maximum and SH minimum occurring in late December at 30 mb. The patterns are similar above 30 mb, but the May values in the SH are larger than the NH maxima in December, as noted earlier.

These plots (and that for 80°N, presented in Gille /17/) show long term (seasonal) changes, probably due to photochemical effects, and short period variations, especially during the winter, that are related to dynamical effects. There are marked decreases during the times of major disturbances in the stratosphere, which are to be expected when the downward motions which lead to stratospheric warmings through adiabatic compression bring down air that is poorer in HNO_3.

Table 3. Monthly average zonal mean mixing ratios (parts per billion by volume)

October

Pressure (mb)	-64	-60	-50	-40	-30	-20	-10	0	10	20	30	40	50	60	70	80
2.00	0.29	0.30	0.32	0.32	0.32	0.33	0.33	0.34	0.35	0.34	0.34	0.34	0.39	0.40	0.45	0.55
3.00	0.44	0.44	0.46	0.46	0.47	0.48	0.47	0.49	0.51	0.49	0.51	0.53	0.58	0.63	0.72	0.84
5.00	1.15	1.14	1.22	1.29	1.39	1.52	1.49	1.42	1.41	1.61	1.56	1.48	1.53	1.78	1.90	1.92
7.00	1.82	1.80	1.85	1.92	2.05	2.02	1.94	1.90	1.93	2.18	2.25	2.20	2.48	2.92	3.21	3.30
10.00	2.95	2.98	3.00	2.94	3.09	2.63	2.27	2.26	2.60	3.09	3.30	3.60	4.10	4.77	5.34	5.99
16.00	5.46	5.45	5.23	4.95	4.94	4.25	2.97	2.71	3.29	4.65	5.17	6.10	6.94	7.69	8.69	10.09
30.00	7.45	7.53	7.45	6.94	6.40	5.31	3.42	2.41	2.91	4.00	5.62	7.30	8.40	9.38	10.84	12.39
50.00	6.21	6.46	6.62	6.71	4.62	2.08	1.78	1.21	1.53	2.22	3.74	5.17	6.60	7.56	8.77	9.90
70.00	4.71	4.80	4.63	3.66	2.33	1.02	0.67	0.66	0.73	0.96	1.85	3.11	4.41	5.30	6.32	6.97
100.00	3.18	3.07	2.55	1.70	0.84	0.43	0.39	0.41	0.60	0.59	0.76	1.38	2.30	3.08	3.71	4.01

November

Pressure (mb)	-64	-60	-50	-40	-30	-20	-10	0	10	20	30	40	50	60	70	80
2.00	0.27	0.27	0.28	0.30	0.31	0.32	0.34	0.33	0.34	0.33	0.33	0.36	0.41	0.45	0.52	0.59
3.00	0.39	0.40	0.43	0.44	0.46	0.48	0.50	0.49	0.50	0.49	0.54	0.57	0.62	0.71	0.86	1.05
5.00	1.09	1.10	1.15	1.23	1.39	1.49	1.46	1.44	1.42	1.58	1.55	1.50	1.68	1.97	2.17	2.36
7.00	1.72	1.72	1.71	1.82	2.06	2.00	1.92	1.90	1.93	2.19	2.27	2.40	2.80	3.23	3.43	3.58
10.00	2.85	2.81	2.70	2.75	3.00	2.69	2.31	2.28	2.68	3.11	3.49	3.92	4.66	5.30	5.85	6.40
16.00	5.24	5.15	4.86	4.67	4.69	4.34	3.10	2.78	3.38	4.76	5.64	6.67	7.64	8.58	9.78	11.10
30.00	7.54	7.42	6.97	6.40	6.15	5.08	3.35	2.44	2.97	4.30	6.10	7.85	8.68	9.82	11.39	12.74
50.00	6.30	6.27	6.95	6.17	4.23	2.76	1.76	1.17	1.60	2.44	4.09	5.64	6.61	7.70	9.08	9.93
70.00	4.63	4.52	4.14	3.25	2.10	0.98	0.76	0.60	0.74	0.98	2.01	3.43	4.56	5.50	6.64	7.04
100.00	2.87	2.77	2.26	1.51	0.77	0.44	0.63	0.52	0.61	0.53	0.78	1.59	2.48	3.44	4.03	4.11

December

Pressure (mb)	-64	-60	-50	-40	-30	-20	-10	0	10	20	30	40	50	60	70	80
2.00	0.25	0.25	0.27	0.30	0.32	0.34	0.35	0.34	0.34	0.33	0.35	0.37	0.39	0.45	0.56	0.64
3.00	0.38	0.39	0.42	0.44	0.48	0.52	0.51	0.51	0.51	0.49	0.53	0.57	0.61	0.76	1.04	1.20
5.00	1.05	1.08	1.15	1.25	1.38	1.52	1.46	1.46	1.47	1.60	1.60	1.57	1.71	2.00	2.51	2.85
7.00	1.65	1.66	1.71	1.82	2.02	2.07	1.95	1.95	2.01	2.22	2.31	2.48	2.81	3.14	3.54	3.90
10.00	2.71	2.69	2.68	2.72	2.93	2.82	2.48	2.35	2.61	3.10	3.50	4.07	4.80	5.28	5.68	6.10
16.00	4.90	4.84	4.67	4.51	4.53	4.34	3.39	2.88	3.48	5.09	6.02	7.08	8.24	9.09	9.70	10.05
30.00	7.10	7.01	6.65	6.15	5.68	4.71	3.29	2.42	3.09	5.28	6.97	8.21	9.28	10.41	10.91	11.02
50.00	6.18	6.02	6.43	4.64	3.68	2.47	1.68	1.18	1.77	3.14	4.59	5.88	7.19	8.30	8.65	8.46
70.00	4.34	4.17	3.57	2.78	1.80	0.86	0.78	0.63	0.82	1.12	2.16	3.74	5.34	6.26	6.40	6.30
100.00	2.55	2.40	1.87	1.24	0.67	0.41	0.72	0.58	0.63	0.47	0.81	1.88	3.34	3.99	4.09	4.10

January

Pressure (mb)	-64	-60	-50	-40	-30	-20	-10	0	10	20	30	40	50	60	70	80
2.00	0.24	0.25	0.28	0.30	0.33	0.34	0.34	0.35	0.34	0.32	0.34	0.36	0.38	0.41	0.51	0.60
3.00	0.38	0.39	0.42	0.46	0.50	0.53	0.53	0.53	0.53	0.49	0.51	0.53	0.57	0.76	1.07	1.32
5.00	1.07	1.10	1.14	1.28	1.48	1.55	1.49	1.52	1.57	1.58	1.45	1.50	1.68	2.23	2.96	3.40
7.00	1.70	1.71	1.73	1.88	2.09	2.13	1.96	1.97	2.05	2.18	2.20	2.38	2.66	3.16	3.72	4.04
10.00	2.79	2.76	2.74	2.80	2.88	2.88	2.51	2.34	2.50	2.94	3.35	3.82	4.32	4.72	5.07	5.25
16.00	4.98	4.94	4.75	4.54	4.39	4.17	3.34	2.79	3.31	4.83	5.90	6.72	7.43	8.07	8.61	8.77
30.00	7.15	7.09	6.63	6.03	5.24	4.13	3.00	2.23	3.08	5.63	7.51	8.37	9.17	10.20	10.88	10.95
50.00	6.12	5.92	6.19	4.24	3.20	2.14	1.56	1.15	1.76	3.36	5.23	6.47	7.29	8.39	8.91	9.22
70.00	4.18	3.98	3.29	2.39	1.45	0.87	0.78	0.64	0.80	1.17	2.69	4.41	5.40	6.43	6.84	7.17
100.00	2.35	2.19	1.66	1.00	0.55	0.51	0.70	0.62	0.67	0.52	1.06	2.41	3.47	4.19	4.41	4.58

February

Pressure (mb)	-90	-80	-70	-60	-50	-40	-30	-20	-10	0	10	20	30	40	50	60	70	80
2.00	0.26	0.27	0.29	0.32	0.33	0.35	0.34	0.33	0.32	0.32	0.34	0.36	0.37	0.38	0.38	0.38		
3.00	0.40	0.41	0.44	0.47	0.51	0.54	0.52	0.54	0.52	0.47	0.49	0.52	0.56	0.61	0.64	0.67		
5.00	1.16	1.18	1.21	1.36	1.50	1.60	1.53	1.46	1.57	1.61	1.35	1.36	1.57	1.90	2.10	2.30		
7.00	1.90	1.88	1.86	2.00	2.11	2.15	2.00	1.87	2.00	2.13	2.03	2.19	2.62	3.04	3.20	3.42		
10.00	3.17	3.11	2.99	2.97	2.92	2.81	2.46	2.20	2.36	2.72	3.21	3.82	4.38	4.70	4.76	4.78		
16.00	5.62	5.50	5.16	4.79	4.40	3.92	3.04	2.51	2.90	3.97	5.32	6.50	7.14	7.26	7.22	7.09		
30.00	7.77	7.57	6.97	6.13	4.90	3.61	2.67	2.03	2.95	5.00	7.29	8.58	9.27	9.58	9.74	9.94		
50.00	6.47	6.18	5.31	4.23	2.90	1.79	1.31	1.09	1.66	3.30	6.36	6.88	7.84	8.55	8.90	9.25		
70.00	4.37	4.11	3.27	2.33	1.28	0.72	0.67	0.57	0.73	1.02	2.76	4.57	5.68	6.63	7.23	7.82		
100.00	2.40	2.21	1.58	0.91	0.47	0.41	0.63	0.38	0.65	0.60	1.13	2.45	3.48	4.42	5.05	5.55		

March

Pressure (mb)	-90	-80	-70	-60	-50	-40	-30	-20	-10	0	10	20	30	40	50	60	70	80
2.00	0.32	0.32	0.32	0.33	0.35	0.35	0.33	0.33	0.34	0.33	0.34	0.35	0.35	0.37	0.40	0.44		
3.00	0.50	0.49	0.49	0.51	0.53	0.53	0.51	0.50	0.49	0.50	0.51	0.50	0.54	0.57	0.61	0.64		
5.00	1.37	1.33	1.37	1.46	1.59	1.69	1.48	1.40	1.48	1.54	1.35	1.26	1.31	1.46	1.59	1.70		
7.00	2.32	2.20	2.12	2.18	2.20	2.15	1.94	1.78	1.94	1.99	1.87	1.85	2.06	2.46	2.61	2.71		
10.00	3.97	3.76	3.44	3.28	3.07	2.84	2.41	2.14	2.34	2.67	2.87	3.12	3.66	4.21	4.32	4.32		
16.00	6.74	6.47	5.90	5.38	4.64	3.89	2.93	2.43	2.72	3.60	4.90	6.46	8.24	6.97	7.04	6.86		
30.00	8.76	8.42	7.65	6.76	5.19	3.46	2.51	2.05	2.96	5.00	6.73	7.49	8.18	8.65	8.84	8.81		
50.00	7.16	6.73	5.69	4.60	3.11	1.68	1.17	1.05	1.70	3.35	5.02	6.46	7.35	8.17	8.91	9.27		
70.00	4.90	4.40	3.52	2.54	1.40	0.66	0.58	0.57	0.79	1.25	2.70	4.39	5.45	6.38	7.47	8.01		
100.00	2.65	2.37	1.66	1.01	0.51	0.34	0.43	0.41	0.61	0.61	1.12	2.39	3.26	4.03	5.26	5.93		

April

Pressure (mb)	-90	-80	-70	-60	-50	-40	-30	-20	-10	0	10	20	30	40	50	60	70	80
2.00	0.42	0.41	0.39	0.37	0.36	0.35	0.33	0.34	0.33	0.33	0.33	0.33	0.31	0.32	0.33	0.35		
3.00	0.64	0.63	0.58	0.55	0.56	0.56	0.61	0.60	0.60	0.60	0.50	0.47	0.46	0.48	0.51	0.52		
5.00	1.78	1.72	1.62	1.68	1.61	1.66	1.52	1.34	1.43	1.54	1.30	1.21	1.17	1.20	1.31	1.49		
7.00	3.22	3.02	2.65	2.43	2.32	2.14	1.93	1.79	1.90	2.04	1.95	1.81	1.77	1.86	2.12	2.55		
10.00	5.40	5.06	4.33	3.78	3.39	2.91	2.41	2.19	2.35	2.63	2.78	2.92	2.88	3.08	3.50	4.10		
16.00	8.62	8.17	7.19	6.27	5.17	4.21	2.99	2.50	2.86	3.76	4.47	4.87	4.95	5.30	5.86	6.40		
30.00	10.16	9.64	8.63	7.79	6.67	3.79	2.67	2.23	3.16	5.09	6.20	6.72	7.04	7.42	7.84	7.98		
50.00	7.93	7.32	6.14	5.18	3.70	2.00	1.19	1.00	1.07	3.41	4.72	5.82	0.78	7.40	7.60	7.09		
70.00	5.60	5.01	3.84	2.89	1.73	0.74	0.56	0.55	0.92	1.26	2.42	3.88	5.14	5.92	6.20	6.30		
100.00	3.21	2.83	1.95	1.27	0.65	0.35	0.41	0.41	0.65	0.55	1.04	2.15	3.18	3.81	4.19	4.62		

May

Pressure (mb)	-90	-80	-70	-60	-50	-40	-30	-20	-10	0	10	20	30	40	50	60	70	80
2.00	0.52	0.51	0.47	0.42	0.38	0.34	0.35	0.36	0.34	0.33	0.33	0.32	0.30	0.29	0.27	0.27		
3.00	0.80	0.79	0.72	0.63	0.60	0.55	0.53	0.52	0.51	0.52	0.51	0.48	0.45	0.44	0.42	0.39		
5.00	2.22	2.23	2.02	1.80	1.72	1.73	1.60	1.42	1.41	1.56	1.42	1.24	1.17	1.13	1.14	1.16		
7.00	4.06	3.92	3.34	2.79	2.48	2.26	2.07	1.92	1.93	2.06	1.97	1.84	1.74	1.73	1.83	1.97		
10.00	6.79	6.39	5.33	4.37	3.69	3.02	2.52	2.34	2.44	2.71	2.78	2.87	2.78	2.81	2.93	3.24		
16.00	10.50	9.89	8.45	7.08	6.00	4.66	3.26	2.65	3.14	3.98	4.39	4.60	4.68	4.83	4.98	5.44		
30.00	11.39	10.79	9.47	7.94	6.79	4.32	2.71	2.45	3.37	5.17	6.11	6.45	6.64	6.89	7.02	7.21		
50.00	8.53	7.96	6.81	5.35	4.32	2.66	1.30	1.14	2.23	3.54	4.59	5.58	0.32	6.76	6.93	6.87		
70.00	6.01	5.54	4.26	3.14	2.05	1.01	0.57	0.56	1.11	1.49	2.41	3.61	4.65	5.21	5.56	5.62		
100.00	3.51	3.25	2.35	1.61	0.79	0.45	0.36	0.36	0.83	0.69	1.02	1.94	2.83	3.27	3.65	3.81		

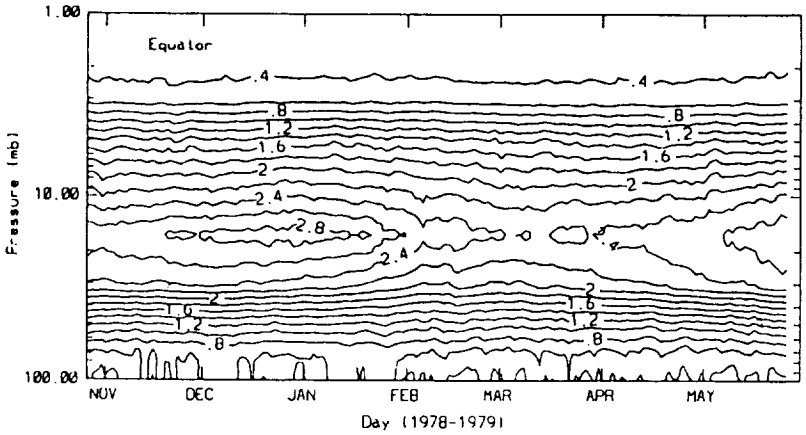

Figure 12. Time-height cross section of HNO_3 at the equator. Contour interval is 0.2 ppbv.

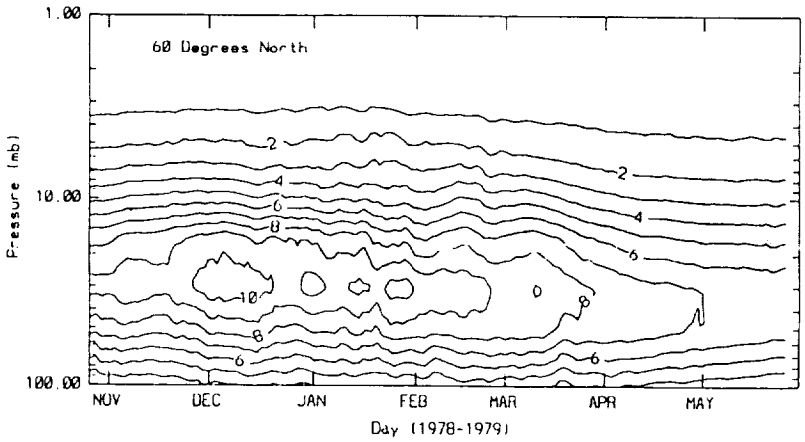

Figure 13. Time-height cross section of HNO_3 at 60°N. Contour interval is 1 ppbv.

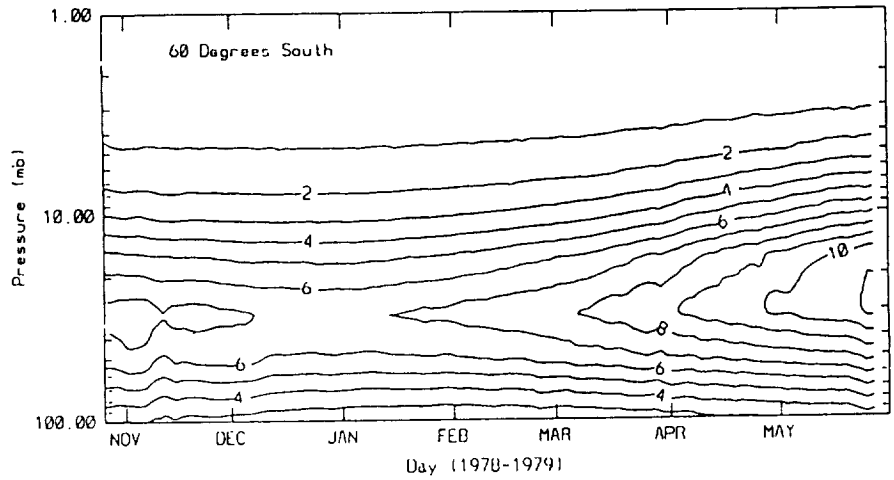

Figure 14. Time-height cross section of HNO_3 at 60°S. Contour interval is 1 ppbv.

CONCLUSIONS

The values of HNO_3 mixing ratio above 10 mb presented here have been corrected for an instrumental effect. The vertical mixing ratio profiles show a layered distribution, with the peak near 20 mb and low values in the tropics, where there is a small semi-annual variation. Poleward of 30° latitude the peak is at 30 mb and there is an annual variation, with maxima during late fall or winter and minima during summer. Cross-sections of monthly averaged zonal means emphasize the strong poleward gradients, and indicate a hemispheric asymmetry. In addition, there are slightly higher values at the upper levels near the winter pole.

Acknowledgments This work was supported by the National Aeronautics and Space Administration under Interagency Agreement W-16215.

REFERENCES

1. D. G. Murcray, T. G. Kyle, F. H. Murcray, and W. J. Williams, Nitric acid and nitric oxide in the lower stratosphere, *Nature* 218, 78-79 (1968).

2. WMO, *Atmospheric Ozone 1985*, World meteorological organization global ozone research and monitoring project report no. 16, see Table 10-3 on p. 517 (1986).

3. WMO, *Atmospheric Ozone 1985*, World meteorological organization global ozone research and monitoring project report no. 16, see Table 10-4 on p. 526 (1986).

4. J. M. Russell III, C. B. Farmer, C. P. Rinsland, R. Zander, L. Froidevaux, G. C. Toon, B. Gao, J. Shaw and M. Gunson, Measurements of odd nitrogen compounds in the stratosphere by the ATMOS experiment on Spacelab 3, *J. Geophys. Res.*, 93, 1718-1736 (1988).

5. A. L. Lazrus and B. W. Gandrud, Distribution of stratospheric nitric acid vapor, *J. Atmos. Sci.* 31, 1102-1108 (1974).

6. G. Brasseur and S. Solomon, *Aeronomy of the Middle Atmosphere*, D. Reidel, Dordrecht, 1984.

7. J. C. Gille and J. M. Russell III, The Limb Infrared Monitor of the Stratosphere: Experiment description, performance, and results, *J. Geophys. Res.* 89, 5125-5140 (1984).

8. J. M. Russell III and J. C. Gille, The Limb Infrared Monitor of the Stratosphere (LIMS) experiment, in: *The Nimbus 7 Users Guide*, ed. C. R. Madrid, NASA Goddard Space Flight Center, Greenbelt, Maryland, 1978, pp. 71-103.

9. J. C. Gille, P. L. Bailey, and J. M. Russell III, Temperature and composition measurements from the LRIR and LIMS experiments on Nimbus 6 and 7, *Phil. Trans. R. Soc. Lond. Ser. A* 296, 205-218 (1980).

10. C. D. Rodgers, Statistical principles of inversion theory, in: *Inversion Methods in Atmospheric Remote Sounding*, ed. A. Deepak, Academic Press, New York, 1977, pp. 117-138.

11. W. J. Kohri, LRIR observations of the structure and propagation of the stationary planetary waves in the Northern Hemisphere during December 1975, Ph.D. thesis, *Cooperative Thesis No. 83*, Drexel Univ. and National Center for Atmospheric Research, Boulder, CO, 1981.

12. J. C. Gille, J. M. Russell III, P. L. Bailey, E. E. Remsberg, L. L. Gordley, W.F.J. Evans, H. Fischer, B. W. Gandrud, A. Girard, J. E. Harries, and S. A. Beck, Accuracy and precision of the nitric acid concentrations determined by the limb infrared monitor of the stratosphere experiment on Nimbus 7, *J. Geophys. Res.* 89, 5179-5190 (1984).

13. C. H. Jackman, J. A. Kaye, and P. D. Guthrie, LIMS HNO_3 data above 5 mbar: Corrections based on simultaneous observations of other species, *J. Geophys. Res.* 90, 7923-7930 (1985).

14. P. L. Bailey and J. C. Gille, A correction to LIMS derived HNO_3 mixing ratios, in preparation (1989).

15. J. C. Gille, P. L. Bailey and C. A. Craig, Proposed reference model for nitric acid, *Adv. Space Res.*, 7, 25-35 (1987).

16. J. C. Gille, L. V. Lyjak, and A. K. Smith, The global residual mean circulation in the middle atmosphere for the northern winter period, *J. Atmos. Sci.* 44, 1437-1452 (1987).

17. J. C. Gille, Distributions of ozone and nitric acid measured by the Limb Infrared Monitor of the Stratosphere (LIMS), in Transport Processes in the Middle Atmosphere, G. Visconti and R. Garcia, Eds., D. Riedel, Dordrecht, 73-85 (1987).

7

PROPOSED REFERENCE MODELS FOR CO_2 AND HALOGENATED HYDROCARBONS

P. Fabian

Max-Planck-Institut für Aeronomie
D-3411 Katlenburg-Lindau, Federal Republic of Germany

ABSTRACT

The vertical distribution of carbon dioxide, halocarbons and their sink products, HCl and HF, have become available, mainly by means of balloon measurements. Most measurements were made at northern mid-latitudes, but some constituents were measured at tropical latitudes and in the southern hemisphere as well. This report attempts to combine the available data for presentation of reference models for CO_2, CCl_4, CCl_3F, CCl_2F_2, $CClF_3$, CF_4, CCl_2F-$CClF_2$, $CClF_2$-$CClF_2$, $CClF_2$-CF_3, CF_3-CF_3, CH_3Cl, $CHClF_2$, CH_3-CCl_3, $CBrClF_2$, $CBrF_3$, HCl and HF.

INTRODUCTION

CO_2 is a natural constituent of the atmosphere thought to be well mixed up to the turbopause. Due to the burning of fossil fuel, however, CO_2 abundances increase steadily at ground level resulting in CO_2 profiles which fall off with altitude in the stratosphere.

Halogenated hydrocarbons (halocarbons) are source gases for ClO_x, FO_x- and BrO_x-radicals in the stratosphere. Besides methyl chloride (CH_3Cl), the halocarbons discussed here originate almost entirely from anthropogenic sources: While CFC-10 (CCl_4), CFC-113 (CCl_2F-$CClF_2$), and CFC-140 (CH_3-CCl_3) are mainly used as solvents, CFC-22 ($CHClF_2$) and CFC-13 ($CClF_3$) are chiefly applied as refrigerants. CFC-114 ($CClF_2$-$CClF_2$), CFC-115 ($CClF_2$-CF_3), CFC-11 (CCl_3F), and CFC-12 (CCl_2F_2) are used as propellants and refrigerants, the two latter ones for foam blowing as well. CFC-14 (CF_4) and CFC-116 (CF_3-CF_3) are released from aluminium plants, but CF_4 is likely to have natural sources as well. The bromine containing species CFC-12B1 ($CBrClF_2$) and CFC-13B1 ($CBrF_3$) are released from fire extinguishers. Most halocarbons have long overall atmospheric life times. Thus the abundances of those emitted from anthropogenic sources are growing with time (see table 1). The same holds for the sink products HCl and HF.

EXPERIMENTAL

Stratospheric CO_2 and halocarbon data presented here were obtained by analyses of cryogenically collected air samples. CO_2 was analysed by infrared absorption /1/, while halocarbon analyses were made by gas chromatography (GC) employing electron capture detectors (ECD) as well as mass spectrometers (MS) for detection (e.g. /2-6/). The balloon-borne cryogenic whole-air samplers flown by the Max-Planck-Institut für Aeronomie (MPAE) and the Kernforschungsanlage Jülich (KFA) are described in /7/ and /8/, respectively. The stratospheric data are limited to balloon altitudes, i.e. up to about 35 km. Tropospheric data available from analyses of air samples collected aboard aircraft are also presented.

Vertical profiles of HCl and HF were obtained by various IR spectroscopic techniques, mainly through the efforts of the international Balloon Intercomparison Campaigns (BIC) conducted during 1982 and 1983. Since these are discussed in detail in the NASA Stratospheric Ozone Assessment Report 1985 /9/, they are not presented here.

RESULTS

CO_2

Cryogenically collected air samples from 3 balloon flights carried out at 44°N during November 1979, September 1982 and September 1984 were analysed for CO_2 using IR absorption. Employing this techniques, flask samples can be analysed with a total error of ±0.2 ppmV corresponding to ±0.06%. The results are plotted in fig.1 supplemented by aircraft data obtained close to the balloon site during the same time periods /10/. A striking feature of the CO_2 profiles is the overall similarity of the stratospheric portions above 20 km. Obviously, the general increase of the tropospheric abundance of CO_2, resulting from the burning of fossil fuel, is reflected by a stratospheric increase at a corresponding rate. Mid-stratospheric mixing ratios, as averaged over the height range above 22 km, are 325.4±0.5, 329.6±0.2, and 331.6±0.3 ppmV for 1979, 1982, and 1984, respectively. Average annual increase rates thus amount to 1.2 ppmV/y between 1979 and 1984

Table 1
Average vertical distribution of halocarbons at northern midlatitudes, units: pptV (10^{-12} by volume). These profiles correspond to the times given at the bottom of each column. Overall atmospheric lifetimes, N/S ratios and trends are also given. Trend values marked by an asterisk were derived from time-dependent model computations, they are as yet not confirmed by measurements.

layer	CCl_4 (CFC-10)	CCl_3F (CFC-11)	CCl_2F_2 (CFC-12)	$CClF_3$ (CFC-13)	CF_4 (CFC-14)	CClF-$CClF_2$ (CFC-113)	$CClF_2$-$CClF_2$ (CFC-114)
surface & lower troposphere	130	190	350	4	70	23	11
10-11 km	96.5	177.7	329.3			21.93	10.36
11-12 km	86.5	171.7	321.8			20.71	10.02
12-13 km	80.1 ±10%	171.3	314.7			20.68	9.89
13-14 km	73.2	167.2	310.7 ±5%			21.68 ±20%	9.57
14-15 km	69.3	163.7	307.4	3.9	65.2	21.95	9.31
15-16 km	66.0	156.9 ±6%	298.5			22.83	9.03 ±8%
16-17 km	60.8 ±17%	147.2	284.4			22.32	8.59
17-18 km	52.4 ±21%	133.5	267.4			20.99	8.17
18-19 km	44.2 ±28%	118.3	246.9	3.5	66.6	17.81	7.62
19-20 km	34.1 ±36%	98.0	218.2 ±7%			15.51	6.91
20-21 km	22.5 ±46%	76.0	189.7			12.25	6.13
21-22 km	13.6 ±59%	53.9 ±36%	160.3			10.01	5.53
22-23 km	8.9 ±73%	35.7 ±40%	137.4 ±12%	3.0 ±10%	66.5	8.43 ±32%	5.17
23-24 km	4.9 ±90%	20.3 ±47%	113.3 ±22%		±10%	7.40	4.79
24-25 km	2.3	11.1 ±50%	93.6 ±25%			6.54	4.28
25-26 km	1.2 ±100%	5.8 ±64%	81.5 ±28%			5.49	4.39
26-27 km	0.3	3.5 ±79%	69.2	2.7	58.8	4.79	4.16
27-28 km	0.1	1.4 ±90%	55.9 ±18%			3.94	3.79
28-29 km		0.6	46.1 ±50%	2.5		3.15	3.65 ±18%
29-30 km		0.5 ±100%	40.5			2.46	3.72
30-31 km		0.3	29.9			1.90	3.33
31-32 km		0.2 ±50%	24.3 ±30%	2.1	61.8	1.39 ±65%	3.16
32-33 km		0.2	16.9			1.03	3.04
33-34 km			15.6			0.54	2.85
34-35 km							
Corresponding to time	Sept/Oct. 1982-83	Sept./Oct. 1980-83	Sept./Oct. 1980-83	Sept. 1980	Sept. 1980	Sept./Oct. 1982-84	Sept./Oct. 1982-84
overall life time	60-100y	55-93 y	105-169y	180-450y	10000y	63-122y	126-310y
N/S ratio	1.07	1.12	1.07	≈1	≈1	1.12	1.05
trend	2%/y	6%/y	5%/y	5%/y*	2%/y*	10%/y*	6%/y

which is quite comparable with those observed at tropospheric levels. Annual means of tropospheric CO_2, for the years discussed here, were found to be in excess of 6.8±0.9 ppmV over the stratospheric mixing ratios corresponding to a time lag of 5.2±0.8 years. The transition occurs between 10 and 22 km altitude, while there is almost no height dependence of the CO_2 VMR above that height.

The tropospheric CO_2 profiles shown in fig. 1 are representative of late summer/fall conditions, when the cumulative uptake of CO_2 by plants reaches its maximum. Thus at ground level, an annual minimum is obtained in August/September. In late winter/spring, when CO_2 is returned to the atmosphere, a maximum occurs in April/May. This seasonal variation, having a total amplitude of about 7 ppmV in the northern troposphere, is almost undetectable within the lower stratosphere.

The existence of a shaped CO_2 profile as shown in fig. 1 may be relevant for satellite sounders that use the assumption of well-mixed CO_2 in the stratosphere to retrieve temperatures from infrared spectral features.

Halogenated hydrocarbons (halocarbons)

Vertical profiles of halocarbons are plotted in figures 2-12. Every data point corresponds to an air sample with sampling altitude ranges typically varying between 1-2 km at 35 km and about 0.2-0.4 km at 10 km. The plotted altitudes correspond to the centers of the sampling ranges. A careful error analysis has to take into account the following

Table 1 contd.

layer	$CClF_2$-CF_3 (CFC-115)	CF_3-CF_3 (CFC-116)	CH_3Cl (CFC-40)	$CHClF_2$ (CFC-22)	CH_3-CCl_3 (CFC-140)	$CBrClF_2$ (CFC-12BI)	$CBrF_3$ (CFC-13BI)
surface & lower troposphere	4.1	4	617	73	175	1.3	1.0
10-11 km				60.8	104.4	1.32	0.9
11-12 km				55.9	80.6	1.23	
12-13 km				56.2	76.0 ±10%	1.26	
13-14 km				53.8	69.1	1.15 ±20%	
14-15 km	3.1		424]	53.0	67.1	1.08	0.68
15-16 km			372.4	52.0	69.7	0.99	
16-17 km			348.1	50.6	66.7 ±20%	0.84	±10%
17-18 km			306.3 ±20%	48.1	61.8	0.68	
18-19 km	2.3	3.7	262.6	45.8	56.5	0.56	
19-20 km	±10%		214.9	42.6 ±11%	49.8	0.40 ±26%	
20-21 km			161.5	38.6	29.7 ±30%	0.28	0.44
21-22 km			125.4 ±35%	34.9	19.5	0.15 ±50%	
22-23 km	1.7	3.47	116.4	32.0	11.4	0.06	0.17
23-24 km			100.9	29.8	6.32 ±50%	0.02	
24-25 km			83.3 ±50%	27.6	3.96		
25-26 km		±10%	75.8	27.0	2.16		
26-27 km	1.36	3.12	65.1	26.1	1.24		0.06
27-28 km			42.1	25.3	0.1 ±100%		
28-29 km	1.26	2.93	30.5	24.0			
29-30 km			29.6	24.6			
30-31 km			22.9 ±30%	23.5			
31-32 km			20.9	21.7			
32-33 km	1.0	2.53	19.8	19.7			
33-34 km							
34-35 km							
Corresponding to time overall life time	Sept. 1980 230-550y	Sept. 1980 10 000 y	Sept./Oct. 1980-83 2-3 y	Sept. 1982/83 12-20y	Sept./Oct. 1982/83 5.7-10y	Sept./Oct. 1982-84 29-42y	Sept. 1980 62-117y
N/S ratio	≈1	≈1	1	1.18	1.36	1.43	?
trend	9%/y*	6%/y*	-	12%/y	8%/y	20%/y	5%/y*

contributions: The sampling altitude range and its errors due to the fact that measured pressures were converted into altitudes using the temperature distribution of a standard atmosphere, the statistical errors related to sampling, possible contamination and analysis leading to an overall precision of ± (5-10)%, and the errors of the absolute calibration which are ±10% or less. The lowest detection limits are about 0.02 pptV for CFC-12BI, 0.1 pptV for CFC-10, CFC-11, CFC-113, CFC-140, and CFC-13BI, and 1 pptV for CFC-12, CFC-13, CFC-14, CFC-114, CFC-115, CFC-116, CFC-40, and CFC-22.

The data points of the figures show a scatter, however, which is often considerably larger than the quoted precision of 5-10%. This certainly reflects some natural variability, but no seasonal effects as all data represent September/October conditions. The scatter is particularly large in those portions of the profiles which show a large vertical gradient of the mixing ratio suggesting that sampling height errors may be involved. CH_3Cl (fig. 9) is exceptional in revealing extremely large scatter between 20 and 30 km altitude. It is not clear whether real natural variability or sample contamination may account for this effect.

Thus, for calculating reference models for the different species, the individual errors were not analysed for every data point. Instead, the points were averaged within 1-km layers, and the standard deviations from the respective mean values were calculated. It appears that this mean standard deviation is a reasonable estimate of all statistical errors within each layer. The average profiles thus obtained and the standard deviations are plotted in the figures. They are also compiled in table 1.

For CFC-13, CFC-14, CFC-115, CFC-116, and CFC-13BI, only one measured profile was available at all (see fig. 5, 6, 12, data points compiled in table 1). Thus no averaging was possible. More data points will become available soon. At MPAE, air samples collected during balloon flights made 1983, 1984 and 1985 have already been analysed for those constituents. The absolute calibration, however, has not been finished yet. It can be concluded, however, that these new data confirm the vertical slopes of the species, shown

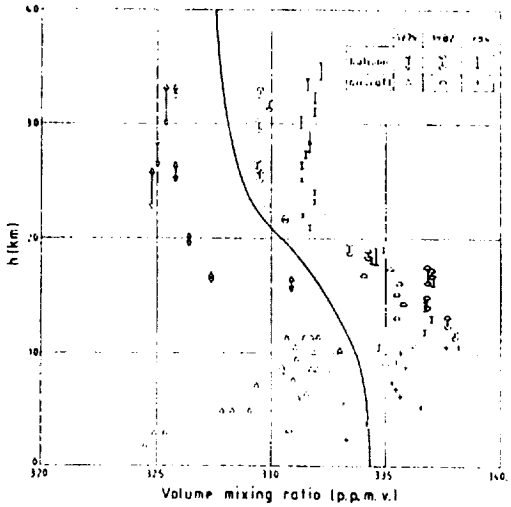

Figure 1. Vertical distribution of CO_2 between the ground and 35-km altitude as analysed by infrared absorption of whole air samples collected aboard balloon and aircraft platforms, for 1979, 1982, and 1984. The height range of the balloon samples is shown by the symbols. The modelled profile (solid line) computed by means of a one-dimensional time-dependent model corresponds to 1980 conditions /10/.

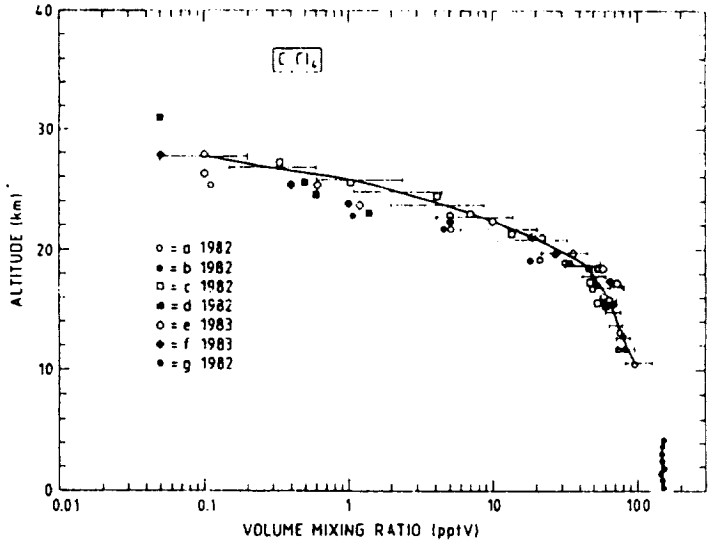

Figure 2. Vertical distribution of CCl_4 (CFC-10) at northern midlatitudes. Every data point represents one whole-air sample collected during the year listed in the figure. Each symbol represents data from a different flight or group of investigators, respectively. The average profile and its error bars were obtained by averaging all data points within 1 km layers. The points of this profile are compiled in Table 1. Sources: a,b /4/; c-f /6/; g /11/.

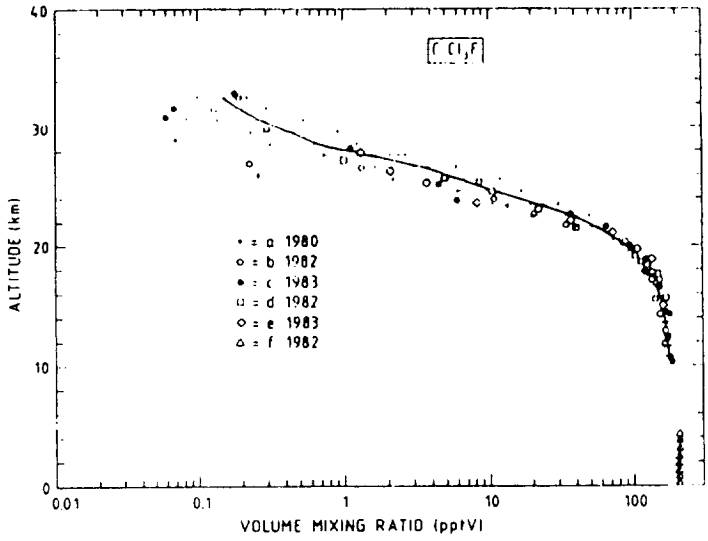

Figure 3. Same as Figure 2 but for CCl_3F (CFC-11). Sources: a /3/; b /12/; c,e /13/; d /6,8/; f /11/.

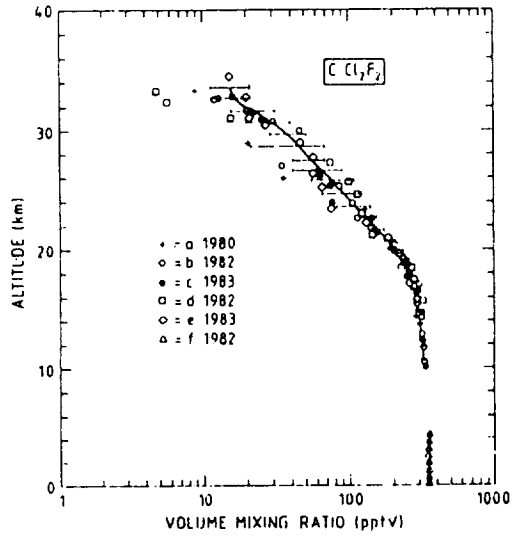

Figure 4. Same as Figure 2 but for CCl_2F_2 (CFC-12). Sources: a /3/; b /12/; c,e /13/; d /6,8/; f /11/.

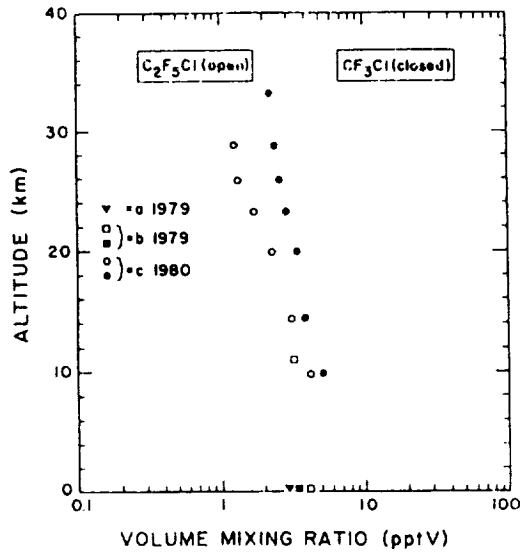

Figure 5. Vertical distribution of $CClF_3$ (CFC-13) and $CClF_2$-CF_3) (CFC-115) at northern midlatitudes. Sources: a /14/; b /15/; c /3/.

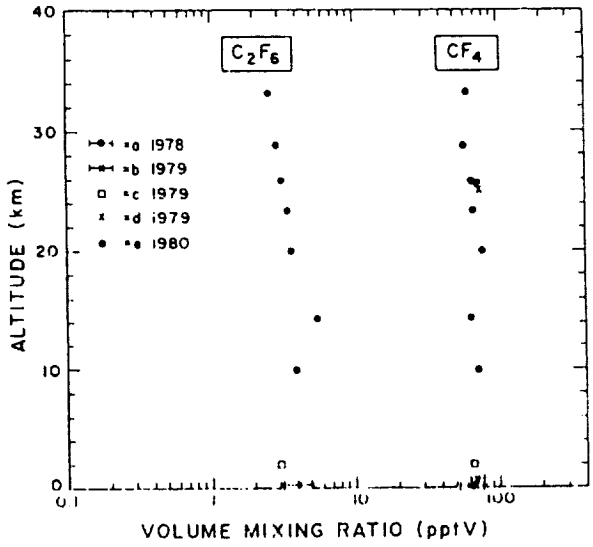

Figure 6. Vertical distribution of CF_4 (CFC-14) and CF_3-CF_3 (CFC-116) at northern midlatitudes. Sources: a/16/; b /15/; c /14/; d /17/; e /3/.

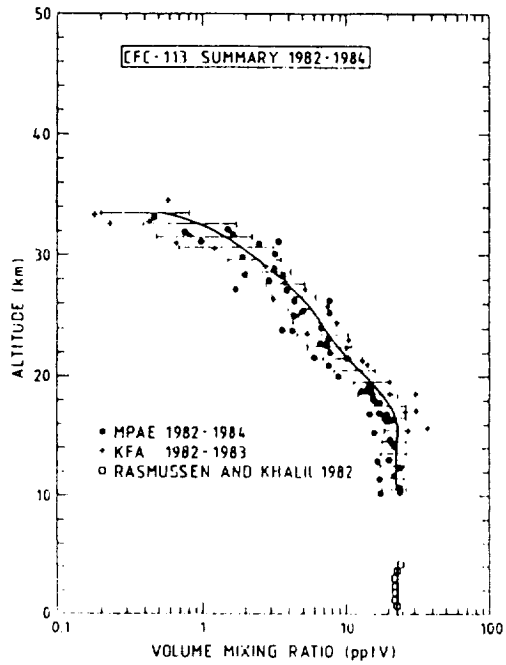

Figure 7. Same as Figure 2 but for CCl_2F-$CClF_2$ (CFC-113). Source: /18/.

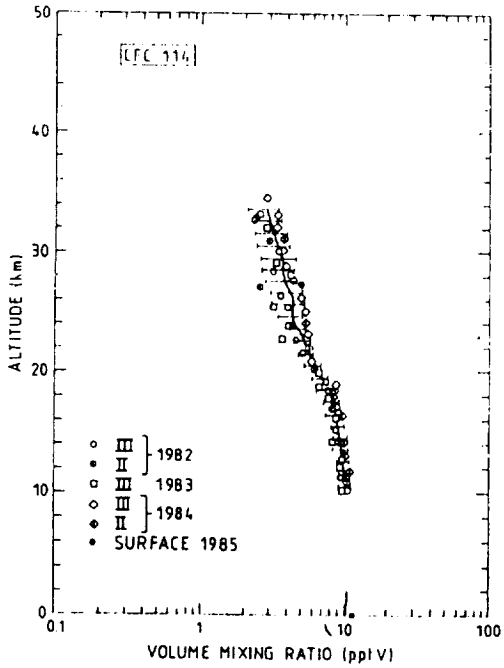

Figure 8. Same as Figure 2 but for $CClF_2$-$CClF_2$ (CFC-114). Source: /19/.

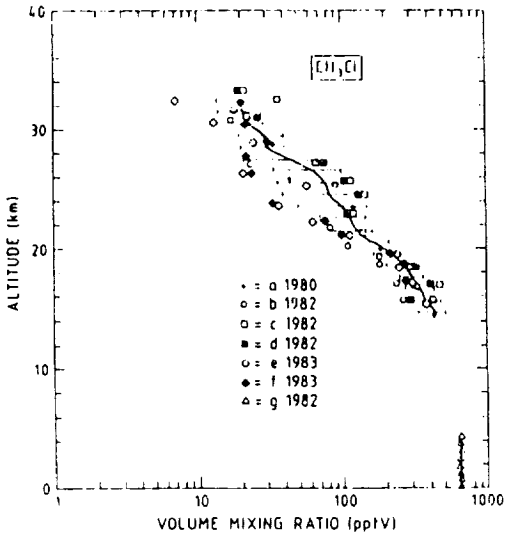

Figure 9. Same as Figure 2 but for CH_3Cl (CFC-40). Sources: a /3/; b /12/; c-f /6/; g /11/.

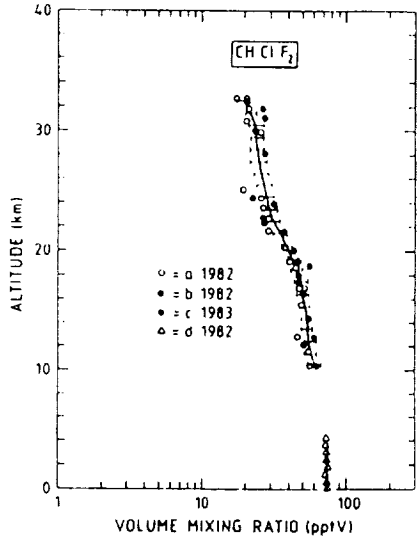

Figure 10. Same as Figure 2 but for $CHClF_2$ (CFC-22). Sources: a-c /20/; d /11/.

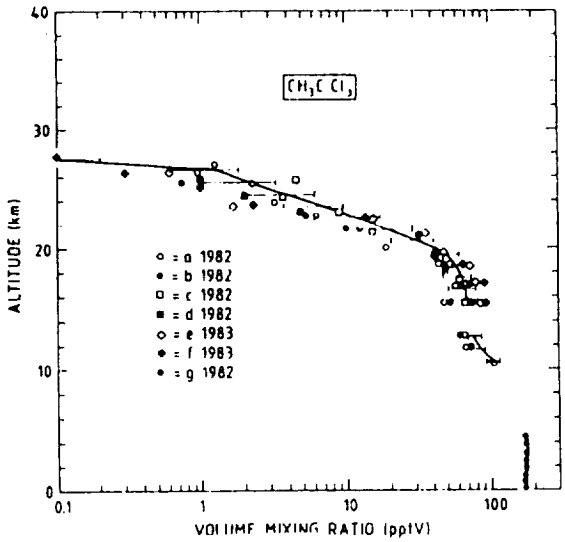

Figure 11. Same as Figure 2 but for CH_3-CCl_3 (CFC-140). Sources: a,b /4/; c-f /6/; g /11/.

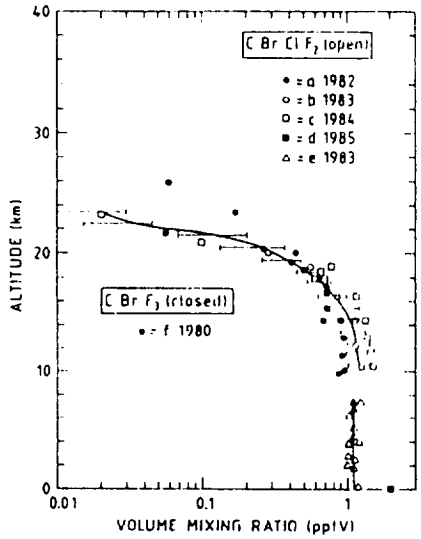

Figure 12. Same as Figure 2 but for $CBrClF_2$ (CFC-12BI). Vertical distribution of $CBrF_3$ (CFC-13BI) is also given. Sources: a-d /21/; e /11/; f /3/.

in figures 5,6, and 12.

The proposed reference models of halocarbons are compiled in table 1. Due to the errors related to the absolute calibration, every profile is accurate to within ±10% for the time period given at the bottom of the respective column. The same accuracy may be assumed for the surface and lower tropospheric mixing ratios shown in the first line of table 1. These were obtained by averaging all published field data.

Since all stratospheric measurements presented here were made during September/October, the tabulated values correspond to this time of year. On the basis of measurements made at KFA, Schmidt et al. /8/ have argued that seasonal variations do occur. These are small, however, and thus most likely included in the quoted standard deviations.

The given halocarbon profiles reflect northern midlatitude conditions. Corresponding southern midlatitude data may be obtained by applying the N/S ratios also given in table 1, which were derived from all available tropospheric halocarbons measurements. Tropical profiles of CFC-11 and CFC-12 are known to fall with height less rapidly than midlatitude profiles /22/ as upward motion partly counteracts decomposition in this region. A similar effect can be expected for other halocarbons, but except for a few first exploratory data /23/ no conclusive measurements are documented yet.

Due to continuing anthropogenic emission, atmospheric halocarbon abundances increase with time. Present annual increase rates were evaluated and also listed in table 1. These trend values base, wherever available on measured data. The trend values marked by an asterisk were derived from time-dependent model computations at MPAE based on available global emission scenarios.

ACKNOWLEDGEMENT

The source gas research program at the Max-Planck-Institut für Aeronomie has been sponsored by the Federal Ministry of Research and Technology through grants No.FKW-03 and KBF-MT-0450-0704563 2.

REFERENCES

/ 1/ Bischof, W., Tellus 29, 435 (1977)
/ 2/ Penkett, S.A., Toxicol.Environ.Chem. 3, 291 (1981)
/ 3/ Fabian, P., Borchers, R., Penkett, S.A., Prosser, N.J.D., Nature 294, 733 (1981)
/ 4/ Borchers, R., Fabian, P., Penkett, S.A., Naturwiss. 70, 514 (1983)
/ 5/ Fabian, P., Gömer, D., Fresenius Z. Anal.Chem. 319, 890 (1984)
/ 6/ Knapska, D., Schmidt, U., Jebsen, C., Kulessa, G., Rudolph, J., Penkett, S.A., Atmospheric Ozone (C.S. Zerefos, A. Ghazi, Eds.) 117, Reidel-Dordrecht (1985)
/ 7/ Fabian, P., Adv. Space Res. 1, 17 (1981)
/ 8/ Schmidt, U., Khedim, A., Knapska, D., Kulessa, G., Johnen, F.J., Adv. Space Res. 4, 131 (1984)
/ 9/ NASA, Stratospheric Ozone Assessment Report 1985, Washington, D.C. (1986)
/10/ Bischof, W., Borchers, R., Fabian, P., Krüger, B.C., Nature 316, 708 (1985)
/11/ Rasmussen, R.A., Khalil, M.A.K., Dept.of Env. Sci. Oregon Grad. Center, Beaverton, manuscript (1983)
/12/ Borchers, R., Fabian, P., unpublished data.
/13/ Schmidt, U., Kulessa, G., Klein, E., Röth, E.P., Fabian, P., Borchers, R., to appear in Plan. Space Sci. (accepted 1986)
/14/ Rasmussen, R.A., Khalil, M.A.K., in M. Nicolet, A.C. Aikin (eds.) NATO Adv. Study Inst. Atmosph. Ozone, Report FAA-EE-80-20, 209 (1984)
/15/ Penkett, S.A., Prosser, N.J.D., Rasmussen, R.A., Khalil, M.A.K., J. Geophys. Res. 86, 5172 (1981)
/16/ Rasmussen, R.A., Penkett, S.A., Prosser, N.J.D., Nature 277, 549 (1979)
/17/ Goldman, A., Murcray, D., Murcray, F., Cook, G., van Allen, J., Bonomo, F., Blatherwick R., Geophys. Res. Lett. 6, 609 (1979)
/18/ Borchers, R., Fabian, P., Krüger, B.C., Lal, S., Schmidt, U., Knapska, D., Penkett, S.A., to appear in Plan. Space Sci. (accepted 1986)
/19/ Fabian, P., Borchers, R., Krüger, B.C., Lal, S., J. Geophys. Res. 90, 13091 (1985)
/20/ Fabian, P., Borchers, R., Krüger, B.C., Lal, S., Penkett, S.A., Geophys. Res. Lett. 12, 1 (1985)
/21/ Lal, S., Borchers, R., Fabian, P., Krüger, B.C., Nature 316, 135 (1985)
/22/ Ehhalt, D.H., Proc. Ozone Symposium Boulder 1980 (J. London, Ed.) 728 (1981)
/23/ Borchers, R., Fabian, P., Lal, S., Subbaraya, B.H., Acharya, Y.B., Jayaraman, A., this issue

8

BACKGROUND STRATOSPHERIC AEROSOL REFERENCE MODEL

M. P. McCormick* and P. Wang**

*Atmospheric Sciences Division, NASA Langley Research Center, Hampton, VA 23666
**Science and Technology Corporation, Hampton, VA 23666

INTRODUCTION

The objective of this paper is to present a proposed reference model for the background stratospheric aerosol based on currently available data from satellite observations. Information on the characteristics of stratospheric aerosols is important to climate and remote sensing studies through radiative transfer processes. Measurements of stratospheric aerosols actually date back nearly 30 years. Using balloon-borne particle counters, Junge et al. /1/ discovered a layer of high particle concentration several kilometers thick in the lower stratosphere which has become known as the Junge layer. Primarily, measurements of stratospheric aerosols have been made by two different approaches, either using in situ mechanical/optical particle counters or by remote optical sensing techniques. In order to obtain more information on the stratospheric aerosol layer, NASA has launched three satellite instruments since October 1978: the Stratospheric Aerosol Measurement (SAM II) on Nimbus 7, and the Stratospheric Aerosol and Gas Experiments I and II (SAGE I and II) on the Applications Explorer Mission 2 satellite and the Earth Radiation Budget Satellite, respectively. These satellite instruments all utilize the solar occultation technique to measure vertical profiles of limb attenuated solar intensity at desired wavelengths during each sunrise and sunset experienced by the satellite. The SAM II instrument is a one-channel sunphotometer measuring aerosol extinction at 1.0 μm in the polar regions. The SAGE I instrument is a four-channel sunphotometer which measures aerosol extinction at 1.0 μm and 0.45 μm with nearly global coverage. In addition, it also provides simultaneous observations of stratospheric O_3 and NO_2 at 0.60- and 0.45-μm wavelengths, respectively. The detailed aspects of the SAM II and SAGE I systems have been described by McCormick et al. /4/. The SAGE II satellite instrument was launched in 1984 and is an advanced version of SAGE I. It has three additional channels centered at 0.448-, 0.525-, and 0.94-μm wavelengths which provide a differential NO_2 measurement, additional aerosol extinction data, and an H_2O vapor concentration channel. Thus, the SAGE II satellite instrument measures aerosol extinction at four different wavelengths, and the simultaneously determined stratospheric H_2O is of particular importance in understanding the aerosol microphysical processes as well as their composition. The data processing of SAGE II observations is currently in progress, and the data set will be available to the scientific community beginning in 1987.

Unlike the stratospheric gaseous species, which can be fully characterized by determining their concentration (number density or mixing ratio), a complete description of aerosol particles requires information about their composition/refractive index, size distribution, and shape. A complete set of such information is very much needed, especially in order to understand the radiative implications of aerosols. Fortunately, there is sufficient evidence that the stratospheric aerosol can be described reasonably well by assuming they are spherical liquid droplets of approximately 75 percent H_2SO_4 and 25 percent H_2O in composition by weight (Rosen, /7/); see also the Standard Radiation Atmosphere (SRA), /10/. In addition, analytic models have been recommended for the background stratospheric aerosol size distribution and composition by Russell et al. /8/ which have proved quite successful in the validation of SAM II and SAGE I (Russell et al., /9/). The current understanding of sources and sinks, and their distributions have been reviewed by Turco et al. /11/ who also pointed out which experimental and theoretical analysis are needed in order to enhance our knowledge about stratospheric aerosols.

Since aerosol extinction at 1.0-μm wavelength inferred from SAGE I satellite observations constitute the only available multi-year aerosol data set with nearly global-scale coverage, it is reasonable to use this data set to derive a reference model of stratospheric aerosols. It should be kept in mind that strictly speaking, this proposed reference model is an optical one. Nevertheless, it summarizes the general global-scale features of the stratospheric aerosol layer and can be used, for example, to derive parameters which are important to climate studies (McCormick, /5/; Lenoble and Brogniez, /3/; SRA, /10/).

REFERENCE MODEL

During its operation lifetime from February 1979 to November 1981, the SAGE I instrument produced 34 months of aerosol extinction data with nearly global coverage. Except for the very minor volcanic eruption of La Soufriere (13.3°N, 61.2°W; 17 April 1979), the stratospheric aerosol layer was practically unperturbed during the SAGE measuring period from February 1979 to May 1980 (Kent and McCormick, /2/). After that time, a number of large volcanic perturbations occurred. As a result, the SAGE aerosol 1.0-mm extinction data set obtained during this period will be adopted in this paper to establish a simple reference model for the background stratospheric aerosol. The meridional distribution of the zonal mean stratospheric aerosol extinction at 1.0-mm wavelength on a seasonal basis has been documented in tabulations and in graphic representations by McCormick /6/. This distribution is reproduced in Figure 1.

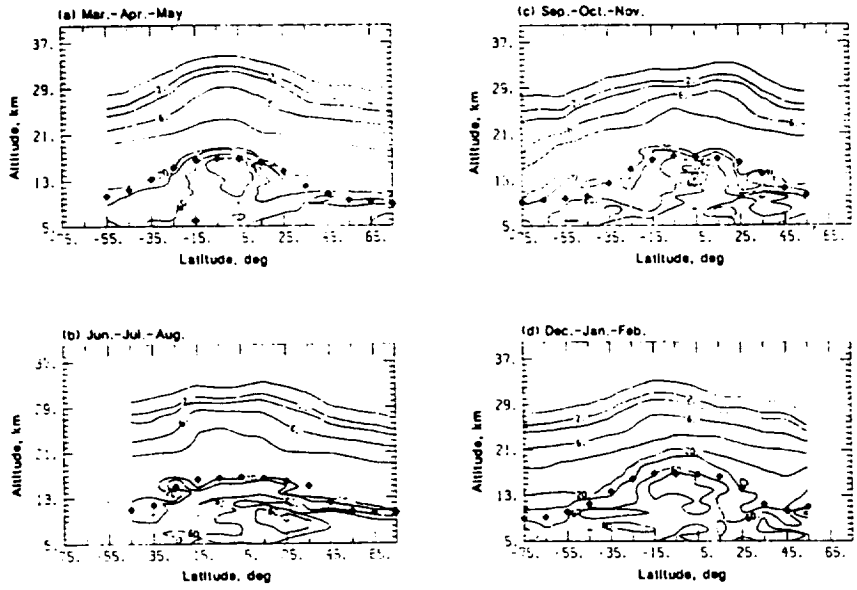

Fig. 1. Seasonal meridional distribution of aerosol extinction at 1.0 μm, in units of 10^{-3} km^{-1}, (a) March-April-May (1979), (b) June-July-August (1979), (c) September-October-November (1979), and (d) December (1979)-January-February (1980).

In order to obtain the vertical distribution of stratospheric aerosols in a climatological manner, the averaged profiles are computed for five different latitudinal bins: 75°S-40°S, 40°S-20°S, 20°S-20°N, 20°N-40°N, and 40°N-75°N on a seasonal basis. These latitude bins roughly correspond to the tropics and the mid- and high latitudes in both hemispheres. The results are tabulated in Tables 1-4 and Figures 2-5 using the northern seasonal period nomenclature, starting with spring, and are in all cases referenced to the tropopause height. The remarkable feature in Figures 2-5 is the similar vertical distribution of the averaged profiles from the five different latitudinal bins when referenced to the tropopause and the similarity in the four different seasonal plots. Figure 6 presents a plot of all the data of Figures 2-5 on one graph and shows the striking similarity in the data. This very similar vertical distribution of the 1.0-μm aerosol extinction in Figures 2-6 suggests that it is reasonable to construct a simple analytic representation for profiles from the five different latitudinal bins. The following third order polynomial is used for this representation:

$$\mathrm{Log}_{10}(\beta) = a + bZ + cZ^2 + dZ^3 \qquad (1)$$

where β is the 1.0-μm aerosol extinction at altitude z measured from the tropopause and a, b, c, and d are coefficients to be determined from the SAGE I satellite data set. This calculation was carried out to 20 km above the tropopause, the range over which the data are the most accurate. The results of the derived coefficients are given in Table 5. The computed profile using these coefficients for each of the seasonal periods is indicated in Figures 2-5 by the heavy curve. As one can see, the computed profiles represent the average of the vertical profiles from the five different latitudinal bins very well. It is understood that

TABLE 1 Zonally Averaged Stratospheric Aerosol Extinction at 1.0 Micrometer (1/km) for March, April, and May 1979

	LATITUDE				
ALT*(km)	75S-40S	40S-20S	20S-20N	20N-40N	40N-75N
0	1.921E-04	1.371E-04	5.779E-04	2.871E-04	7.013E-04
1	1.668E-04	1.189E-04	3.254E-04	1.771E-04	3.337E-04
2	1.507E-04	1.096E-04	1.708E-04	1.376E-04	1.973E-04
3	1.260E-04	1.109E-04	1.239E-04	1.221E-04	1.597E-04
4	1.276E-04	1.141E-04	1.136E-04	1.156E-04	1.433E-04
5	1.315E-04	1.128E-04	1.087E-04	1.130E-04	1.331E-04
6	1.323E-04	1.067E-04	1.020E-04	1.098E-04	1.262E-04
7	1.261E-04	9.676E-05	9.433E-05	1.044E-04	1.195E-04
8	1.140E-04	8.482E-05	8.748E-05	9.576E-05	1.118E-04
9	9.858E-05	7.255E-05	8.047E-05	8.750E-05	1.032E-04
10	8.205E-05	6.083E-05	7.300E-05	7.781E-05	9.428E-05
11	6.591E-05	4.967E-05	6.586E-05	6.748E-05	8.538E-05
12	5.152E-05	4.001E-05	5.865E-05	5.638E-05	7.626E-05
13	3.860E-05	3.203E-05	4.982E-05	4.599E-05	6.615E-05
14	2.900E-05	2.520E-05	3.829E-05	3.678E-05	5.468E-05
15	2.163E-05	1.954E-05	2.771E-05	2.806E-05	4.250E-05
16	1.594E-05	1.477E-05	1.935E-05	2.184E-05	3.139E-05
17	1.164E-05	1.083E-05	1.319E-05	1.642E-05	2.272E-05
18	8.423E-06	7.894E-06	8.857E-06	1.230E-05	1.663E-05
19	6.171E-06	5.720E-06	5.905E-06	9.026E-06	1.196E-05
20	4.596E-06	4.191E-06	4.000E-06	6.506E-06	8.653E-06
TROP-HEIGHT	10.75	14.21	16.60	13.15	9.54

*Altitude above tropopause

TABLE 2 Zonally Averaged Stratospheric Aerosol Extinction at 1.0 Micrometer (1/km) for June, July, and August 1979

	LATITUDE				
ALT* (km)	75S-40S	40S-20S	20S-20N	20N-40N	40N-75N
0	2.165E-04	1.542E-04	1.513E-04	1.475E-04	4.835E-04
1	1.795E-04	1.384E-04	1.157E-04	1.346E-04	2.241E-04
2	1.618E-04	1.275E-04	1.120E-04	1.128E-04	1.541E-04
3	1.489E-04	1.229E-04	1.108E-04	1.115E-04	1.338E-04
4	1.418E-04	1.235E-04	1.125E-04	1.096E-04	1.274E-04
5	1.405E-04	1.251E-04	1.101E-04	1.022E-04	1.258E-04
6	1.386E-04	1.209E-04	1.065E-04	9.679E-05	1.232E-04
7	1.329E-04	1.144E-04	1.023E-04	8.899E-05	1.169E-04
8	1.233E-04	1.049E-04	9.853E-05	7.755E-05	1.091E-04
9	1.095E-04	9.334E-05	9.290E-05	6.694E-05	1.005E-04
10	9.288E-05	7.913E-05	8.388E-05	5.731E-05	8.945E-05
11	7.709E-05	6.511E-05	7.292E-05	4.870E-05	7.697E-05
12	6.224E-05	5.282E-05	5.620E-05	3.756E-05	6.293E-05
13	5.038E-05	4.238E-05	3.679E-05	2.860E-05	4.820E-05
14	4.118E-05	3.448E-05	2.420E-05	2.182E-05	3.510E-05
15	3.332E-05	2.834E-05	1.660E-05	1.610E-05	2.496E-05
16	2.691E-05	2.160E-05	1.142E-05	1.199E-05	1.746E-05
17	2.010E-05	1.642E-05	7.904E-06	8.819E-06	1.251E-05
18	1.439E-05	1.242E-05	5.544E-06	6.572E-06	8.851E-06
19	1.026E-05	9.112E-06	3.947E-06	4.961E-06	6.327E-06
20	7.347E-06	6.616E-06	2.858E-06	3.771E-06	4.604E-06
TROP-HEIGHT	10.98	12.82	16.57	15.36	10.50

*Altitude above tropopause

TABLE 3 Zonally Averaged Stratospheric Aerosol Extinction at 1.0 Micrometer (1/km) for September, October, and November 1979

ALT* (km)	LATITUDE 75S-40S	40S-20S	20S-20N	20N-40N	40N-75N
0	3.843E-04	2.396E-04	3.432E-04	1.440E-04	2.702E-04
1	3.007E-04	1.639E-04	2.770E-04	1.205E-04	1.721E-04
2	2.393E-04	1.533E-04	1.691E-04	1.152E-04	1.423E-04
3	2.033E-04	1.411E-04	1.240E-04	1.170E-04	1.348E-04
4	1.818E-04	1.390E-04	1.148E-04	1.197E-04	1.349E-04
5	1.654E-04	1.354E-04	1.084E-04	1.187E-04	1.402E-04
6	1.488E-04	1.290E-04	1.044E-04	1.122E-04	1.407E-04
7	1.314E-04	1.180E-04	1.007E-04	1.023E-04	1.376E-04
8	1.129E-04	1.061E-04	9.502E-05	8.859E-05	1.291E-04
9	9.593E-05	9.340E-05	8.691E-05	7.723E-05	1.149E-04
10	7.863E-05	7.880E-05	7.521E-05	6.596E-05	9.819E-05
11	6.550E-05	6.656E-05	5.682E-05	5.494E-05	7.950E-05
12	5.398E-05	5.469E-05	3.977E-05	4.490E-05	6.220E-05
13	4.396E-05	4.190E-05	2.710E-05	3.619E-05	4.704E-05
14	3.387E-05	3.246E-05	1.848E-05	2.726E-05	3.524E-05
15	2.658E-05	2.487E-05	1.286E-05	2.029E-05	2.513E-05
16	2.052E-05	1.890E-05	9.053E-06	1.511E-05	1.827E-05
17	1.523E-05	1.442E-05	6.423E-06	1.082E-05	1.316E-05
18	1.107E-05	1.022E-05	4.640E-06	7.896E-06	9.563E-06
19	8.083E-06	7.369E-06	3.421E-06	5.762E-06	6.992E-06
20	5.920E-06	5.310E-06	2.555E-06	4.267E-06	5.128E-06
TROP-HEIGHT	9.70	13.49	16.77	14.99	10.77

*Altitude above tropopause

TABLE 4 Zonally Averaged Stratospheric Aerosol Extinction at 1 Micrometer (1/km) for December 1979, January and February 1988

ALT* (km)	LATITUDE 75S-40S	40S-20S	20S-20N	20N-40N	40N-75N
0	3.798E-04	2.909E-04	5.149E-04	2.479E-04	2.738E-04
1	3.044E-04	2.349E-04	4.376E-04	2.237E-04	2.340E-04
2	2.418E-04	1.930E-04	3.385E-04	2.286E-04	2.341E-04
3	2.121E-04	1.640E-04	2.939E-04	2.277E-04	2.376E-04
4	1.952E-04	1.439E-04	2.132E-04	2.182E-04	2.341E-04
5	1.743E-04	1.211E-04	1.342E-04	2.004E-04	2.175E-04
6	1.483E-04	1.024E-04	1.047E-04	1.778E-04	1.935E-04
7	1.252E-04	8.859E-05	9.617E-05	1.563E-04	1.682E-04
8	1.075E-04	7.722E-05	8.760E-05	1.311E-04	1.454E-04
9	9.471E-05	6.697E-05	7.679E-05	1.101E-04	1.242E-05
10	8.263E-05	5.818E-05	6.183E-05	9.256E-05	1.075E-04
11	7.141E-05	4.709E-05	4.638E-05	7.784E-05	9.328E-05
12	5.955E-05	3.762E-05	3.444E-05	6.337E-05	7.888E-05
13	4.800E-05	2.899E-05	2.496E-05	5.087E-05	6.676E-05
14	3.796E-05	2.174E-05	1.750E-05	3.915E-05	5.466E-05
15	2.940E-05	1.612E-05	1.247E-05	2.883E-05	4.197E-05
16	2.197E-05	1.145E-05	8.842E-06	2.047E-05	3.087E-05
17	1.596E-05	8.205E-06	6.294E-06	1.384E-05	2.134E-05
18	1.147E-05	5.860E-06	4.522E-06	9.776E-06	1.493E-05
19	8.272E-06	4.219E-06	3.276E-06	6.858E-06	1.054E-05
20	5.974E-06	3.065E-06	2.425E-06	4.885E-06	7.409E-06
TROP-HEIGHT	10.14	14.74	16.65	12.52	10.42

*Altitude above tropopause

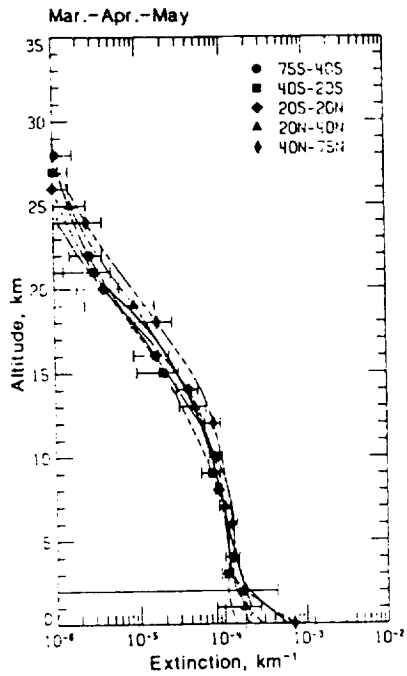

Fig. 2. Vertical distributions of aerosol 1.0-μm extinction for March-April-May (1979) at the tropics, and mid- and high latitudes in both hemispheres above the tropopause.

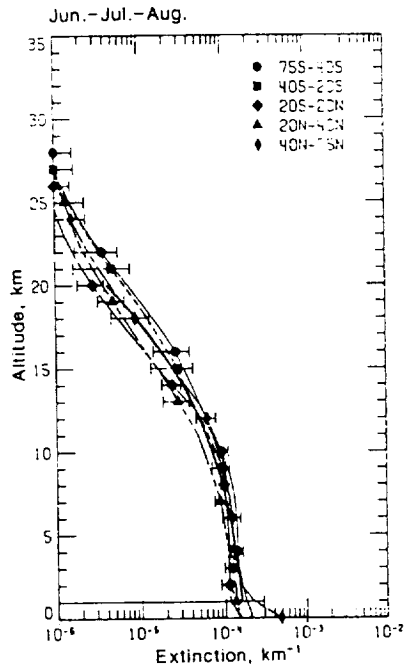

Fig. 3. Vertical distribution of aerosol 1.0-μm extinction for June-July-August (1979) at the tropics, and mid- and high latitudes in both hemispheres above the tropopause.

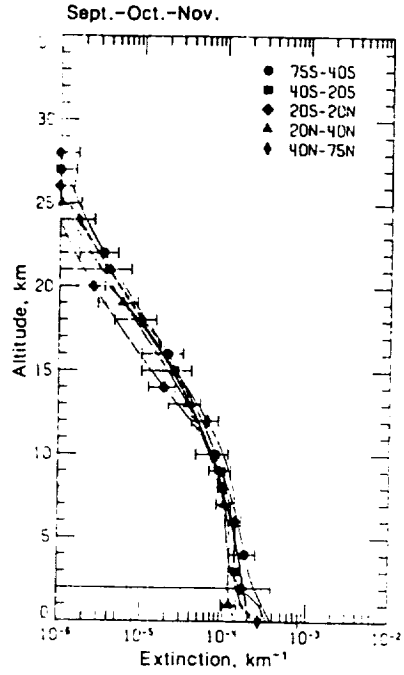

Fig. 4. Vertical distribution of aerosol 1.0-μm extinction for September-October-November (1979) at the tropics, and mid- and high latitudes in both hemispheres above the tropopause.

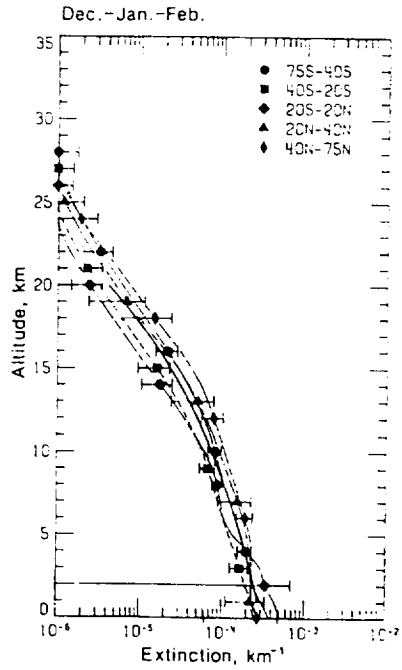

Fig. 5. Vertical distribution of aerosol 1.0-μm extinction for December (1979)-January-February (1980) at the tropics, and mid- and high latitudes in both hemispheres above the tropopause.

these heavy curves are only approximate representations of the globally-averaged vertical distribution since we have only used 1 year of the SAGE I data set, but it does appear to be a reasonable representation. Also listed in Table 5 is a separate fit to the data of Figure 6.

TABLE 5 Coefficients of the Polynomial (Eq. 1) Derived from SAGE 1.0-μm Aerosol Extinction (March 1979 to February 1980)

	COEFFICIENTS			
PERIOD*	a	b	c	d
MAM	-3.60	-8.59E-02	6.30E-03	-3.17E-04
JJA	-3.78	-1.79E-02	-5.66E-04	-1.27E-04
SON	-3.67	-3.26E-02	-2.99E-04	-1.20E-04
DJF	-3.50	-5.42E-02	4.01E-04	-1.21E-04
YEARLY MEAN	-3.64	-4.77E-02	-1.46E-03	-1.71E-04

*MAM (March, April, May)
JJA (June, July, August)
SON (September, October, November)
DJF (December, January, February)

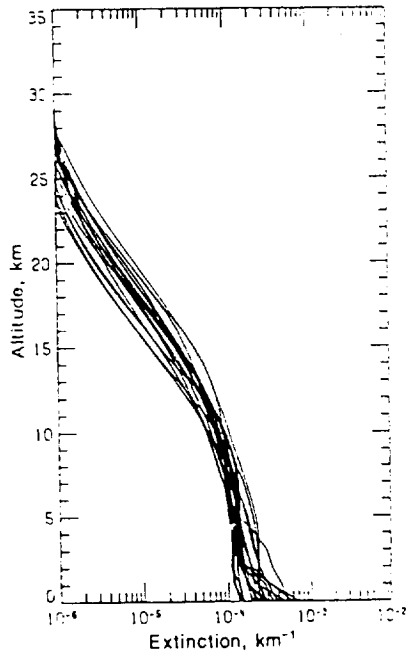

Fig. 6. The spreading of the vertical profiles from all the different seasons and latitudinal bins given in Figures 2-5.

SUMMARY

In this analysis, a reference background stratospheric aerosol optical model is developed based on the nearly global SAGE I satellite observations in the non-volcanic period from March 1979 to February 1980. Zonally averaged profiles of the 1.0-μm aerosol extinction for the tropics and the mid- and high altitudes for both hemispheres are obtained and presented in graphical and tabulated form for the different seasons. In addition, analytic expressions for these seasonal global zonal means, as well as the yearly global mean, are determined according to a third order polynomial fit to the vertical profile data set. This proposed background stratospheric aerosol model can be useful in modeling studies of stratospheric aerosols and for simulations of atmospheric radiative transfer and radiance calculations in atmospheric remote sensing.

REFERENCES

1. Junge, C. E., C. W. Chagnon, and J. E. Manson, Stratospheric aerosols, J. Meterol. 18, 81 (1961)

2. Kent, G. S. and M. P. McCormick, SAGE and SAM II measurements of global stratospheric aerosol optical depth and mass loading, Geophys. Res., 89, 804, 5303 (1984)

3. Lenoble, J. and C. Brogniez, Information on stratospheric aerosol characteristics contained in the SAGE satellite multi-wavelength extinction measurements, Appl. Opt., 24, 1054 (1985)

4. McCormick, M. P., P. Hamill, T. J. Pepin, W. P. Chu, T. J. Swissler, and L. R. McMaster, Satellite studies of the stratospheric aerosol, Bull. Amer. Meteor. Soc. 60, 1038 (1979)

5. McCormick, M. P., Aerosol observations for climate studies. Adv. Space Res., 5, 67 (1985a)

6. McCormick, M. P., SAGE aerosol measurements Volume I - February 21, 1979 to December 31, 1979, NASA RP 1145 (1985b)

7. Rosen, J. M., The boiling point of stratospheric aerosols, J. Appl. Meteorol., 10, 1044 (1971)

8. Russell, P. B., M. P. McCormick, T. J. Swissler, W. P. Chu, J. M. Livingston, W. H. Fuller, J. M. Rosen, D. J. Hofmann, L. R. McMaster, D. C. Woods, and T. Pepin, Satellite and correlative measurements of the stratospheric aerosol, I: An optical model for data conversions, J. Atmos. Sci., 38, 1279 (1981)

9. Russell, P. B., M. P. McCormick, T. J. Swissler, J. M. Rosen, D. J. Hofmann, and L. R. McMaster, Satellite and correlative measurements of the stratospheric aerosol III: Comparison of measurements by SAM II, SAGE, dustsondes, filters, impactors, and lidar, J. Atmos. Sci., 41, 1791 (1984)

10. Standard Radiation Atmosphere Radiation Commission of IAMAP, A preliminary cloudless standard atmosphere for radiation computation, Boulder, Colorado, USA, (1984)

11. Turco, R. P., R. C. Whitten, and O. B. Toon, Stratospheric aerosols: Observation and theory, Rev. Geophys. and Space Phys., 20, 233 (1982)

9

COMPARISON BETWEEN OBSERVED AND CALCULATED DISTRIBUTIONS OF TRACE SPECIES IN THE MIDDLE ATMOSPHERE

G. Brasseur* and A. DeRudder**

*National Center for Atmospheric Research, Boulder, CO 80307
**Belgian Institute for Space Aeronomy, 1180 Brussels, Belgium

INTRODUCTION

The number density of atmospheric minor constituents is characterized by large temporal and spatial variability. In the case of long-lived species such as the "source gases" (N_2O, CH_4, the chlorofluorocarbons, etc.), transport processes may account for much of this variability. In the case of fast-reacting species such as chemical radicals (OH, HO_2, O, NO, Cl, etc.), a large fraction of the variability is produced by the diurnal and seasonal variation of the solar insolation. However, as these radicals are usually produced by chemical or photochemical decomposition of long-lived species, their distribution is also indirectly controlled by transport processes. Finally, in the case of species whose chemical lifetime is approximately equal to the transport characteristic time of the atmosphere (ozone and nitric acid in the middle stratosphere, temporary reservoirs such as HO_2NO_2, $ClONO_2$, HOCl in given altitude ranges), chemistry and dynamics play an equally important role.

With the measurement, over a significant period of time and over a wide spatial range, of a number of trace species concentrations, it has become possible to produce climatological distributions of these compounds and even, for some of them, to infer reliable empirical models. As most of these models result from averaging a large number of observations, they may be compared to theoretical models which intend to simulate global average conditions by solving the conservation equations based on chemical, radiative and dynamical considerations. Such comparison allows the validation of both observational data and theoretical calculations. Moreover, such study leads to a better understanding of the basic processes which control the observed distributions and to the identification of inconsistencies between theory and observations.

Ideally, in order to investigate all processes involved, a comparison between theory and observations require on the one hand multidimensional models and on the other hand atmospheric data sets covering the entire earth. However, because the data available are limited and accurate multidimensional transport schemes are computationally expensive and difficult to achieve, "first order" validation of the currently known chemical processes in the stratosphere can be based on simpler one-dimensional calculations.

The purpose of this short paper is to identify major discrepancies between empirical models and theoretical models and to stress the need for additional observations in the atmosphere and for further laboratory work, since these differences suggest either problems associated with observation techniques or errors in chemical kinetics data (or the existence of unknown processes which appear to play an important role). The model used for this investigation [1] extends from the earth's surface to the lower thermosphere. It includes the important chemical and photochemical processes related to the oxygen, hydrogen, carbon, nitrogen and chlorine families. The chemical code is coupled with a radiative scheme which provides the heating rate due to absorption of solar radiation by ozone and the cooling rate due to the emission and absorption of terrestrial radiation by CO_2, H_2O and O_3.[2] The vertical transport of the species is expressed by an eddy diffusion parameterization.

COMPARISON BETWEEN THEORETICAL MODELS AND OBSERVATIONS

As the model used hereafter is one-dimensional and produces global average vertical profiles, the present

* National Center for Atmospheric Research is funded by the National Science Foundation

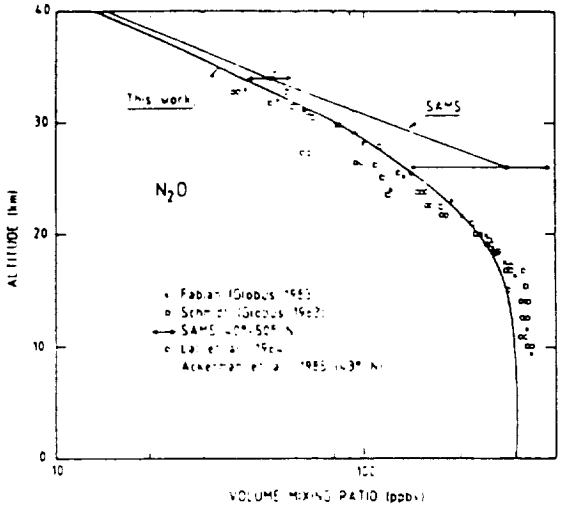

Fig. 1. Comparison between several observed distributions of nitrous oxide [3, 4, 5, 6] and a 1-D theoretical profile.

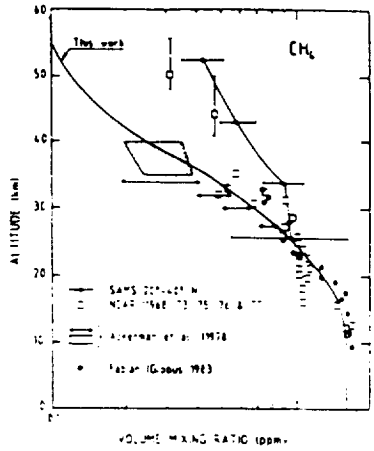

Fig. 2. Comparison between observed distributions of methane [3, 4, 7] and a 1-D theoretical profile.

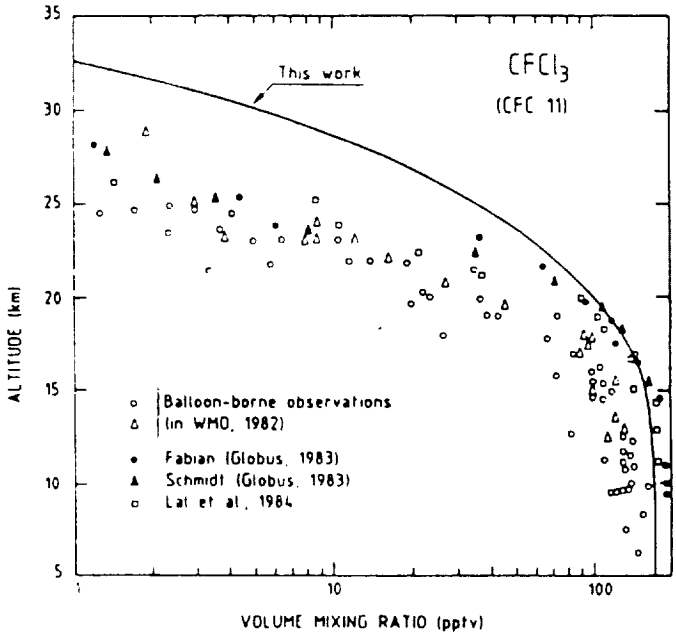

Fig. 3. Comparison between observed distributions of CFC-11 [3, 5] and a 1-D theoretical profile.

study will focus essentialiy on the long-lived trace gases. However, some important and unexplained discrepancies concerning the fast-reacting species will also be mentioned.

Source Gases

The calculated distributions of N_2O, CH_4, CCl_4, CH_3CCl_3, CFC-11 and CFC-12, are displayed in Figures 1-6. The agreement between theoretical and observed vertical distributions is good for N_2O

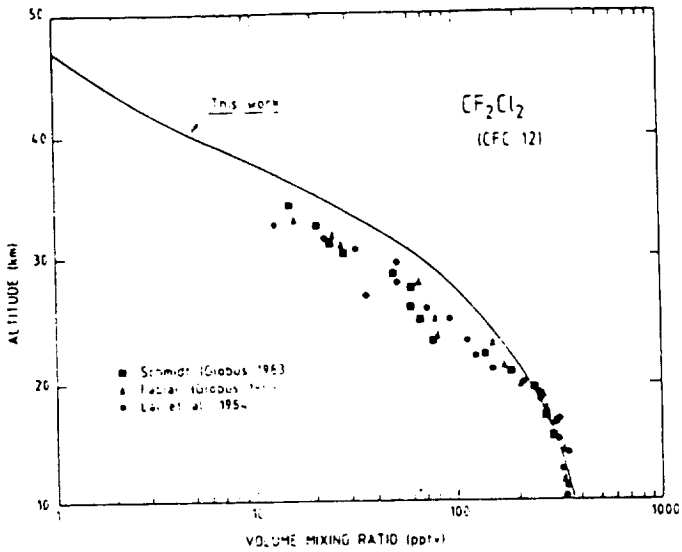

Fig. 4. Comparison between observed distributions of CFC-12 [3, 5] and a 1-D theoretical profile.

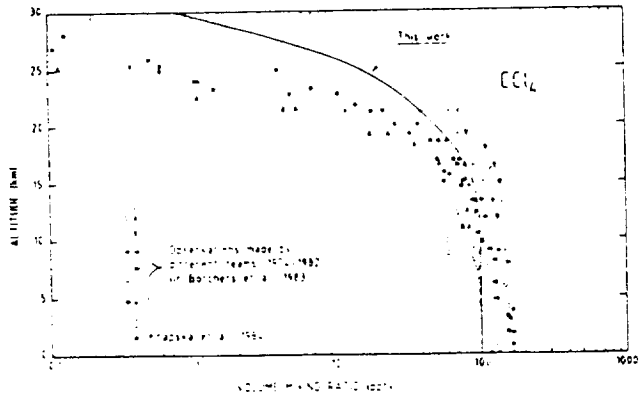

Fig. 5. Comparison between observed distributions of carbon tetrachloride [8, 9] a nd a 1-D theoretical profile.

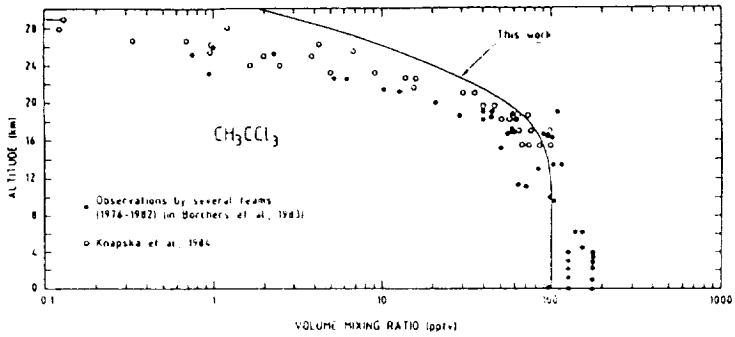

Fig. 6. Comparison between observed distributions of methyl chloroform [8, 9] and a 1-D theoretical profile.

and for CH_4. In the latter case however large differences in the observations exist above 30 km, making the comparison between model and observation difficult. The relatively good agreement, in the case of N_2O, is not surprising as the eddy diffusion coefficients which are used in the models (including the present model) are usually tuned to fit the vertical profile of this particular gas. For the precursor gases of active chlorine (e.g., the CFCs), the model tends to overestimate the mixing ratio, especially in the higher levels, except for CFC-12. Such discrepancy which appears in essentially all 1-D models has not yet been resolved. It can be due either to the use of an inadequate eddy diffusion coefficient or to an underestimated loss rate (or to both). Indeed, it has been shown from theoretical considerations [10] that the specified value of the 1-D eddy diffusion coefficient should be a function of the lifetime of the trace-constituent. Moreover, uncertainties remain in the calculation of the penetration of sunlight in the Schumann-Runge bands, leading to uncertain photodissociation rates of the chlorofluorocarbons.

The calculated lifetime of the source gases playing a major role in the stratosphere is given in Table 1.

TABLE 1 Calculated Lifetime of the Source Gases

Species	Lifetime (yrs)
N_2O	165.6
CH_4	10.0
CH_3Cl	1.5
CCl_4	68.8
CH_3CCl_3	6.6
$CFCl_3$(CFC-11)	86.6
CF_2Cl_2(CFC-12)	154.3
$CFCl_2CF_2Cl$(CFC-113)	129.8
CHF_2Cl(CFC-22)	16.2

Active Gases and Temporary Reservoirs

The concentration of active gases such as OH, HO_2, O, Cl, ClO, etc. is difficult to measure since their concentration is low and their chemical reactivity very high. A reliable comparison between theoretical model results and the few available data requires the knowledge of the solar zenith angle at the time of the measurement and the concentration in the observed air mass of the transport dependent long-live species which are the progenitor of the fast reacting compounds. From an examination of Figures 7 and 8, it can however be deduced that the most recent measurements of the OH radical [11, 12, 13, 14] have the same order of magnitude than values provided by theoretical models but that, in the case of HO_2, the values reported by Helten et al. [15] are in the lower stratosphere a factor 100 larger than predicted by

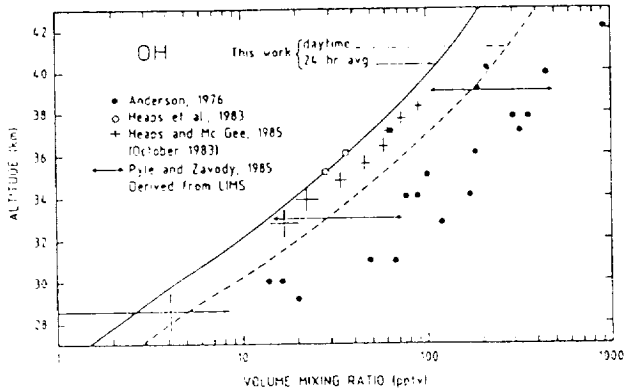

Fig. 7. Comparison between observed or indirectly deduced mixing ratio of OH [11, 12, 13, 14] and theoretical profiles (24 hour average and daytime average; mid-latitude; equinox).

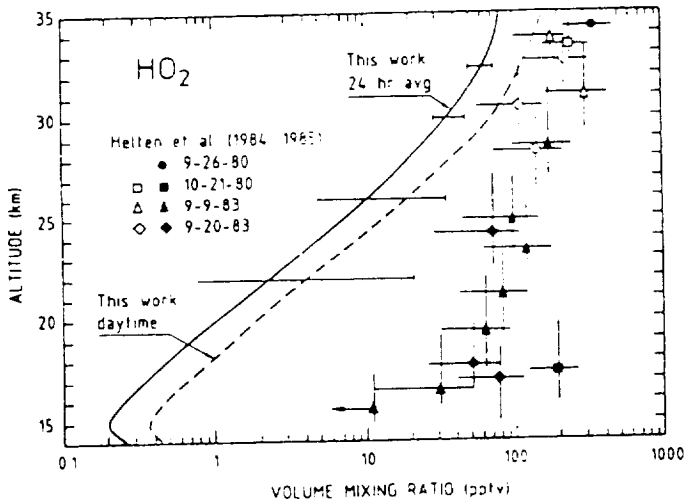

Fig. 8. Comparison between observed mixing ratio of HO_2 [15] and theoretical profiles (24 hour average and daytime average; mid-latitude; equinox).

theory. If additional measurements tend to confirm these data, the presently accepted chemical scheme is in error for the hydrogen species, at least, in the atmospheric layer where the ozone concentration is the largest.

Efforts to measure the vertical distribution of temporary reservoirs have been reported only recently. Figures 9 and 10 show that, especially for $ClONO_2$, the data deduced from infra-red measurements, for example from the ATMOS experiment, are consistent with a 24 hour-averaged model calculation.

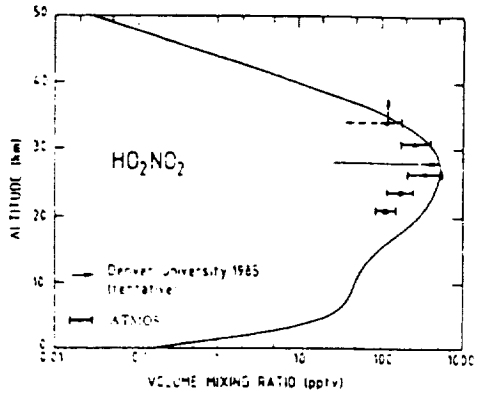

Fig. 9. Comparison between observations of HO_2NO_2 [16] and a 24-hour average theoretical profile (mid-latitude, equinox).

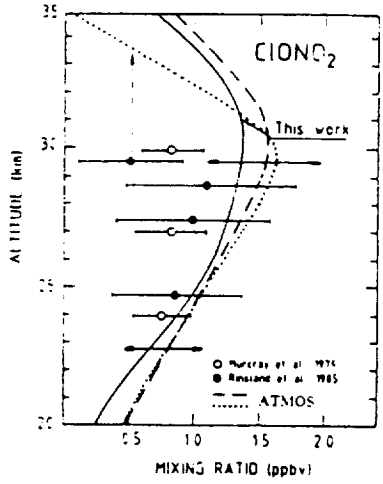

Fig. 10. Comparison between observations of $ClONO_2$ [17, 18, 19] and a 24-hour average theoretical profile (mid-latitude, equinox). The dotted line and the dashed line refer to ATMOS data at 30°N (sunset) at 47°S (sunrise) respectively.

Nitric Acid and Ozone

Finally, a comparison between theory and observations is performed for 2 gases (HNO_3 and O_3) which are produced in the stratosphere and whose lifetime varies significantly with altitude and latitude. In the case of HNO_3 (Figure 11), the agreement is fairly good between theory and observation below 30 km but above this height, most models seem to overestimate the HNO_3 mixing ratio. This discrepancy is emphasized by the fact that a new treatment of the HNO_3 LIMS data [20] indicates that the mixing ratio retrieved in the upper stratosphere should be reduced by as much as a factor 2-5.

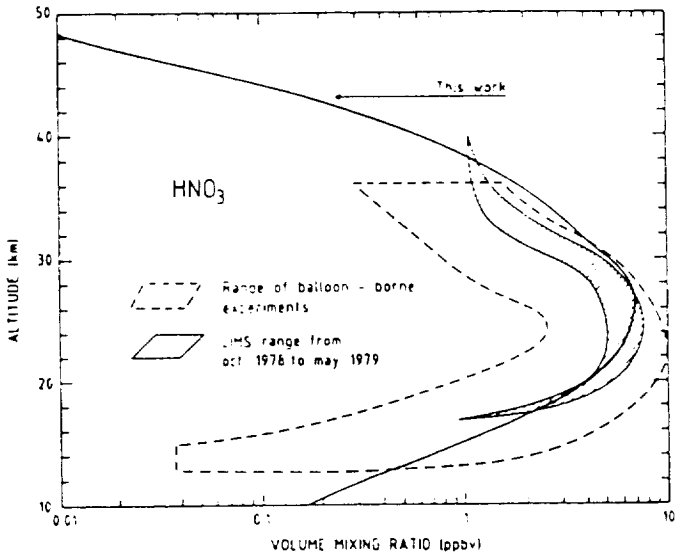

Fig. 11. Comparison between observations of nitric acid (balloon-borne experiments and LIMS data) and a theoretical profile (24 hour average, mid-latitude, equinox).

Ozone has been measured rather systematically and by different techniques over a number of years. The vertical profile provided by the US Standard Atmosphere [21] which is in close agreement with other data bases is compared in Figure 12 with a model calculation. The theoretical concentrations are obviously 20 to 40% lower than the observed values in the upper stratosphere. This ozone imbalance which was noted in several investigations [22, 23] is not yet explained. It could be due either to unknown additional production processes of ozone or to errors in some chemical or photochemical parameters. This problem is a major question as it reflects some unknown processes occurring in the atmospheric region where photochemical conditions apply and where the largest relative ozone depletions are predicted as a response to the emission of CFCs.

CONCLUSIONS

Models reproduce most of the observed distributions of the trace species belonging to the oxygen, hydrogen, nitrogen and chlorine families. Some discrepancies however remain, which reflect errors or uncertainties in the chemical scheme currently adopted in the models. More work is thus needed to identify the physical or chemical processes which could explain the cause of these discrepancies. A more detail comparison between observations and theory, which should account for the latitudinal and seasonal variation of the trace species concentration, should involve multi-dimensional models.

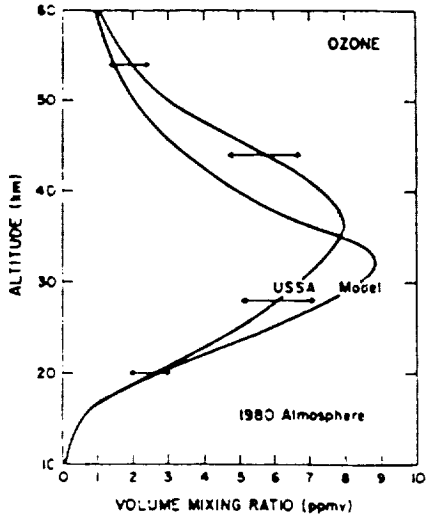

Fig. 12. Comparison between the U.S. Standard atmosphere model of ozone [21] and a theoretical vertical distribution.

REFERENCES

1. G. Brasseur, A. De Rudder and C. Tricot, *J. Atmos. Chem.*, **3**, 261 (1985).
2. J. J. Morcrette, Ph.D. Thesis, University of Lille, France (1984).
3. U. Schmidt, G. Kulessa, E. Klein, E. P. Röth, P. Fabian and R. Borchers, *Planet. Space Science*, to be published (1986).
4. R. L. Jones and J. A. Pyle, *J. Geophys. Res.*, **89**, 5263 (1984).
5. S. Lal, R. Borchers and P. Fabian, in *Atmospheric Ozone* (C. S. Zerefos and A. Ghazi, eds.), pp. 134-138 (1985).
6. M. Ackerman, C. Lippens, C. Muller, J. Vercheval, J. Besson, A. Girard, J. Laurent and M. P. Lemaitre, *Geophys. Res. Lett.*, **10**, 667 (1985).
7. M. Ackerman, D. Frimont, C. Muller and D. J. Wuebbles, *Pure Appl. Geophys.*, **117**, 367 (1978).
8. R. Borchers, P. Fabian and S. A. Penkelt, *Naturwiss*, **70**, 514 (1983).
9. D. Knapska, U. Schmidt, C. Jebsen, G. Kulessa and J. Rudolph in *Atmospheric Ozone* (C. S. Zerefos and A. Ghazi, eds.) pp. 117-121, D. Reidel Publishing Co., Dordrecht, The Netherlands (1985).
10. J. R. Holton, *J. Geophys. Res.*, **91**, 2681 (1986).
11. J. G. Anderson, *Geophys. Res. Lett.*, **3**, 165 (1976).
12. W. S. Heaps and T. J. McGee, *J. Geophys. Res.*, **88**, 5281 (1983).
13. W. S. Heaps and T. J. McGee, *J. Geophys. Res.*, **90**, 7913 (1985).

14. J. A. Pyle and A. M. Zavody, *Quart. J. Roy. Meteorol. Soc.*, 111 (1985).

15. M. Helten, W. Patz, D. H. Ehhalt and E. P. Röth, in *Atmospheric Ozone* (C. S. Zerefos and A. Ghazi, eds.) pp. 196-200, D. Reidel Publishing Co., Dordrecht, The Netherlands (1985).

16. C. P. Rinsland, R. Zander, C. B. Farmer, R. H. Norton, L. R. Brown, J. M. Russell III and J. H. Park, *Geophys. Res. Lett.*, 13, 761 (1986).

17. D. G. Murcray, A. Goldman, F. H. Murcray, F. J. Murcray and W. J. Williams, *Geophys. Res. Lett.*, 6, 857 (1979).

18. C. P. Rinsland, A. Goldman, D. G. Murcray, F. J. Murcray, F. S. Bonomo, R. D. Blatherwick, V. M. Devi, M.A.H. Smith and P. L. Rinsland, *J. Geophys. Res.*, 90, 7931 (1985).

19. R. Zander, C. P. Rinsland, C. B. Farmer, L. R. Brown and R. H. Norton, *Geophys. Res. Lett.*, 13, 757 (1986).

20. J. C. Gille and P. A. Bailey, private communication (1986).

21. U. S. Standard Atmosphere, NOAA - S/T76-1562, U.S. Printing Office, Washington, D.C. (1976).

22. P. J. Crutzen and U. Schmailzl, *Planet. Space Sci.*, 31, 1009 (1983).

23. L. Froidevaux, Ph.D. Thesis, California Institute of Technology (1983).

10

N91-27642

REFERENCE MODELS FOR THERMOSPHERIC NO

C. A. Barth

University of Colorado
Boulder, CO 80309

Nitric oxide has been measured with an ultraviolet spectrometer on the polar-orbiting satellite Solar Mesosphere Explorer (SME) for the period January 1982 to August 1986. The nitric oxide database contains densities at all latitudes sorted into 5°-bins and at altitudes between 100 and 140 km sorted into 3.3-km-bins. The largest densities occur at latitudes in the auroral zones where the density varies as a function of geomagnetic activity. Variations of a factor of 10 occur between times of intense activity and quiet times. At low latitudes, the nitric oxide density at 110 km varies from a mean value of 3×10^7 molecules/cm^3 in January 1982 to a mean value of 4×10^6 molecules/cm^3 during solar minimum conditions in 1986. In addition, the low-latitude nitric oxide density varies ±50% with a period of 27 days during times of high solar activity.

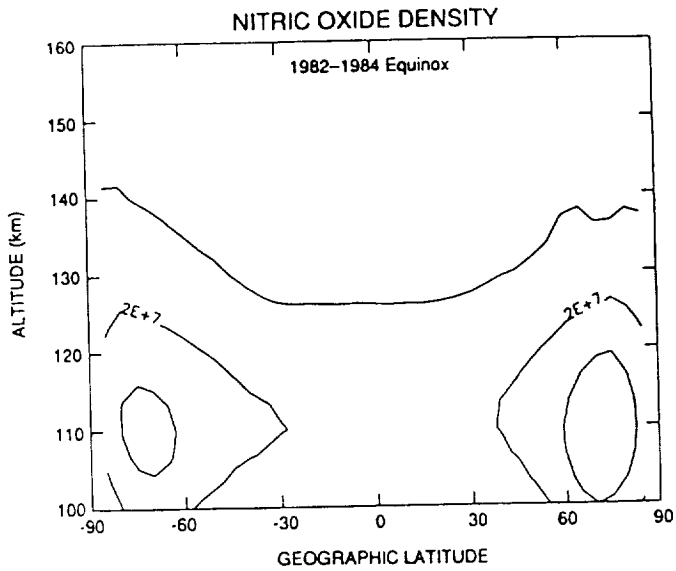

Figure 1. Nitric oxide density for the 1982-1984 equinox periods as a function of geographic latitude and altitude. Observations for the periods March 7 to April 2 and September 10 to October 6 for the years 1982, 1983, and 1984 are averaged together. The contour interval is 1×10^7 molecules cm^{-3} and the lowest contour level is 1×10^7 molecules cm^{-3}.

Table 1. NO Density (x 10^6 molecules/cm^3)

	Geographic Latitude																		
Alt	-90	-85	-80	-75	-70	-65	-60	-55	-50	-45	-40	-35	-30	-25	-20	-15	-10	5	0
160		1	2	2	3	3	3	1	1	1	1	1	1	1	1	1	1	1	1
157		3	2	4	4	3	3	3	4	3	1	1	1	1	1	1	1	1	2
153		3	4	5	5	5	3	5	5	5	4	4	4	3	1	1	1	3	3
150		5	7	7	7	7	6	6	6	4	5	5	5	5	4	5	4	3	3
147		10	9	8	8	8	8	8	7	7	5	4	4	4	4	4	4	4	4
143		10	10	9	9	8	8	8	7	6	6	5	5	4	4	4	4	4	4
140		10	10	10	9	9	9	8	7	7	6	5	5	4	4	4	4	4	4
137		11	12	11	11	10	9	9	8	7	6	6	5	5	5	5	5	5	5
133		12	14	13	12	11	11	10	9	8	7	7	6	6	6	6	6	6	6
130		14	16	15	15	14	13	12	11	10	9	8	8	7	7	7	7	7	7
127		17	19	19	18	16	15	14	13	12	11	10	10	9	10	9	9	10	9
123		19	22	22	21	20	19	17	16	15	14	13	12	12	12	12	12	12	12
120		22	26	26	25	24	22	20	19	18	17	16	15	15	15	15	15	15	15
117		23	29	29	29	27	25	23	22	20	19	18	18	18	18	17	17	17	17
113		24	30	32	31	30	28	25	24	22	21	20	20	19	19	19	19	19	18
110		24	30	33	33	31	29	26	24	22	21	21	20	20	20	20	19	19	19
107		22	29	31	32	31	28	25	23	21	20	20	19	19	19	19	18	18	18
103		18	25	28	29	28	25	23	21	19	18	17	17	16	16	16	16	16	16
100		14	20	24	25	24	21	19	17	15	14	14	13	13	13	13	13	12	12

	0	5	10	15	20	25	30	35	40	45	50	55	60	65	70	75	80	85	90
160	1	1	1	1	1	1	1	0	0	0	1	1	1	1	1	1	1	1	
157	1	1	2	2	1	1	1	1	1	1	1	1	1	1	1	1	1	1	
153	2	2	3	2	2	1	2	3	1	2	2	1	1	1	1	2	1	5	
150	3	3	3	3	3	3	4	4	3	3	3	2	3	5	4	6	7	7	
147	4	4	4	5	4	4	4	5	4	6	6	6	6	7	8	8	8	7	
143	4	4	5	4	4	5	5	5	6	7	6	6	8	8	8	8	8	8	
140	4	5	5	5	5	5	5	6	6	7	7	7	8	9	9	9	9	8	
137	5	5	5	5	5	6	6	7	7	7	8	9	10	11	13	12	12	13	12
133	6	6	6	6	6	7	7	8	8	8	9	10	11	13	14	15	16	15	14
130	7	7	8	8	8	8	8	9	10	10	11	12	13	14	15	16	15	14	
127	9	9	10	9	10	10	10	11	12	12	13	15	16	17	19	20	18	16	
123	12	12	12	12	12	12	13	13	14	15	16	18	20	21	23	24	22	19	
120	15	14	14	14	14	15	15	16	17	18	19	21	23	26	28	29	26	22	
117	17	17	17	17	16	17	17	18	19	20	22	24	27	30	33	33	30	25	
113	18	18	18	18	18	18	19	19	20	21	23	26	29	34	37	37	33	27	
110	19	19	18	18	18	18	19	19	20	22	24	27	31	35	39	38	34	27	
107	18	18	17	17	17	17	18	18	19	21	23	26	30	35	38	37	33	26	
103	16	15	15	15	15	15	15	16	17	18	21	24	28	33	35	34	29	23	
100	12	12	12	12	11	12	12	12	13	15	17	20	24	28	30	28	24	19	

Table 1. Nitric oxide density for the 1982-1984 equinox periods as a function of geographic latitude and altitude. Observations for the periods March 7 to April 2 and September 10 to October 6 for the years 1982, 1983, and 1984 are averaged together. The averaged densities are given in units of 10^6 molecules cm^{-3}.

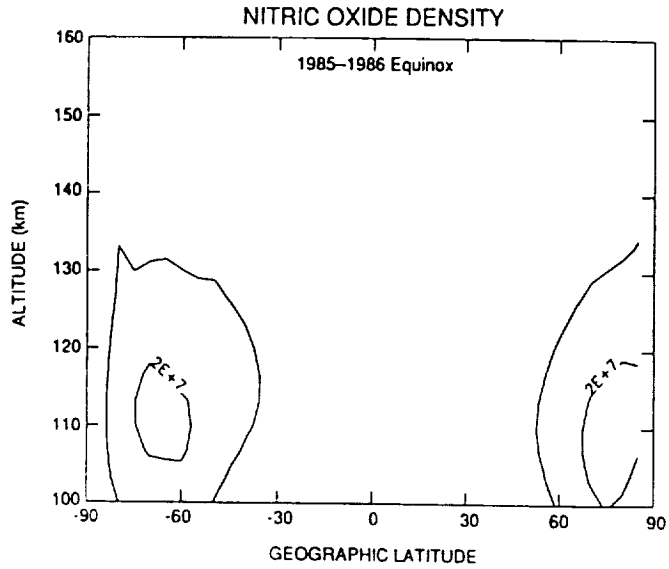

Figure 2. Nitric oxide density for the 1985-1986 equinox periods as a function of geographic latitude and altitude. Observations for the periods March 7 to April 2 of 1985 and 1986 and September 10 to October 6 for the year 1985 are averaged together. The contour interval is 1×10^7 molecules cm^{-3} and the lowest contour level is 1×10^7 molecules cm^{-3}.

Table 2. NO Density (x 10^6 molecules/cm^3)

Geographic Latitude

Alt	-90	-85	-80	-75	-70	-65	-60	-55	-50	-45	-40	-35	-30	-25	-20	-15	-10	-5	0
160		0	0	0	0	0	0	0	0	0	0	0	0	0	0	0	0	0	0
157		0	0	0	0	0	0	0	0	0	0	0	0	0	0	0	0	0	0
153		0	0	0	0	0	0	0	0	0	0	0	0	0	0	0	0	0	0
150		0	0	2	2	2	2	3	0	0	0	0	0	0	0	0	1	1	0
147		0	3	2	2	3	3	3	3	2	1	1	0	1	0	3	1	2	2
143		0	3	6	8	6	5	4	5	5	2	1	4	2	2	3	3	3	2
140		0	8	8	7	8	7	6	7	8	6	4	3	3	3	3	3	3	3
137		3	9	8	8	8	8	7	7	7	6	5	4	4	3	3	3	3	3
133		3	10	8	9	9	9	8	8	7	7	6	5	4	4	4	3	3	3
130		3	11	10	11	11	10	10	10	8	8	6	6	5	5	4	4	4	4
127		4	12	12	13	13	12	11	11	10	9	7	7	6	5	5	5	5	5
123		5	13	14	16	16	14	13	12	11	10	8	7	7	6	6	6	6	5
120		6	15	17	19	18	17	15	14	12	11	9	8	8	7	7	7	6	6
117		6	17	19	21	21	19	17	15	13	11	10	9	8	8	7	7	7	6
113		7	18	20	22	22	21	18	15	13	11	10	9	8	8	7	7	7	6
110		7	17	20	22	22	22	19	15	12	11	9	9	8	7	7	7	7	6
107		7	16	18	21	21	21	18	14	11	9	8	7	7	7	6	6	6	6
103		6	13	16	18	18	19	17	12	9	7	6	6	5	5	5	5	4	5
100		5	10	12	14	15	16	14	10	7	5	4	4	4	4	3	3	3	4
	0	5	10	15	20	25	30	35	40	45	50	55	60	65	70	75	80	85	90
160	0	0	0	0	0	0	0	0	0	0	0	0	0	0	0	0	0	0	
157	0	0	0	0	0	0	0	0	0	0	0	0	0	0	0	0	0	0	
153	0	0	0	0	0	0	0	1	0	0	0	0	0	0	0	0	0	0	
150	0	1	1	1	1	1	1	1	1	0	0	0	0	0	0	0	0	0	
147	2	1	1	1	2	1	2	1	2	2	1	0	1	0	0	1	0	0	
143	2	3	2	2	2	2	2	2	5	6	2	3	4	1	1	2	4	3	
140	3	3	3	3	2	3	2	3	4	5	6	6	7	6	5	4	5	5	
137	3	3	3	3	3	3	3	3	4	5	4	5	7	7	7	8	8	9	
133	3	3	3	3	3	3	3	3	4	5	5	5	7	7	8	9	9	10	
130	4	4	4	4	4	4	4	4	4	5	5	6	7	8	10	10	11	12	
127	5	5	4	4	4	4	4	5	5	5	6	6	8	10	11	12	13	14	
123	5	5	5	5	5	5	5	5	6	6	6	7	9	11	13	15	16	16	
120	6	6	6	6	6	6	6	6	6	7	7	9	11	13	16	18	19	19	
117	6	6	6	6	6	6	6	6	7	7	8	10	12	15	19	21	22	21	
113	6	6	6	6	6	6	7	7	7	8	9	11	14	17	21	24	24	22	
110	6	6	6	6	6	6	6	6	7	8	9	11	14	18	22	26	25	22	
107	5	5	5	5	5	5	6	6	7	7	8	11	14	18	22	26	24	20	
103	4	4	4	4	4	4	5	5	6	6	7	10	13	17	21	24	22	17	
100	3	3	3	3	3	3	3	3	4	5	6	8	11	15	18	21	18	14	

Table 2. Nitric oxide density for the 1985-1986 equinox periods as a function of geographic latitude and altitude. Observations for the periods March 7 to April 2 of 1985 and 1986 and September 10 to October 6 for the year 1985 are averaged together. The averaged densities are given in units of 10^6 molecules cm^{-3}.

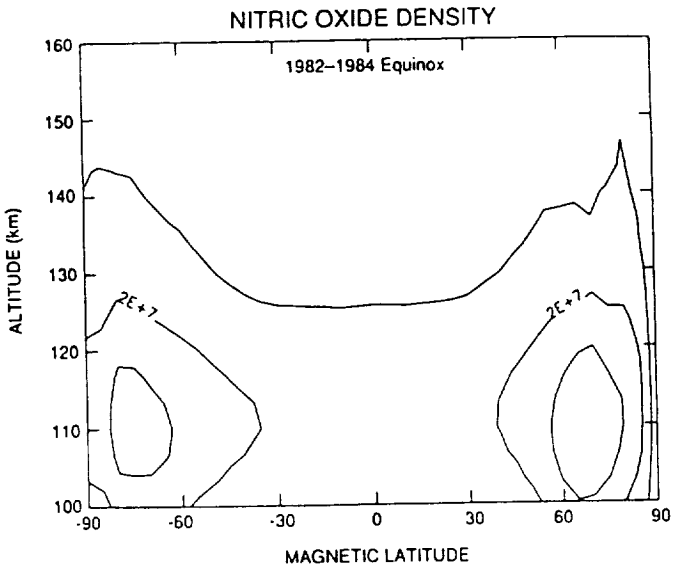

Figure 3. Nitric oxide density for the 1982-1984 equinox periods as a function of geomagnetic latitude and altitude. Observations for the periods March 7 to April 2 and September 10 to October 6 for the years 1982, 1983, and 1984 are averaged together. The contour interval is $1x10^7$ molecules cm^{-3} and the lowest contour level is $1x10^7$ molecules cm^{-3}.

Table 3. NO Density (x 10^6 molecules/cm^3)

Geomagnetic Latitude

Alt	-90	-85	-80	-75	-70	-65	-60	-55	-50	-45	-40	-35	-30	-25	-20	-15	-10	5	0
160	1	1	2	2	3	3	3	1	1	1	1	1	1	1	1	1	1	1	1
157	1	3	2	2	3	4	4	4	3	1	1	1	1	1	1	1	1	1	1
153	3	3	4	4	5	5	5	5	6	5	4	4	4	3	1	1	1	2	1
150	5	7	6	9	7	7	7	7	6	5	4	4	5	5	5	4	3	3	2
147	8	8	8	10	9	8	8	7	6	5	5	4	4	4	4	4	4	4	4
143	10	10	10	10	9	9	8	7	6	5	5	4	4	4	4	4	4	4	4
140	10	11	11	11	10	9	9	8	7	6	5	5	4	4	4	4	4	4	4
137	11	12	12	12	11	10	10	9	7	6	5	5	5	5	5	5	5	5	5
133	12	13	14	14	12	12	11	10	9	8	6	6	6	6	6	6	6	6	6
130	14	15	17	17	15	14	13	12	10	9	8	7	7	7	7	7	7	7	7
127	16	17	20	20	18	16	15	14	13	11	10	10	9	9	9	9	9	9	9
123	19	20	24	24	21	20	18	17	15	14	13	12	12	12	12	12	12	12	12
120	21	22	28	28	25	24	22	20	18	17	16	15	15	15	15	14	14	14	14
117	24	25	31	31	29	27	25	23	21	20	19	18	17	17	17	17	17	17	17
113	25	26	34	34	32	30	27	25	23	22	20	20	19	19	19	19	19	19	19
110	25	26	34	34	33	31	28	26	24	22	21	20	19	19	20	19	19	19	19
107	22	25	33	33	32	30	28	25	23	21	20	19	18	18	18	18	19	18	18
103	20	22	29	29	29	28	25	22	20	19	17	16	16	16	16	16	16	16	16
100	16	17	24	24	25	23	21	19	17	15	14	13	12	12	13	13	13	13	12

	0	5	10	15	20	25	30	35	40	45	50	55	60	65	70	75	80	85	90
160	1	1	1	1	1	0	1	1	0	1	1	1	1	1	1	1	1	1	0
157	1	1	2	1	2	2	2	1	1	1	1	1	1	1	1	.1	1	1	0
153	1	2	3	3	2	3	2	1	2	2	3	2	1	1	1	1	5	2	0
150	2	3	3	3	3	4	4	5	3	4	4	4	3	5	4	6	8	2	0
147	4	4	4	4	5	5	5	6	4	6	7	7	8	8	8	8	10	8	0
143	4	4	4	4	5	5	5	6	7	7	8	7	8	8	8	8	11	8	2
140	4	4	5	5	5	5	5	6	7	7	8	9	9	9	9	11	12	9	2
137	5	5	5	5	5	6	6	6	7	8	9	10	11	11	10	11	12	10	2
133	6	6	6	6	6	6	7	7	8	9	10	11	12	13	13	13	13	11	2
130	7	7	7	8	8	8	8	9	10	11	12	14	14	15	16	15	16	14	2
127	9	9	9	9	9	10	10	11	12	13	15	16	18	19	20	18	18	16	3
123	12	12	12	12	12	12	12	13	14	16	17	19	22	24	25	22	22	17	3
120	14	14	14	14	14	14	15	16	17	18	20	23	25	29	30	26	25	19	3
117	17	17	16	16	16	16	17	18	19	20	23	25	29	33	34	30	28	21	3
113	19	18	18	18	18	18	18	19	20	22	24	28	32	37	38	33	29	21	3
110	19	18	18	18	18	18	18	19	20	22	25	29	34	38	39	34	29	21	3
107	18	18	17	17	17	17	17	18	19	21	24	28	33	38	38	33	28	20	3
103	16	15	15	15	15	15	15	16	17	19	22	26	31	35	34	30	24	18	2
100	12	12	12	11	11	12	12	12	13	15	18	22	26	30	29	25	20	15	2

Table 3. Nitric oxide density for the 1982-1984 equinox periods as a function of geomagnetic latitude and altitude. Observations for the periods March 7 to April 2 and September 10 to October 6 for the years 1982, 1983, and 1984 are averaged together. The averaged densities are given in units of 10^6 molecules cm^{-3}.

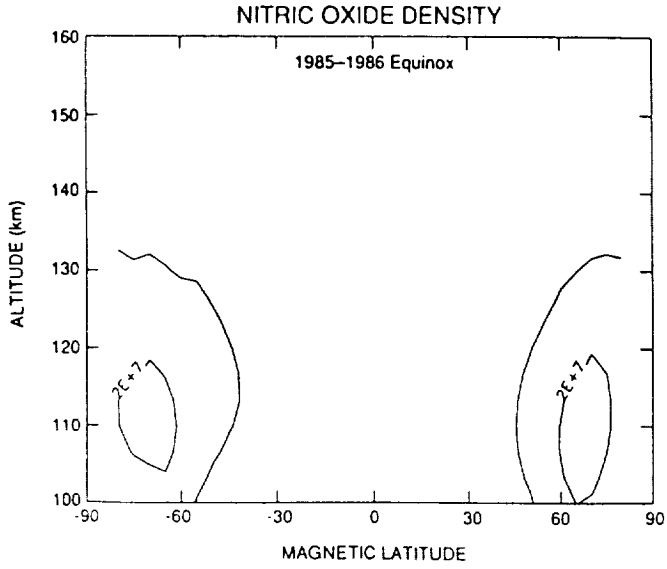

Figure 4. Nitric oxide density for the 1985-1986 equinox periods as a function of geomagnetic latitude and altitude. Observations for the periods March 7 to April 2 of 1985 and 1986 and September 10 to October 6, 1985, are averaged together. The contour interval is $1x10^7$ molecules cm^{-3} and the lowest contour level is $1x10^7$ molecules cm^{-3}.

Table 4. NO Density (x 10^6 molecules/cm^3)

Geomagnetic Latitude

Alt	-90	-85	-80	-75	-70	-65	-60	-55	-50	-45	-40	-35	-30	-25	-20	-15	-10	5	0
160			0	0	0	0	0	0	0	0	0	0	0	0	0	0	0	0	0
157			0	0	0	0	0	0	0	0	0	0	0	0	0	0	0	0	0
153			0	0	0	0	0	0	0	0	0	0	0	0	0	0	0	0	0
150			0	2	2	2	3	0	0	0	0	0	0	0	0	1	1	0	1
147			2	2	3	3	3	3	2	1	0	1	0	2	2	2	2	2	1
143			2	3	5	5	4	5	5	1	1	3	2	2	3	3	3	2	3
140			4	7	8	7	6	6	8	5	3	3	3	3	3	3	3	3	3
137			9	8	8	8	7	7	7	6	5	4	4	3	3	3	3	3	3
133			10	9	9	9	8	8	7	6	6	5	4	4	3	3	3	3	3
130			11	11	11	10	9	9	8	7	6	5	5	4	4	4	4	4	4
127			12	13	13	12	11	11	9	8	7	6	6	5	5	5	5	5	5
123			15	16	16	15	13	12	11	9	8	7	7	6	6	6	5	5	5
120			17	19	19	17	15	14	12	10	9	8	7	7	7	6	6	6	6
117			19	21	21	20	17	15	13	11	9	9	8	7	7	7	6	6	6
113			20	22	23	22	19	15	13	11	9	9	8	8	7	7	7	6	6
110			20	22	23	22	19	15	12	10	9	8	8	7	7	7	6	6	6
107			18	21	21	22	18	14	11	9	8	7	7	7	6	6	5	5	5
103			16	18	19	20	17	12	9	7	6	6	5	5	5	5	4	4	4
100			12	14	15	16	14	9	7	5	4	4	4	4	3	3	3	3	3

Alt	0	5	10	15	20	25	30	35	40	45	50	55	60	65	70	75	80	85	90
160	0	0	0	0	0	0	0	0	0	0	0	0	0	0	0	0	0		
157	0	0	0	0	0	0	0	0	0	0	0	0	0	0	0	0	0		
153	0	0	0	0	0	0	1	0	0	0	0	0	0	0	0	0	0		
150	1	1	1	1	1	1	1	1	2	0	0	0	0	0	0	0	2		
147	1	1	1	1	2	1	1	2	3	1	1	0	0	1	0	0	2		
143	3	2	3	2	3	2	3	5	6	2	4	3	3	4	4	2	2		
140	3	3	3	3	3	2	3	4	5	2	6	5	5	4	4	7	8		
137	3	3	3	3	3	3	3	4	4	4	6	6	6	8	6	8	8		
133	3	3	3	3	3	3	4	4	5	5	6	7	8	9	9	10	9		
130	4	4	4	4	4	4	4	5	5	5	6	7	9	10	11	11	11		
127	5	4	5	4	4	5	5	5	5	6	7	9	10	12	14	13	12		
123	5	5	5	5	5	5	5	6	6	7	8	10	12	15	17	16	13		
120	6	6	6	6	6	6	6	7	7	8	10	12	15	18	20	18	14		
117	6	6	6	6	6	6	7	7	8	9	11	14	17	21	22	20	16		
113	6	6	6	6	6	7	7	8	8	10	12	16	19	23	25	21	16		
110	6	6	6	6	6	6	7	8	8	10	13	16	20	25	25	21	16		
107	5	5	5	5	6	6	6	7	8	9	12	16	20	25	25	20	15		
103	4	4	4	4	4	5	5	6	7	8	11	15	19	23	22	17	13		
100	3	3	3	3	3	3	4	5	5	7	9	13	17	20	19	14	10		

Table 4. Nitric oxide density for the 1985-1986 equinox periods as a function of geomagnetic latitude and altitude. Observations for the periods March 7 to April 2 of 1985 and 1986 and September 10 to October 6, 1985, are averaged together. The averaged densities are given in units of 10^6 molecules cm^{-3}.

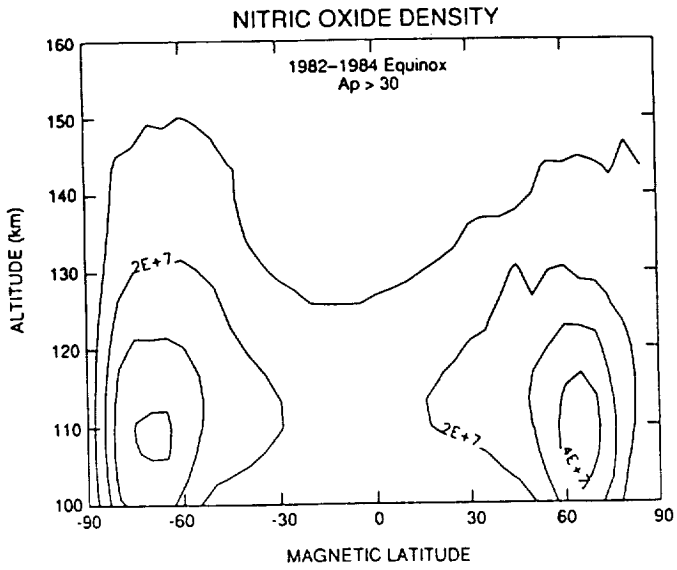

Figure 5. Nitric oxide density for the 1982-1984 equinox periods as a function of geomagnetic latitude and altitude for days when Ap>30. Observations for the periods March 7 to April 2 and September 10 to October 6 for the years 1982, 1983, and 1984 are averaged together. The contour interval is $1x10^7$ molecules cm^{-3} and the lowest contour level is $1x10^7$ molecules cm^{-3}.

Table 5. NO Density (x 10^6 molecules/cm^3)

Geomagnetic Latitude

Alt	-90	-85	-80	-75	-70	-65	-60	-55	-50	-45	-40	-35	-30	-25	-20	-15	-10	-5	0
160	0	0	1	1	2	2	2	0	0	0	0	0	0	0	0	1	1	1	0
157	0	2	1	1	3	3	3	4	3	1	1	1	1	1	1	1	1	1	1
153	0	2	3	3	3	5	4	5	5	4	4	3	3	3	1	1	1	1	1
150	0	3	5	7	9	8	10	9	7	6	5	5	4	4	4	3	3	1	1
147	0	4	9	10	12	13	13	12	11	7	5	5	5	6	5	5	5	2	3
143	2	6	11	13	14	14	14	13	12	11	8	6	5	5	5	6	6	4	4
140	2	7	12	14	15	15	16	15	13	11	8	7	5	5	5	5	5	4	4
137	2	7	13	16	16	17	17	16	15	12	9	8	5	6	5	5	5	5	5
133	2	8	15	18	18	18	19	18	17	14	10	9	8	7	6	6	6	6	6
130	2	9	17	20	20	21	21	20	19	15	12	11	9	8	7	7	7	7	8
127	2	11	20	24	23	24	24	23	21	17	15	13	11	11	9	9	9	9	10
123	2	13	23	28	27	28	27	25	23	20	17	15	14	13	12	12	12	12	13
120	2	15	27	32	32	32	30	28	25	22	20	18	16	16	14	14	14	15	15
117	2	17	31	36	36	36	33	30	27	24	22	20	19	18	17	17	17	17	17
113	3	18	34	39	39	39	36	31	27	24	23	21	20	19	18	18	18	19	19
110	3	19	36	40	41	41	36	31	26	24	23	21	20	19	19	19	19	19	19
107	3	18	36	40	41	41	35	29	24	23	22	20	19	17	18	18	18	18	18
103	3	17	33	37	38	38	31	25	21	20	19	17	16	15	16	16	16	16	15
100	2	14	29	32	33	33	26	20	17	16	15	13	13	11	12	13	12	12	12

Alt	0	5	10	15	20	25	30	35	40	45	50	55	60	65	70	75	80	85	90
160	0	1	1	0	0	0	0	0	0	0	1	1	1	1	1	1	1	1	
157	1	1	1	1	1	2	1	1	1	1	1	2	1	1	1	1	1	1	
153	1	1	1	2	2	2	1	1	1	1	2	2	2	1	2	1	1	2	
150	1	2	1	2	3	4	3	4	2	1	4	2	2	5	3	4	6	2	
147	3	3	3	4	4	4	4	5	4	6	7	8	5	9	8	9	10	8	
143	4	4	3	5	6	6	5	6	9	6	9	11	11	11	10	10	11	10	
140	4	4	5	5	6	7	7	7	8	7	10	12	13	12	11	11	12	11	
137	5	5	6	7	8	8	10	10	10	11	12	14	16	13	13	12	13	13	
133	6	6	7	8	9	10	11	13	16	17	16	18	17	16	15	15	14	14	
130	8	8	9	10	11	12	13	15	18	21	18	20	21	19	17	17	16	15	
127	10	11	11	12	13	14	16	17	20	24	20	24	25	22	24	19	17	16	
123	13	13	14	15	15	17	18	19	23	26	26	27	29	29	28	22	19	17	
120	15	16	16	17	18	19	21	21	25	26	28	30	34	34	33	25	21	17	
117	17	18	18	19	20	21	22	23	26	28	30	33	38	40	37	28	22	17	
113	19	19	19	20	21	22	23	23	26	28	31	35	42	44	40	31	23	17	
110	19	19	19	20	20	21	22	22	25	27	30	36	43	47	42	32	23	16	
107	18	18	18	18	19	20	20	20	23	24	28	35	43	47	41	32	21	15	
103	15	15	15	15	16	16	17	17	19	21	25	32	39	43	38	30	19	13	
100	12	12	11	12	12	13	13	13	15	16	20	27	34	37	32	27	15	10	

Table 5. Nitric oxide density for the 1982-1984 equinox periods as a function of geomagnetic latitude and altitude for days when Ap>30. Observations for the periods March 7 to April 2 and September 10 to October 6 for the years 1982, 1983, and 1984 are averaged together. The averaged densities are given in units of 10^6 molecules cm^{-3}.

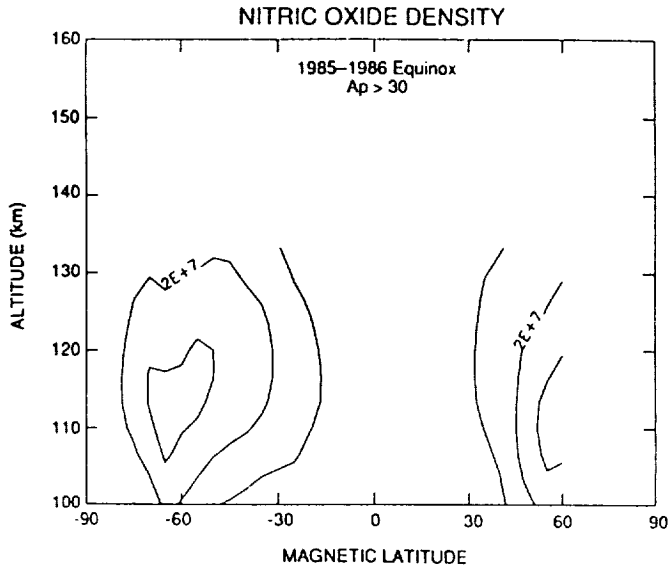

Figure 6. Nitric oxide density for the 1985-1986 equinox periods as a function of geomagnetic latitude and altitude for days when Ap>30. Observations for the periods March 7 to April 2 of 1985 and 1986 and September 10 to October 6, 1985, are averaged together. The contour interval is $1x10^7$ molecules cm^{-3} and the lowest contour level is $1x10^7$ molecules cm^{-3}.

Table 6. NO Density (x 10^6 molecules/cm^3)

Geomagnetic Latitude

Alt	-90	-85	-80	-75	-70	-65	-60	-55	-50	-45	-40	-35	-30	-25	-20	-15	-10	5	0
160			0	0	0	0	0	0	0	0	0	0	0	0	0	0	0	0	0
157			0	0	0	0	0	0	0	0	0	0	0	0	0	0	0	0	0
153			0	0	0	0	0	0	0	0	0	0	0	0	0	0	0	0	0
150			0	9	0	0	0	0	0	0	0	0	0	0	0	0	0	0	0
147			8	10	12	12	0	0	0	0	0	0	0	0	0	0	0	0	0
143			8	11	13	15	0	0	0	0	0	0	0	0	0	0	0	0	0
140			8	12	14	15	12	0	0	12	0	0	0	0	0	3	0	3	0
137			9	14	15	16	15	15	0	16	14	11	8	0	4	3	0	2	2
133			10	15	17	17	17	18	19	18	16	13	10	7	6	4	3	3	2
130			12	17	19	18	20	21	22	21	19	16	13	9	7	5	4	3	3
127			14	20	23	21	23	25	26	24	22	19	15	11	9	6	5	3	3
123			16	22	26	24	26	29	28	26	24	22	17	13	11	8	5	4	3
120			18	24	29	27	29	31	30	27	25	23	18	14	12	9	5	4	3
117			18	25	31	31	31	32	30	27	25	23	19	15	12	9	6	5	4
113			18	24	31	33	32	32	28	25	24	21	17	14	11	9	5	5	4
110			17	22	28	33	31	29	25	23	21	18	15	13	10	8	5	5	4
107			15	18	24	31	28	25	21	18	17	14	12	11	8	7	4	4	4
103			12	14	19	28	24	20	16	14	12	10	9	8	6	5	4	3	3
100			9	10	13	22	19	14	11	9	7	5	5	6	4	3	3	2	2

Alt	0	5	10	15	20	25	30	35	40	45	50	55	60	65	70	75	80	85	90
160	0	0	0	0	0	0	0	0	0	0	0	0	0						
157	0	0	0	0	0	0	0	0	0	0	0	0	0						
153	0	0	0	0	0	0	0	0	0	0	0	0	0						
150	0	0	0	0	0	0	0	0	0	0	0	0	0						
147	0	0	0	0	0	0	0	0	0	0	0	0	0						
143	0	0	0	0	2	0	0	0	0	0	0	0	0						
140	0	2	0	2	2	0	0	0	0	0	0	0	0						
137	2	2	2	2	2	3	4	7	0	0	0	0	0						
133	2	3	2	2	3	3	5	9	10	11	17	0	0						
130	3	3	2	3	3	4	6	10	11	13	16	16	19						
127	3	3	3	4	4	5	7	11	12	15	19	19	23						
123	3	4	3	4	5	6	8	12	13	16	22	22	26						
120	3	4	4	5	6	6	8	13	14	17	24	26	30						
117	4	4	4	5	6	6	9	13	14	19	27	30	32						
113	4	4	4	5	6	6	8	12	14	20	28	32	34						
110	4	4	4	5	6	5	8	10	13	20	28	33	33						
107	4	3	4	4	5	4	6	8	12	19	26	32	31						
103	3	2	3	3	4	3	5	6	10	17	23	29	27						
100	2	2	2	2	3	2	4	4	7	14	19	24	22						

Table 6. Nitric oxide density for the 1985-1986 equinox periods as a function of geomagnetic latitude and altitude for days when Ap>30. Observations for the periods March 7 to April 2 of 1985 and 1986 and September 10 to October 6, 1985, are averaged together. The averaged densities are given in units of 10^6 molecules cm^{-3}.

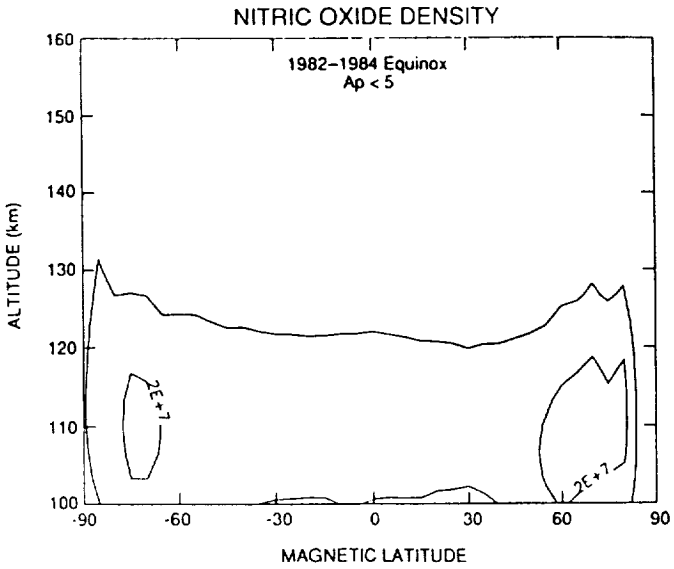

Figure 7. Nitric oxide density for the 1982-1984 equinox periods as a function of geomagnetic latitude and altitude for days when Ap<5. Observations for the periods March 7 to April 2 and September 10 to October 6 for the years 1982, 1983, and 1984 are averaged together. The contour interval is $1x10^7$ molecules cm^{-3} and the lowest contour level is $1x10^7$ molecules cm^{-3}.

Table 7. NO Density (x 10^6 molecules/cm^3)

Geomagnetic Latitude

Alt	-90	-85	-80	-75	-70	-65	-60	-55	-50	-45	-40	-35	-30	-25	-20	-15	-10	5	0
160	0	1	1	1	1	1	1	1	1	1	1	1	1	1	1	1	1	1	1
157	1	1	1	1	1	1	1	1	1	1	1	1	1	1	1	1	1	1	1
153	1	1	1	1	1	1	1	1	1	1	1	1	1	1	1	1	1	1	1
150	1	4	2	2	2	3	3	2	2	1	1	2	2	1	1	2	1	1	1
147	3	4	5	4	3	3	3	3	3	2	2	2	2	2	2	2	2	2	2
143	3	5	5	5	4	4	4	4	4	3	3	3	3	3	3	3	3	3	2
140	3	7	6	5	5	5	4	4	3	3	3	4	3	3	3	3	3	3	3
137	3	8	6	5	5	5	5	4	4	4	4	4	3	4	3	3	4	4	4
133	4	9	7	6	6	5	5	5	5	4	4	4	4	4	4	4	4	4	4
130	5	11	8	8	8	6	7	6	6	5	6	5	5	5	5	5	5	5	5
127	5	12	10	10	10	8	8	8	8	7	7	7	7	7	7	7	7	7	7
123	6	14	12	14	13	11	11	11	10	9	9	9	9	9	9	9	9	9	9
120	7	16	14	17	16	13	13	13	12	12	12	11	11	11	11	11	11	11	11
117	8	17	16	20	19	16	16	15	15	14	14	13	13	13	13	13	13	13	13
113	9	18	17	22	22	18	18	17	16	16	15	15	15	14	14	14	15	15	15
110	9	17	17	23	23	19	19	18	17	16	16	15	15	15	15	15	15	15	15
107	8	15	16	22	22	19	19	17	16	16	15	14	14	14	14	14	15	15	14
103	7	13	14	20	20	17	17	15	15	14	13	13	12	12	12	12	13	13	12
100	5	10	11	16	17	14	14	12	12	11	10	10	9	9	9	9	10	10	9

Alt	0	5	10	15	20	25	30	35	40	45	50	55	60	65	70	75	80	85	90
160	1	1	1	1	1	1	0	1	0	1	1	1	1	1	1	1	0	0	
157	1	1	1	1	1	1	1	1	1	1	1	1	1	1	1	1	0	0	
153	1	1	1	1	1	1	1	1	1	1	1	1	1	1	1	1	1	0	
150	1	1	2	2	2	1	1	1	1	1	2	2	1	2	3	1	1	0	
147	2	3	3	3	2	2	2	2	2	2	3	3	3	2	3	2	3	1	
143	2	3	3	3	3	3	3	3	2	2	4	3	3	3	3	3	3	0	
140	3	3	3	3	3	3	3	3	3	3	3	3	4	3	4	4	3	0	
137	4	4	3	3	3	4	3	3	4	3	4	4	4	5	4	5	5	1	
133	4	4	4	4	4	4	4	4	4	4	5	4	4	5	7	6	6	1	
130	5	5	5	5	5	5	5	5	5	5	5	5	6	7	9	7	8	1	
127	7	7	7	7	6	7	6	7	7	6	7	7	9	9	11	9	11	2	
123	9	9	9	8	8	8	8	8	8	9	9	9	12	13	14	13	15	3	
120	11	11	11	11	10	10	10	10	10	11	11	12	15	17	19	16	19	4	
117	13	13	13	12	12	12	12	12	12	13	14	16	18	20	22	19	21	5	
113	15	14	14	14	13	13	13	13	14	14	16	19	22	23	24	21	23	6	
110	15	15	14	14	14	13	13	14	14	15	18	21	24	24	25	23	23	6	
107	14	14	14	14	13	13	12	13	14	15	18	22	25	24	24	22	21	6	
103	12	12	12	12	11	11	11	11	12	14	17	21	24	22	21	21	18	5	
100	9	9	9	9	9	9	8	9	10	12	15	18	21	19	17	17	14	5	

Table 7. Nitric oxide density for the 1982-1984 equinox periods as a function of geomagnetic latitude and altitude for days when Ap<5. Observations for the periods March 7 to April 2 and September 10 to October 6 for the years 1982, 1983, and 1984 are averaged together. The averaged densities are given in units of 10^6 molecules cm^{-3}.

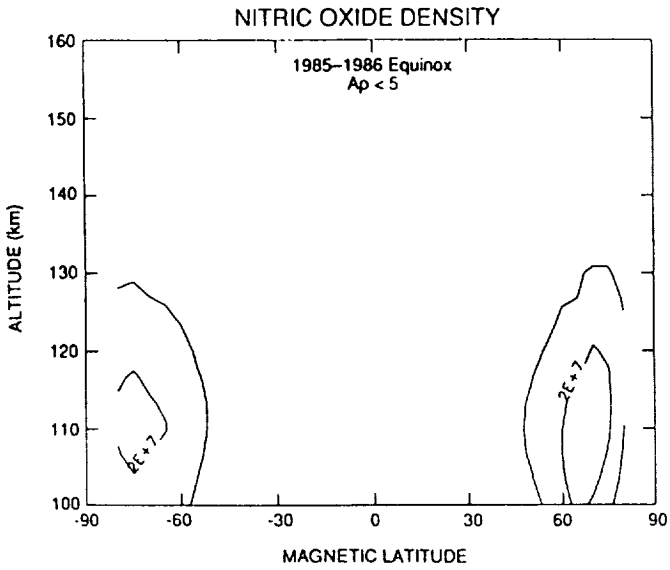

Figure 8. Nitric oxide density for the 1985-1986 equinox periods as a function of geomagnetic latitude and altitude for days when Ap<5. Observations for the periods March 7 to April 2 of 1985 and 1986 and September 10 to October 6, 1985, are averaged together. The contour interval is 1×10^7 molecules cm^{-3} and the lowest contour level is 1×10^7 molecules cm^{-3}.

Table 8. NO Density (x 10^6 molecules/cm^3)

Geomagnetic Latitude

Alt	-90	-85	-80	-75	-70	-65	-60	-55	-50	-45	-40	-35	-30	-25	-20	-15	-10	5	0
160			0	0	0	0	0	0	0	0	0	0	0	0	0	0	0	0	0
157			0	0	0	0	0	0	0	0	0	0	0	0	0	0	0	0	0
153			0	0	0	0	0	0	0	0	0	0	0	0	0	0	0	0	0
150			0	2	2	1	0	0	0	0	0	0	0	0	0	1	1	0	0
147			2	2	2	1	1	0	0	1	0	1	0	2	1	1	2	1	1
143			1	2	3	2	2	0	1	1	1	1	2	2	3	2	3	2	2
140			3	4	4	4	4	2	1	1	2	1	3	3	3	3	3	2	3
137			4	6	6	6	5	5	6	2	3	3	3	3	3	3	3	3	3
133			8	7	7	7	6	6	5	4	5	3	3	3	3	3	3	3	3
130			9	9	8	8	7	6	6	4	5	4	4	4	4	4	4	4	4
127			11	12	10	10	8	7	6	5	5	5	5	5	5	5	5	4	5
123			14	15	13	12	10	8	7	6	6	6	5	5	5	6	5	5	5
120			17	18	16	14	12	9	8	7	7	6	6	6	6	6	6	6	6
117			19	21	19	17	14	10	9	8	7	7	7	6	7	7	6	6	6
113			21	23	21	19	15	11	9	9	7	7	7	7	7	7	6	6	7
110			21	23	21	20	16	11	9	8	7	7	7	6	7	6	6	6	6
107			20	22	21	20	15	11	8	8	6	6	6	6	6	6	5	5	6
103			17	19	19	19	14	10	7	6	5	5	5	5	5	5	4	4	4
100			13	15	15	16	12	8	5	5	4	4	3	3	3	3	3	3	3

Alt	0	5	10	15	20	25	30	35	40	45	50	55	60	65	70	75	80	85	90
160	0	0	0	0	0	0	0	0	0	0	0	0	0	0	0	0	0		
157	0	0	0	0	0	0	0	0	0	0	0	0	0	0	0	0	0		
153	0	0	0	0	0	0	1	0	0	0	0	0	0	0	0	0	0		
150	0	0	1	0	1	1	1	0	0	0	0	0	0	0	0	0	2		
147	1	1	1	0	1	1	1	0	1	0	0	0	0	1	0	0	2		
143	2	2	2	2	2	1	1	2	2	2	1	1	2	1	2	2	2		
140	3	3	3	2	3	2	2	3	3	2	3	2	3	4	4	4	2		
137	3	3	3	3	3	2	3	3	3	4	2	3	3	4	4	4	3		
133	3	3	3	3	3	3	3	3	4	3	5	3	8	8	5	8	7		
130	4	4	4	4	3	4	4	4	4	4	5	6	10	9	12	11	9		
127	5	5	4	4	4	4	4	4	4	5	6	8	10	10	14	13	10		
123	5	5	5	5	5	5	5	5	5	6	7	9	11	13	17	16	10		
120	6	6	6	5	5	6	6	6	6	7	8	10	14	17	21	19	11		
117	6	6	6	6	6	6	6	7	7	8	10	12	16	20	24	21	11		
113	7	6	6	6	6	6	7	7	8	9	11	13	19	24	26	22	11		
110	6	6	6	6	6	6	7	8	8	9	11	14	20	26	26	21	10		
107	6	5	5	5	6	6	6	7	7	9	11	14	20	27	25	19	8		
103	4	4	4	4	5	5	5	6	6	7	10	13	19	26	22	16	7		
100	3	3	3	3	4	4	4	5	5	6	8	11	16	23	18	12	5		

Table 8. Nitric oxide density for the 1985-1986 equinox periods as a function of geomagnetic latitude and altitude for days when Ap<5. Observations for the periods March 7 to April 2 of 1985 and 1986 and September 10 to October 6, 1985, are averaged together. The averaged densities are given in units of 10^6 molecules cm^{-3}.

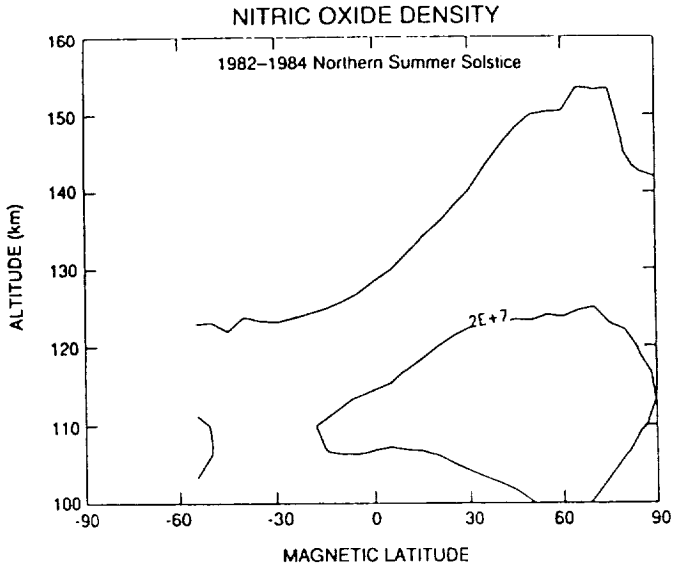

Figure 9. Nitric oxide density for the 1982-1984 northern summer solstice as a function of geomagnetic latitude and altitude. Observations for the periods June 8 to July 4 for the years 1982, 1983, and 1984 are averaged together. The contour interval is $1x10^7$ molecules cm^{-3} and the lowest contour level is $1x10^7$ molecules cm^{-3}.

Table 9. NO Density (x 10^6 molecules/cm^3)

Geomagnetic Latitude

Alt	-90	-85	-80	-75	-70	-65	-60	-55	-50	-45	-40	-35	-30	-25	-20	-15	-10	-5	0
160							0	0	0	1	1	1	1	1	1	1	1	1	1
157							0	0	3	1	1	1	1	1	1	1	1	1	1
153							0	2	2	1	1	1	1	1	1	1	1	2	2
150							1	2	2	1	1	1	1	1	1	1	2	3	4
147							1	1	2	1	1	1	2	3	3	4	4	5	5
143							1	1	2	1	2	3	3	3	4	4	5	5	5
140							1	1	3	3	3	3	3	4	4	4	5	6	6
137							2	2	3	3	3	3	3	4	4	5	5	6	6
133							3	3	4	4	4	4	4	5	5	5	6	7	7
130							1	5	5	5	6	5	5	6	6	7	7	8	9
127							2	7	7	7	8	7	7	8	8	9	9	10	11
123							3	10	10	9	10	10	10	10	11	11	12	13	14
120							5	13	13	12	13	13	13	13	14	14	15	16	16
117							7	16	16	14	16	16	16	16	16	17	18	18	19
113							8	19	18	16	18	18	18	18	19	19	20	20	21
110							10	21	20	17	19	19	19	20	20	20	21	22	21
107							10	21	20	17	19	19	19	19	19	20	20	20	20
103							10	20	19	15	17	18	17	18	18	18	18	18	17
100							10	18	16	13	14	15	14	15	15	15	15	14	14

	0	5	10	15	20	25	30	35	40	45	50	55	60	65	70	75	80	85	90
160	1	1	1	2	2	2	2	2	2	2	2	2	2	3	3	3	3	3	3
157	1	2	2	2	2	2	2	2	2	2	3	3	3	3	3	6	3	3	3
153	2	2	2	2	2	4	2	2	3	3	7	7	7	10	10	10	3	6	5
150	4	5	6	6	6	7	7	9	9	9	10	10	11	11	11	11	9	9	8
147	5	6	6	7	7	8	8	9	10	11	11	12	12	12	12	11	10	9	9
143	5	6	7	7	8	8	9	10	11	12	12	13	13	13	13	11	10	10	10
140	6	6	7	8	9	9	10	11	12	13	13	14	14	14	13	12	11	10	10
137	6	7	8	9	10	11	11	12	13	14	14	14	15	15	14	12	11	11	11
133	7	8	9	10	11	12	13	14	14	15	15	15	15	16	15	13	13	12	12
130	9	10	11	12	13	14	15	15	16	16	16	17	17	17	17	15	14	14	13
127	11	12	13	14	15	16	17	17	18	18	18	18	18	19	19	17	17	16	15
123	14	15	16	17	18	19	19	20	20	20	20	20	20	21	21	20	19	18	17
120	16	17	18	19	20	21	22	22	22	22	22	23	23	24	24	22	21	20	18
117	19	19	20	21	22	23	24	24	24	24	24	25	25	26	27	25	23	21	20
113	21	21	21	22	23	24	25	25	25	25	26	27	28	29	28	26	24	21	20
110	21	21	21	22	22	23	24	24	25	26	27	27	29	30	29	25	23	20	19
107	20	20	20	20	20	21	22	23	24	24	26	27	28	29	27	23	21	18	18
103	17	17	17	17	17	18	19	20	21	22	23	25	26	26	24	20	17	15	15
100	14	14	13	13	13	14	15	16	17	18	20	21	22	22	19	15	13	12	11

Table 9. Nitric oxide density for the 1982-1984 northern summer solstice as a function of geomagnetic latitude and altitude. Observations for the periods June 8 to July 4 for the years 1982, 1983, and 1984 are averaged together. The averaged densities are given in units of 10^6 molecules cm^{-3}.

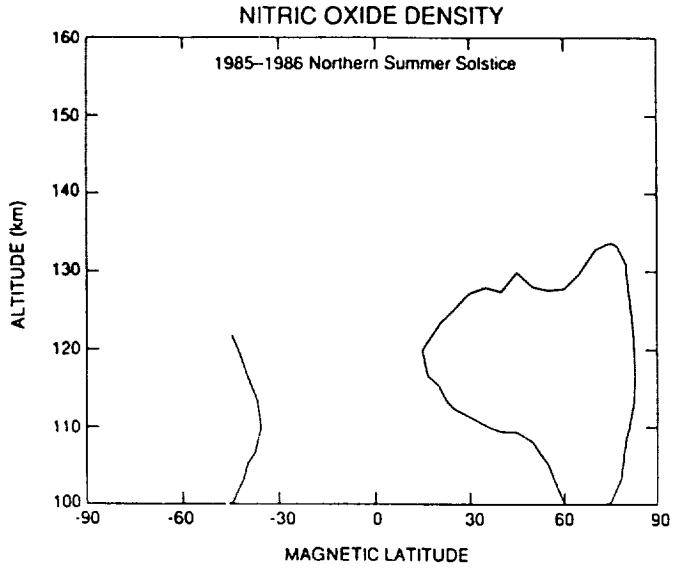

Figure 10. Nitric oxide density for the 1985-1986 northern summer solstice as a function of geomagnetic latitude and altitude. Observations for the periods June 8 to July 4 for the years 1985 and 1986 are averaged together. The contour interval is $1x10^7$ molecules cm^{-3} and the lowest contour level is $1x10^7$ molecules cm^{-3}.

Table 10. NO Density (x 10^6 molecules/cm^3)

Geomagnetic Latitude

Alt	-90	-85	-80	-75	-70	-65	-60	-55	-50	-45	-40	-35	-30	-25	-20	-15	-10	5	0
160									0	0	0	0	0	0	0	0	0	0	0
157									0	0	0	0	0	0	0	0	0	0	0
153									0	0	0	0	0	2	1	2	2	0	1
150									0	0	0	0	0	2	2	2	2	3	3
147									0	0	1	1	1	2	2	2	3	3	3
143									0	2	1	1	2	2	2	2	3	3	3
140									3	2	2	1	2	2	2	2	3	3	4
137									4	3	3	2	2	3	3	3	3	4	4
133									6	4	3	2	3	3	3	3	4	4	5
130									5	4	4	4	3	3	4	4	4	5	5
127									5	7	5	5	4	4	4	4	5	5	6
123									5	9	7	6	5	5	5	5	6	6	7
120									7	11	8	7	6	6	6	6	6	7	8
117									8	13	10	9	8	7	7	7	7	8	9
113									8	15	11	9	8	7	7	7	7	8	9
110									9	15	11	10	9	8	7	7	7	8	8
107									8	15	11	9	8	7	7	7	7	7	7
103									8	13	9	8	7	6	6	6	6	6	6
100									7	10	7	6	6	5	5	4	5	4	4

Alt	0	5	10	15	20	25	30	35	40	45	50	55	60	65	70	75	80	85	90
160	0	0	0	0	0	0	0	0	0	0	0	0	0	0	3	0	0	0	0
157	0	0	0	0	0	0	0	0	0	0	0	3	4	3	3	0	4	0	0
153	1	2	0	0	0	0	0	0	0	0	0	3	4	4	5	6	4	0	0
150	3	3	5	5	6	0	2	0	2	2	3	4	7	7	6	6	4	0	0
147	3	4	5	6	7	7	6	7	7	7	7	7	7	7	6	7	4	4	3
143	3	4	5	6	7	7	7	7	7	7	8	8	8	7	7	7	4	4	3
140	4	4	5	6	7	8	8	8	8	8	8	7	8	8	8	7	4	4	3
137	4	5	6	7	7	7	7	8	8	9	9	8	8	8	9	8	9	4	4
133	5	5	6	7	8	8	9	9	9	9	9	9	9	9	10	10	10	4	4
130	5	6	7	8	9	9	9	9	9	10	10	9	10	10	11	11	10	5	5
127	6	7	8	9	9	10	10	10	10	11	10	10	10	11	13	12	11	5	6
123	7	8	9	10	10	10	11	11	11	11	11	11	11	12	14	13	13	6	6
120	8	9	9	10	10	11	11	11	11	12	12	12	12	14	16	14	13	7	7
117	9	9	9	10	10	11	11	11	12	12	12	12	13	15	16	15	13	8	8
113	9	9	9	9	10	10	11	11	11	11	12	12	13	16	17	16	12	8	8
110	8	8	8	8	9	9	10	10	10	10	11	12	14	16	16	16	11	8	7
107	7	7	7	7	7	8	8	8	9	9	9	11	13	16	15	15	9	7	6
103	6	6	5	5	5	6	6	7	7	7	8	9	12	15	14	14	8	5	5
100	4	4	4	3	4	4	4	5	5	5	5	7	10	13	11	10	6	3	3

Table 10. Nitric oxide density for the 1985-1986 northern summer solstice as a function of geomagnetic latitude and altitude. Observations for the periods June 8 to July 4 for the years 1985 and 1986 are averaged together. The averaged densities are given in units of 10^6 molecules cm^{-3}.

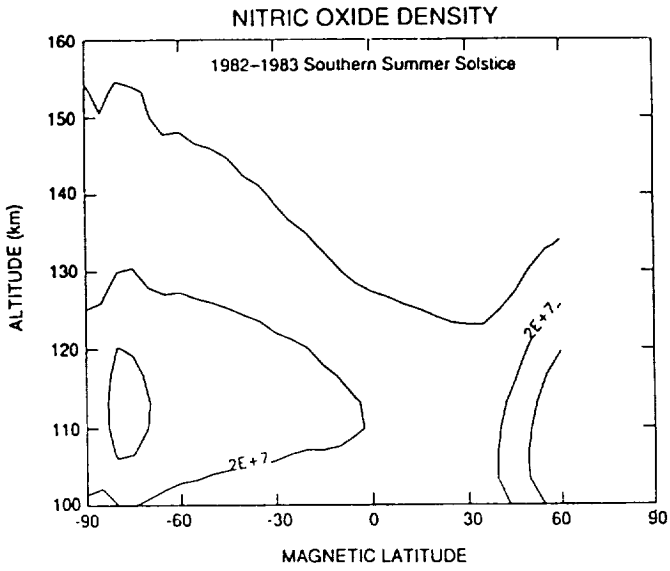

Figure 11. Nitric oxide density for the 1982-1983 southern summer solstice as a function of geomagnetic latitude and altitude. Observations for the period December 9 to January 4 for 1982 and 1983 are averaged together. The contour interval is $1x10^7$ molecules cm^{-3} and the lowest contour level is $1x10^7$ molecules cm^{-3}.

Table 11. NO Density (x 10^6 molecules/cm^3)

Geomagnetic Latitude

Alt	-90	-85	-80	-75	-70	-65	-60	-55	-50	-45	-40	-35	-30	-25	-20	-15	-10	-5	0
160	0	0	0	0	0	0	0	0	0	0	0	0	0	0	0	0	0	1	0
157	5	5	5	6	4	3	2	0	0	0	0	2	0	0	2	0	2	1	1
153	13	5	13	11	10	6	6	3	2	2	2	3	0	3	2	2	2	2	1
150	11	11	12	12	10	9	9	9	8	8	7	7	6	3	3	2	2	2	2
147	12	12	12	13	11	11	11	10	10	9	9	9	8	7	8	7	6	5	4
143	13	12	13	14	12	12	12	12	11	11	10	9	9	8	8	8	6	5	5
140	13	13	14	15	13	13	13	13	12	12	11	10	10	9	8	8	7	6	5
137	14	14	15	16	15	14	15	14	14	13	12	12	11	10	9	8	7	6	6
133	16	16	17	18	16	16	16	16	15	15	14	13	12	11	11	10	9	7	7
130	17	17	20	20	18	18	18	18	17	17	16	15	14	14	13	11	10	9	8
127	19	19	23	23	21	20	20	20	20	19	18	18	16	16	15	14	12	11	10
123	21	22	27	26	24	23	23	22	22	21	21	20	19	19	18	16	15	14	13
120	23	24	30	29	27	25	25	24	24	24	23	22	21	21	20	19	18	16	16
117	25	26	33	32	29	27	27	26	25	25	24	24	23	23	22	21	20	19	18
113	27	27	34	33	30	28	27	26	26	26	25	24	24	23	22	22	21	20	19
110	27	27	34	33	30	28	27	26	25	25	24	23	23	22	22	21	21	20	20
107	25	25	31	30	28	26	24	24	23	22	22	21	21	20	20	20	20	19	18
103	22	22	26	26	24	22	21	20	19	19	18	17	17	16	16	17	17	16	16
100	18	17	20	20	19	17	16	16	15	14	14	13	13	12	12	13	13	13	12

Alt	0	5	10	15	20	25	30	35	40	45	50	55	60	65	70	75	80	85	90
160	0	0	0	0	0	0	0	0	0	0	0	0	0						
157	1	1	2	0	2	0	0	0	0	0	0	0	0						
153	1	1	2	2	2	0	0	0	0	0	0	0	0						
150	2	1	2	2	2	2	1	1	1	2	4	2	4						
147	4	4	4	4	4	4	3	3	3	3	4	4	8						
143	5	4	4	4	4	4	3	3	3	4	4	5	7						
140	5	5	4	4	4	4	4	3	4	4	5	6	9						
137	6	5	5	5	4	4	4	4	4	5	6	7	8						
133	7	6	6	5	5	5	5	5	5	6	8	9	10						
130	8	8	7	7	6	6	6	6	7	8	10	13	13						
127	10	10	9	9	8	8	8	8	9	10	14	17	18						
123	13	13	12	11	11	10	10	10	11	13	17	22	24						
120	16	15	14	14	13	12	12	12	14	16	21	26	30						
117	18	17	17	16	15	15	14	14	16	19	24	30	34						
113	19	19	18	18	17	16	16	16	18	22	28	34	38						
110	20	19	18	18	17	16	16	17	20	25	30	36	39						
107	18	18	17	16	16	16	15	17	21	26	31	36	38						
103	16	15	15	14	14	13	14	16	21	26	30	35	36						
100	12	11	11	11	11	10	11	13	16	22	25	31	31						

Table 11. Nitric oxide density for the 1982-1983 southern summer solstice as a function of geomagnetic latitude and altitude. Observations for the period December 9 to January 4 for 1982 and 1983 are averaged together. The averaged densities are given in units of 10^6 molecules cm^{-3}.

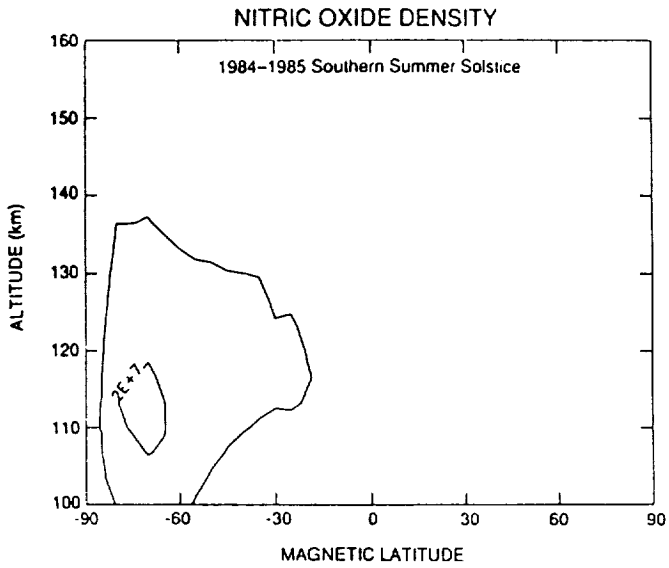

Figure 12. Nitric oxide density for the 1984-1985 northern summer solstice as a function of geomagnetic latitude and altitude. Observations for the periods December 9 to January 4 for the years 1984 and 1985 are averaged together. The contour interval is $1x10^7$ molecules cm^{-3} and the lowest contour level is $1x10^7$ molecules cm^{-3}.

Table 12. NO Density (x 10^6 molecules/cm^3)

Geomagnetic Latitude

Alt	-90	-85	-80	-75	-70	-65	-60	-55	-50	-45	-40	-35	-30	-25	-20	-15	-10	5	0
160	0	0	0	0	0	0	0	0	0	0	0	0	0	0	0	0	0	0	0
157	0	0	0	0	0	0	0	0	0	0	0	0	0	0	0	0	0	0	0
153	0	0	0	4	3	3	0	0	0	2	0	0	2	0	1	0	0	0	0
150	0	0	0	8	7	7	8	4	5	4	4	2	1	2	2	1	1	1	0
147	0	0	6	9	9	8	8	6	5	7	4	4	4	2	4	3	3	3	0
143	5	6	4	9	9	8	8	7	7	7	6	6	5	5	4	4	3	3	2
140	5	6	9	10	9	9	8	7	7	8	7	6	5	5	5	4	4	3	3
137	4	5	10	10	10	10	9	8	9	8	8	7	6	7	6	5	4	3	4
133	5	6	11	12	11	11	10	9	9	9	9	8	8	7	6	6	5	4	4
130	5	6	12	13	13	12	11	11	11	10	10	10	9	8	7	7	6	5	5
127	6	7	14	15	15	14	12	12	11	11	11	11	10	9	8	8	7	6	6
123	7	8	16	17	17	15	13	13	12	12	11	11	10	10	9	9	8	7	6
120	7	9	18	19	19	17	15	14	13	12	12	11	11	11	10	9	9	8	7
117	8	10	19	21	21	19	16	15	13	13	12	11	11	11	10	10	9	8	7
113	9	10	20	21	22	20	17	15	13	12	11	11	10	10	10	9	9	8	7
110	9	10	19	20	22	20	17	15	13	11	10	10	9	9	9	9	8	7	7
107	9	10	17	18	20	19	17	13	11	10	9	8	8	7	7	7	7	6	6
103	8	8	14	15	17	17	15	12	9	8	7	6	6	5	6	6	5	5	5
100	6	7	10	11	13	14	12	9	7	5	5	4	4	3	4	4	3	3	3

Alt	0	5	10	15	20	25	30	35	40	45	50	55	60	65	70	75	80	85	90
160	0	0	0	0	0	0	0	0	0										
157	0	0	0	0	0	0	0	0	0										
153	0	0	0	0	0	0	0	0	0										
150	0	0	0	0	0	0	0	0	0										
147	0	2	0	0	0	0	0	0	0										
143	2	3	1	0	0	0	0	0	0										
140	3	3	3	1	0	1	0	0	0										
137	4	3	3	3	2	1	1	3	0										
133	4	4	3	3	2	2	3	2	2										
130	5	4	4	3	3	2	2	2	2										
127	6	5	5	4	3	3	3	2	2										
123	6	6	5	5	4	3	4	2	2										
120	7	6	6	5	5	4	5	3	2										
117	7	7	6	6	5	5	5	3	2										
113	7	7	7	6	6	5	5	4	3										
110	7	7	6	6	6	5	6	4	5										
107	6	6	6	5	5	5	6	5	7										
103	5	5	5	4	4	5	5	6	10										
100	3	3	3	3	3	4	4	5	8										

Table 12. Nitric oxide density for the 1984-1985 southern summer solstice as a function of geomagnetic latitude and altitude. Observations for the periods December 9 to January 4 for the years 1984 and 1985 are averaged together. The averaged densities are given in units of 10^6 molecules cm^{-3}.

11

PROPOSED REFERENCE MODELS FOR ATOMIC OXYGEN IN THE TERRESTRIAL ATMOSPHERE

E. J. Llewellyn, I. C. McDade*, and M. D. Lockerbie

Institute of Space and Atmospheric Studies
University of Saskatchewan, Saskatoon SK S7N 0W0, Canada

*Present address: Space Physics Research Laboratory, Department of Atmospheric and Oceanic Sciences, University of Michigan, Ann Arbor, MI 48109

ABSTRACT

A provisional Atomic Oxygen Reference model has been derived from average monthly ozone profiles and the MSIS-86 reference model atmosphere. The concentrations are presented in tabular form for the altitude range 40 - 130 km.

INTRODUCTION

While atomic oxygen is an important constituent in the terrestrial atmosphere the measurement of the atmospheric concentration profile is extremely difficult /1/. Those measurements that have been reported (see for example Planetary and Space Science, Volume 36, issue #9, 1988) have certainly not suggested any general agreement on the concentration profile and have indicated that the concentration at the peak of the layer, near 100 km, may vary by as much as two orders of magnitude /2/. This apparent difference is illustrated, in Figure 1, for two profiles /3/ that were taken under similar conditions (latitude, season and time of day), albeit separated by approximately half a solar cycle. However, it should be noted that possible interactions between the measuring instruments and the ambient atmosphere could seriously influence the measured concentrations. As the original source of this atomic oxygen must be the dissociation of molecular oxygen in the thermosphere such large variations would require major fluctuations in either the ultra-violet solar flux, or in those processes that control the loss of atomic oxygen. These latter could be either chemistry or transport dominated. While there is general agreement that the atomic oxygen concentration must exhibit some variation, there is much less agreement as to either the magnitude of these variations or a mean atomic oxygen profile. Thus any proposed reference model for atomic oxygen must either include these large, reported, variations or justify some data selection.

The atomic oxygen profile has been measured with a variety of different experimental techniques and each has its limitation.

1. Mass Spectrometers -- The interactions of the atmospheric constituents with the mass spectrometer walls have been discussed extensively by Offermann et al. /1/ but there seems to be general agreement that the cryo-pumped systems are probably the best design for the lower thermosphere. These systems also offer the advantage that all atmospheric constituents are measured at the same time.

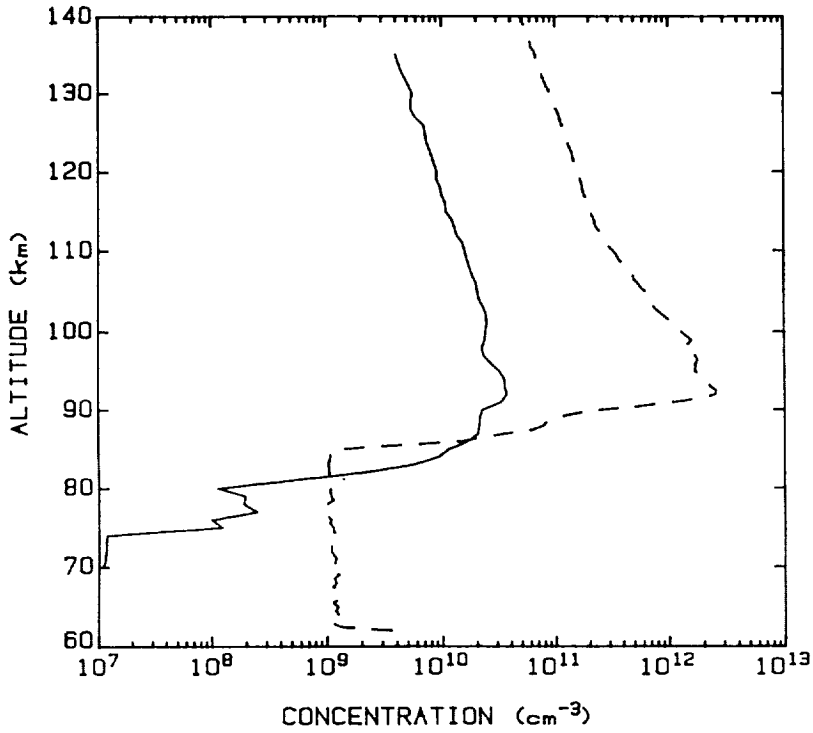

Figure 1. The apparent variation in the measured atomic oxygen concentration height profile for two nighttime profiles taken under similar conditions -- latitude, season, time of day -- but separated by half a solar cycle (P.H.G. Dickinson, private communication).

2. Resonance Lamps -- The details of the scattering appear to be interpreted differently by the various groups /4,5/ using this measurement technique so that the apparent concentrations are quite divergent. Recently there has been some suggestion that interactions between the vehicle and the ambient atmosphere may compromise the measurements /6/.

3. Oxygen recombination emissions -- The details of the oxygen airglow are still uncertain /7/ so that any atomic oxygen determination using these emissions is necessarily limited by the understanding of the airglow excitation process.

4. The OH Meinel emissions -- Recent work by McDade and Llewellyn /8/ has shown that our knowledge of these emissions can be used for atomic oxygen determination but again the accuracy of the derived concentrations are also limited by the knowledge of the airglow processes. However, there have been significant advances since Good /9/ first derived an atomic oxygen profile from the hydroxyl airglow.

5. The quenching of the nitrogen Vegard-Kaplan bands in the aurora -- Although this method has been used for atomic oxygen determination in the aurora there is a requirement for an independent knowledge of the excitation rate of the band system. As with many of the remote sensing methods there is some uncertainty in the appropriate rate constants /10/.

6. The ozone concentration -- The infra-red atmospheric system of oxygen in the airglow can be used to

determine the ozone concentration /11/ and for the assumption that the ozone amounts are in equilibrium it is a simple matter to calculate the atomic oxygen profile /12/. Since the airglow emission is very strong there is little error in the derived atomic oxygen amounts for even strong auroral precipitation.

PROPOSED MODEL

For the mesopause region the available data base for atomic oxygen is somewhat limited. In-situ measurements are necessarily restricted to the locations of available sounding rocket ranges. To overcome this restriction it is believed that the best interim models should concur with the MSIS-86 model /13/. Thus it is proposed that the interim atomic oxygen reference model be a combination of the MSIS-86 model and the atomic oxygen profile derived from the global ozone distribution /14/. It is this combined interim model that is tabulated here. The proposed interim model, for atomic oxygen, makes a smooth transition from the concentrations derived from the global ozone distribution to those of the MSIS-86 model near 100 km. The adopted MSIS-86 atomic oxygen concentrations correspond, in all cases, to quiet solar conditions. The derivation of the atomic oxygen concentration from the ozone concentration follows the technique described by Evans et al. /15/. The calculation of the daytime atomic oxygen profile assumes that the rates of ozone formation and loss may be equated. As the ozone solar dissociation rate, at any altitude, depends on the column concentration of ozone, above that altitude, and the solar elevation angle both factors were included in the determination of the atomic oxygen concentration. For each month the mean solar elevation angle at noon, at that latitude, was used to determine the solar dissociation coefficient. The appropriate atmospheric densities and temperatures were taken from the MAP Reference Atmosphere of Barnett and Corney /16/ and the chemical rate constants were those used by Evans et al. /15/. While the proposed reference model must be considered interim it is expected that with new satellites (e.g. UARS) an improved atomic oxygen reference model should be possible.

Acknowledgements. The authors wish to thank Dr. G. Keating for kindly providing the global ozone profiles in a computer compatible format and Dr. A. Hedin for making a PC version of the MSIS-86 model available. The authors are also indebted to Dr. P.H.G. Dickinson for providing a number of unpublished atomic oxygen profiles.

REFERENCES

1. D. Offermann, Friedrich, V., Ross, P. and U. von Zahn, Neutral Gas Composition Measurements between 80 and 120 km, Planet. Space Sci., **24**, 747 (1981)

2. P.H.G. Dickinson, G. Witt, A. Zuber, D. Murtagh, K.U. Grossman, H.G. Bruckelmann, P. Schwabbauer, K.D. Baker, J.C. Ulwick and R.J. Thomas, Measurements of odd oxygen in the polar region on 10 February 1984 during MAP/WINE. J. Atmos. Terrest. Phys., **49**, 843 (1987)

3. P.H.G. Dickinson, private communication (1987)

4. P.H.G. Dickinson, W.C. Bain, L. Thomas, E.R. Williams, D.B. Jenkins and N.D. Twiddy, The determination of the atomic oxygen concentration and associated parameters in the lower ionosphere. Proc. Roy. Soc. Lond., **A369**, 379 (1980)

5. W.E. Sharp, Absolute concentration of $O(^3P)$ in the lower thermosphere at night. Geophys. Res. Letts., **7**, 485 (1980)

6. G.A. Bird, Aerodynamic Effects on Atmospheric Composition Measurements from Rocket Vehicles in the Thermosphere. Planet. Space Sci., **36**, 921 (1988)

7. I.C. McDade, D.P. Murtagh, R.G.H. Greer, P.H.G. Dickinson, G. Witt, J. Stegman, E.J. Llewellyn, L. Thomas and D.B. Jenkins, ETON 2: Quenching Parameters for Proposed Precursors of $O_2(b^1\Sigma_g^+)$ and $O(^1S)$ in the Terrestrial Nightglow. Planet. Space Sci., **34**, 789 (1986)

8. I.C. McDade and E.J. Llewellyn, Mesospheric Oxygen Atom Densities Inferred from Nighttime OH Meinel Band Emission Rates. Planet. Space Sci., 36, 897 (1988)

9. R.E. Good, Determination of Atomic Oxygen Density from Rocket Borne Measurement of Hydroxyl Airglow. Planet.Space Sci., 24, 389 (1976)

10. I.C. McDade and E.J. Llewellyn, Atomic Oxygen Concentrations in the Auroral Ionosphere. Geophys. Res. Letts., 11, 247 (1984)

11. W.F.J. Evans, D.M. Hunten, E.J. Llewellyn and A. Vallance Jones, Altitude profile of the infrared atmospheric system of oxygen in the dayglow. J. geophys. Res., 73, 2885 (1968)

12. W.F.J. Evans and E.J. Llewellyn, Atomic hydrogen concentrations in the mesosphere and the Hydroxyl emissions. J. geophys.Res., 78, 323 (1973)

13. A.E. Hedin, MSIS-86 Thermospheric Model. J. geophys. Res., 92, 4649 (1987)

14. G.M. Keating and M.C. Pitts, Proposed Reference Models for Ozone. Advances Space Res., 7, #9, 37 (1987)

15. W.F.J. Evans, I.C. McDade, J. Yuen and E.J. Llewellyn, A Rocket Measurement of the O_2 Infrared Atmospheric (0-0) Band Emission in the Dayglow and a Determination of the Mesospheric Ozone and Atomic Oxygen Densities. Can. J. Phys., 66, 941 (1988)

16. J.J. Barnett and M. Corney, Middle Atmosphere Reference Model Derived from Satellite Data. MAP Handbook #16, 47 (1985)

Table 1: Zonally averaged Atomic Oxygen Concentrations (cm^{-3}) in the Southern Hemisphere

[Concentrations shown as 0.0E+00 have not been calculated as either the ozone concentrations are unknown or the atmosphere is in darkness].

January

Latitude	-80	-70	-60	-50	-40	-30	-20	-10
Alt (km)								
130	2.5E+10	2.8E+10	3.1E+10	3.6E+10	3.6E+10	3.7E+10	3.7E+10	3.7E+10
125	3.6E+10	3.9E+10	4.4E+10	5.1E+10	5.1E+10	5.1E+10	5.1E+10	5.0E+10
120	5.4E+10	5.9E+10	6.6E+10	7.6E+10	7.6E+10	7.7E+10	7.5E+10	7.3E+10
115	8.9E+10	9.8E+10	1.1E+11	1.3E+11	1.3E+11	1.3E+11	1.2E+11	1.2E+11
110	1.2E+11	1.4E+11	1.6E+11	1.9E+11	1.9E+11	2.0E+11	2.1E+11	2.2E+11
105	1.7E+11	1.9E+11	2.2E+11	2.8E+11	2.8E+11	3.0E+11	3.2E+11	3.4E+11
100	2.5E+11	2.6E+11	2.9E+11	3.7E+11	3.7E+11	4.0E+11	4.2E+11	4.2E+11
95	3.0E+11	3.0E+11	3.2E+11	3.8E+11	3.8E+11	4.0E+11	4.0E+11	3.9E+11
90	2.4E+11	2.3E+11	2.2E+11	2.4E+11	2.4E+11	2.3E+11	2.2E+11	2.1E+11
85	9.1E+10	8.1E+10	7.3E+10	6.5E+10	6.5E+10	5.8E+10	5.2E+10	4.6E+10
80	4.3E+09	4.5E+09	5.0E+09	7.5E+09	1.1E+10	1.5E+10	1.9E+10	2.1E+10
75	4.9E+09	4.4E+09	4.1E+09	4.2E+09	4.3E+09	4.6E+09	5.2E+09	5.2E+09
70	6.3E+09	5.9E+09	5.6E+09	5.2E+09	4.6E+09	4.1E+09	4.2E+09	4.5E+09
65	7.2E+09	7.0E+09	6.8E+09	6.2E+09	5.8E+09	5.7E+09	5.9E+09	6.1E+09
60	6.4E+09	6.6E+09	6.8E+09	6.8E+09	6.8E+09	6.9E+09	7.2E+09	7.3E+09
55	4.8E+09	5.2E+09	5.6E+09	5.9E+09	6.1E+09	6.3E+09	6.5E+09	6.7E+09
50	3.0E+09	2.8E+09	3.7E+09	4.0E+09	4.3E+09	4.6E+09	4.7E+09	4.8E+09
45	1.2E+09	1.4E+09	1.6E+09	1.8E+09	2.0E+09	2.2E+09	2.3E+09	2.3E+09
40	2.9E+08	3.9E+08	4.6E+08	5.2E+08	5.8E+08	6.1E+08	6.3E+08	6.4E+08

February

Latitude	-80	-70	-60	-50	-40	-30	-20	-10
Alt (km)								
130	2.7E+10	3.0E+10	3.3E+10	3.6E+10	3.8E+10	3.9E+10	3.8E+10	3.7E+10
125	3.8E+10	4.2E+10	4.6E+10	5.1E+10	5.3E+10	5.3E+10	5.2E+10	5.1E+10
120	5.8E+10	6.3E+10	6.9E+10	7.5E+10	7.8E+10	7.8E+10	7.6E+10	7.4E+10
115	9.3E+10	1.0E+11	1.1E+11	1.2E+11	1.3E+11	1.3E+11	1.2E+11	1.2E+11
110	1.3E+11	1.4E+11	1.6E+11	1.8E+11	1.9E+11	2.0E+11	2.1E+11	2.2E+11
105	1.9E+11	2.0E+11	2.3E+11	2.5E+11	2.8E+11	3.0E+11	3.2E+11	3.3E+11
100	2.6E+11	2.7E+11	3.0E+11	3.3E+11	3.7E+11	3.9E+11	4.1E+11	4.0E+11
95	3.0E+11	3.1E+11	3.2E+11	3.4E+11	3.7E+11	3.8E+11	3.8E+11	3.7E+11
90	2.2E+11	2.2E+11	2.1E+11	2.2E+11	2.2E+11	2.2E+11	2.1E+11	2.0E+11
85	7.2E+10	6.8E+10	6.4E+10	6.2E+10	5.8E+10	5.3E+10	4.8E+10	4.3E+10
80	5.0E+09	5.2E+09	6.4E+09	8.9E+09	1.3E+10	1.8E+10	2.2E+10	2.2E+10
75	5.0E+09	3.5E+09	4.6E+09	4.6E+09	4.5E+09	5.2E+09	5.2E+09	5.4E+09
70	6.1E+09	4.6E+09	5.8E+09	5.3E+09	4.9E+09	4.5E+09	4.6E+09	4.6E+09
65	7.4E+09	5.6E+09	6.6E+09	6.2E+09	5.9E+09	5.9E+09	6.1E+09	6.0E+09
60	6.9E+09	5.8E+09	6.7E+09	6.6E+09	6.8E+09	6.9E+09	7.0E+09	7.0E+09
55	5.2E+09	4.8E+09	5.7E+09	5.8E+09	6.0E+09	6.2E+09	6.2E+09	6.5E+09
50	3.2E+09	3.3E+09	3.8E+09	4.1E+09	4.4E+09	4.6E+09	4.7E+09	4.8E+09
45	1.1E+09	1.4E+09	1.6E+09	1.8E+09	2.0E+09	2.2E+09	2.3E+09	2.4E+09
40	2.7E+08	3.6E+08	4.3E+08	4.8E+08	5.4E+08	5.9E+08	6.4E+08	6.8E+08

Table 1: continued

March

Latitude	-80	-70	-60	-50	-40	-30	-20	-10
Alt (km)								
130	3.1E+10	3.3E+10	3.7E+10	4.0E+10	4.1E+10	4.1E+10	4.0E+10	3.9E+10
125	4.3E+10	4.6E+10	5.1E+10	5.5E+10	5.7E+10	5.6E+10	5.5E+10	5.3E+10
120	6.3E+10	6.8E+10	7.4E+10	8.0E+10	8.2E+10	8.2E+10	7.9E+10	7.6E+10
115	1.0E+11	1.1E+11	1.2E+11	1.3E+11	1.3E+11	1.3E+11	1.3E+11	1.2E+11
110	1.4E+11	1.6E+11	1.7E+11	1.9E+11	2.0E+11	2.1E+11	2.1E+11	2.2E+11
105	2.1E+11	2.2E+11	2.4E+11	2.7E+11	2.9E+11	3.1E+11	3.2E+11	3.3E+11
100	2.8E+11	2.9E+11	3.2E+11	3.5E+11	3.8E+11	4.0E+11	4.0E+11	4.0E+11
95	3.0E+11	3.1E+11	3.2E+11	3.5E+11	3.7E+11	3.7E+11	3.7E+11	3.6E+11
90	1.9E+11	2.0E+11	2.0E+11	2.1E+11	2.1E+11	2.1E+11	2.0E+11	2.0E+11
85	5.2E+10	5.3E+10	5.3E+10	5.3E+10	5.1E+10	4.9E+10	4.6E+10	4.2E+10
80	9.8E+09	1.5E+10	1.6E+10	1.9E+10	2.3E+10	2.5E+10	2.3E+10	2.1E+10
75	6.9E+09	6.2E+09	5.8E+09	5.7E+09	5.9E+09	5.8E+09	5.6E+09	5.4E+09
70	6.5E+09	6.3E+09	5.9E+09	5.2E+09	4.9E+09	5.0E+09	4.9E+09	4.7E+09
65	7.2E+09	6.7E+09	6.3E+09	5.9E+09	5.8E+09	6.1E+09	6.2E+09	6.1E+09
60	7.0E+09	6.7E+09	6.6E+09	6.4E+09	6.4E+09	6.6E+09	6.7E+09	6.8E+09
55	5.6E+09	5.2E+09	5.7E+09	5.8E+09	6.0E+09	6.0E+09	6.1E+09	6.4E+09
50	3.5E+09	4.1E+09	4.2E+09	4.4E+09	4.5E+09	4.6E+09	4.6E+09	4.7E+09
45	1.0E+09	1.4E+09	1.7E+09	1.9E+09	2.0E+09	2.2E+09	2.4E+09	2.3E+09
40	2.0E+08	3.0E+08	3.8E+08	4.5E+08	5.1E+08	5.6E+08	6.3E+08	6.7E+08

April

Latitude	-80	-70	-60	-50	-40	-30	-20	-10
Alt (km)								
130	3.4E+10	3.6E+10	3.9E+10	4.1E+10	4.3E+10	4.2E+10	4.1E+10	3.9E+10
125	4.6E+10	4.9E+10	5.3E+10	5.6E+10	5.8E+10	5.7E+10	5.5E+10	5.3E+10
120	6.7E+10	7.1E+10	7.7E+10	8.2E+10	8.4E+10	8.2E+10	7.9E+10	7.6E+10
115	1.0E+11	1.1E+11	1.2E+11	1.3E+11	1.3E+11	1.3E+11	1.3E+11	1.2E+11
110	1.5E+11	1.6E+11	1.8E+11	1.9E+11	2.0E+11	2.1E+11	2.2E+11	2.2E+11
105	2.2E+11	2.3E+11	2.5E+11	2.8E+11	3.0E+11	3.2E+11	3.3E+11	3.3E+11
100	2.9E+11	3.0E+11	3.3E+11	3.6E+11	3.8E+11	4.0E+11	4.0E+11	4.0E+11
95	2.8E+11	3.0E+11	3.2E+11	3.4E+11	3.6E+11	3.7E+11	3.7E+11	3.6E+11
90	1.6E+11	1.7E+11	1.8E+11	1.9E+11	2.0E+11	2.0E+11	2.0E+11	2.0E+11
85	3.7E+10	3.9E+10	4.2E+10	4.5E+10	4.6E+10	4.6E+10	4.5E+10	4.2E+10
80	0.0E+00	0.0E+00	3.0E+10	3.2E+10	3.1E+10	2.7E+10	2.3E+10	2.5E+10
75	0.0E+00	0.0E+00	1.6E+10	1.1E+10	7.8E+09	6.2E+09	5.7E+09	5.5E+09
70	0.0E+00	0.0E+00	7.2E+09	5.8E+09	5.3E+09	2.7E+07	5.0E+09	4.6E+09
65	0.0E+00	0.0E+00	7.4E+09	6.6E+09	6.3E+09	6.5E+09	6.3E+09	5.9E+09
60	0.0E+00	0.0E+00	7.3E+09	6.9E+09	6.6E+09	6.7E+09	6.8E+09	6.7E+09
55	0.0E+00	0.0E+00	6.6E+09	6.4E+09	6.1E+09	6.1E+09	6.2E+09	6.4E+09
50	3.0E+09	5.2E+09	4.5E+09	4.5E+09	4.7E+09	4.6E+09	4.6E+09	4.7E+09
45	6.1E+08	1.4E+09	1.6E+09	1.8E+09	2.0E+09	2.1E+09	2.2E+09	2.2E+09
40	1.1E+08	2.4E+08	3.1E+08	3.7E+08	4.3E+08	4.0E+08	5.6E+08	6.2E+08

Table 1: continued

May

Latitude	-80	-70	-60	-50	-40	-30	-20	-10
Alt (km)								
130	3.3E+10	3.5E+10	3.8E+10	4.0E+10	4.1E+10	4.0E+10	3.9E+10	3.7E+10
125	4.6E+10	4.8E+10	5.2E+10	5.4E+10	5.6E+10	5.5E+10	5.2E+10	5.0E+10
120	6.6E+10	7.0E+10	7.4E+10	7.8E+10	8.0E+10	7.8E+10	7.5E+10	7.2E+10
115	1.0E+11	1.1E+11	1.1E+11	1.2E+11	1.2E+11	1.2E+11	1.2E+11	1.2E+11
110	1.5E+11	1.6E+11	1.8E+11	1.9E+11	2.0E+11	2.0E+11	2.1E+11	2.1E+11
105	2.2E+11	2.3E+11	2.5E+11	2.8E+11	3.0E+11	3.1E+11	3.2E+11	3.2E+11
100	2.7E+11	2.9E+11	3.2E+11	3.5E+11	3.7E+11	3.9E+11	3.9E+11	3.9E+11
95	2.5E+11	2.7E+11	3.0E+11	3.3E+11	3.5E+11	3.6E+11	3.6E+11	3.6E+11
90	1.3E+11	1.4E+11	1.6E+11	1.7E+11	1.9E+11	1.9E+11	2.0E+11	2.0E+11
85	2.8E+10	3.1E+10	3.4E+10	3.9E+10	4.3E+10	4.5E+10	4.6E+10	4.3E+10
80	0.0E+00	0.0E+00	0.0E+00	3.7E+10	3.1E+10	2.8E+10	6.9E+10	3.2E+10
75	0.0E+00	0.0E+00	0.0E+00	1.4E+10	9.1E+09	6.8E+09	6.1E+09	3.8E+09
70	0.0E+00	0.0E+00	0.0E+00	7.8E+09	5.8E+09	5.4E+09	4.8E+09	4.3E+09
65	0.0E+00	0.0E+00	0.0E+00	7.2E+09	7.0E+09	6.5E+09	6.3E+09	5.9E+09
60	0.0E+00	0.0E+00	0.0E+00	5.9E+09	7.0E+09	6.8E+09	7.0E+09	7.0E+09
55	0.0E+00	0.0E+00	0.0E+00	7.4E+09	6.4E+09	6.0E+09	6.2E+09	6.5E+09
50	0.0E+00	3.4E+09	5.4E+09	4.4E+09	4.5E+09	1.2E+11	8.9E+10	4.5E+09
45	0.0E+00	6.8E+08	1.4E+09	1.5E+09	1.8E+09	2.3E+09	2.4E+09	2.0E+09
40	0.0E+00	1.3E+08	2.4E+08	2.9E+08	3.5E+08	4.6E+08	5.4E+08	5.5E+08

June

Latitude	-80	-70	-60	-50	-40	-30	-20	-10
Alt (km)								
130	3.2E+10	3.3E+10	3.5E+10	3.7E+10	3.8E+10	3.7E+10	3.6E+10	3.4E+10
125	4.4E+10	4.6E+10	4.9E+10	5.1E+10	5.2E+10	5.1E+10	4.9E+10	4.6E+10
120	6.3E+10	6.6E+10	7.0E+10	7.4E+10	7.5E+10	7.3E+10	7.0E+10	6.6E+10
115	9.8E+10	1.0E+11	1.1E+11	1.1E+11	1.2E+11	1.1E+11	1.1E+11	1.1E+11
110	1.5E+11	1.6E+11	1.7E+11	1.8E+11	1.9E+11	1.9E+11	2.0E+11	2.0E+11
105	2.1E+11	2.2E+11	2.5E+11	2.7E+11	2.8E+11	3.0E+11	3.0E+11	3.0E+11
100	2.6E+11	2.8E+11	3.1E+11	3.4E+11	3.6E+11	3.7E+11	3.8E+11	3.7E+11
95	2.3E+11	2.5E+11	2.8E+11	3.1E+11	3.4E+11	3.5E+11	3.5E+11	3.5E+11
90	1.2E+11	1.3E+11	1.4E+11	1.6E+11	1.8E+11	1.9E+11	1.9E+11	1.9E+11
85	2.4E+10	2.7E+10	3.0E+10	3.6E+10	4.1E+10	4.5E+10	4.6E+10	4.4E+10
80	0.0E+00	0.0E+00	0.0E+00	0.0E+00	3.1E+10	2.6E+10	2.4E+10	2.5E+10
75	0.0E+00	0.0E+00	0.0E+00	0.0E+00	9.4E+09	6.8E+09	5.7E+09	5.1E+09
70	0.0E+00	0.0E+00	0.0E+00	0.0E+00	6.4E+09	5.7E+09	4.7E+09	4.2E+09
65	0.0E+00	0.0E+00	0.0E+00	0.0E+00	7.7E+09	6.5E+09	6.1E+09	6.0E+09
60	0.0E+00	0.0E+00	0.0E+00	0.0E+00	7.4E+09	7.0E+09	7.0E+09	7.2E+09
55	0.0E+00	0.0E+00	0.0E+00	0.0E+00	6.5E+09	5.9E+09	6.1E+09	6.4E+09
50	0.0E+00	0.0E+00	4.4E+09	5.4E+09	4.4E+09	4.3E+09	4.4E+09	4.5E+09
45	0.0E+00	0.0E+00	9.9E+08	1.5E+09	1.6E+09	1.7E+09	1.8E+09	1.9E+09
40	0.0E+00	0.0E+00	2.1E+08	2.6E+08	3.0E+08	3.7E+08	4.4E+08	5.0E+08

Table 1: continued

July

Latitude	-80	-70	-60	-50	-40	-30	-20	-10
Alt (km)								
130	3.1E+10	3.3E+10	3.5E+10	3.6E+10	3.7E+10	3.6E+10	3.5E+10	3.3E+10
125	4.3E+10	4.5E+10	4.8E+10	5.0E+10	5.1E+10	5.0E+10	4.7E+10	4.5E+10
120	6.2E+10	6.5E+10	6.9E+10	7.2E+10	7.3E+10	7.1E+10	6.8E+10	6.5E+10
115	9.7E+10	1.0E+11	1.1E+11	1.1E+11	1.1E+11	1.1E+11	1.1E+11	1.1E+11
110	1.5E+11	1.5E+11	1.7E+11	1.8E+11	1.9E+11	1.9E+11	1.9E+11	1.9E+11
105	2.1E+11	2.2E+11	2.4E+11	2.6E+11	2.8E+11	2.9E+11	3.0E+11	3.0E+11
100	2.6E+11	2.8E+11	3.1E+11	3.3E+11	3.6E+11	3.7E+11	3.7E+11	3.7E+11
95	2.3E+11	2.5E+11	2.8E+11	3.1E+11	3.3E+11	3.4E+11	3.4E+11	3.4E+11
90	1.2E+11	1.3E+11	1.5E+11	1.6E+11	1.8E+11	1.9E+11	1.9E+11	1.9E+11
85	2.5E+10	2.7E+10	3.1E+10	3.6E+10	4.1E+10	4.4E+10	4.5E+10	4.3E+10
80	0.0E+00	0.0E+00	0.0E+00	2.5E+10	2.5E+10	2.5E+10	2.3E+10	2.1E+10
75	0.0E+00	0.0E+00	0.0E+00	1.2E+10	8.8E+09	6.6E+09	5.5E+09	4.9E+09
70	0.0E+00	0.0E+00	0.0E+00	7.6E+09	5.8E+09	5.4E+09	4.6E+09	4.4E+09
65	0.0E+00	0.0E+00	0.0E+00	7.9E+09	7.1E+09	6.4E+09	6.1E+09	6.0E+09
60	0.0E+00	0.0E+00	0.0E+00	0.0E+00	6.9E+09	6.7E+09	6.8E+09	7.1E+09
55	0.0E+00	0.0E+00	0.0E+00	0.0E+00	6.1E+09	5.9E+09	6.1E+09	6.4E+09
50	0.0E+00	0.0E+00	3.8E+09	4.8E+09	4.1E+09	4.3E+09	4.4E+09	4.6E+09
45	0.0E+00	0.0E+00	8.8E+08	1.4E+09	1.5E+09	1.6E+09	3.9E+08	2.0E+09
40	0.0E+00	0.0E+00	1.8E+08	2.6E+08	2.9E+08	3.6E+08	3.3E+08	4.8E+08

August

Latitude	-80	-70	-60	-50	-40	-30	-20	-10
Alt (km)								
130	3.2E+10	3.4E+10	3.6E+10	3.8E+10	3.9E+10	3.8E+10	3.7E+10	3.5E+10
125	4.4E+10	4.6E+10	5.0E+10	5.2E+10	5.3E+10	5.2E+10	5.0E+10	4.7E+10
120	6.4E+10	6.7E+10	7.2E+10	7.6E+10	7.7E+10	7.5E+10	7.2E+10	6.8E+10
115	1.0E+11	1.0E+11	1.1E+11	1.2E+11	1.2E+11	1.2E+11	1.1E+11	1.1E+11
110	1.5E+11	1.6E+11	1.7E+11	1.8E+11	1.9E+11	2.0E+11	2.0E+11	2.0E+11
105	2.1E+11	2.3E+11	2.5E+11	2.7E+11	2.9E+11	3.0E+11	3.0E+11	3.1E+11
100	2.7E+11	2.9E+11	3.2E+11	3.4E+11	3.6E+11	3.8E+11	3.8E+11	3.8E+11
95	2.6E+11	2.8E+11	3.0E+11	3.3E+11	3.4E+11	3.5E+11	3.5E+11	3.4E+11
90	1.4E+11	1.5E+11	1.6E+11	1.8E+11	1.9E+11	1.9E+11	1.9E+11	1.9E+11
85	3.1E+10	3.3E+10	3.7E+10	4.1E+10	4.4E+10	4.5E+10	4.5E+10	4.2E+10
80	0.0E+00	0.0E+00	2.9E+10	2.8E+10	2.8E+10	2.6E+10	2.4E+10	2.1E+10
75	0.0E+00	0.0E+00	1.4E+10	1.1E+10	9.2E+09	7.6E+09	6.0E+09	5.3E+09
70	0.0E+00	0.0E+00	8.0E+09	6.6E+09	6.3E+09	5.8E+09	5.0E+09	4.4E+09
65	0.0E+00	0.0E+00	7.4E+09	7.4E+09	7.1E+09	6.3E+09	6.0E+09	6.0E+09
60	0.0E+00	0.0E+00	7.0E+09	6.8E+09	6.6E+09	6.7E+09	6.7E+09	7.0E+09
55	0.0E+00	0.0E+00	5.1E+09	6.0E+09	5.8E+09	6.0E+09	6.2E+09	6.5E+09
50	0.0E+00	1.3E+09	3.2E+09	3.7E+09	4.0E+09	4.3E+09	4.5E+09	4.7E+09
45	0.0E+00	3.0E+08	1.0E+09	1.3E+09	1.5E+09	1.7E+09	2.0E+09	2.1E+09
40	0.0E+00	1.0E+08	2.5E+08	2.9E+08	3.2E+08	3.9E+08	4.7E+08	5.4E+08

Table 1: continued

September

Latitude	-80	-70	-60	-50	-40	-30	-20	-10
Alt (km)								
130	3.3E+10	3.5E+10	3.8E+10	4.1E+10	4.2E+10	4.2E+10	4.0E+10	3.9E+10
125	4.5E+10	4.8E+10	5.2E+10	5.6E+10	5.8E+10	5.7E+10	5.5E+10	5.3E+10
120	6.6E+10	7.1E+10	7.6E+10	8.1E+10	8.3E+10	8.2E+10	7.9E+10	7.5E+10
115	1.0E+11	1.1E+11	1.2E+11	1.3E+11	1.3E+11	1.3E+11	1.3E+11	1.2E+11
110	1.5E+11	1.6E+11	1.8E+11	1.9E+11	2.0E+11	2.1E+11	2.2E+11	2.2E+11
105	2.2E+11	2.3E+11	2.5E+11	2.8E+11	3.0E+11	3.2E+11	3.3E+11	3.3E+11
100	2.9E+11	3.0E+11	3.3E+11	3.6E+11	3.8E+11	4.0E+11	4.1E+11	4.0E+11
95	3.0E+11	3.1E+11	3.3E+11	3.5E+11	3.7E+11	3.7E+11	3.7E+11	3.6E+11
90	1.8E+11	1.8E+11	1.9E+11	2.0E+11	2.1E+11	2.0E+11	2.0E+11	2.0E+11
85	4.3E+10	4.5E+10	4.7E+10	4.9E+10	4.9E+10	4.8E+10	4.6E+10	4.3E+10
80	2.5E+10	2.8E+10	3.1E+10	3.3E+10	3.2E+10	2.9E+10	2.5E+10	2.2E+10
75	1.4E+10	1.6E+10	1.4E+10	1.2E+10	9.4E+09	7.3E+09	6.2E+09	5.5E+09
70	7.8E+09	8.1E+09	7.2E+09	6.7E+09	6.3E+09	5.8E+09	5.2E+09	4.4E+09
65	6.0E+09	7.3E+09	7.3E+09	7.3E+09	6.9E+09	6.1E+09	5.7E+09	5.6E+09
60	0.0E+00	7.0E+09	6.8E+09	6.7E+09	6.6E+09	6.5E+09	6.5E+09	6.7E+09
55	0.0E+00	5.8E+09	5.8E+09	5.8E+09	5.8E+09	6.0E+09	6.1E+09	6.4E+09
50	1.0E+09	3.1E+09	3.7E+09	4.0E+09	4.3E+09	4.5E+09	4.5E+09	4.6E+09
45	2.5E+08	1.0E+09	1.4E+09	1.6E+09	1.8E+09	2.0E+09	2.1E+09	2.2E+09
40	1.1E+08	2.9E+08	3.7E+08	3.7E+08	4.0E+08	4.7E+08	5.4E+08	6.0E+08

October

Latitude	-80	-70	-60	-50	-40	-30	-20	-10
Alt (km)								
130	3.2E+10	3.4E+10	3.8E+10	4.2E+10	4.4E+10	4.4E+10	4.3E+10	4.2E+10
125	4.4E+10	4.8E+10	5.3E+10	5.7E+10	6.0E+10	6.0E+10	5.8E+10	5.7E+10
120	6.6E+10	7.1E+10	7.8E+10	8.4E+10	8.7E+10	8.7E+10	8.4E+10	8.2E+10
115	1.0E+11	1.1E+11	1.2E+11	1.3E+11	1.4E+11	1.4E+11	1.4E+11	1.3E+11
110	1.5E+11	1.6E+11	1.8E+11	2.0E+11	2.1E+11	2.2E+11	2.3E+11	2.4E+11
105	2.1E+11	2.3E+11	2.5E+11	2.8E+11	3.1E+11	3.3E+11	3.5E+11	3.6E+11
100	2.9E+11	3.0E+11	3.3E+11	3.6E+11	4.0E+11	4.2E+11	4.3E+11	4.3E+11
95	3.2E+11	3.3E+11	3.4E+11	3.7E+11	3.9E+11	4.0E+11	4.0E+11	3.9E+11
90	2.2E+11	2.2E+11	2.2E+11	2.2E+11	2.3E+11	2.2E+11	2.1E+11	2.1E+11
85	6.3E+10	6.2E+10	6.0E+10	5.9E+10	5.7E+10	5.3E+10	4.9E+10	4.5E+10
80	1.8E+10	2.4E+10	2.8E+10	2.9E+10	2.8E+10	2.5E+10	2.3E+10	2.4E+10
75	9.1E+09	8.9E+09	9.0E+09	8.8E+09	7.6E+09	6.6E+09	6.2E+09	6.5E+09
70	8.0E+09	7.7E+09	7.7E+09	7.1E+09	6.4E+09	5.6E+09	5.3E+09	4.7E+09
65	7.0E+09	6.9E+09	7.0E+09	6.8E+09	6.4E+09	6.0E+09	5.7E+09	5.3E+09
60	6.8E+09	6.7E+09	6.6E+09	6.6E+09	6.5E+09	6.5E+09	6.4E+09	6.5E+09
55	5.1E+09	5.6E+09	6.2E+09	5.8E+09	5.9E+09	6.0E+09	6.1E+09	6.3E+09
50	2.7E+09	3.6E+09	4.0E+09	4.3E+09	4.5E+09	4.6E+09	4.6E+09	4.7E+09
45	9.9E+08	1.4E+09	1.6E+09	1.9E+09	2.1E+09	2.2E+09	2.2E+09	2.3E+09
40	3.1E+08	4.1E+08	4.3E+08	4.6E+08	5.1E+08	5.5E+08	6.0E+08	6.3E+08

Table 1: continued

November

Latitude	-80	-70	-60	-50	-40	-30	-20	-10
Alt (km)								
130	2.9E+10	3.1E+10	3.5E+10	3.9E+10	4.1E+10	4.2E+10	4.2E+10	4.1E+10
125	4.1E+10	4.4E+10	4.9E+10	5.4E+10	5.7E+10	5.8E+10	5.7E+10	5.7E+10
120	6.1E+10	6.7E+10	7.4E+10	8.1E+10	8.5E+10	8.6E+10	8.4E+10	8.2E+10
115	9.9E+10	1.1E+11	1.2E+11	1.3E+11	1.4E+11	1.4E+11	1.4E+11	1.3E+11
110	1.4E+11	1.5E+11	1.7E+11	1.9E+11	2.1E+11	2.2E+11	2.3E+11	2.4E+11
105	1.9E+11	2.1E+11	2.4E+11	2.7E+11	3.0E+11	3.3E+11	3.5E+11	3.6E+11
100	2.7E+11	2.9E+11	3.1E+11	3.5E+11	4.0E+11	4.3E+11	4.5E+11	4.5E+11
95	3.2E+11	3.2E+11	3.4E+11	3.7E+11	4.0E+11	4.2E+11	4.2E+11	4.1E+11
90	2.5E+11	2.3E+11	2.3E+11	2.4E+11	2.4E+11	2.4E+11	2.3E+11	2.2E+11
85	8.4E+10	7.7E+10	7.1E+10	6.8E+10	6.4E+10	5.8E+10	5.3E+10	4.8E+10
80	6.1E+09	7.4E+09	9.8E+09	1.2E+10	1.6E+10	1.8E+10	2.0E+10	2.4E+10
75	5.7E+09	5.5E+09	5.9E+09	5.5E+09	5.9E+09	5.8E+09	6.0E+09	6.4E+09
70	6.7E+09	6.5E+09	6.4E+09	6.2E+09	5.8E+09	5.4E+09	4.7E+09	4.7E+09
65	6.7E+09	6.6E+09	6.5E+09	6.3E+09	6.0E+09	5.8E+09	5.6E+09	5.4E+09
60	6.6E+09	6.6E+09	6.6E+09	7.2E+09	6.6E+09	6.7E+09	6.6E+09	6.9E+09
55	5.0E+09	5.3E+09	5.7E+09	5.9E+09	6.2E+09	6.2E+09	6.2E+09	6.4E+09
50	2.9E+09	3.4E+09	3.8E+09	4.1E+09	4.4E+09	4.6E+09	4.6E+09	4.6E+09
45	1.1E+09	1.4E+09	1.7E+09	2.0E+09	2.2E+09	2.3E+09	2.3E+09	2.3E+09
40	3.2E+08	4.0E+08	4.6E+08	5.4E+08	6.1E+08	6.4E+08	6.5E+08	6.5E+08

December

Latitude	-80	-70	-60	-50	-40	-30	-20	-10
Alt (km)								
130	2.6E+10	2.8E+10	3.2E+10	3.6E+10	3.8E+10	3.9E+10	3.9E+10	3.9E+10
125	3.7E+10	4.0E+10	4.5E+10	5.0E+10	5.3E+10	5.4E+10	5.3E+10	5.3E+10
120	5.6E+10	6.1E+10	6.9E+10	7.6E+10	8.0E+10	8.0E+10	7.9E+10	7.8E+10
115	9.2E+10	1.0E+11	1.1E+11	1.3E+11	1.3E+11	1.3E+11	1.3E+11	1.3E+11
110	1.3E+11	1.4E+11	1.6E+11	1.9E+11	2.0E+11	2.1E+11	2.2E+11	2.3E+11
105	1.8E+11	2.0E+11	2.3E+11	2.6E+11	2.9E+11	3.2E+11	3.4E+11	3.5E+11
100	2.5E+11	2.7E+11	3.0E+11	3.4E+11	3.8E+11	4.2E+11	4.4E+11	4.4E+11
95	3.1E+11	3.1E+11	3.2E+11	3.6E+11	3.9E+11	4.2E+11	4.2E+11	4.1E+11
90	2.5E+11	2.4E+11	2.3E+11	2.4E+11	2.5E+11	2.4E+11	2.3E+11	2.3E+11
85	9.7E+10	8.5E+10	7.6E+10	7.2E+10	6.8E+10	6.1E+10	5.4E+10	4.8E+10
80	4.6E+09	5.1E+09	5.7E+09	7.8E+09	1.1E+10	1.4E+10	1.8E+10	2.2E+10
75	5.0E+09	4.6E+09	4.8E+09	4.6E+09	4.6E+09	4.6E+09	5.3E+09	5.7E+09
70	6.6E+09	6.3E+09	5.9E+09	5.5E+09	5.3E+09	2.4E+09	4.5E+09	4.8E+09
65	7.1E+09	7.1E+09	6.8E+09	6.5E+09	6.1E+09	6.0E+09	6.1E+09	6.1E+09
60	6.6E+09	6.9E+09	7.0E+09	7.0E+09	6.9E+09	7.2E+09	7.4E+09	7.5E+09
55	4.8E+09	5.2E+09	5.6E+09	6.0E+09	6.2E+09	6.4E+09	6.5E+09	6.8E+09
50	2.9E+09	3.3E+09	3.7E+09	4.0E+09	4.3E+09	4.5E+09	4.7E+09	4.8E+09
45	1.2E+09	1.4E+09	1.7E+09	1.9E+09	2.1E+09	2.2E+09	2.3E+09	2.3E+09
40	3.3E+08	4.0E+08	4.8E+08	5.5E+08	6.1E+08	6.4E+08	6.4E+08	6.3E+08

Table 2: Zonally averaged Atomic Oxygen Concentrations (cm^{-3}) in the Northern Hemisphere

[Concentrations shown as 0.0E+00 have not been calculated as either the ozone concentrations are unknown or the atmosphere is in darkness].

January

Latitude	0	10	20	30	40	50	60	70	80
Alt (km)									
130	3.2E+10	3.1E+10	3.1E+10	3.1E+10	3.0E+10	2.9E+10	2.7E+10	2.6E+10	2.4E+10
125	4.3E+10	4.3E+10	4.3E+10	4.3E+10	4.2E+10	4.1E+10	3.9E+10	3.6E+10	3.4E+10
120	6.3E+10	6.2E+10	6.3E+10	6.4E+10	6.4E+10	6.2E+10	5.9E+10	5.5E+10	5.2E+10
115	1.0E+11	1.0E+11	1.0E+11	1.1E+11	1.1E+11	1.0E+11	9.7E+10	9.0E+10	8.5E+10
110	1.9E+11	1.9E+11	1.8E+11	1.7E+11	1.6E+11	1.5E+11	1.4E+11	1.3E+11	1.2E+11
105	2.9E+11	2.9E+11	2.7E+11	2.5E+11	2.3E+11	2.1E+11	1.9E+11	1.7E+11	1.6E+11
100	3.6E+11	3.6E+11	3.5E+11	3.4E+11	3.1E+11	2.8E+11	2.5E+11	2.4E+11	2.3E+11
95	3.3E+11	3.3E+11	3.4E+11	3.4E+11	3.2E+11	3.0E+11	2.8E+11	2.7E+11	2.8E+11
90	1.9E+11	1.8E+11	1.9E+11	2.0E+11	2.0E+11	2.0E+11	2.0E+11	2.1E+11	2.3E+11
85	3.9E+10	3.9E+10	4.4E+10	4.9E+10	5.5E+10	6.0E+10	6.5E+10	7.4E+10	8.6E+10
80	3.8E+10	2.3E+10	2.4E+10	2.4E+10	2.4E+10	2.9E+10	2.5E+10	0.0E+00	0.0E+00
75	5.2E+09	5.7E+09	7.1E+09	9.7E+09	1.3E+10	1.5E+10	1.4E+10	0.0E+00	0.0E+00
70	4.7E+09	4.5E+09	4.7E+09	5.4E+09	6.3E+09	9.4E+09	1.2E+10	0.0E+00	0.0E+00
65	6.0E+09	5.8E+09	5.8E+09	6.0E+09	7.6E+09	7.6E+09	4.9E+09	0.0E+00	0.0E+00
60	7.2E+09	6.9E+09	6.6E+09	6.4E+09	6.0E+09	7.2E+09	6.4E+09	0.0E+00	0.0E+00
55	6.7E+09	6.5E+09	6.2E+09	5.8E+09	5.5E+09	5.4E+09	0.0E+00	0.0E+00	0.0E+00
50	4.8E+09	4.7E+09	4.4E+09	4.1E+09	3.7E+09	2.8E+09	1.9E+09	0.0E+00	0.0E+00
45	2.3E+09	2.1E+09	2.0E+09	1.7E+09	1.3E+09	8.9E+08	4.5E+08	0.0E+00	0.0E+00
40	6.2E+08	5.6E+08	4.9E+08	4.0E+08	2.9E+08	2.0E+08	1.1E+08	0.0E+00	0.0E+00

February

Latitude	0	10	20	30	40	50	60	70	80
Alt (km)									
130	3.4E+10	3.3E+10	3.3E+10	3.3E+10	3.3E+10	3.1E+10	3.0E+10	2.8E+10	2.7E+10
125	4.6E+10	4.5E+10	4.5E+10	4.6E+10	4.5E+10	4.4E+10	4.1E+10	3.9E+10	3.7E+10
120	6.6E+10	6.6E+10	6.6E+10	6.7E+10	6.7E+10	6.5E+10	6.2E+10	5.8E+10	5.6E+10
115	1.1E+11	1.1E+11	1.1E+11	1.1E+11	1.1E+11	1.1E+11	1.0E+11	9.4E+10	9.0E+10
110	2.0E+11	1.9E+11	1.9E+11	1.8E+11	1.7E+11	1.6E+11	1.5E+11	1.3E+11	1.3E+11
105	3.0E+11	3.0E+11	2.8E+11	2.6E+11	2.4E+11	2.2E+11	2.0E+11	1.9E+11	1.8E+11
100	3.7E+11	3.6E+11	3.6E+11	3.5E+11	3.2E+11	2.9E+11	2.7E+11	2.5E+11	2.5E+11
95	3.4E+11	3.4E+11	3.4E+11	3.4E+11	3.2E+11	3.0E+11	2.9E+11	2.9E+11	2.9E+11
90	1.9E+11	1.8E+11	1.9E+11	1.9E+11	2.0E+11	2.0E+11	2.0E+11	2.0E+11	2.2E+11
85	3.9E+10	3.9E+10	4.3E+10	4.7E+10	5.2E+10	5.5E+10	5.9E+10	6.5E+10	7.1E+10
80	2.3E+10	2.4E+10	2.8E+10	2.8E+10	2.7E+10	2.6E+10	2.4E+10	1.7E+10	0.0E+00
75	5.7E+09	6.0E+09	7.3E+09	9.5E+09	1.4E+10	1.8E+10	1.8E+10	1.5E+10	0.0E+00
70	4.5E+09	4.6E+09	5.0E+09	5.5E+09	6.2E+09	7.8E+09	1.1E+10	1.2E+10	0.0E+00
65	5.9E+09	5.5E+09	5.5E+09	5.7E+09	6.1E+09	7.6E+09	8.2E+09	6.5E+09	0.0E+00
60	6.8E+09	6.6E+09	6.2E+09	6.0E+09	5.7E+09	5.8E+09	6.2E+09	5.6E+09	0.0E+00
55	6.5E+09	6.5E+09	6.1E+09	5.8E+09	5.6E+09	5.4E+09	5.2E+09	2.7E+09	0.0E+00
50	4.8E+09	4.7E+09	4.5E+09	4.3E+09	4.1E+09	3.7E+09	2.8E+09	7.6E+08	0.0E+00
45	2.4E+09	2.2E+09	2.1E+09	1.9E+09	1.6E+09	1.2E+09	7.6E+08	1.9E+08	0.0E+00
40	6.7E+08	6.2E+08	5.5E+08	4.6E+08	3.7E+08	2.7E+08	1.6E+08	7.2E+07	0.0E+00

Table 2: continued

March

Latitude / Alt (km)	0	10	20	30	40	50	60	70	80
130	3.8E+10	3.9E+10	3.9E+10	4.0E+10	3.9E+10	3.8E+10	3.7E+10	3.5E+10	3.5E+10
125	5.2E+10	5.2E+10	5.3E+10	5.4E+10	5.4E+10	5.3E+10	5.1E+10	4.9E+10	4.7E+10
120	7.4E+10	7.5E+10	7.6E+10	7.8E+10	7.8E+10	7.7E+10	7.4E+10	7.1E+10	6.9E+10
115	1.2E+11	1.2E+11	1.2E+11	1.2E+11	1.2E+11	1.2E+11	1.2E+11	1.1E+11	1.1E+11
110	2.2E+11	2.2E+11	2.1E+11	2.0E+11	1.9E+11	1.8E+11	1.7E+11	1.6E+11	1.6E+11
105	3.3E+11	3.3E+11	3.2E+11	3.0E+11	2.8E+11	2.6E+11	2.5E+11	2.3E+11	2.3E+11
100	4.0E+11	4.0E+11	3.9E+11	3.8E+11	3.6E+11	3.4E+11	3.2E+11	3.1E+11	3.0E+11
95	3.6E+11	3.6E+11	3.6E+11	3.6E+11	3.5E+11	3.3E+11	3.2E+11	3.1E+11	3.1E+11
90	2.0E+11	1.9E+11	1.9E+11	2.0E+11	2.0E+11	1.9E+11	1.9E+11	1.9E+11	1.8E+11
85	4.0E+10	4.2E+10	4.5E+10	4.6E+10	4.7E+10	4.7E+10	4.7E+10	4.6E+10	4.6E+10
80	2.0E+10	2.2E+10	2.6E+10	2.9E+10	3.2E+10	3.1E+10	2.8E+10	2.3E+10	1.8E+10
75	5.4E+09	5.9E+09	6.7E+09	8.6E+09	1.2E+10	1.7E+10	2.1E+10	1.9E+10	1.4E+10
70	4.5E+09	4.5E+09	5.1E+09	5.8E+09	6.0E+09	7.2E+09	9.4E+09	1.2E+10	1.1E+10
65	5.8E+09	5.6E+09	5.7E+09	5.8E+09	6.2E+09	6.6E+09	7.0E+09	7.4E+09	6.7E+09
60	6.8E+09	6.6E+09	6.2E+09	6.1E+09	6.1E+09	6.1E+09	5.9E+09	5.9E+09	4.2E+09
55	6.5E+09	6.4E+09	6.2E+09	6.0E+09	5.8E+09	5.7E+09	5.5E+09	5.3E+09	2.2E+09
50	4.8E+09	4.7E+09	4.6E+09	4.5E+09	4.4E+09	4.2E+09	3.9E+09	3.0E+09	7.0E+08
45	2.3E+09	2.3E+09	2.2E+09	2.1E+09	2.0E+09	1.7E+09	1.3E+09	8.1E+08	1.9E+08
40	6.8E+08	6.5E+08	6.0E+08	5.3E+08	4.8E+08	4.0E+08	1.4E+08	1.7E+08	7.4E+07

April

Latitude / Alt (km)	0	10	20	30	40	50	60	70	80
130	3.8E+10	3.8E+10	3.8E+10	3.8E+10	3.7E+10	3.6E+10	3.4E+10	3.2E+10	3.1E+10
125	5.2E+10	5.1E+10	5.2E+10	5.2E+10	5.2E+10	5.0E+10	4.7E+10	4.5E+10	4.3E+10
120	7.4E+10	7.4E+10	7.5E+10	7.6E+10	7.6E+10	7.4E+10	7.0E+10	6.6E+10	6.4E+10
115	1.2E+11	1.2E+11	1.2E+11	1.2E+11	1.2E+11	1.2E+11	1.1E+11	1.1E+11	1.0E+11
110	2.2E+11	2.1E+11	2.0E+11	1.9E+11	1.8E+11	1.7E+11	1.6E+11	1.5E+11	1.4E+11
105	3.3E+11	3.2E+11	3.1E+11	2.9E+11	2.7E+11	2.5E+11	2.3E+11	2.1E+11	2.0E+11
100	3.9E+11	3.9E+11	3.9E+11	3.7E+11	3.5E+11	3.2E+11	3.0E+11	2.8E+11	2.8E+11
95	3.6E+11	3.5E+11	3.6E+11	3.5E+11	3.4E+11	3.2E+11	3.1E+11	3.0E+11	3.1E+11
90	1.9E+11	1.9E+11	1.9E+11	2.0E+11	2.0E+11	2.0E+11	2.0E+11	2.0E+11	2.1E+11
85	3.9E+10	4.1E+10	4.4E+10	4.7E+10	5.0E+10	5.3E+10	5.5E+10	5.8E+10	6.1E+10
80	2.5E+10	2.5E+10	2.6E+10	3.0E+10	3.1E+10	2.9E+10	2.8E+10	2.5E+10	1.8E+10
75	5.5E+09	5.4E+09	6.0E+09	7.5E+09	9.2E+09	1.0E+10	1.2E+10	1.3E+10	1.2E+10
70	4.4E+09	4.7E+09	5.4E+09	5.9E+09	6.2E+09	6.6E+09	8.9E+09	7.8E+09	8.7E+09
65	5.7E+09	5.6E+09	5.9E+09	6.0E+09	6.2E+09	6.4E+09	1.8E+10	6.7E+09	1.9E+10
60	6.7E+09	6.6E+09	6.4E+09	6.4E+09	6.5E+09	6.5E+09	6.4E+09	6.2E+09	6.0E+09
55	6.5E+09	6.4E+09	6.1E+09	6.1E+09	6.1E+09	6.0E+09	5.8E+09	5.6E+09	5.4E+09
50	4.0E+09	4.7E+09	4.3E+09	1.7E+12	4.6E+09	4.3E+09	4.1E+09	3.7E+09	2.8E+09
45	2.2E+09	2.3E+09	2.2E+09	2.2E+09	2.2E+09	2.0E+09	5.1E+09	1.2E+09	2.4E+09
40	6.4E+08	6.5E+08	6.2E+08	5.9E+08	5.8E+08	5.2E+08	4.6E+08	2.8E+08	1.8E+08

Table 2: continued

May

Latitude	0	10	20	30	40	50	60	70	80
Alt (km)									
130	3.6E+10	3.5E+10	3.5E+10	3.5E+10	3.4E+10	3.3E+10	3.1E+10	2.9E+10	2.8E+10
125	4.8E+10	4.8E+10	4.8E+10	4.8E+10	4.8E+10	4.6E+10	4.3E+10	4.1E+10	3.9E+10
120	7.0E+10	6.9E+10	7.0E+10	7.1E+10	7.1E+10	6.9E+10	6.5E+10	6.1E+10	5.8E+10
115	1.1E+11	1.1E+11	1.1E+11	1.2E+11	1.2E+11	1.1E+11	1.1E+11	9.8E+10	9.3E+10
110	2.1E+11	2.0E+11	1.9E+11	1.8E+11	1.8E+11	1.6E+11	1.5E+11	1.4E+11	1.3E+11
105	3.2E+11	3.1E+11	2.9E+11	2.7E+11	2.5E+11	2.3E+11	2.1E+11	1.9E+11	1.8E+11
100	3.8E+11	3.8E+11	3.8E+11	3.6E+11	3.3E+11	3.0E+11	2.7E+11	2.6E+11	2.5E+11
95	3.5E+11	3.5E+11	3.5E+11	3.5E+11	3.4E+11	3.1E+11	2.9E+11	2.9E+11	3.0E+11
90	1.9E+11	1.9E+11	1.9E+11	2.0E+11	2.0E+11	2.0E+11	2.0E+11	2.1E+11	2.3E+11
85	4.0E+10	4.0E+10	4.5E+10	4.9E+10	5.4E+10	5.8E+10	6.3E+10	7.0E+10	7.9E+10
80	3.3E+10	3.0E+10	2.7E+10	2.3E+10	1.9E+10	1.6E+10	1.2E+10	9.9E+09	7.4E+09
75	5.8E+09	5.7E+09	5.7E+09	6.2E+09	5.8E+09	5.9E+09	5.4E+09	5.1E+09	5.3E+09
70	4.5E+09	4.7E+09	5.2E+09	5.2E+09	5.5E+09	5.8E+09	6.0E+09	6.4E+09	6.9E+09
65	5.7E+09	6.0E+09	6.2E+09	6.1E+09	6.1E+09	6.4E+09	6.8E+09	6.8E+09	6.7E+09
60	6.9E+09	6.9E+09	6.8E+09	6.7E+09	6.5E+09	6.7E+09	6.7E+09	6.6E+09	6.5E+09
55	6.5E+09	6.3E+09	6.2E+09	6.2E+09	6.2E+09	6.1E+09	5.9E+09	5.6E+09	5.2E+09
50	4.6E+09	4.6E+09	4.7E+09	4.7E+09	4.5E+09	4.3E+09	4.0E+09	3.6E+09	3.1E+09
45	2.1E+09	2.2E+09	2.2E+09	2.2E+09	2.2E+09	2.0E+09	1.8E+09	1.3E+09	1.1E+09
40	5.9E+08	6.2E+08	6.1E+08	6.0E+08	6.0E+08	5.5E+08	4.7E+08	3.7E+08	2.7E+08

June

Latitude	0	10	20	30	40	50	60	70	80
Alt (km)									
130	3.3E+10	3.2E+10	3.2E+10	3.2E+10	3.1E+10	3.0E+10	2.8E+10	2.6E+10	2.5E+10
125	4.4E+10	4.4E+10	4.4E+10	4.4E+10	4.4E+10	4.2E+10	4.0E+10	3.7E+10	3.5E+10
120	6.4E+10	6.4E+10	6.5E+10	6.6E+10	6.6E+10	6.4E+10	6.0E+10	5.6E+10	5.3E+10
115	1.1E+11	1.1E+11	1.1E+11	1.1E+11	1.1E+11	1.1E+11	9.9E+10	9.2E+10	8.7E+10
110	2.0E+11	1.9E+11	1.8E+11	1.7E+11	1.7E+11	1.6E+11	1.4E+11	1.3E+11	1.2E+11
105	3.0E+11	2.9E+11	2.8E+11	2.6E+11	2.4E+11	2.2E+11	2.0E+11	1.8E+11	1.7E+11
100	3.7E+11	3.6E+11	3.6E+11	3.4E+11	3.2E+11	2.9E+11	2.6E+11	2.4E+11	2.3E+11
95	3.4E+11	3.4E+11	3.4E+11	3.4E+11	3.3E+11	3.0E+11	2.8E+11	2.8E+11	2.9E+11
90	1.9E+11	1.9E+11	1.9E+11	2.0E+11	2.1E+11	2.0E+11	2.0E+11	2.1E+11	2.4E+11
85	4.0E+10	4.0E+10	4.5E+10	5.1E+10	5.7E+10	6.1E+10	6.6E+10	7.6E+10	8.9E+10
80	2.5E+10	2.3E+10	2.0E+10	1.7E+10	1.3E+10	1.2E+11	6.2E+09	4.8E+09	4.4E+09
75	5.1E+09	5.0E+09	5.1E+09	5.1E+09	4.9E+09	5.2E+10	4.5E+09	4.3E+09	4.9E+10
70	4.2E+09	4.4E+09	4.5E+09	4.9E+09	4.9E+09	5.1E+09	5.5E+09	5.9E+09	6.2E+09
65	6.0E+09	6.2E+09	6.4E+09	6.1E+09	6.2E+09	6.7E+09	7.2E+09	7.3E+09	7.2E+09
60	7.3E+09	7.4E+09	7.4E+09	7.1E+09	7.0E+09	7.2E+09	7.2E+09	6.9E+09	6.5E+09
55	6.5E+09	6.4E+09	6.3E+09	6.2E+09	6.1E+09	6.0E+09	5.6E+09	5.3E+09	4.8E+09
50	4.6E+09	4.7E+09	4.7E+09	4.6E+09	4.3E+09	4.1E+09	3.7E+09	3.3E+09	2.9E+09
45	2.1E+09	2.1E+09	2.2E+09	2.2E+09	2.1E+09	1.9E+09	1.7E+09	1.4E+09	1.1E+09
40	5.5E+08	5.8E+08	5.8E+08	5.8E+08	5.6E+08	5.2E+08	4.6E+08	3.8E+08	3.0E+08

Table 2: continued

July

Latitude	0	10	20	30	40	50	60	70	80
Alt (km)									
130	3.2E+10	3.1E+10	3.1E+10	3.1E+10	3.0E+10	2.9E+10	2.7E+10	2.6E+10	2.4E+10
125	4.3E+10	4.3E+10	4.3E+10	4.3E+10	4.2E+10	4.1E+10	3.9E+10	3.6E+10	3.4E+10
120	6.3E+10	6.2E+10	6.3E+10	6.4E+10	6.4E+10	6.2E+10	5.9E+10	5.5E+10	5.2E+10
115	1.0E+11	1.0E+11	1.0E+11	1.1E+11	1.1E+11	1.0E+11	9.7E+10	9.0E+10	8.5E+10
110	1.9E+11	1.9E+11	1.8E+11	1.7E+11	1.6E+11	1.5E+11	1.4E+11	1.3E+11	1.2E+11
105	2.9E+11	2.9E+11	2.7E+11	2.5E+11	2.3E+11	2.1E+11	1.9E+11	1.7E+11	1.6E+11
100	3.6E+11	3.6E+11	3.5E+11	3.4E+11	3.1E+11	2.8E+11	2.5E+11	2.4E+11	2.3E+11
95	3.3E+11	3.3E+11	3.4E+11	3.4E+11	3.2E+11	3.0E+11	2.8E+11	2.7E+11	2.8E+11
90	1.9E+11	1.8E+11	1.9E+11	2.0E+11	2.0E+11	2.0E+11	2.0E+11	2.1E+11	2.3E+11
85	3.9E+10	3.9E+10	4.4E+10	4.9E+10	5.5E+10	6.0E+10	6.5E+10	7.4E+10	8.6E+10
80	2.0E+10	2.0E+10	1.8E+10	1.7E+10	1.3E+10	8.9E+09	5.6E+09	4.6E+09	4.3E+09
75	5.2E+09	5.3E+09	5.3E+09	5.1E+09	4.8E+09	4.8E+09	4.2E+09	4.1E+09	4.7E+09
70	4.4E+09	4.3E+09	4.1E+09	4.3E+09	4.9E+09	5.2E+09	5.3E+09	5.8E+09	6.2E+09
65	6.1E+09	6.3E+09	6.3E+09	6.2E+09	6.3E+09	6.6E+09	7.1E+09	7.5E+09	7.4E+09
60	7.3E+09	7.5E+09	7.5E+09	7.3E+09	7.1E+09	7.2E+09	7.2E+09	7.1E+09	6.6E+09
55	6.6E+09	6.6E+09	6.4E+09	6.3E+09	6.0E+09	5.9E+09	5.6E+09	5.2E+09	4.7E+09
50	4.7E+09	4.7E+09	4.7E+09	4.6E+09	4.4E+09	4.0E+09	3.6E+09	3.3E+09	2.9E+09
45	2.1E+09	2.2E+09	2.2E+09	2.1E+09	2.0E+09	1.8E+09	1.6E+09	1.4E+09	1.1E+09
40	5.5E+08	5.7E+08	5.7E+08	5.5E+08	5.3E+08	4.9E+08	4.3E+08	3.6E+08	2.9E+08

August

Latitude	0	10	20	30	40	50	60	70	80
Alt (km)									
130	3.4E+10	3.3E+10	3.3E+10	3.3E+10	3.3E+10	3.1E+10	3.0E+10	2.8E+10	2.7E+10
125	4.6E+10	4.5E+10	4.5E+10	4.6E+10	4.5E+10	4.4E+10	4.1E+10	3.9E+10	3.7E+10
120	6.6E+10	6.6E+10	6.6E+10	6.7E+10	6.7E+10	6.5E+10	6.2E+10	5.8E+10	5.6E+10
115	1.1E+11	1.1E+11	1.1E+11	1.1E+11	1.1E+11	1.1E+11	1.0E+11	9.4E+10	9.0E+10
110	2.0E+11	1.9E+11	1.9E+11	1.8E+11	1.7E+11	1.6E+11	1.5E+11	1.3E+11	1.3E+11
105	3.0E+11	3.0E+11	2.8E+11	2.6E+11	2.4E+11	2.2E+11	2.0E+11	1.9E+11	1.8E+11
100	3.7E+11	3.6E+11	3.6E+11	3.5E+11	3.2E+11	2.9E+11	2.7E+11	2.5E+11	2.5E+11
95	3.4E+11	3.4E+11	3.4E+11	3.4E+11	3.2E+11	3.0E+11	2.9E+11	2.9E+11	2.9E+11
90	1.9E+11	1.8E+11	1.9E+11	1.9E+11	2.0E+11	2.0E+11	2.0E+11	2.0E+11	2.2E+11
85	3.9E+10	3.9E+10	4.3E+10	4.7E+10	5.2E+10	5.5E+10	5.9E+10	6.5E+10	7.1E+10
80	2.0E+10	3.1E+10	2.1E+10	1.9E+10	1.4E+10	1.0E+10	7.0E+09	5.4E+09	5.4E+09
75	5.1E+09	5.2E+09	5.8E+09	5.5E+09	4.8E+09	4.7E+09	4.4E+09	4.3E+09	4.8E+09
70	4.6E+09	4.8E+09	4.7E+08	4.6E+09	4.8E+09	5.2E+09	5.5E+09	5.6E+09	6.0E+09
65	6.1E+09	6.3E+09	6.1E+09	6.1E+09	6.1E+09	6.2E+09	6.6E+09	7.0E+09	7.2E+09
60	7.1E+09	7.1E+09	7.1E+09	7.0E+09	6.9E+09	6.8E+09	6.8E+09	6.8E+09	6.7E+09
55	6.6E+09	6.5E+09	6.2E+09	6.1E+09	5.9E+09	5.7E+09	5.5E+09	5.3E+09	4.9E+09
50	4.8E+09	4.8E+09	4.7E+09	4.7E+09	4.4E+09	4.1E+09	3.7E+09	3.4E+09	3.0E+09
45	2.3E+09	2.3E+09	2.3E+09	2.2E+09	2.0E+09	1.8E+09	1.6E+09	1.3E+09	1.0E+09
40	5.9E+08	6.0E+08	5.8E+08	5.5E+08	5.1E+08	4.6E+08	4.0E+08	3.3E+08	2.8E+08

Table 2: continued

September

Latitude	0	10	20	30	40	50	60	70	80
Alt (km)									
130	3.8E+10	3.8E+10	3.8E+10	3.8E+10	3.8E+10	3.7E+10	3.5E+10	3.3E+10	3.2E+10
125	5.1E+10	5.1E+10	5.2E+10	5.2E+10	5.2E+10	5.0E+10	4.8E+10	4.6E+10	4.4E+10
120	7.4E+10	7.3E+10	7.5E+10	7.6E+10	7.6E+10	7.4E+10	7.1E+10	6.7E+10	6.5E+10
115	1.2E+11	1.2E+11	1.2E+11	1.2E+11	1.2E+11	1.2E+11	1.1E+11	1.1E+11	1.0E+11
110	2.2E+11	2.1E+11	2.1E+11	2.0E+11	1.9E+11	1.8E+11	1.6E+11	1.5E+11	1.5E+11
105	3.3E+11	3.2E+11	3.1E+11	2.9E+11	2.7E+11	2.5E+11	2.3E+11	2.2E+11	2.1E+11
100	4.0E+11	3.9E+11	3.9E+11	3.8E+11	3.5E+11	3.3E+11	3.1E+11	2.9E+11	2.9E+11
95	3.6E+11	3.6E+11	3.6E+11	3.6E+11	3.5E+11	3.3E+11	3.2E+11	3.1E+11	3.1E+11
90	2.0E+11	1.9E+11	1.9E+11	2.0E+11	2.0E+11	2.0E+11	2.0E+11	2.0E+11	2.0E+11
85	4.0E+10	4.1E+10	4.5E+10	4.7E+10	4.9E+10	5.1E+10	5.3E+10	5.4E+10	5.5E+10
80	2.1E+10	2.0E+10	2.2E+10	2.3E+10	8.6E+12	1.9E+10	1.5E+10	1.5E+10	1.2E+10
75	5.5E+09	5.6E+09	5.7E+09	6.0E+09	6.0E+09	6.1E+09	5.7E+09	6.3E+09	7.5E+09
70	4.3E+09	4.6E+09	4.7E+09	4.6E+09	2.0E+10	4.9E+09	5.4E+09	5.6E+09	6.1E+09
65	5.8E+09	5.8E+09	5.7E+09	5.6E+09	5.5E+09	3.3E+05	5.7E+09	6.0E+09	6.5E+09
60	6.7E+09	6.6E+09	6.7E+09	6.5E+09	6.3E+09	4.0E+08	6.4E+09	6.2E+09	6.1E+09
55	6.4E+09	2.2E+12	6.1E+09	6.0E+09	5.8E+09	3.8E+08	5.5E+09	5.4E+09	5.3E+09
50	4.7E+09	4.8E+09	4.7E+09	4.7E+09	4.9E+09	3.7E+08	4.1E+09	3.8E+09	3.1E+09
45	2.3E+09	2.3E+09	2.3E+09	2.2E+09	2.1E+09	3.0E+08	1.6E+09	1.3E+09	9.0E+08
40	6.4E+08	6.3E+08	6.0E+08	5.4E+08	5.0E+08	1.6E+08	3.6E+08	2.7E+08	1.8E+08

October

Latitude	0	10	20	30	40	50	60	70	80
Alt (km)									
130	4.2E+10	4.2E+10	4.3E+10	4.4E+10	4.4E+10	4.3E+10	4.1E+10	4.0E+10	3.9E+10
125	5.6E+10	5.7E+10	5.8E+10	5.9E+10	6.0E+10	5.9E+10	5.7E+10	5.4E+10	5.3E+10
120	8.0E+10	8.1E+10	8.3E+10	8.5E+10	8.6E+10	8.5E+10	8.2E+10	7.9E+10	7.7E+10
115	1.3E+11	1.3E+11	1.3E+11	1.3E+11	1.3E+11	1.3E+11	1.3E+11	1.2E+11	1.2E+11
110	2.4E+11	2.4E+11	2.3E+11	2.2E+11	2.1E+11	2.0E+11	1.9E+11	1.8E+11	1.8E+11
105	3.6E+11	3.6E+11	3.5E+11	3.3E+11	3.1E+11	2.9E+11	2.7E+11	2.6E+11	2.5E+11
100	4.3E+11	4.3E+11	4.3E+11	4.2E+11	4.0E+11	3.7E+11	3.5E+11	3.4E+11	3.3E+11
95	3.9E+11	3.9E+11	3.9E+11	3.9E+11	3.8E+11	3.6E+11	3.5E+11	3.3E+11	3.2E+11
90	2.1E+11	2.1E+11	2.1E+11	2.1E+11	2.1E+11	2.0E+11	2.0E+11	1.9E+11	1.8E+11
85	4.3E+10	4.6E+10	4.9E+10	4.9E+10	4.9E+10	4.8E+10	4.7E+10	4.5E+10	4.3E+10
80	2.5E+10	2.3E+10	2.1E+10	2.4E+10	2.8E+10	2.8E+10	2.6E+10	2.3E+10	1.6E+10
75	6.6E+09	6.0E+09	6.3E+09	6.6E+09	7.3E+09	9.7E+09	1.4E+10	1.6E+10	1.5E+10
70	4.4E+09	4.4E+09	4.7E+09	4.8E+09	5.1E+09	5.2E+09	7.0E+09	1.0E+10	1.1E+10
65	5.1E+09	5.1E+09	6.1E+09	6.0E+09	6.2E+09	6.3E+09	6.7E+09	7.3E+09	0.0E+00
60	6.5E+09	6.4E+09	6.5E+09	6.3E+09	6.1E+09	6.0E+09	1.0E+10	6.7E+09	0.0E+00
55	6.5E+09	6.4E+09	6.8E+09	6.0E+09	5.9E+09	6.0E+09	6.0E+09	6.0E+09	0.0E+00
50	4.7E+09	4.7E+09	4.6E+09	4.6E+09	4.6E+09	4.5E+09	4.4E+09	3.9E+09	3.1E+09
45	2.3E+09	2.2E+09	2.2E+09	2.1E+09	2.0E+09	1.8E+09	1.5E+09	1.1E+09	6.3E+08
40	6.4E+08	6.2E+08	5.7E+08	5.1E+08	4.5E+08	3.8E+08	3.0E+08	2.0E+08	1.0E+08

Table 2: continued

November

Latitude	0	10	20	30	40	50	60	70	80
Alt (km)									
130	4.2E+10	4.3E+10	4.5E+10	4.6E+10	4.7E+10	4.6E+10	4.6E+10	4.5E+10	4.4E+10
125	5.7E+10	5.8E+10	6.1E+10	6.3E+10	6.4E+10	6.4E+10	6.2E+10	6.1E+10	6.0E+10
120	8.2E+10	8.4E+10	8.7E+10	9.0E+10	9.2E+10	9.2E+10	9.0E+10	8.8E+10	8.6E+10
115	1.3E+11	1.4E+11	1.4E+11	1.4E+11	1.4E+11	1.4E+11	1.4E+11	1.4E+11	1.3E+11
110	2.5E+11	2.5E+11	2.4E+11	2.4E+11	2.3E+11	2.2E+11	2.1E+11	2.0E+11	2.0E+11
105	3.7E+11	3.7E+11	3.7E+11	3.5E+11	3.4E+11	3.2E+11	3.0E+11	2.9E+11	2.8E+11
100	4.5E+11	4.5E+11	4.6E+11	4.5E+11	4.3E+11	4.1E+11	3.9E+11	3.7E+11	3.5E+11
95	4.1E+11	4.1E+11	4.2E+11	4.1E+11	4.0E+11	3.8E+11	3.6E+11	3.4E+11	3.2E+11
90	2.3E+11	2.3E+11	2.3E+11	2.2E+11	2.2E+11	2.1E+11	1.9E+11	1.8E+11	1.7E+11
85	4.6E+10	5.0E+10	5.3E+10	5.2E+10	5.0E+10	4.6E+10	4.2E+10	3.8E+10	3.6E+10
80	2.8E+10	2.9E+10	2.6E+08	2.9E+10	3.2E+10	3.3E+10	2.9E+10	0.0E+00	0.0E+00
75	6.6E+09	6.5E+09	6.8E+09	8.3E+09	9.9E+09	1.4E+10	1.6E+10	0.0E+00	0.0E+00
70	4.4E+09	4.3E+09	4.5E+09	5.3E+09	6.1E+09	7.7E+09	1.1E+10	0.0E+00	0.0E+00
65	5.2E+09	5.3E+09	5.9E+09	6.6E+09	6.9E+09	7.4E+09	8.1E+09	0.0E+00	0.0E+00
60	6.8E+09	6.7E+09	6.3E+09	6.5E+09	6.2E+09	6.3E+09	7.3E+09	0.0E+00	0.0E+00
55	6.6E+09	6.5E+09	5.9E+09	6.1E+09	6.1E+09	6.2E+09	0.0E+00	0.0E+00	0.0E+00
50	4.7E+09	4.5E+09	4.1E+09	4.5E+09	4.4E+09	4.5E+09	4.4E+09	3.0E+09	0.0E+00
45	2.2E+09	2.1E+09	2.0E+09	2.0E+09	1.9E+09	1.6E+09	1.2E+09	6.0E+08	0.0E+00
40	6.3E+08	5.8E+08	5.3E+08	4.7E+08	3.9E+08	3.1E+08	2.2E+08	1.1E+08	0.0E+00

December

Latitude	0	10	20	30	40	50	60	70	80
Alt (km)									
130	3.9E+10	4.1E+10	4.3E+10	4.5E+10	4.6E+10	4.6E+10	4.6E+10	4.5E+10	4.5E+10
125	5.4E+10	5.6E+10	5.9E+10	6.1E+10	6.3E+10	6.3E+10	6.3E+10	6.2E+10	6.1E+10
120	7.8E+10	8.0E+10	8.4E+10	8.8E+10	9.0E+10	9.1E+10	9.0E+10	8.9E+10	8.8E+10
115	1.3E+11	1.3E+11	1.3E+11	1.4E+11	1.4E+11	1.4E+11	1.4E+11	1.4E+11	1.4E+11
110	2.4E+11	2.4E+11	2.4E+11	2.3E+11	2.3E+11	2.2E+11	2.1E+11	2.1E+11	2.0E+11
105	3.6E+11	3.7E+11	3.6E+11	3.6E+11	3.4E+11	3.3E+11	3.1E+11	3.0E+11	2.9E+11
100	4.4E+11	4.5E+11	4.6E+11	4.5E+11	4.3E+11	4.1E+11	3.9E+11	3.7E+11	3.5E+11
95	4.1E+11	4.2E+11	4.2E+11	4.2E+11	4.0E+11	3.8E+11	3.6E+11	3.3E+11	3.1E+11
90	2.3E+11	2.3E+11	2.3E+11	2.3E+11	2.2E+11	2.0E+11	1.8E+11	1.7E+11	1.6E+11
85	4.8E+10	5.2E+10	5.5E+10	5.3E+10	4.9E+10	4.4E+10	3.8E+10	3.5E+10	3.2E+10
80	2.3E+10	2.4E+10	2.5E+10	2.6E+10	3.1E+10	3.3E+10	0.0E+00	0.0E+00	0.0E+00
75	5.8E+09	5.9E+09	6.8E+09	9.0E+09	1.2E+10	1.6E+10	0.0E+00	0.0E+00	0.0E+00
70	4.6E+09	4.4E+09	4.7E+09	5.8E+09	7.2E+09	1.0E+10	0.0E+00	0.0E+00	0.0E+00
65	5.9E+09	5.8E+09	5.8E+09	2.0E+10	8.1E+09	8.6E+09	0.0E+00	0.0E+00	0.0E+00
60	7.4E+09	7.2E+09	6.9E+09	6.8E+09	6.3E+09	8.1E+09	0.0E+00	0.0E+00	0.0E+00
55	6.9E+09	6.7E+09	6.2E+09	5.8E+09	5.7E+09	6.6E+09	0.0E+00	0.0E+00	0.0E+00
50	4.8E+09	4.6E+09	4.3E+09	4.1E+09	3.8E+09	3.4E+09	3.2E+09	0.0E+00	0.0E+00
45	2.2E+09	2.1E+09	1.9E+09	1.7E+09	1.5E+09	1.1E+09	7.1E+08	0.0E+00	0.0E+00
40	6.0E+08	5.5E+08	5.0E+08	4.2E+08	3.2E+08	2.2E+08	1.3E+08	0.0E+00	0.0E+00

12

NUMERICAL SIMULATIONS OF THE SEASONAL/LATITUDINAL VARIATIONS OF ATOMIC OXYGEN AND NITRIC OXIDE IN THE LOWER THERMOSPHERE AND MESOSPHERE

D. Rees and T. J. Fuller-Rowell

Department of Physics and Astronomy, University College London
Gower Street, London WC1E 6BT, United Kingdom

ABSTRACT:

A 2-Dimensional zonally-averaged thermospheric model and the global UCL thermospheric model have been used to investigate the seasonal, solar activity and geomagnetic variation of atomic oxygen and nitric oxide. The 2-Dimensional model includes detailed oxygen and nitrogen chemistry, with appropriate completion of the energy equation, by adding the thermal infrared cooling by [O] and [NO]. This solution includes solar and auroral production of odd nitrogen compounds and metastable species. This model has been used for three investigations: firstly, to study the interactions between atmospheric dynamics and minor species transport and density, secondly, to examine the seasonal variations of atomic oxygen and nitric oxide within the upper mesosphere and thermosphere and their response to solar and geomagnetic activity variations; thirdly, to study the factor of 7 - 8 peak nitric oxide density increase as solar $F_{10.7}$ cm flux increases from 70 to 240 reported from the Solar Mesospheric Explorer. Auroral production of [NO] is shown to be the dominant source at high latitudes, generating peak [NO] densities a factor of 10 greater than typical number densities at low latitudes. At low latitudes, the predicted variation of the peak [NO] density, near 110 km, with the solar $F_{10.7}$ cm flux is rather smaller than is observed. This is most likely due to an overestimate of the soft X-ray flux at low solar activity, for times of extremely low sunspot number, as occurred in June 1986. As observed on pressure levels, the variation of [O] density is small. The global circulation during solstice and periods of elevated geomagnetic activity causes depletion of [O] in regions of upwelling, and enhancements in regions of downwelling.

INTRODUCTION.

This paper provides a brief review of some two and three-dimensional model studies of the inter-relationships between the major and minor species of the lower thermosphere and upper mesosphere. Several timely questions are addressed by the model simulations. The data from the Solar Mesospheric Explorer (SME /1/) show a factor of about 7 - 8 variation of peak low-latitude number density as the solar $F_{10.7}$ cm flux increases from 70 to 240 units, compared with a variation of approximately a factor of 4 found in previous numerical studies /2/. The degree of possible variability of atomic oxygen number densities in the lower thermosphere and upper mesosphere consistent with major meteorological, seasonal and geomagnetic variability of the atmosphere is also of interest. Previous studies (for example a special issue of Planetary and Space Science, 1988) have shown up to a factor of at least 100 variability in the density of atomic oxygen at and below the peak density of the species, normally observed around 105 km.

ATOMIC OXYGEN AND NITRIC OXIDE: KEY MINOR CONSTITUENTS.

Atomic oxygen is created by the photodissociation of molecular oxygen within the thermosphere. Having approximately half the molecular mass of O_2 and N_2, its scale height is double that of O_2 and N_2 for the same temperature. Since recombination is very slow at middle and upper thermospheric densities and collision rates and if diffusive equilibrium prevails, [O] becomes the major constituent above around 150 km /3,4,5,6/. Given the long recombination time, the species can be transported globally by mean winds. When large-scale upwelling and advection occurs, particularly at solstice, and also associated with the intense large-scale heating during geomagnetic storms, diffusive equilibrium no longer fully controls the vertical profiles of [O] and [N_2, O_2]. Under such conditions /7,8/, the process known as wind-driven diffusion may cause large relative departures of individual light or heavy species from diffusive equilibrium, although hydrostatic equilibrium will

still be generally observed. Relative to density values which would be expected for the appropriate kinetic temperature, N_2 is strongly enhanced in regions of persistent upwelling and outflow, where atomic oxygen is strongly depleted. In regions of persistent convergence and downwelling, the converse is true. The major direct consequences are an excess of molecular nitrogen at the summer pole, particularly at times of high geomagnetic activity, while the winter pole (at quiet times) and winter mid-latitudes (under more disturbed conditions) contains the highest densities of atomic oxygen and helium.

These perturbations of minor species density extend to lower thermosphere altitudes, and wind-driven diffusion is one significant cause of variability of atomic oxygen in the lower thermosphere. Eddy diffusion can also cause vertical transport of minor species, and can change the vertical profile of atomic oxygen and other minor constituents /8/.

Nitric Oxide is primarily created through the reaction of the atomic nitrogen species $N(^2D)$ and $N(^4S)$ with molecular oxygen /3,9/. $N(^2D)$ and $N(^4S)$ are produced by auroral dissociation /10/, by photodissociation /11/ and various ion chemical reactions involving N_2^+ /12/.

Although nitric oxide is chemically and radiatively active, its chemical lifetime in the lower thermosphere is long enough for wind transport to be important. Its diffusion into the mesosphere is also important, and it has been shown /13/ that in the winter polar stratosphere, it also has a long effective lifetime in non-sunlit regions. Increased production, at times of high solar activity, or associated with enhanced auroral production during geomagnetic storms, may create very large lower thermospheric densities of [NO]. Given enhanced vertical transport due to turbulence, this may result in large [NO] densities in the mesosphere and even in the upper stratosphere at winter high-latitudes, where there is no solar photodestruction of nitric oxide. There are a number of major consequences of such enhancements, affecting the chemical and radiative balance of the mesosphere and thermosphere, and properties of the ionosphere.

THE NUMERICAL MODEL.

The three-dimensional atmospheric model has been well-described in a number of papers, including Fuller-Rowell and Rees /14,15/ and Fuller-Rowell et al /16/. The zonally-averaged model evolved from the nested grid model of Fuller-Rowell /17/ and is further described in Rees and Fuller-Rowell /8/.

The seasonal, latitudinal and solar activity variations of atomic oxygen density will be considered, as will the response to variable geomagnetic forcing at high geomagnetic latitude. Large-scale Hadley-type circulation cells are generated within the thermosphere, closing in the upper mesosphere, as the result of the solar diurnal heating variation, the seasonal / hemispheric asymmetry of solar heating, and due to geomagnetic heating, usually at high latitudes. These large-scale circulation systems force a partial breakdown of diffusive equilibrium as the result of the combination of vertical convection and horizontal advection. The full 3-dimensional global coupled ionosphere - thermosphere UCL model will be used for these simulations /14,15,16/.

A second series of simulations uses the zonally-averaged 2-dimensional model. Nitric oxide and other 'odd nitrogen' compounds are included as minor species. With this model, it is possible to examine, in addition, the seasonal, latitudinal, solar activity and geomagnetic response of [NO]. It is also possible to evaluate the transport and thermal effects of variable eddy turbulence within the lower thermosphere and upper mesosphere. The model takes into account the thermal radiation from nitric oxide, which has very important effects on the thermal balance, and consequences for the mean circulation.

The two-dimensional, zonally-averaged model of the thermosphere solves the non-linear energy, momentum, continuity and three-constituent composition equation self-consistently and time-dependently. The finite-difference grid covers the latitude range from the north to the south geographic pole in steps of 5^o latitude, and the seventeen pressure levels, one scale height apart, cover altitudes from 70km to approximately 500km, depending on solar activity. The model has been adapted from the high-resolution, nested-grid model of Fuller-Rowell /17/, which contains a complete description of the numerical procedure, the set of equations, boundary conditions and parameterisation required to simulate the thermospheric neutral wind, temperature and density. The same paper also describes the photochemistry, and the dissociation and recombination rate constants included in the computation of the mass mixing ratio of the major species of atomic oxygen, and of molecular nitrogen and oxygen.

A further addition has been made to the model to include the production, loss and transport of $N(^2D)$, $N(^4S)$, and NO (Nitric Oxide). The evolution of the concentrations of these minor species are computed self-consistently in parallel with the development of the structure, dynamics and energy budget of the major species. The creation of nitric oxide occurs through the odd-nitrogen chemistry primarily through the reactions of $N(^2D)$ and $N(^4S)$ with molecular

oxygen. The $N(^2D)$ and $N(^4S)$ are produced by ion chemical reactions involving N_2^+, and by direct dissociation of N_2 by auroral particles /10/ or solar radiation /11/. The odd-nitrogen chemistry, branching ratios, and rate coefficients, included in the model are as described in Roble et al /2/.

All three production sources of atomic nitrogen are included in the zonally averaged model. The sources of $N(^2D)$ and $N(^4S)$ through the ion chemical reactions are evaluated within the UCL-Sheffield coupled thermosphere-ionosphere model. The reference spectra appropriate for high and low solar activity, together with the ionisation frequencies of the major species, are taken from Torr et al /18/. The solar production function thus produced is used within the zonally averaged code, where solution of the odd nitrogen chemistry and transport proceeds in parallel with that of the dynamics, energy budget and composition of the major species.

The particle precipitation source is derived from the TIROS/NOAA satellite data /19/ and is used to describe the high-latitude auroral heating rate, ionization rate, and molecular nitrogen dissociation /10/, self-consistently within the model. The direct particle heating acts in addition to the Joule dissipation which together modify the global circulation pattern. The circulation, which transports and mixes the major species and is described fully in Fuller-Rowell /17/, also acts as a source of transport to the minor species. The distribution of nitric oxide, as a strong radiative cooler /9/, has a strong influence on the latitudinal temperature gradient, and on the global mean thermospheric temperature as has been shown by Roble and Emery /20/. The latitudinal distribution of temperature and NO, and the global circulation pattern, is a highly coupled and interacting system of variables.

The auroral precipitation also produces ionization which enhances the ion densities above the quiet background levels described by Chiu /21/. This additional source of ionization has been included, where the auroral enhancement is assumed to be in chemical equilibrium, and is added to the background solar-produced values of Chiu /21/ by the square root of the sum of the squares. This is a less sophisticated approach than is used in the 3-D fully-coupled ionosphere - thermosphere model, but produces an overall result which is adequate for the purposes of these 2-D simulations, where we are not yet concerned with the details of the ionospheric predictions.

RESULTS OF THE SIMULATIONS.

Global distributions with seasonal, latitudinal and geomagnetic variations.

Figure 1 shows the global distributions of temperature, mean molecular mass, atomic oxygen density and molecular nitrogen density at pressure level 7 (125 km) of the UCL three-dimensional, time-dependent model (E-Region, approximately 125 km). The seasonal / latitudinal variation of atomic oxygen density shows a very distinct minimum at the summer pole, and a maximum at the winter pole. For moderately active solar ($F_{10.7}$ = 185), and quiet geomagnetic activity conditions, there is a factor of more than 2 variation of E-region atomic oxygen density from global minimum to global maximum. This simulation includes the effect of lower atmosphere tides introduced via lower boundary forcing /22/.

Figure 2 shows the global distributions of temperature, mean molecular mass, atomic oxygen density and molecular nitrogen density at pressure level 12 of the UCL three-dimensional, time-dependent model (F-Region, approximately 320 km). There is a very large seasonal / latitudinal variation of atomic oxygen density. The minimum oxygen density is at the summer pole, however, the maximum values are displaced from the winter pole, towards high winter mid-latitudes, as a result of high-latitude energy input. This simulation is for moderately active solar ($F_{10.7}$ = 185), and moderately disturbed geomagnetic activity conditions (Kp = 3). Atomic oxygen number density varies by more than a factor of 6 from global minimum to global maximum, consistent with empirical model results /16/.

Figure 3 shows the global distributions of temperature, mean molecular mass, atomic oxygen density and molecular nitrogen density at pressure level 7 of the UCL three-dimensional, time-dependent model (E-Region, approximately 125 km) taken from the same simulation as that shown in Figure 2. It shows that a similar, if somewhat smaller seasonal / latitudinal variation of atomic oxygen density occurs at the lower altitudes. The minimum oxygen density is again at the summer pole and, as at F-region altitudes, the maximum values are displaced from the winter pole, towards high winter mid-latitudes, as a result of high-latitude energy input. There is a surprisingly large variation of atomic oxygen density from global minimum to global maximum, about a factor of 5, resulting from the seasonal asymmetry of solar insolation, combined with the high-latitude geomagnetic energy input. This factor of 5 atomic oxygen density variation at~125 km altitude greatly exceeds the latitudinal / seasonal total density variation. It is necessary to recall that the majority of species density profiles are measured with sole reference to geometric altitude, and no reference to pressure level or to total gas density.

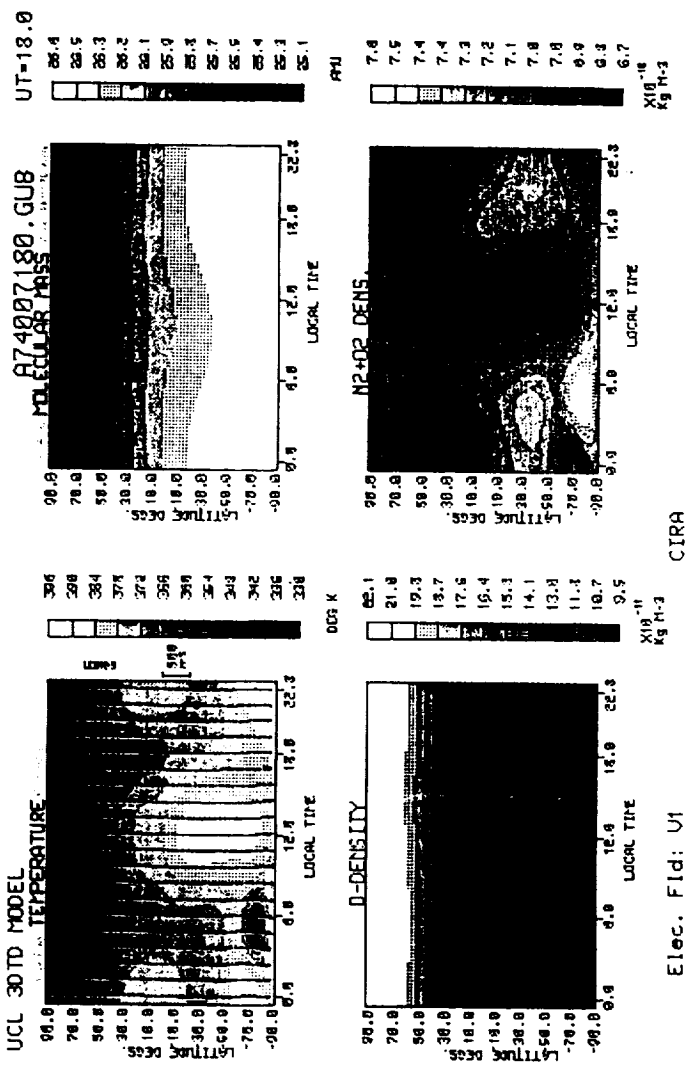

FIGURE 1. Pressure level 7 of the UCL three-dimensional, time-dependent model (E-REGION, approximately 125 km) for moderately active solar conditions ($F_{10.7}$ = 185) and quiet geomagnetic activity conditions. There is a factor of more than 2 variation of E-region atomic oxygen density from global minimum to global maximum.

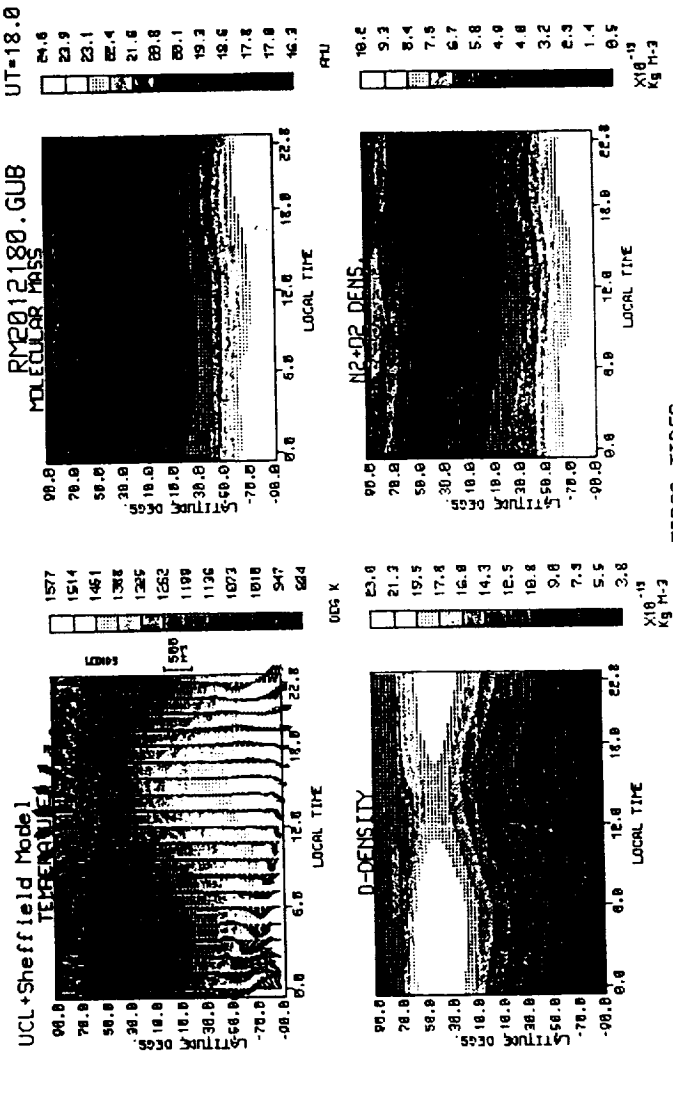

FIGURE 2. Pressure level 12 of the UCL three-dimensional, time-dependent model (F-REGION, approximately 320 km) from a simulation for moderately disturbed geomagnetic activity conditions, and for moderately active solar conditions ($F_{10.7}$ = 185). The minimum oxygen density is at the summer pole, but the maximum values are displaced from the winter pole, towards high winter mid-latitudes.

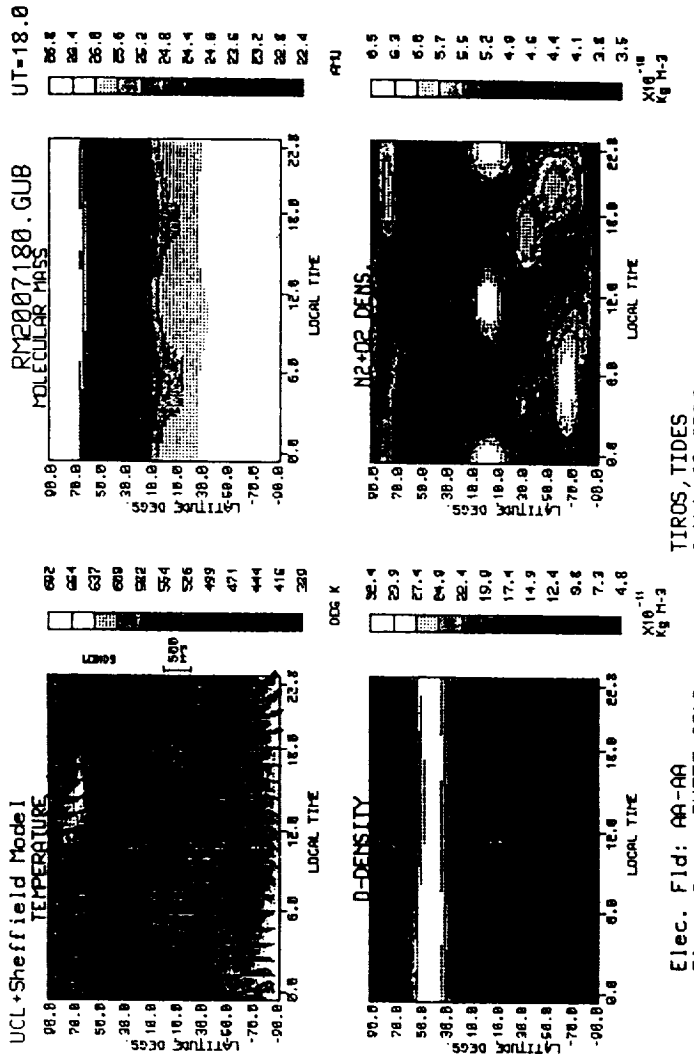

FIGURE 3. Pressure level 7 of the UCL three-dimensional, time-dependent model (E-REGION, approximately 125 km) for the same simulation as that shown in Figure 2. The minimum oxygen density is again at the summer pole and, as at F-region altitudes, however, the maximum values are displaced from the winter pole, towards high winter mid-latitudes.

Latitudinal distributions for equinox and variations with solar and geomagnetic activity.

Figure 4 shows variations of atmospheric structure and composition as a function of altitude and latitude simulated using the two-dimensional, time-dependent model. Panel A shows the density distributions of atomic oxygen, nitric oxide, molecular oxygen and molecular nitrogen. Panel B shows Temperature, Meridional and vertical neutral wind, and mean molecular mass. Panel C displays nitric oxide density distribution from 100 to 160 km, for comparison with the results obtained from SME /1/. The conditions depicted are equinox, low solar ($F_{10.7}$ cm = 80) and low geomagnetic (Kp = 1) activity. There is a weak latitudinal variation of atomic oxygen density, caused by the high-latitude geomagnetic energy inputs. Nitric oxide density is structured by two peaks, one at low-latitudes, due to solar production, and the other in the auroral oval, resulting from auroral particle dissociation.

Figure 5 shows variations of atmospheric structure and composition as a function of altitude and latitude simulated using the two-dimensional, time-dependent model. The displays are as for Figure 4. The conditions simulated are low solar ($F_{10.7}$ cm = 80) and moderate geomagnetic activity (Kp = 3), at equinox. There is now a small latitudinal variation of atomic oxygen density, with decreased density in regions of increased high-latitude geomagnetic energy inputs. The major feature in nitric oxide density is the enhanced high-latitude peaks, resulting from increased auroral production. There is a ratio of about 4:1 between low-latitude and high latitude values of nitric oxide.

Figure 6 shows variations of atmospheric structure and composition as a function of altitude and latitude simulated using the two-dimensional, time-dependent model. The displays are as for Figure 4. The conditions which are simulated are low solar ($F_{10.7}$ cm = 80) and high geomagnetic activity (Kp =5), at equinox. The latitudinal variation is further enhanced. Atomic oxygen is further depleted, and molecular nitrogen further enhanced, in those regions which correspond to the enhanced auroral energy and particle inputs. Nitric oxide densities vary by an order of magnitude from low to high latitudes. The broad latitude extension of elevated nitric oxide densities correspond mainly to the extended regions of energetic particle precipitation described by the statistical models of energetic electron precipitation. Marked changes of nitric oxide extend to the lower altitude limits (70 km) of the model, while significant changes of atomic oxygen density extend below 86 km. These low-altitude disturbances are primarily due to intense geomagnetic energy inputs within the auroral oval.

Figure 7 shows variations of atmospheric structure and composition as a function of altitude and latitude simulated using the two-dimensional, time-dependent model. The displays are as for Figure 4. The conditions which are simulated are high solar activity ($F_{10.7}$ cm = 200), and low geomagnetic activity (Kp = 2) at equinox. There are considerable enhancements of molecular nitrogen, molecular oxygen and nitric oxide densities and a marked decrease of atomic oxygen density within both auroral ovals. At this high level of solar activity, the low latitude values of nitric oxide density are considerably increased, by about a factor of 4, compared with those for low solar activity ($F_{10.7}$ cm = 80). This factor is smaller than the factor of 7 - 8 reported for the same range of solar activity by Barth /1/. This apparent discrepancy will be discussed in the following section. Even at high solar activity, the low latitude values remain below the peak auroral oval values, except for very quiet geomagnetic conditions, Kp = 1 or lower. This indicates that except for prolonged periods of geomagnetic quiet during periods of high solar radio and UV / EUV fluxes, high latitude peaks, corresponding to enhanced auroral production, will still be a distinctive feature of the global distribution of nitric oxide.

Latitudinal distributions for solstice.

Figure 8 shows variations of atmospheric structure and composition as a function of altitude and latitude simulated using the two-dimensional, time-dependent model. The displays are as for Figure 4. The conditions which are simulated are moderately high solar activity ($F_{10.7}$ cm = 150), and low geomagnetic activity (Kp = 2) at the December solstice. A significant seasonal / latitudinal asymmetry develops in the distribution of all constituents. There is a large summer high latitude enhancement of molecular nitrogen and of nitric oxide, and depletion of atomic oxygen. For nitric oxide, there is approximately a factor of 50 % summer high latitude enhancement, the combination of solar and auroral production. For atomic oxygen and molecular nitrogen, the behaviour in the summer and winter hemispheres is quite opposite, due to the influence of global, pole to pole circulation. For nitric oxide, there is still an enhancement in the winter auroral oval, as well as the rather larger enhancement in the summer auroral oval.

DISCUSSION.

Atomic oxygen in the upper thermosphere shows large seasonal / latitudinal variations in response to asymmetric solar insolation. Such variations have been well known for many years, and have now been successfully simulated by theoretical and numerical modelling.

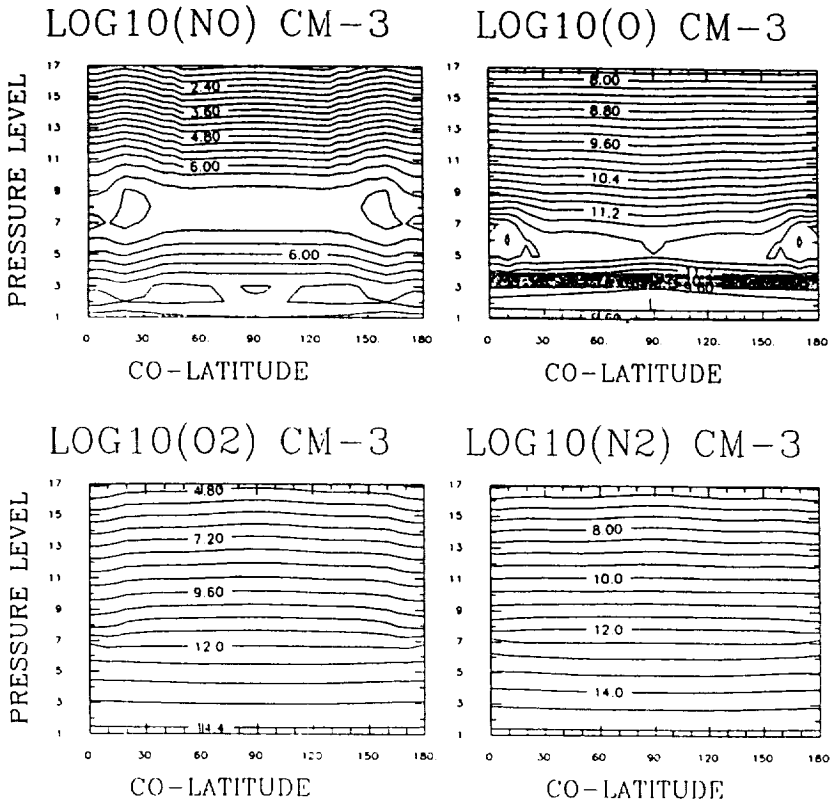

Figure 4. Variations of atmospheric structure and composition as a function of altitude and latitude, simulated using the UCL two-dimensional, time-dependent model. Panel A shows the density distributions of atomic oxygen, nitric oxide, molecular oxygen and molecular nitrogen. Panel B shows temperature, meridional and vertical neutral wind, and mean molecular mass. The conditions depicted are equinox, low solar ($F_{10.7}$ cm = 80) and low geomagnetic activity (Kp = 1). Panel C depicts the distribution of nitric oxide between 100 and 160 km, for direct comparison with the data from SME.

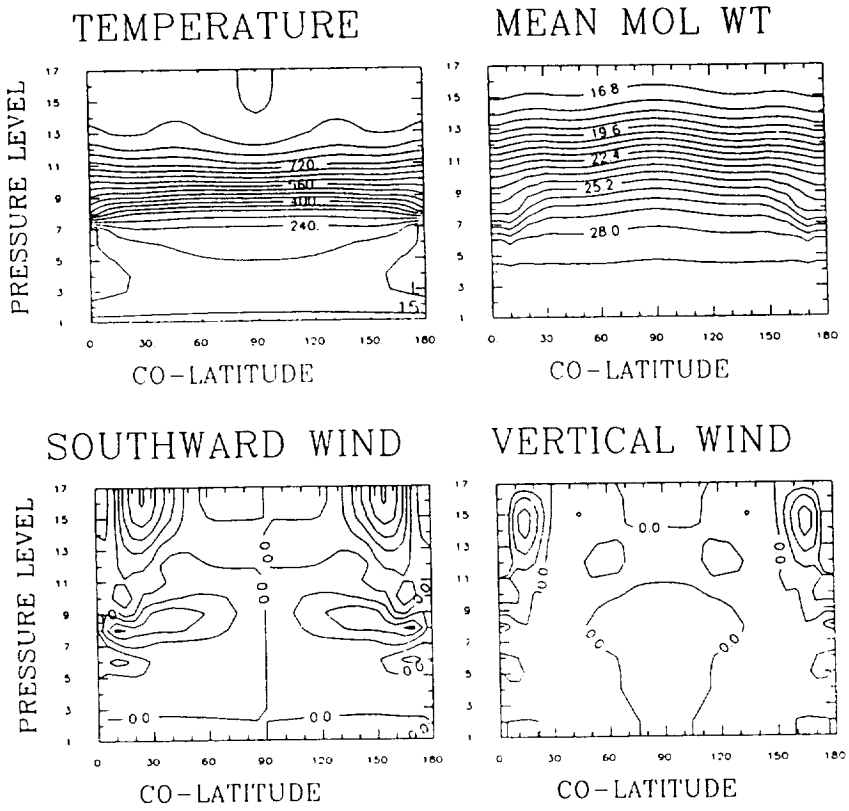
TEMPERATURE
MEAN MOL WT
PRESSURE LEVEL
720.
300.
240.
15.
16.8
19.6
22.4
25.2
28.0
CO-LATITUDE
CO-LATITUDE
SOUTHWARD WIND
VERTICAL WIND
PRESSURE LEVEL
0.0
0.0
0.0
CO-LATITUDE
CO-LATITUDE

Figure 4B.

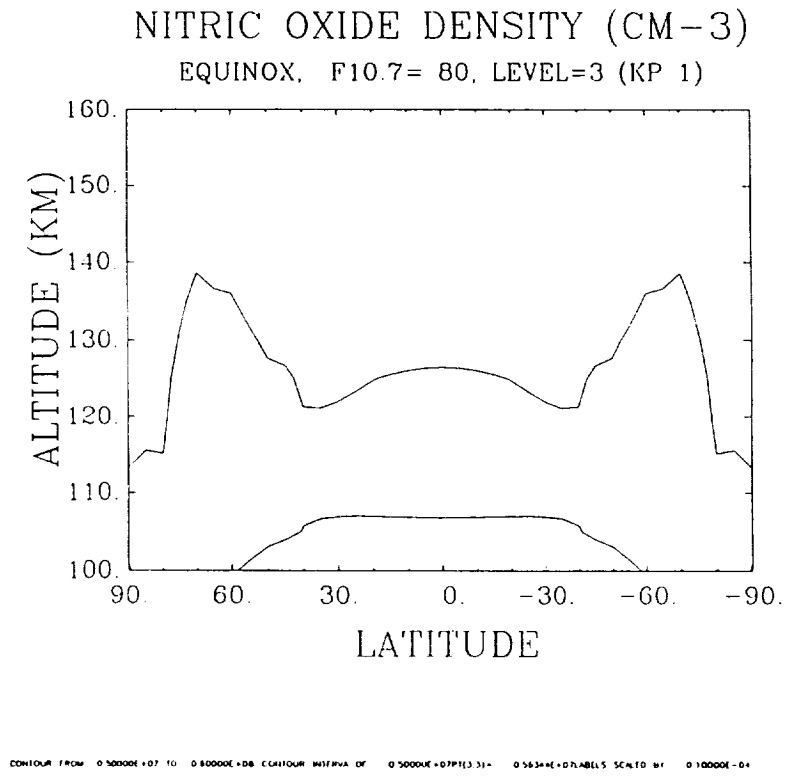
NITRIC OXIDE DENSITY (CM-3)
EQUINOX, F10.7= 80, LEVEL=3 (KP 1)
ALTITUDE (KM)
160.
150.
140.
130.
120.
110.
100.
90.
60.
30.
0.
-30.
-60.
-90.
LATITUDE

Figure 4C.

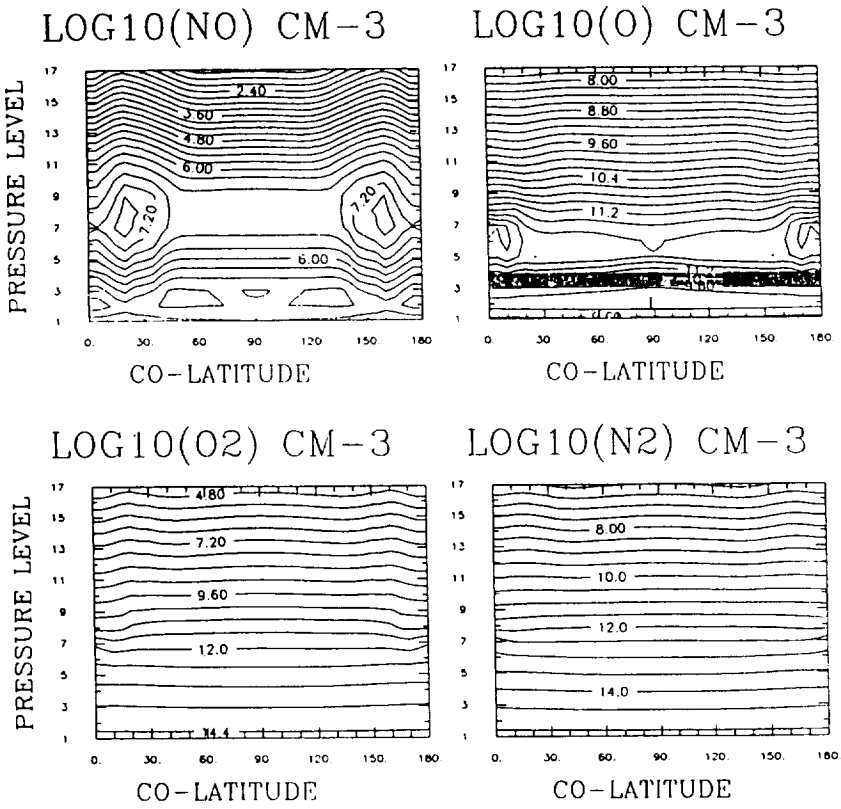

Figure 5. Variations of atmospheric structure and composition as a function of altitude and latitude simulated using the two-dimensional, time-dependent model. The display is as for Figure 4. The conditions simulated are low solar ($F_{10.7}$ cm = 80) and moderate geomagnetic activity (Kp = 3) at equinox.

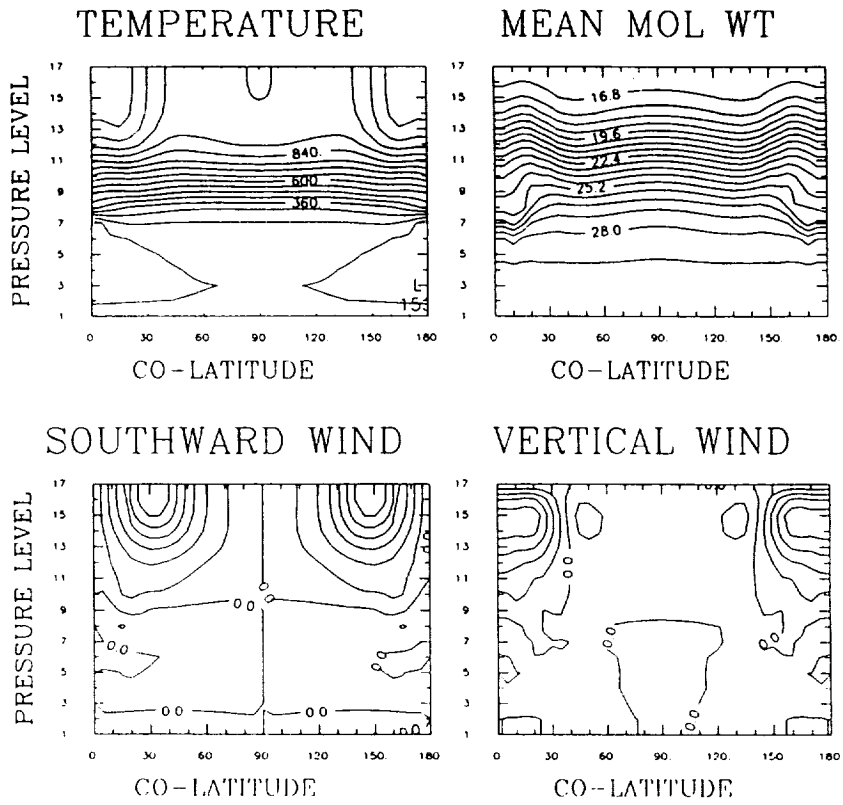
TEMPERATURE
MEAN MOL WT
PRESSURE LEVEL
840.
600
360
15
16.8
19.6
22.4
25.2
28.0
CO-LATITUDE
CO-LATITUDE
SOUTHWARD WIND
VERTICAL WIND
PRESSURE LEVEL
0.0
CO-LATITUDE
CO-LATITUDE

Figure 5B.

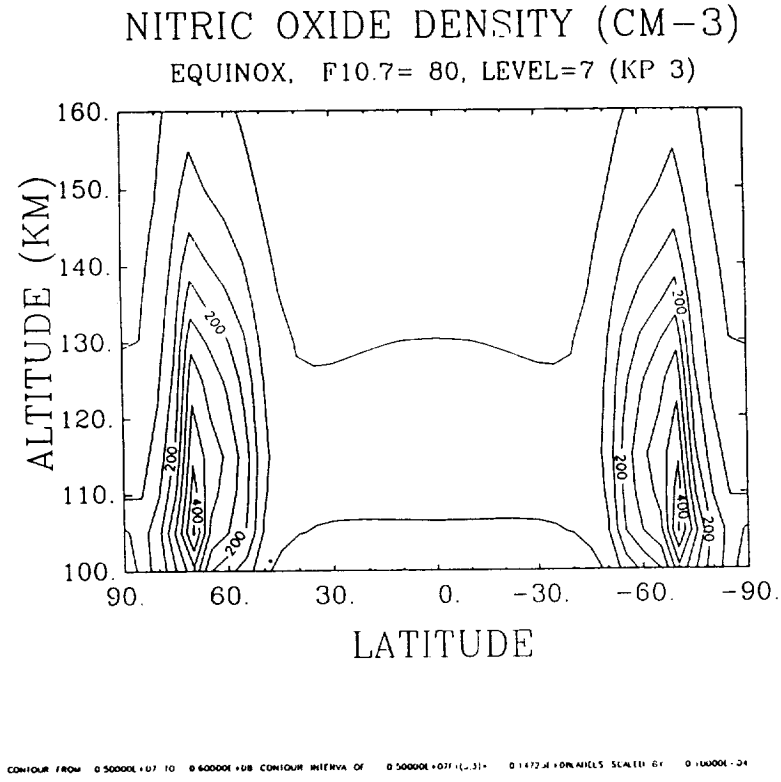
NITRIC OXIDE DENSITY (CM-3)
EQUINOX, F10.7= 80, LEVEL=7 (KP 3)
ALTITUDE (KM)
160.
150.
140.
130.
120.
110.
100.
90.
60.
30.
0.
-30.
-60.
-90.
LATITUDE
200
100

Figure 5C.

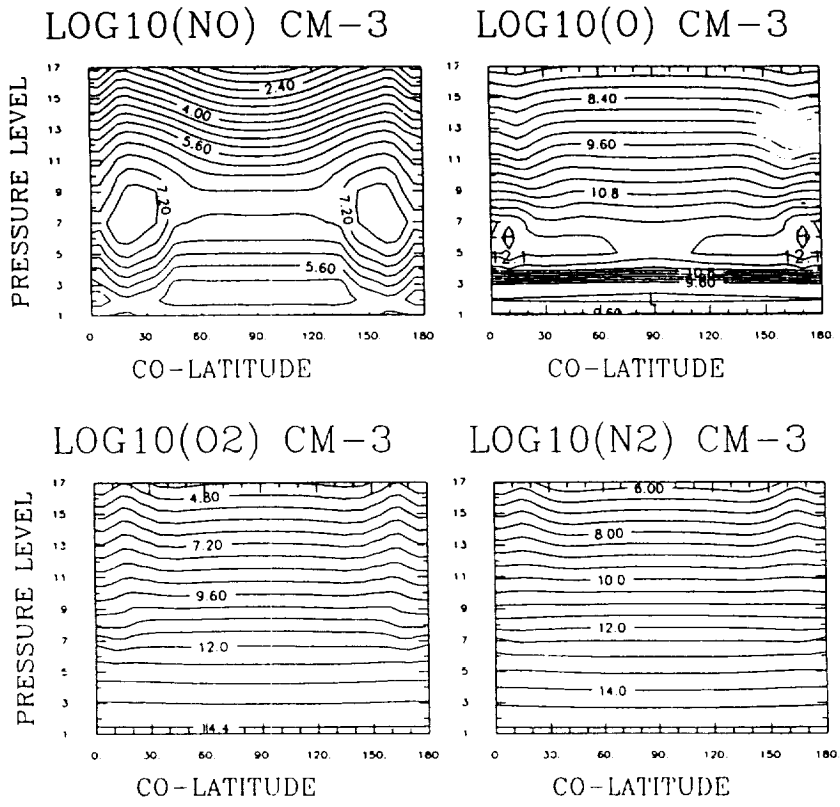

Figure 6. Variations of atmospheric structure and composition as a function of altitude and latitude simulated using the two-dimensional, time-dependent model. The display is as for Figure 4. The conditions which are simulated are low solar ($F_{10.7}$ cm = 80) and moderately high geomagnetic activity (Kp = 5) at equinox.

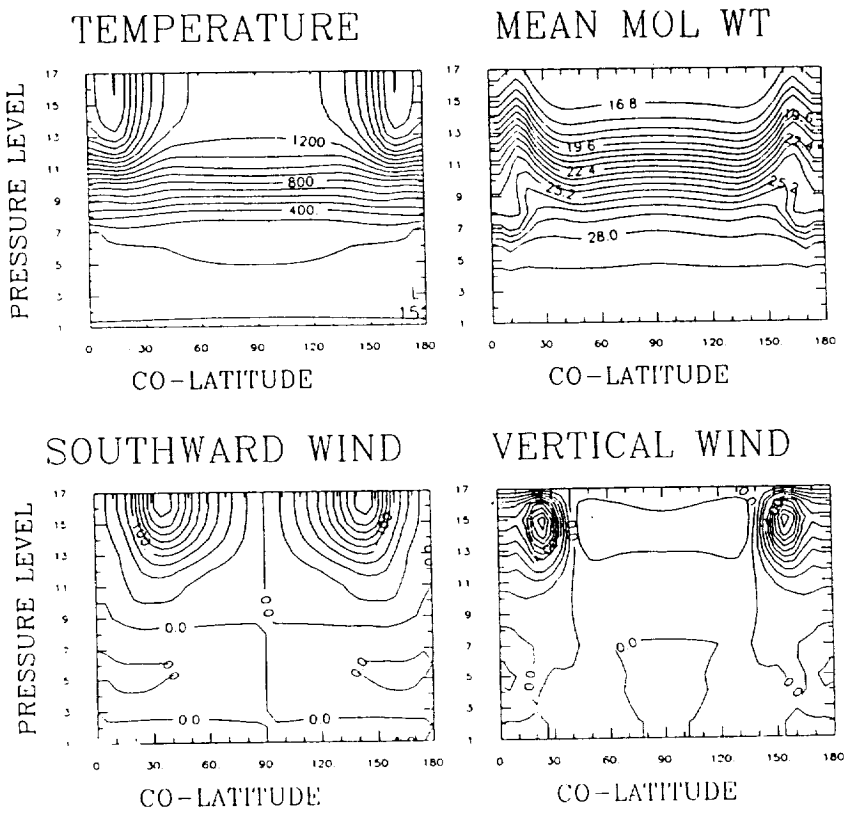
TEMPERATURE
MEAN MOL WT
PRESSURE LEVEL
1200
800
400
168
196
224
252
280
CO-LATITUDE
CO-LATITUDE
SOUTHWARD WIND
VERTICAL WIND
PRESSURE LEVEL
0.0
0.0
0.0
CO-LATITUDE
CO-LATITUDE

Figure 6B.

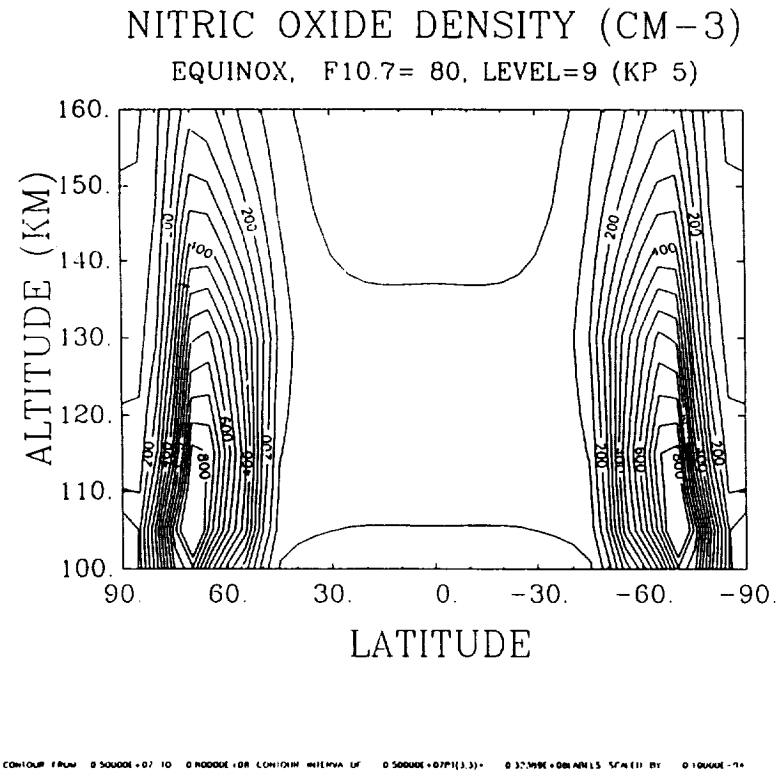
NITRIC OXIDE DENSITY (CM-3)
EQUINOX, F10.7= 80, LEVEL=9 (KP 5)
ALTITUDE (KM)
160.
150.
140.
130.
120.
110.
100.
90.
60.
30.
0.
-30.
-60.
-90.
LATITUDE

Figure 6C.

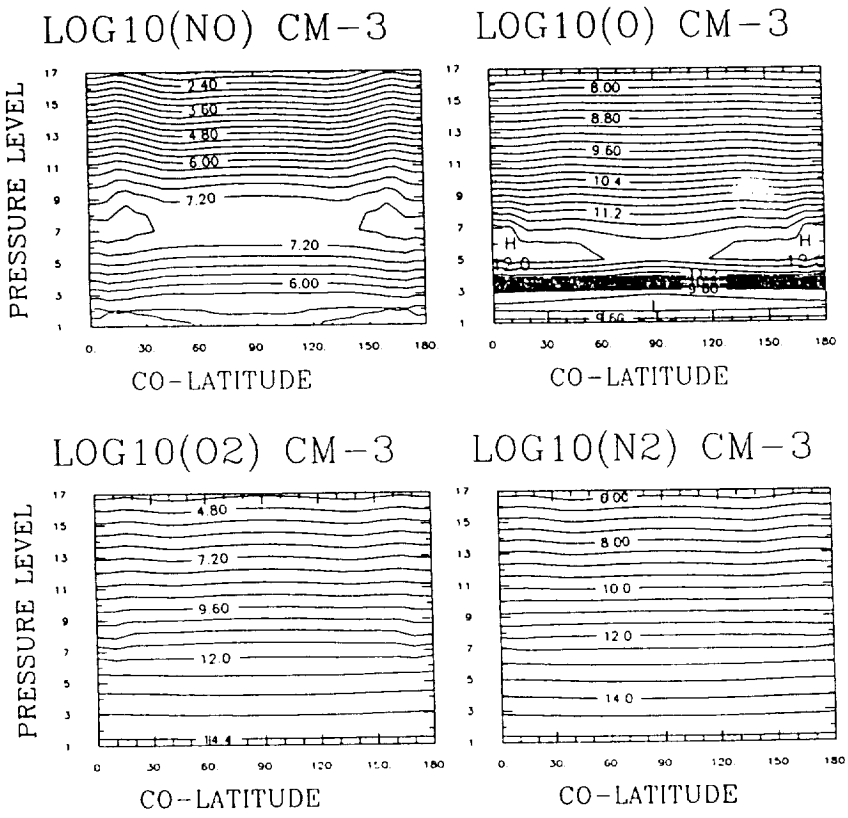

Figure 7. Variations of atmospheric structure and composition as a function of altitude and latitude simulated using the two-dimensional, time-dependent model. the display is as for Figure 4. The conditions which are simulated are high solar ($F_{10.7}$ cm = 200) and low geomagnetic activity (Kp = 2) at equinox.

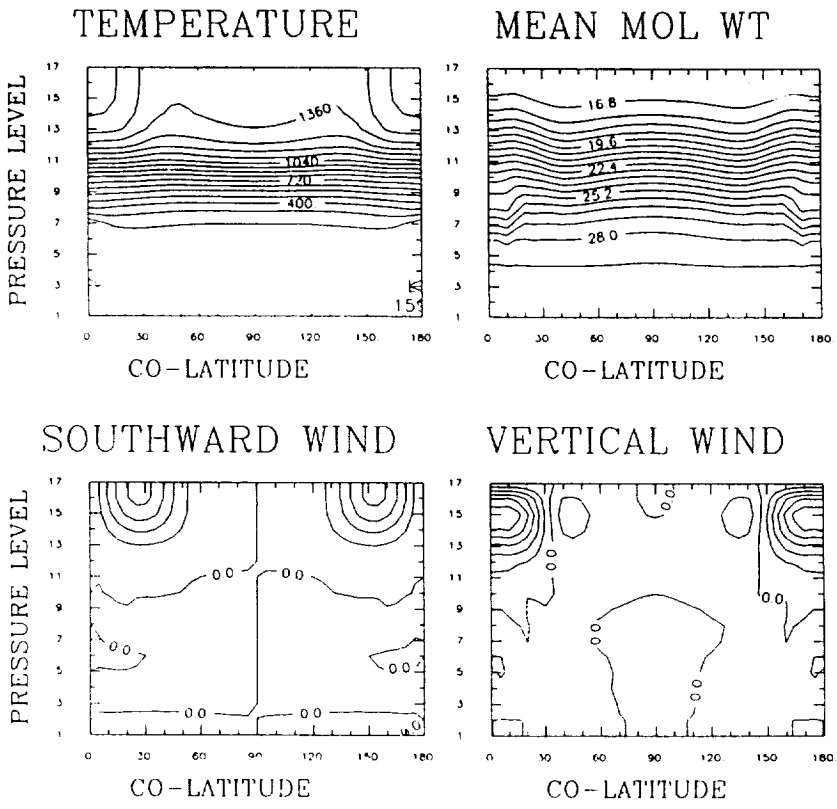
TEMPERATURE
MEAN MOL WT
PRESSURE LEVEL
CO-LATITUDE
1360
1040
720
400
15
16.8
19.6
22.4
25.2
28.0
SOUTHWARD WIND
VERTICAL WIND
0.0

Figure 7B.

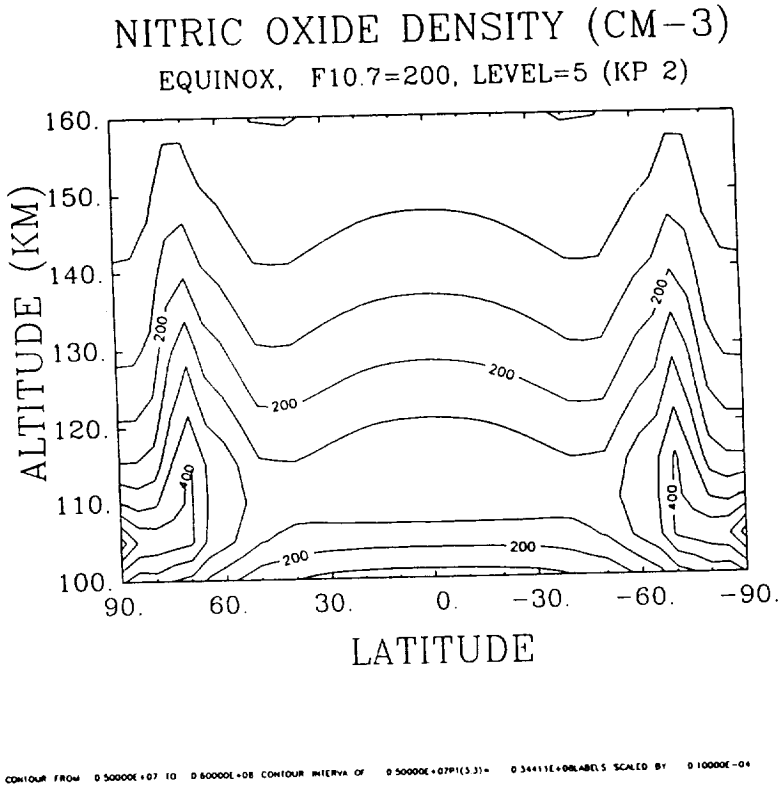
NITRIC OXIDE DENSITY (CM-3)
EQUINOX, F10.7=200, LEVEL=5 (KP 2)
ALTITUDE (KM)
160.
150.
140.
130.
120.
110.
100.
90.
60.
30.
0.
-30.
-60.
-90.
LATITUDE
200
400

Figure 7C.

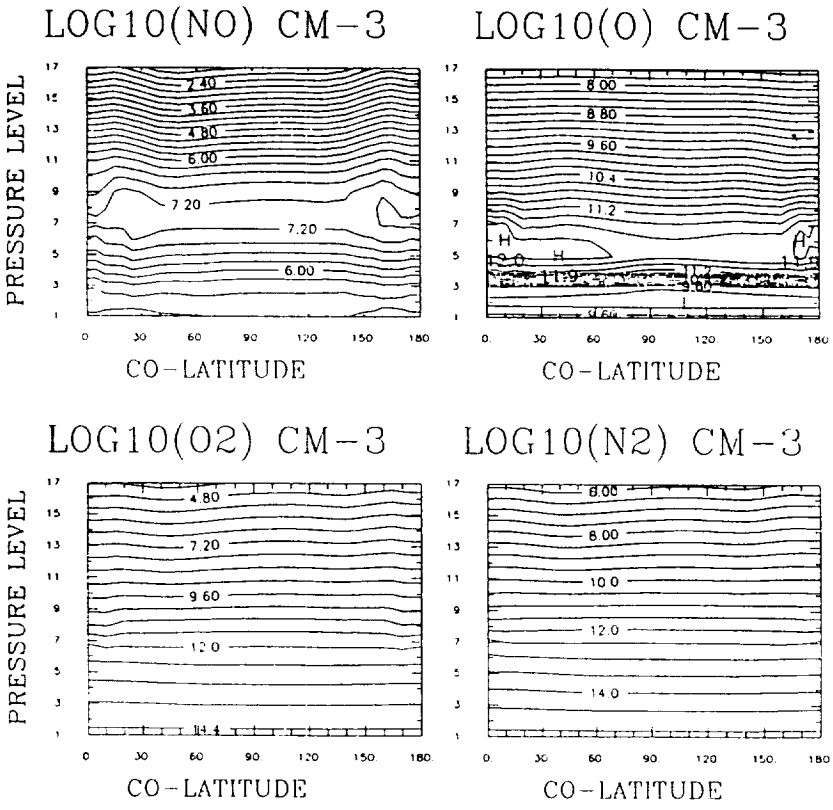

Figure 8. Variations of atmospheric structure and composition as a function of altitude and latitude simulated using the two-dimensional, time-dependent model. The display is as for Figure 4. The conditions depicted are moderately high solar activity ($F_{10.7}$ cm = 150) and low geomagnetic activity (Kp = 2) at the December solstice.

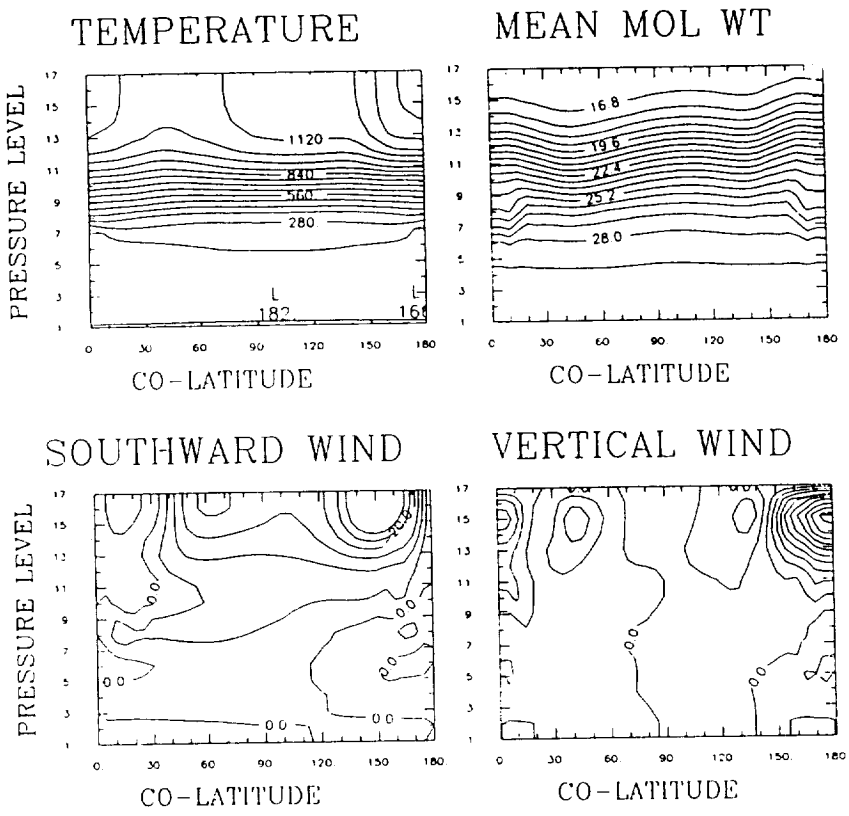
TEMPERATURE
MEAN MOL WT
SOUTHWARD WIND
VERTICAL WIND
PRESSURE LEVEL
CO-LATITUDE
1120
840
560
280
16.8
19.6
22.4
25.7
28.0
0 30 60 90 120 150 180

Figure 8B.

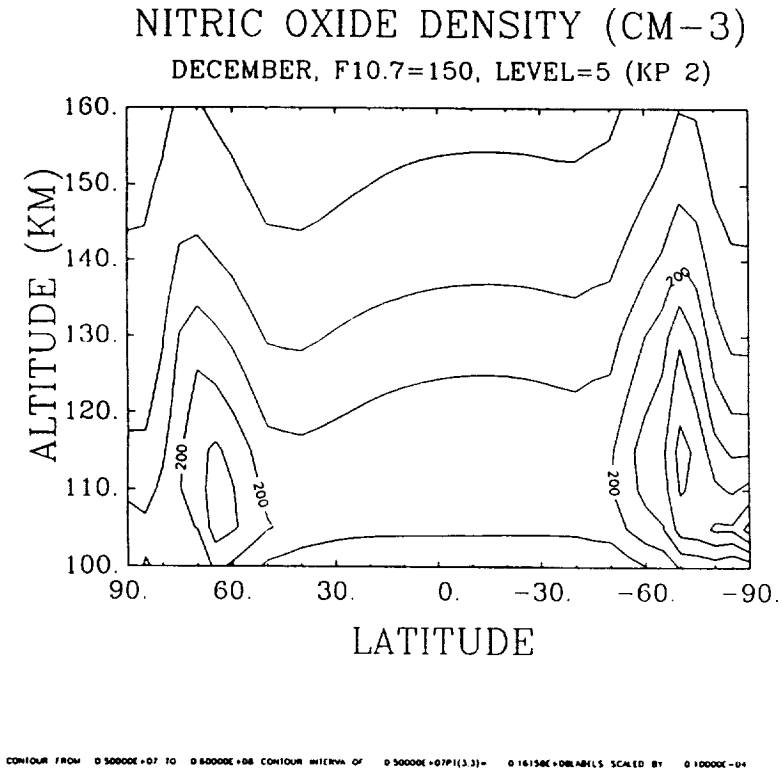
NITRIC OXIDE DENSITY (CM-3)
DECEMBER, F10.7=150, LEVEL=5 (KP 2)
ALTITUDE (KM)
160.
150.
140.
130.
120.
110.
100.
90.
60.
30.
0.
-30.
-60.
-90.
LATITUDE
200
200
200
CONTOUR FROM 0.500000E+07 TO 0.800000E+08 CONTOUR INTERVAL OF 0.500000E+07P1(3,3)= 0.161586E+08LABELS SCALED BY 0.100000E-04

Figure 8C.

Wind-driven diffusion /23/ caused by systematic upwelling over the summer pole, downwelling near the winter pole, with an interconnecting mean meridional flow of the order of 50 m/sec, partly overcomes diffusive equilibrium within the thermosphere. This causes the enhancement of heavy atomic and molecular species relative to light atomic species in the summer polar region and the converse in the region of downwelling near the winter pole.

At higher levels of geomagnetic activity, the wind-driven diffusion process is enhanced, causing a further enrichment of heavy and molecular species in the summer geomagnetic polar cap, where the strongest combined solar and geomagnetic heating occurs. At such times, the latitudinal variations of the atomic oxygen mixing ratio in the upper thermosphere become both larger and more complex, particularly at the solstice. Using coupled ionosphere - thermosphere models, the structures observed during major disturbances can be reasonably well simulated, and related to the locally-enhanced heating and upwelling caused, in the polar regions, by enhanced ion-neutral coupling (ion drag / frictional / Joule heating) resulting from the enhancement of E-region plasma densities by particle precipitation.

Under disturbed geomagnetic conditions at solstice, there can be a factor of 10 latitude variation in atomic oxygen concentration at the same F-region altitude (300 km). Even at E-region altitudes (around 125 km), a factor of 5 variation can occur. In both cases, minimum [O] values are within the summer geomagnetic polar cap, while maximum [O] values are at high winter mid-latitudes, equatorward of the auroral oval.

It is clear from the figures that the dominant influence on global [NO] production is from the auroral dissociation of N_2 at high latitudes. For all but the most quiet geomagnetic conditions, the high latitude peak NO number density is considerably greater than values observed at equatorial latitudes. At low latitudes, however, a large variation over the solar cycle has been observed /1/. This is a direct result of the solar cycle-related flux increase in the wavelength range up to 100 nm.

The solar production of $N(^2D)$ and (N^4S), the precursors of [NO], occurs primarily through the ion chemical reactions, particularly N_2^+ with neutral oxygen. A small additional source has also been identified by Richards et al /11/, namely the predissociation of N_2 in the wavelength range 80 - 100 nm. The peak [NO] density, near 105 km, is strongly controlled at low latitudes by the strength of the solar ionising flux able to penetrate to these levels. The wavelength region of most interest therefore, is the 1 - 14 nm soft X-ray flux.

The present simulations have used the solar fluxes and ionisation frequencies of the major species described by Torr et al /18/. The reference spectrum for low solar activity is from rocket-borne measurements in April 1974, when the $F_{10.7}$ cm radio flux was about 70 units. For high solar activity, the period in June 1979 was used, when the $F_{10.7}$ cm flux was in excess of 240 units. Using these reference spectra to define the range of solar flux in the model, the peak low-latitude [NO] density around 110 km varied from 0.8 * 106 cm-3 at low solar activity, to 3 * 106 cm-3 at high solar activity. The [NO] values differ from the observations of Barth /1/ over the last solar cycle. He reported a variation of a factor of 7 - 8 for the ratio of peak equatorial [NO] from high to low solar activity. The only fundamental difference with the present results is that the model appears to underestimate the minimum values by a factor of 2, and hence underestimates the ratio of equatorial [NO] density from high to low solar activity.

The most plausible explanation is that the soft X-ray flux was actually lower during the last solar cycle minimum in June 1986, than in the April 1974 minimum period, when direct solar EUV radiance measurements were available. Although the $F_{10.7}$ cm radio flux was similar during the two periods, the sunspot numbers differed considerably. In April 1974, the sunspot number was 40, in 1986, the minimum value was 1 during June, and the 1986 average only 14. In view of the strong correlation of the E-region critical frequency with the Zurich sunspot number, a direct relationship between [NO] density and the soft X-ray flux appears the most likely explanation. The $F_{10.7}$ cm radio index is thus not a particularly good indicator of [NO] equatorial density, and an index related to sunspot number might provide a better key for prediction.

We have previously shown /8/ that increased eddy turbulence causes enhanced downward transport of nitric oxide from the upper thermosphere to the mesosphere. The number density of nitric oxide is increased in the lower thermosphere, at the mesopause, and in the upper mesosphere by more than a factor of 10 by enhanced values of eddy turbulence (within published values).

The dominant consequence of the enhanced downward transport of nitric oxide is strong mesopause cooling in the vicinity of the region of enhanced eddy diffusion coefficient. The cooling is due to increased I.R. radiation from regions of elevated nitric oxide density. There is a change in the mean meridional wind and flow towards regions of increased eddy turbulence, which causes a complex sequence of inter-related effects.

If eddy turbulence is increased systematically on a large scale, for a period of several days, mesospheric nitric oxide densities increase. This causes, via increased radiative cooling, mesopause cooling of the order of 30 K, in the region of enhanced eddy turbulence. The increased eddy transport also enhances upper mesospheric atomic oxygen densities, but less dramatically than for nitric oxide, since atomic oxygen is removed rather rapidly below about 95 to 100 km.

SUMMARY.

In this study, we have attempted to use the numerical models to study the range of variability of atomic oxygen and nitric oxide which might be expected to occur as the result of four fundamental processes of change affecting the lower and upper thermosphere.

(i) Seasonal / latitudinal variations.

The effect of global convection and advection induced by asymmetric solar isolation near solstice causes a strong latitudinal variation in the composition of the thermosphere. Systematic upwelling and outflow near the summer pole, the connecting circulation and systematic convergence and downwelling towards the winter pole disturb diffusive equilibrium. The result is the enhancement of heavy atomic and molecular species, as viewed at constant pressure levels, in the summer polar regions, and a complementary enhancement of light atomic species near the winter polar region (again relative to constant pressure levels). The effects are well-determined empirically, and the seasonal / latitudinal variation is further enhanced by the high latitude heating during periods of high geomagnetic activity.

In the summer polar region, the mean molecular mass at pressure level 12 (F-region, around 300 km) may increase to above 24 / 25 amu (high solar activity, $F_{10.7}$ = 185, and for moderately disturbed geomagnetic conditions, Kp = 3^+ - 5). The minimum mean molecular mass at pressure level 12 (around 280 km) is now at high winter mid-latitudes (rather than in the winter polar region) but still has a value close to 17 amu.

Such compositional disturbances are not confined to the F-region, and even at 125 km, variations of a factor of 5 in atomic oxygen density can be generated at high geomagnetic activity levels.

For nitric oxide, there is approximately a 50 % modulation in number density caused by seasonal variations.

Solar Activity variations.

The latitude variations observed at constant pressure levels in atomic oxygen and molecular nitrogen caused by seasonal asymmetries of illumination and heating are only marginally changed by variations of solar activity. However, nitric oxide responds quite dramatically. The simulated variation of a factor of 4, as solar $F_{10.7}$ cm flux increases from 70 to 240, is smaller than the ratio reported from SME observations - a factor of 7 - 8. This difference is most likely associated with smaller X-ray fluxes during the 1986 solar minimum than during 1074, the previous solar cycle minimum. During 1986, the sunspot number was exceptionally low.

Geomagnetic Activity Variations.

The relatively localised energy inputs associated with elevated levels of geomagnetic activity generally decrease atomic oxygen concentrations (when observed on constant pressure levels). In the summer polar cap, this decrease can be an order of magnitude at F-region altitudes (around 300 km), and a factor of 5 at E-region altitudes (125 km). Normally, molecular nitrogen densities are elevated as the atomic oxygen density decreases. Nitric oxide generally responds quickly and increases rapidly in response to an increase of auroral production, varying by more than one order of magnitude from quiet to disturbed geomagnetic conditions.

Effects of eddy turbulence transport:

Atomic Oxygen.

Increased eddy turbulence causes enhanced downward transport of atomic oxygen from the upper thermosphere into the mesosphere. Where eddy turbulence is enhanced, the mixing ratio of [O] is increased at all altitudes, not only in the vicinity of the mesopause and lower thermosphere.

Nitric Oxide.

Nitric Oxide is readily transported downward by enhanced eddy diffusion around and above the mesopause. This may enhance radiative cooling of the upper mesosphere caused by nitric oxide, with further signatures in temperature and wind distributions.

A combination of seasonal, solar activity and geomagnetic variations discussed in this paper can cause unusual values or profiles of nitric oxide or atomic oxygen within the lower thermosphere and upper mesosphere. Generally, there should be a correlation or anticorrelation between variations of different major and minor constituents within the lower thermosphere and upper mesosphere, which may also leave a signature in temperature, density or wind profiles. We have previously shown that variations in the eddy diffusion coefficient, can cause a wide range of significant correlated composition, thermal and wind changes.

ACKNOWLEDGEMENTS

The work at UCL was supported with computer time allocated on the University of London Computers, by grants from the UK Science and Engineering Research Council, and from the Air Force Geophysics Laboratory (AFOSR-86-341).

REFERENCES

/1/ BARTH C.A., Reference Models for thermospheric NO., Adv. Space Res. (1989), (in press).
/2/ ROBLE R.G., E.C. RIDLEY and R.E. DICKINSON, On the global mean structure of the thermosphere, J. Geophys. Res., 92, 8745-87, (1987)
/3/ BANKS P.M. and G. KOCKARTS, Aeronomy, Parts A and B, Academic Press, New York, (1973).
/4/ Cospar Working Group IV, COSPAR International Reference Atmosphere (CIRA) 1972, Akademie-Verlag, Berlin, 1972.
/5/ HEDIN A.E., A revised thermospheric model based on mass spectrometer and incoherent scatter data: MSIS-83, J. Geophys. Res. 88, 10170, (1983).
/6/ HEDIN A.E., MSIS-86 thermospheric model, J. Geophys. Res. 92, 4649, (1987).
/7/ REES D., R. GORDON, T.J. FULLER-ROWELL, M.F. SMITH, G.R. CARIGNAN, T.L. KILLEEN, P.B. HAYS, N.W. SPENCER, The composition, structure, temperature and dynamics of the upper thermosphere in the polar regions during October to December 1981, Planet. Space. Sci. 33, 617, (1985).
/8/ REES D. and T.J. FULLER-ROWELL, Understanding the transport of atomic oxygen within the thermosphere, using a numerical global thermospheric model, Planet. Space Sci. 36, 935-948, (1988)
/9/ KOCKARTS, G., Nitric oxide cooling in the terrestrial thermosphere, Geophys. Res. Lett., 7, 137-140, (1980).
/10/ REES M.H., B.A. EMERY, R.G. ROBLE, and K. STAMNES, Neutral and ion gas heating by auroral electron precipitation, J. Geophys. Res., 88, 6289-6300, (1983).
/11/ RICHARDS P.G, M.R. TORR and D.G. TORR, Photo-dissociation of N_2, a significant source of thermospheric atomic nitrogen, J. Geophys. Res., 86, 1498-1498, (1981).
/12/ TORR M.R. and D.G. TORR, Chemistry of the thermosphere and ionosphere, J.Atm. Terr. Phys. 41, 797-839, (1979).
/13/ GARCIA R.R. and S. SOLOMON, J. Geophys Res 90, 3859, (1985)
/14/ FULLER-ROWELL T.J. and D. REES, A three-dimensional, time-dependent, global model of the thermosphere, J. Atmos. Sci., 37, 2545, (1980).
/15/ FULLER-ROWELL T.J. and D. REES, Derivation of a conservative equation for mean molecular weight for a two constituent gas within a three-dimensional, time-dependent model of the thermosphere, Planet. Space Sci., 31, 1209, (1983).
/16/ FULLER-ROWELL T.J., S. QUEGAN, D. REES, R.J. MOFFETT, G.J. BAILEY, Interactions between neutral thermospheric composition and the polar ionosphere using a coupled ionosphere-thermosphere model, J. Geophys. Res., 92, 7744, (1987).
/17/ FULLER-ROWELL T.J., Two-dimensional high resolution nested grid model of the thermosphere: 1 Neutral response to an electric field spike. J. Geophys. Res., 89, 2971-2990, (1984).
/18/ TORR M.R., D.E. TORR and R.A. ONG, Geophys. Res. Lett., 6, 771-774, (1979).
/19/ FULLER-ROWELL T.J. and D.S. EVANS, Height-integrated Pedersen and Hall conductivity patterns inferred from TIROS/NOAA satellite data. J. Geophys. Res. 92, 7606, (1987).
/20/ ROBLE R.G., and B.A. EMERY, On the global mean temperature of the thermosphere, Planet. Space Sci., 31, 597-614, (1983).
/21/ CHIU Y.T., An improved phenomenological model of ionospheric density, J. Atmos. Terr. Phys. 37, 1563-1570, (1975).
/22/ PARISH H., T.J. FULLER-ROWELL, D. REES, T.S VIRDI and P.J.S. WILLIAMS, Numerical simulations of the seasonal response of the thermosphere to propagating tides, Adv. Space Res., (1989), (in press)
/23/ MAYR H.G. and I. HARRIS, Some properties of upper atmosphere dynamics, Rev. Geophys and Space Phys., 16, 539, (1978).

AUTHOR INDEX

CUMULATIVE LISTING FOR THE MAP HANDBOOK

Volume	Contents	Publication Date
1	National Plans, PMP-1 , PMP-2, PMP-3 Reports, Approved MAP Projects	June 1981
2	Symposium on Middle Atmosphere Dynamics and Transport	June 1981
3	PMP-5, MSG-1, MSG-2, MSG-3 Reports, Antarctic Middle Atmosphere Project (AMA), EXOS-C Scientific Observations, WMO Report No. 5., Updated Chapter 2 of MAP Planning Document, Condensed Minutes of MAPSC Meetings	November 1981
4	Proceedings of MAP Assembly, Edinburgh, August 1981 Condensed Minutes of MAPSC Meetings, Edinburgh, Proceedings of MAP Open Meeting, Hamburg, August 1981,	April 1982
5	A Catalogue of Dynamic Parameters Describing the Variability of the Middle Stratosphere during the Northern Winters	May 1982
6	MAP Directory	November 1982
7	Acronyms, Condensed Minutes of MAPSC Meetings, Ottawa, May 1982, MAP Projects, National Reports, Committee, PMP, MSG, Workshop Reports, Announcements, Corrigendum	December 1982
8	MAP Project Reports: DYNAMICS, GLOBUS, and SSIM, MSG-7 Report, National Reports: Czechoslovakia, USA	July 1983
9	URSI/SCOSTEP Workshop on Technical Aspects of MST Radar, Urbana, May 1983	December 1983
10	International Symposium on Ground-Based Studies of the Middle Atmosphere, Schwerin, May 1983	May 1984
11	Condensed Minutes of MAPSC Meetings, Hamburg, 1983, Research Recommendations for Increased US Participation in the Middle Atmosphere Program, GRATMAP and MSG-7 Reports	June 1984
12	Coordinated Study of the Behavior of the Middle Atmosphere in Winter (PMP-1) Workshops	July 1984
13	Ground-Based Techniques	November 1984
14	URSI/SCOSTEP Workshop on Technical Aspects of MST Radar, Urbana, May 1984	December 1984
15	Balloon Techniques	June 1985
16	Atmospheric Structure and its Variation in the Region 20 to 120 km: Draft of a New Reference Middle Atmosphere	July 1985
17	Condensed Minutes of MAPSC Meeting, Condensed Minutes of MAP Assembly, MAP Project, MSG, and National Reports	August 1985
18	MAP Symposium, Kyoto, November 1984	December 1985
19	Rocket Techniques	March 1986
20	URSI/SCOSTEP Workshop on Technical and Scientific Aspects of MST Radar, Aguadilla, October 1985	June 1986
21	MAPSC Minutes, ATMAP Workshop, Atmospheric Tides Workshop, MAP/WINE Experimenters Meetings, National Reports: Coordinated Study of the Behavior of the Middle Atmosphere in Winter	July 1986 July 1986
22	Middle Atmosphere Composition Revealed by Satellite Observations	September 1986
23	Condensed Minutes of MAPSC Meetings, Toulouse, June/July 1986	December 1986
24	MAP Directory	May 1987
25	First GLOBMET Symposium, Dushanbe, August 1985	August 1987
26	MAPSC Minutes, Abstracts and Report of Workshop on Noctilucent Clouds, Boulder,	June 1988 October 1985
27	COSPAR Symposium 6, The Middle Atmosphere After MAP,Espoo, July 1988, MAPSC Minutes, Espoo, July 1988; Workshop on Noctilucent Clouds, Tallinn, July 1988	April 1989
28	URSI/SCOSTEP Workshop on Technical and Scientific Aspects of MST Radar, Kyoto, November/December 1988	August 1989
29	International Symposium on Solar Activity Forcing of the Middle Atmosphere, Liblice, Czechoslovakia, April 1989; MASH Workshop, Williamsburg, April 1986	September 1989
30	International School on Atmospheric Radar, Kyoto, November 1988	October 1989
31	Reference Models of Trace Species for the COSPAR International Reference Atmosphere (Draft)	December 1989